ANALYSIS AND SYNTHESIS OF MILLIMETRIC E-PLANE DIPLEXERS IN RECTANGULAR WAVEGUIDE

Antonio Morini, Tullio Rozzi
Dipartimento di Elettronica e Automatica, Università di Ancona

ABSTRACT

A novel E-plane diplexer is proposed and discussed.
Its feature is the matching section of the three-port junction, obtained by means of an E-plane septum, realized on the same mask as the branching filters and placed in the cavity of an abrupt E-plane junction.
The latter is designed in such a way that, when combine d with two reasonably -good filters, separately designed and suitably positioned, the resulting diplexer gives good performances without further optimization.
This design technique, based on the properties of the scattering parameters of a reciprocal lossless three-port junction, is , as such, of general validity and easily extended to other structures.

INTRODUCTION

The more expensive part of an E-plane circuit in rectangular waveguide for millimetric application is its housing. In fact, its fabrication requires high precision milling machines and it is difficult to reduce tolerances below 10 μ for each half housing. Therefore, it becomes important to simplify as much as possible the housing geometry, even increasing the complexity of the mask.
For this reason, we study an E-plane diplexer based on an abrupt three-port junction, in lieu of a tapered junction, Dittlof and Arndt (1-2), Vahldieck and Varailhon de la Filolie(3), requiring more expensive mechanical construction.
The junction is tuned by a single inductive post, built on the same mask as the E-plane filters and placed between the junction and the bifurcation, as shown in fig.1, Morini et al. (4). Consequently, the resulting diplexer consists of just three parts: a single mask containing filters and tuning post and the two halves of the housing wherefrom junction and guides are made.The diplexer is then assembled by sandwiching the mask between the two halves of the housing . Modelling the junction, inclusive of the post, involves a rigorous treatment of the interaction between adjacent discontinuities by the concept of accessible modes, Rozzi et al. (5). As contrasted to (5), modes of both TE and TM polarization occur, depending on two indices.

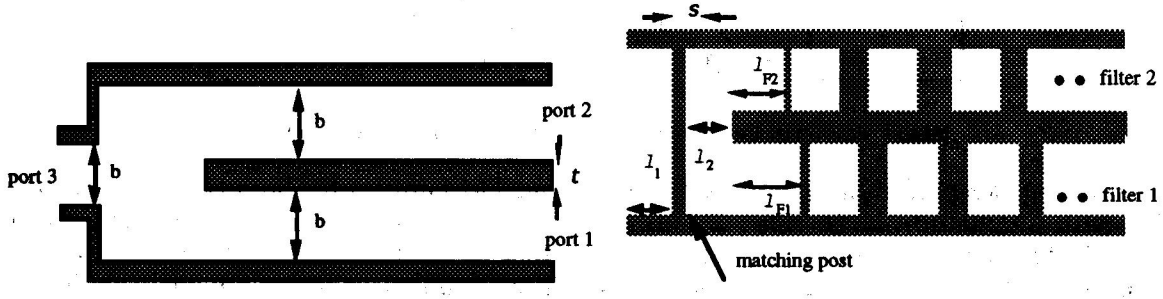

fig.1 Geometry of the E-plane diplexer
(l) E-section of the junction (r) mask containing filters and matching post

Particular attention was also given to the problem of 'optimum' synthesis of the whole diplexer with two given good filters, not amenable to modification.
It is a common misconception that optimum results are achieved by utilizing a good power divider closed by the branching filters.
In a recent paper we showed this assumption to be groundless, and, by exploiting some general properties of lossless reciprocal three-port junctions endowed with a plane of symmetry, we recovered some conditions to be satisfied in order to obtain an 'optimum' three-port for diplexer application with two given filters, Morini and Rozzi (6).
The technique here described, based on the above conditions, permits to separate the synthesis of the junction from that of the filters, giving an explicit formula for the correct positioning of the filters, without any further optimization.

JUNCTION ANALYSIS

We shall now focus on the analysis of the junction (4), whereas reference is made to (5) for that of the filters. Symmetry of the junction about its longitudinal mid-plane implies $s_{11} = s_{22}$ and $s_{13} = s_{23}$, moreover by adopting even and odd excitations the three-port junction reduces to the two two-port situations shown in fig.2.

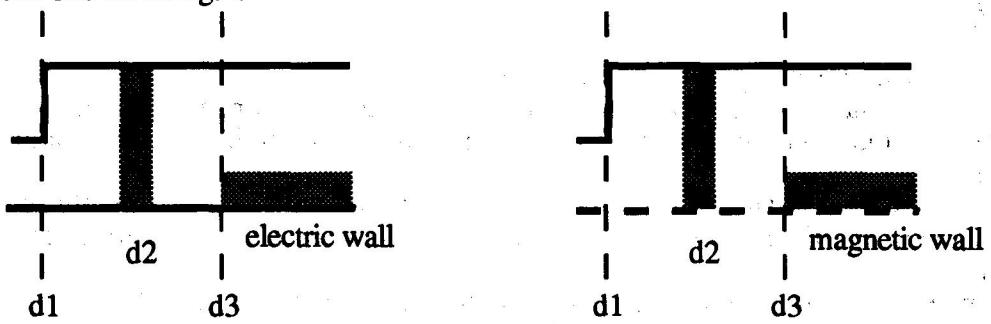

fig.2 even/odd excitation at ports 1 and 2: resulting structures

Both comprize the cascade of three discontinuities d1, d2, d3 separated by short sections of guide and, as such, interacting. These discontinuities are analyzed individually as 2N- port, N being the number of ' accessible modes '. These are chosen according to the following considerations:

Discontinuities 1 and 3, that is two E-plane steps, under the excitation of an incident TE_{10} -mode, excite in turn just LSE_{1n} -modes with n=1,2,3, due to their uniformity with respect to x.

On the other hand, discontinuity 2, i.e. the metal septum, due to its uniformity with respect to y, when excited by LSE_{1n} -modes excites in turn the TE_{mn} and TM_{mn} families with m=1,3,5... Finally, the latter impinging on discontinuities 1 and 3 excite TE_{mn} and TM_{mn} modes with n=1,2,3..

This complex mechanism is summarized in table I.

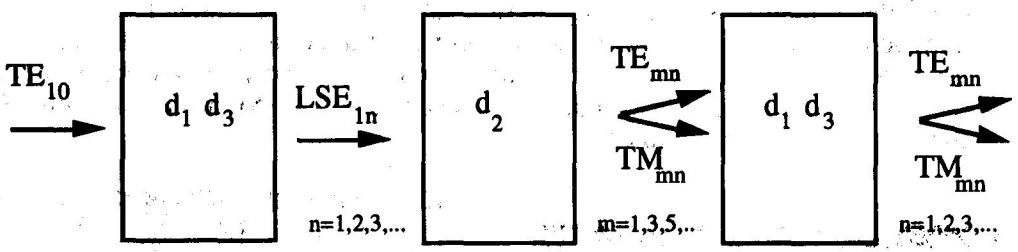

table I scheme of the modal interactions occurring between discontinuities

For this reason, we preferred to work with the TE and TM families for both types of discontinuity. Modes with attenuation larger than 20 dB between successive discontinuities were considered 'localized'. Applying the above criteria we found that in the case of interest it was sufficient to consider the first five modes as accessible. The six discontinuities occurring are analyzed by deriving variational expressions for the multiport impedance matrix $\mathbf{Z}_k^e$ and $\mathbf{Z}_k^o$ (k=1, 2, 3) of each. The discontinuity fields are expanded in polynomials with weight functions singular at the sharp edges, Collin (7), leading to singular integral equations. Having computed $\mathbf{Z}_k^e$ and $\mathbf{Z}_k^o$ (k=1, 2, 3), the behavior of the whole junction is determined by cascading the corresponding transmission matrices $\mathbf{T}_k^e$ and $\mathbf{T}_k^o$ .In fact , denoting by $\mathbf{U}^e(l)$ e $\mathbf{U}^o(l)$ the standard transmission matrices of a waveguide section of length l, for the even/odd excitations respectively , the global transmission matrix becomes, in the even case,

$$\mathbf{T}_E(l_1,l_2;\, s,b,t,f) = \mathbf{T}_1^e(b,t,f)\cdot\mathbf{U}^e(l_1,f)\cdot\mathbf{T}_2^e(s;2b+t,f)\cdot\mathbf{U}^e(l_2,f)\cdot\mathbf{T}_3^e(b,t,f) \quad : \text{dim } 3x3 \qquad (1a)$$

and, in the odd case,

$$T_O(l_1,l_2;\ s,b,t,f) = T_1^o(b,t,f)\cdot U^o(l_1,f)\cdot T_2^o(s;2b+t,f)\cdot U^o(l_2,f)\cdot T_3^o(b,t,f) \quad : \text{dim } 2x2 \qquad (1b)$$

When the interaction between junction and filters via modes below-cutoff is negligible, the matrices just obtained can be reduced by closing the ports corresponding to those modes on their characteristic impedances. From the latter circuits it is easy to derive the scattering parameters and then the response of the diplexer by standard network methods .

DIPLEXER SYNTHESIS

As mentioned in the introduction, a common misconception is that an "optimum" diplexer need be designed starting from a good power divider. Really, this assumption yields good results only when geometries of the branching filters, and consequently their electrical parameters, are substantially modified in such a way that the whole diplexer satisfies specifications, H. Yao et al. (8). In that case, the computer optimization (manipulation) of the filters is so intensive that the original choice of a power divider does not seem to be particularly significant.

The method we will follow permits instead to design separately junction and filters.

In fact we showed (6) that a three-port symmetrical junction in conjunction with two pass-band filters gives good diplexer performance if the junction satisfies the following specifications:

$$|s_{11}| = |s_{22}| \cong |s_{33}| \qquad f=f_1,\ f=f_2 \qquad (2a)$$

$$|s_{33}| \geq 1/3 \qquad (2b)$$

$$s'_{11} \cong s'_{12} \cong s'_{22} \cong 0 \qquad f=f_1,\ f=f_2 \qquad (2c)$$

Where $s_{ij}(\upsilon)$ is a scattering parameter of the junction, $s'_{ij}(\upsilon)$ its derivative with respect to the effective frequency $\upsilon = \beta a$; β is the propagation constant of the fundamental mode for the waveguide feeds, a is the guide wider wall; finally f_1 and f_2 are the midband frequencies of the two branching filters.

We can consider the performance of the three-port junction, by closing one of its arm on a filter Fi (i=1,2) and by evaluating the bandwidth of the resulting two-port, centered on the midband frequency of the second filter, f_j, over which the reflection magnitude is lower than a fixed ε. The distance l_{Fi} at which filter Fi need be located is given by the formula (6):

$$l_{Fi} = -\frac{1}{2j\beta(f_j)} \ln\left[\frac{s_{ij}}{\Delta s\ s^*_{33}\ \rho_{Fi}(f_j)}\right] \qquad (3)$$

when i=1, j=2 and when i=2 j=1, $\rho_{Fi}(f)$ is the reflection of the filter Fi.

It is found that the maximum bandwidth $2\Delta\upsilon$ of the two-port so obtained, and then of each channel of the diplexer, depends on the reflection magnitude at the common port of the junction,

$$2\Delta\upsilon \leq \frac{1 - |s_{33}|^2}{|s_{33}|^2}\frac{\varepsilon a}{2l} \qquad (4)$$

Fig 3 shows a plot of eq.4, for a given reflection ε = -30 dB and for different $|s_{33}|$ comprised between -9.5 dB an -3 dB, representing the maximum banwidth of the diplexer versus the normalized distance l_{Fi}/a . It is seen that $|s_{33}|$ decreases as the bandwidth increases.

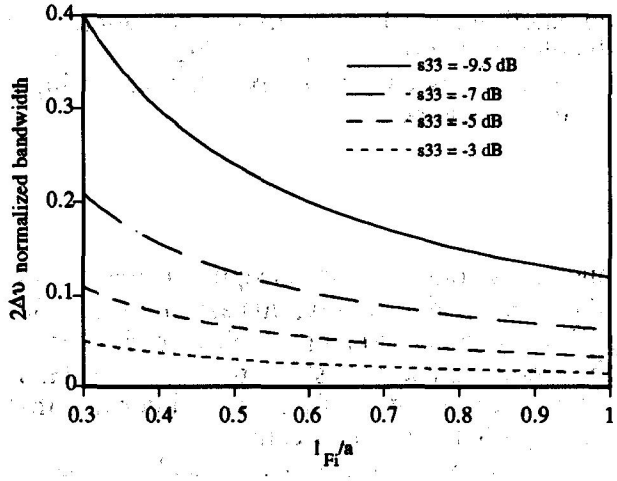

fig. 3 Maximum normalized bandwidth vs. filter positioning for a given ε = - 30 dB

RESULTS

In the present case, we had to design a diplexer with the following specifications:

b1 37.482 - 37.782 GHz
b2 38.742 - 39.042 GHz
mrl in the pass-band 26 dB
5 poles filters

This corresponds to a normalized bandwidth for each channel given by $2\,\Delta\upsilon \cong 0.06$ (considering a WR 28 rectangular waveguide). By comparison with fig.3 we see that, once 2a-c are verified, $|s_{33}| \leq -5$ dB.
Therefore we designed first the branching filters (minimum return loss 26 dB) by using a classical synthesis technique, Rhodes (9), and by E-plane program developed by ourselves (5). Their dimensions are summarized in the following table:

posts(p) cavities (c)	p1=p6	c1=c5	p2=p5	c2=c4	p3=p4	c3
filter1	1.730	7.812	5.549	7.781	6.376	7.781
filter2	2.026	7.301	6.442	7.259	7.360	7.258

table 2 dimensions of the two branching filters

Secondly, we designed the junction. From equations (1a-b) we recover the scattering matrix of the three-port junction and optimized its geometrical parameters l_1, l_2 by minimizing the objective function F, given by:

$$F(l_1,l_2;\, s,t;\, a,b) = \sqrt{\sum_i \left(\left|\frac{s_{11}}{s_{33}}\right| - 1\right)^2} + \sum_i \sqrt{\left(|s_{11}| - \frac{1}{3}\right)^2 + \left(|s_{33}| - \frac{1}{3}\right)^2}$$

being $s_{ii} \doteq s_{ii}(l_1,l_2;\, s,t,f_i,\, a,b)$. The summation is made on the frequency points belonging to the pass-bands of the two filters, tipically 5-10 points in each band.
For the minimization of F, we made use of a library routine based on the quasi Newton method, NAG (10). As distances l_1 and l_2 range from 200 μ to 6 mm, we may obtain distances shorter than those for which the first higher order mode is attenuated less than 20 dB. A more accurate equivalent circuit, making use of additional accessible modes is then employed. The length of the matching

septum, s, and the thickness of the wall separating the two output guides, t, range respectively from 100 μ to 600 μ by 50 μ steps and from 2 mm to 4 mm, by 200 μ steps, and finally a=7.112 mm and b=3.556 mm. A good result was found for l_1= 4.465 mm, l_2= 4.885 mm, s= 0.200 mm, t= 3.550 mm. The corresponding distances at which to locate the filters, calculated by means of (3), are: l_{F1}= 3.023 mm and l_{F2}= 2.934 mm.

In our case, the configuration employed does not comply with (2c), causing a reduction of the maximum obtainable bandwidth. Moreover, in all cases encountered, the two bands were separated by a region of considerable mismatch , as shown in fig.4 for a typical junction.

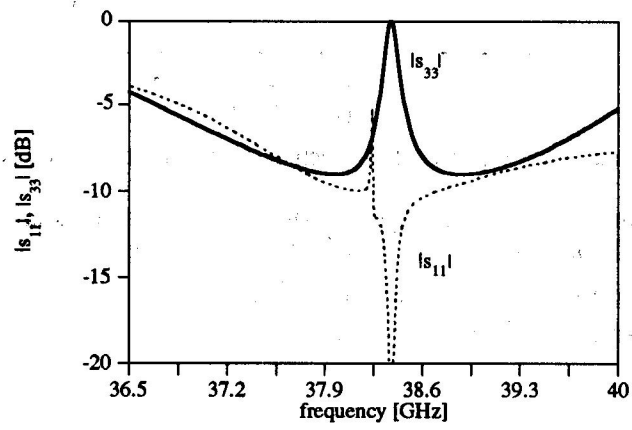

fig. 4 comparison between |s11| and |s33| for a tipical junction employed

This fact does not constitute a limitation in itself, provided this mismath region is narrower than the band separating the passbands of the two filters: on the contrary, the isolation between diplexer channels is enhanced.

In K_a-band, one recovers channels of 500-600 MHz spaced by about 1 GHz, with match better than -30 dB: these characteristics were more than sufficient for the design of the diplexer prototype.

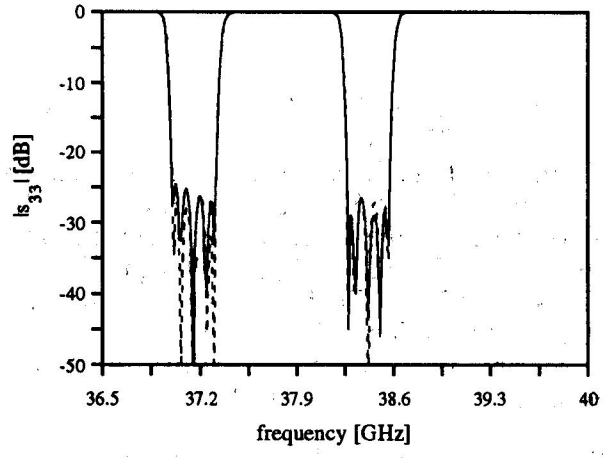

fig.5 Comparison between theoretical reflection magnitude at common port of the diplexer with those of the single branching filters .

In fact fig. 5 shows the theoretical reflection magnitude at the common port of the diplexer compared with those of the two filters. It is noted that the diplexer response, designed according to the criteria above, is seen as transparent by the filters without the need for costly optimization. Finally, fig 6 shows the measured magnitude of the reflection at the common port of the diplexer prototype that was actually built. Deviations are due to mechanical tolerances. We also simulated three contiguous diplexers in the band 37 - 39 GHz, each with 300 MHz bandwidth wide, by using, in all cases, the same fixed housing, tuning only by varying the length of the matching post and its position inside the cavity.

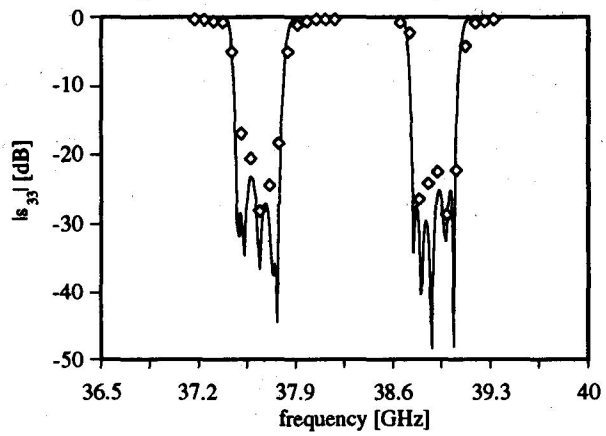

fig.6 Comparison between theoretical and experimental reflection magnitude at common port of the diplexer realized.

This arrangement affords considerable savings in fabrication, as individual diplexers differ only by just an inexpensive mask. Moreover, it is to be noted that, by suppressing low frequency spurious passbands, these selective frequency characteristics allow filters with longer cavities (λ_g,$3/2\lambda_g$) to be employed, which substantially reduce ohmic losses.

CONCLUSIONS

We have proposed a novel ' E-plane ' diplexer junction of compact and inexpensive fabrication and developed a rigorous analysis for its characterization.
This solution seems to be advantageous when filter bands are less than 2% wide. A prototype was built and tested showing good performance in close agreement with the theoretical prediction.

ACKNOWLEDGMENTS

The authors are pleased to thank Dr. H. Yao for his useful suggestions and helpful discussions.

REFERENCES

(1) J. Dittloff, and F. Arndt, "Rigorous design of septate multiplexers with printed circuit elements", IEEE MTT-S Digest 1988, pp.431-434;
(2) J. Dittloff, and F. Arndt, "Rigorous field theory design of millimeter-wave E-plane integrated circuit multiplexers", IEEE Trans. on MTT, vol. MTT-37, No. 2, Feb. 1989, pp 340-350;
(3) R. Vahldieck , B. Varailhon de la Filolie, " Computer aided design of parallel-connected millimeter-wave diplexers/multiplexers, IEEE MTT-S Digest 1988, pp 435-438;
(4) A. Morini, T. Rozzi, D. De Angelis,W. Gulloch: "A novel matched diplexer configuration in E-plane technology", IEEE MTT-S Digest 1993, pp 1077-1080;
(5) T. Rozzi, F. Moglie, A. Morini, W. Gulloch, M. Politi: "Accurate full-band equivalent circuits of inductive posts in rectangular waveguide", IEEE Trans. on MTT, vol. MTT-40, No. 5, May 1992;
(6) A. Morini, T. Rozzi: "Design of 'optimum' three port symmetrical junctions for diplexer application", IEEE MTT-S Digest 1994;
(7) R.E. Collin, " Field Theory of guided waves, II Edition", IEEE press, 1990;
(8) H. Yao, A. Abdelmonem, J. liang, X. Liang, K. Zaki and A. Martin: "Wide-band waveguide and ridge waveguide T-junction for diplexer applications", IEEE Trans. on MTT, vol. MTT-41, No. 12, Dec. 1993, pp 2166-2173;
(9) D. Rhodes, "Theory of electrical filters", John Wiley & Sons, 1976
(10) Nag Fortran Library Manual, Mark 15, 1991 The Numerical Group Limited

Constraints to the Optimum Performance and Bandwidth Limitations of Diplexers Employing Symmetric Three-Port Junctions

Antonio Morini, *Member, IEEE*, and Tullio Rozzi, *Fellow, IEEE*

***Abstract*—This work addresses the problem of the fundamental limitations to the optimum performance of diplexers employing three-port junctions and preassigned branching filters. In this situation it is a common misconception that optimum results are achieved by utilizing a good power divider closed by two good branching filters. From the properties of the S-matrix of a three-port junction, we show this not to be the case and derive a set of necessary conditions to be satisfied in order that the junction be successfully employed in the realization of diplexers. We derive explicit expressions for the positions at which the filters must be placed in the junction arms for optimum diplexer performance, resulting in considerable simplification of the difficult diplexer synthesis problem. A theorem on the maximum achievable bandwidth is proved and validated by means of two practical examples.**

I. Introduction

AT MILLIMETER frequencies it is expedient to employ reciprocal circuits for the realization of diplexers and multiplexers and some interesting examples have appeared in the recent literature [1]–[4]. These are constituted essentially by three-port junctions closed by two filters, which select the RX signal at port 1 and the TX signal at port 2, while port 3 is the input port in Fig. 1. The junction must be realized in such a way that port 3 and 1, 3, and 2 be perfectly matched over the RX band and the TX band, respectively.

A general theory for the synthesis of diplexers-multiplexers is indeed presented in [5]–[7]. However, its application is not immediate since the deviations between prototype and actual physical structure require a further process of optimization. Therefore, for the practical purpose of design, the geometry of the junction, including the distances from the junction at which the filters need to be positioned, is often determined by making use of either of the two following approaches [8].

1) Separate design of the three-port junction, of the branching filters and selection of the optimum distances of the filters from the junction.
2) Global optimization of the whole diplexer by varying either filter dimensions or junction geometry and filter distances or both together.

The latter approach may seem more satisfactory, but, in practice is rendered problematic by the large number of variables and by the "error function" not being analytically available, so that a number of local minima occur.

With a view to bypassing such difficulties, some researchers have employed segmentation techniques (evolution strategy method) in the solution space, that while yielding some very good results [1], [2], appear to be computationally cumbersome. The first approach would seem more expedient, but, unfortunately, its results so far are disappointing until and unless either the filters, the junction or both are altered essentially, falling back therefore into case 2) above.

This work examines the reasons for this failure starting from the properties of the S-matrix of the lossless reciprocal three-port junction. It is shown that, contrary to common belief, the ideal junction is not provided by a matched power splitter and that , in fact, it has to satisfy some necessary conditions. These will be derived and illustrated in the following by means of two examples of diplexer designs, the first one from the literature, the second a new one.

Once the junction is well defined, we obtain by means of a simple analytical formula the distances of the filters from the junction for optimum performance.

Moreover, there is a direct design application of the above criteria: often, in fact, one has to assemble a diplexer starting from two given filters and a three-port junction, with just the possibility of experimental tuning. In this case, the analytical results here obtained permit to simplify considerably the procedure, concentrating attention just upon the junction, whose characteristics can be modified in order to satisfy simple prescribed specifications. The two filters are then connected to the junction at distances determined from separate measurements of junction and filters.

It is noted that, for the sake of simplicity, the analytical model is developed on the basis of just fundamental mode interaction between junction and filters. In cases where optimum distances are so short that higher modes may cause interaction, the single mode result may be considered as an excellent starting point for an optimization routine anyway. It is emphasized that said criteria are based on the analysis of the scattering matrix of the junction and they are, as such, of general application, independently of the technology adopted.

II. Analysis

In Fig. 1, the diplexer is modeled as a lossless reciprocal three-port junction (J) with ports 1 and 2 closed by filters $F1$

Manuscript received December 8, 1994; revised November 12, 1995.
The author is with the Dipartimento di Elettronica e Automatica, Università di Ancona, via Brecce Bianche, 60100 Ancona, Italy.
Publisher Item Identifier S 0018-9480(96)01447-0.

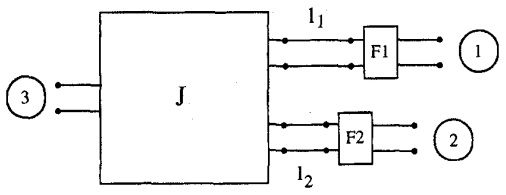

Fig. 1. Black box equivalent circuit of the diplexer; J is a three-port junction, $F1$ and $F2$ are the two filters.

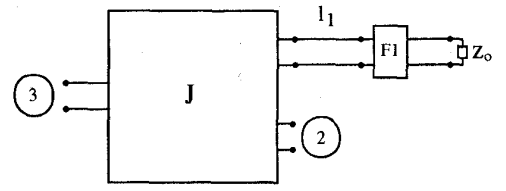

Fig. 2. Two-port network obtained by closing port 1 of J by $F1$, located at distance l_1 from the junction.

and $F2$ with passbands b_1 and b_2, respectively. We require:

1) perfect transmission between ports 3 and 2 over the band b_2;
2) perfect transmission between ports 3 and 1 over the band b_1.

Let us consider the first requirement:

This is certainly satisfied, if by closing port 1 by filter $F1$, terminated by a matched load (Fig. 2), the resulting two-port junction is perfectly matched and lossless over the band b_2.

Let ρ_{L1} denote the reflection coefficient of $F1$, located at a distance l_1 from port 1 of the junction, the scattering matrix of the resulting 2-port network (3-2) is given by

$$\begin{bmatrix} S_{22} & S_{23} \\ S_{23} & S_{33} \end{bmatrix} = \begin{bmatrix} s_{22} & s_{23} \\ s_{23} & s_{33} \end{bmatrix} + \frac{1}{\frac{1}{\rho_{L1} e^{-j2\upsilon l_1/a}} - s_{11}} \times \begin{bmatrix} s_{12}^2 & s_{12}s_{13} \\ s_{12}s_{13} & s_{13}^2 \end{bmatrix}. \quad (1)$$

Where s_{ij} are the parameters of the scattering matrix $\mathbf{S}$ of the junction J and $\upsilon = \beta a$ is the effective frequency, β being the propagation constant of the fundamental mode of the waveguide feeds and a being an appropriate transverse dimension. Requirement 1) therefore implies

$$S_{22}(\upsilon) = 0 \qquad \text{(over the band } b_2\text{)} \quad (2)$$

Hence, using the fact that for a lossless junction $s_{33}^* = \frac{s_{11}s_{22} - s_{12}^2}{\Delta s}$, where Δs is the determinant of $\mathbf{S}$, we derive

$$\rho_{L1} e^{-j2\upsilon l_1/a} = \frac{s_{22}}{s_{11}s_{22} - s_{12}^2} = \frac{s_{22}}{\Delta s\, s_{33}^*}. \quad (3)$$

Since $F1$ operates in its stopband over band b_2, we have $|\rho_{L1}| \cong 1$ to a good approximation, $|\Delta s| = 1$ due to losslessness and consequently from (3), in order for constraint i) to be satisfied, we must require

$$|s_{22}| = |s_{33}| \qquad \text{over the band } b_2. \quad (4a)$$

In analogous manner, we may show that in order for requirement 2) to be satisfied, we must have

$$|s_{11}| = |s_{33}| \qquad \text{over the band } b_1 \quad (4b)$$

It is noted that (4a) and (4b) above involve just the scattering parameters of the junction independently of the filters and of their spacings from the junction. In order that requirement 1) be satisfied at the frequency f_2, we choose the distance l_1 by solving (3) at $f = f_2$, yielding the spacing

$$l_1 = -\frac{a}{2j\upsilon} \ln\left[\frac{s_{22}}{\Delta s\, s_{33}^* \rho_{L1}}\right] \qquad f = f_2. \quad (5a)$$

Proceeding in analogous fashion for ports 2–3, we recover

$$l_2 = -\frac{a}{2j\upsilon} \ln\left[\frac{s_{11}}{\Delta s\, s_{33}^* \rho_{L2}}\right] \qquad f = f_1. \quad (5b)$$

The spacings l_1, l_2, obtained from (5a) and (5b), together with (4a) and (4b), ensure ideal diplexer behavior at the midband frequencies f_1 and f_2 of the two filters.

We shall now consider the question of the maximum achievable bandwidth under the constraint of junction symmetry.

A. Symmetrical Junctions

Let us now consider the important class of three-port junctions endowed with a plane of symmetry. To this class belong many common junctions, e.g., considering only rectangular waveguide junctions, the abrupt E-plane and H-plane junctions, T-junctions, Y-junctions with arbitrary angle of aperture and junctions such as those described in [2], [9], and [10] containing more complicated matching sections.

The above symmetry implies [11]

$$s_{11} = s_{22} \qquad \text{for } E\text{-plane junctions} \quad (6a)$$

$$s_{11} = -s_{22} \qquad \text{for } H\text{-plane junctions.} \quad (6b)$$

Consequently, by combining property (6) above with constraint (4a)–(4b), we deduce that the geometry is to be selected in such a way that

$$|s_{11}| = |s_{22}| \cong |s_{33}| \quad (7)$$

over the bands b_1 and b_2.

We may now state the following lemma:

Lemma: A necessary condition in order for (7) to be satisfied is that

$$|s_{33}| \geq 1/3. \quad (8)$$

Proof: We will first deal with E-plane junctions.

The above statement can be proved by means of geometrical considerations. In fact, define by Γ_e, Γ_o the reflection coefficients at port 1 corresponding to an even, odd excitation respectively at ports 1 and 2. We have then

$$s_{11} = \frac{\Gamma_e + \Gamma_o}{2} \quad (9a)$$

$$s_{12} = \frac{\Gamma_e - \Gamma_o}{2}. \quad (9b)$$

Because of losslessness we have $s_{33} = -\frac{s_{13}}{s_{13}^*}(s_{11}^* + s_{12}^*)$, so that

$$|s_{33}| = |\Gamma_e|. \quad (9c)$$

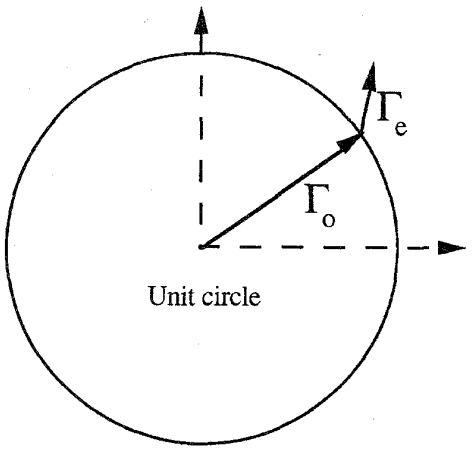

Fig. 3. Representation of the reflection coefficients Γ_e and Γ_o, corresponding to even/odd excitation, in the complex plane.

The condition $|s_{22}| = |s_{33}|$ over the band b_2 (4a) requires, however

$$|\Gamma_e| = \left|\frac{\Gamma_e + \Gamma_o}{2}\right|. \tag{10}$$

Let us plot the reflection coefficients as vectors in the complex plane (see Fig. 3). By virtue of the assumed symmetry, in the odd excitation case, the amplitude of the wave transmitted to port 3, $b_3 = s_{13}\left(\frac{1}{2}\right) + s_{13}\left(-\frac{1}{2}\right) = 0$, hence $|\Gamma_o| = 1$.

Noting, moreover, that the minimum of s_{11} is obtained if Γ_e and Γ_o have opposite phases, we obtain

$$\left|\frac{\Gamma_e + \Gamma_o}{2}\right| \geq \frac{1 - |\Gamma_e|}{2} \tag{11}$$

which together with (10) proves the statement (8).

The H-plane case follows simply by exchanging Γ_e with Γ_o. □

A direct consequence is that an optimum junction behavior for the purpose of realizing a diplexer is rather different from that of a power splitter, for which $|s_{33}| = 0$. We shall now consider the problem of diplexer bandwidth. Although the actual achievable bandwidth depends on the specific junction and filter characteristics, we will determine an upper limit to its value with the help of the following theorem.

Theorem: The maximum achievable bandwidth, for a given a reflection ε, of the two-port junction obtained by closing one arm of a symmetrical three-port on a given filter is given by

$$2\Delta v \leq \frac{1 - |s_{33}|^2}{|s_{33}|^2}\frac{\varepsilon}{2\bar{l}}$$

where s_{33} is the reflection at the common port of the junction, $\bar{l}$ is an "effective" normalized distance at which the filter is positioned.

Proof: By closing port 1 of the junction on $F1$ (Fig. 2), the reflection coefficient of the resulting two-port network $S_{22}(v)$ is expressed in terms of the s-parameters of the junction J and of $F1$ as

$$S_{22}(v) = s_{22}(v) + \frac{s_{12}^2(v)}{\frac{1}{\rho_{L1}e^{-j2vl_1/a}} - s_{11}(v)}. \tag{12}$$

We have seen that, according to (11), $S_{22}(v_2) = 0$. Therefore in a neighborhood of the midband frequency f_2, corresponding to v_2, considering the first order Taylor approximation to S_{22} we have

$$S_{22}(v) \approx \frac{d}{dv}S_{22}(v_2)\Delta v. \tag{13}$$

Now, we require that $|S_{22}(v)| < \varepsilon$ over the band Δv, ε being the maximum reflection coefficient of the junction that is compatible with the diplexer specifications, that is

$$\left|\frac{d}{dv}S_{22}(v_2)\right| \leq \frac{\varepsilon}{\Delta v}. \tag{14}$$

By differentiating (12) with respect v, we obtain

$$\begin{aligned}\frac{d}{dv}S_{22}(v_2) &= s'_{22} + \frac{2s'_{12}s_{12}}{\frac{1}{\rho_{L1}e^{-j2v_2l_1/a}} - s_{11}} \\ &+ \frac{s_{12}^2\left(-2j\frac{l_1}{a}\frac{e^{+j2v_2l_1/a}}{\rho_{L1}} + \frac{\rho'_{L1}e^{+j2v_2l_1/a}}{\rho_{L1}^2} + s'_{11}\right)}{\left(\frac{1}{\rho_{L1}e^{-j2v_2l_1/a}} - s_{11}\right)^2}.\end{aligned} \tag{15}$$

The best situation occurs when $s'_{11} = s'_{12} = s'_{22} = 0$, corresponding to a junction whose parameters do not depend on frequency. Moreover, considering that $\rho_{L1}(v) \approx e^{-j\phi(v)}$ outside its band-pass and that $\phi'(v) \geq 0$ owing to the Foster's reactance theorem, by virtue of (14), we recover

$$\left|s_{12}^2\frac{\phi'(v) + 2\frac{l_1}{a}}{\left(\frac{1}{\rho_{L1}e^{-j2v_2l_1/a}} - s_{11}\right)^2}\right|_{v=v_2} \leq \frac{\varepsilon}{\Delta v} \tag{16}$$

which, in consideration of (2), reduces to

$$\left|s_{22}^2\frac{\phi'(v) + 2\frac{l_1}{a}}{s_{12}^2}\right|_{v=v_2} \leq \frac{\varepsilon}{\Delta v} \tag{17}$$

finally, recalling (9c) and (10), we obtain the following inequality

$$\left|\frac{s_{22}^2}{s_{12}^2}\right| = \left|\frac{\Gamma_e}{\frac{\Gamma_e - \Gamma_o}{2}}\right|^2 \leq \frac{\varepsilon}{\Delta v(\phi'(v) + 2l_1/a)} \quad v = v_2. \tag{18}$$

For an E-plane junction, we set now

$$\Gamma_e = |\Gamma_e|e^{j\phi_e} \tag{19a}$$

$$\Gamma_o = e^{j\phi_o}. \tag{19b}$$

For a H-plane one we set instead $\Gamma_e = e^{j\phi_e}, \Gamma_o = e^{j\phi_o}|\Gamma_o|$ and proceed along similar lines.

By defining $\Delta\phi = \phi_e - \phi_o$ and by substituting expressions (19) into (10), we obtain

$$\cos\Delta\phi = \frac{3|\Gamma_e|^2 - 1}{2|\Gamma_e|}. \tag{20}$$

The latter equation permits us to solve (18) with respect to the normalized bandwidth $2\Delta v$

$$2\Delta v \leq \frac{1 - |\Gamma_e|^2}{|\Gamma_e|^2}\frac{\varepsilon}{\phi'(v_2) + 2l_1/a}. \tag{21}$$

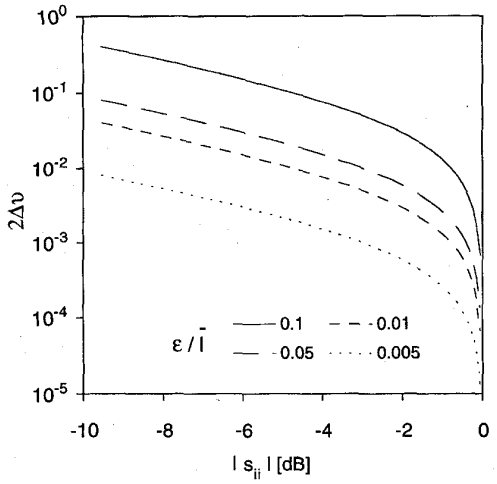

Fig. 4. Normalized bandwidth Δv versus the reflection coefficient at the common port of the three-port junction.

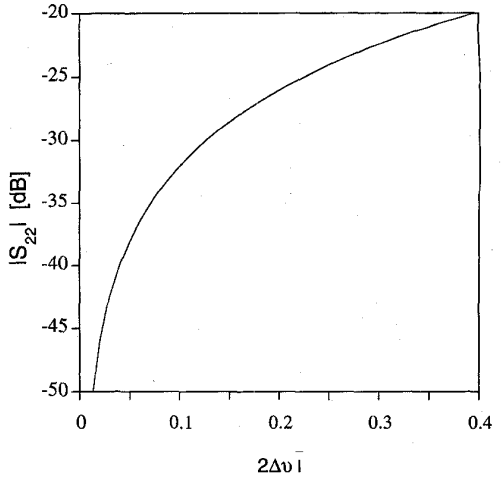

Fig. 5. Reflection coefficient at port 2 of the best junction possible ($|\Gamma_e| = 1/3$) when port 1 is closed on $F1$ (Fig. 2) versus $2\Delta v\bar{l}$.

Now, by introducing the effective normalized distance $\bar{l} = \phi'(v_2)/2 + l_1/a$ and remembering (9c), the theorem is proved. □

Inequality (21) gives the maximum normalized bandwidth, centered at f_2, of the two-port junction obtained by closing port 1 by filter $F1$ (Fig. 2), versus the reflection coefficient of the junction, as illustrated in Fig. 4. The ratio between ε, the maximum reflection coefficient admissible of the two-port so obtained, and the length $\bar{l}$, is taken as a parameter.

As we will see in detail in the Section III, the phase differential $\phi'(v_2)$ of the reflection of the load filter $F1$ plays a very important role in determining the maximum diplexer bandwidth; this variation being strongest near the passband for typical minimum phase filters, it is much more difficult to realize contiguous diplexers than noncontiguous ones.

The best situation occurs when $|\Gamma_e| = 1/3$. In that case, inequality (21) becomes

$$2\Delta v \leq \frac{4\varepsilon}{\bar{l}}. \tag{22}$$

On the contrary, it is noted that Δv tends to 0 as $|\Gamma_e|$ tends to 1.

The magnitude of the reflection for the two-port just described as a function of the bandwidth $2\Delta v\bar{l}$, as derived from (22), is shown in Fig. 5.

It is also interesting to note that in the most favorable case, the scattering matrix of the three-port junction assumes the following expression

$$\frac{1}{3}\begin{bmatrix} e^{j\phi} & -2e^{j\phi} & 2e^{j\xi} \\ -2e^{j\phi} & e^{j\phi} & 2e^{j\xi} \\ 2e^{j\xi} & 2e^{j\xi} & e^{j(2\xi-\phi)} \end{bmatrix}$$

ϕ, ξ being two constant phases. Finally note that the latter is the scattering matrix of an ideal Y-junction, which, therefore, seems to be the best choice with a view to designing diplexers with the criteria illustrated.

In conclusion, returning to the general case, the necessary conditions on the parameters of an optimum three-port symmetrical junction in order to obtain optimum perfomance when the junction is used in combination with two given filters in a diplexer configuration can be summarized by the following formulas

$$|s_{11}| = |s_{22}| \cong |s_{33}| \quad f = f_1,\ f = f_2 \tag{23a}$$

$$|s_{33}| \geq 1/3, \quad \text{preferably} \quad |s_{33}| = 1/3 \tag{23b}$$

$$s'_{11} \cong s'_{12} \cong s'_{22} \cong 0 \quad f = f_1,\ f = f_2. \tag{23c}$$

The maximum achievable bandwidth of the diplexer is then stated by (21), and, moreover, having selected a junction with the above characteristics, the two filters have to be positioned as indicated by (6).

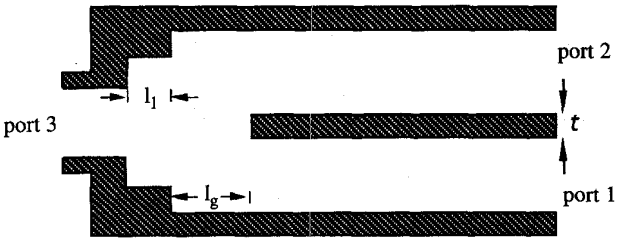

Fig. 6. E-plane section of the three-port junction employed in [1, 2].

III. Examples

In the following, we will demonstrate the validity of the foregoing criteria by means of two examples. The first one concerns a diplexer configuration designed, built and tested in [2], employing a symmetrical junction whose E-plane section is shown in Fig. 6.

This example was recomputed by making explicit use of the condition (5) within a simple optimization routine for the junction: The dimension we obtained are virtually identical to those reported in [2], as shown in Table I.

The results of the diplexer simulations are also virtually identical to those of Fig. 8 of [2]. Fig. 7 shows a comparison of the reflection magnitudes at ports 3 and 1 of the junction

TABLE I
COMPARISON BETWEEN DISTANCES CALCULATED IN [2] WITH THOSE CALCULATED BY OURSELVES BY OPTIMIZATION OF THE JUNCTION AND FORMULA (5)

distances	[2] (mm)	present method (mm)
l_1	2.434	2.430
l_g	12.977	12.975
c_1	9.074	9.066
c_2	8.285	8.280

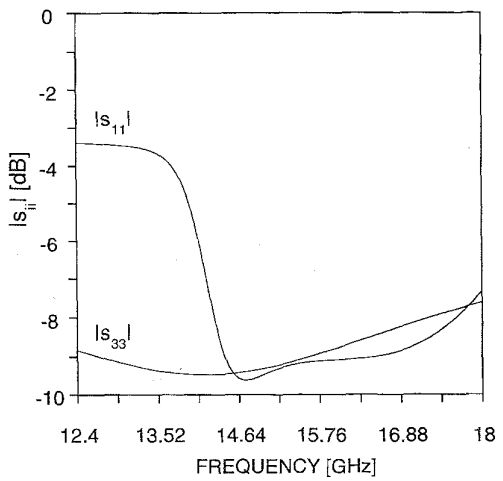

Fig. 7. Magnitudes of the reflection coefficients of the junction used in [2] at ports 1 and 3.

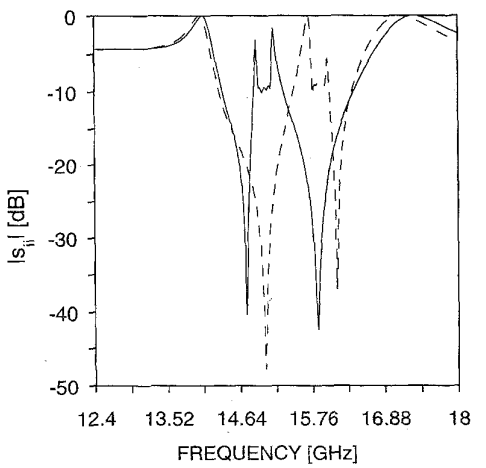

Fig. 8. Magnitude of the reflection coefficients for the junction of [2] at the common port 3 when port 1 is loaded by $F1$ (continuous) and port 2 is loaded by $F2$ (dashed).

without the filters; as it can be inferred, these values are very close to each other over the band of operation of the diplexer, as required by conditions (7), and they also satisfy

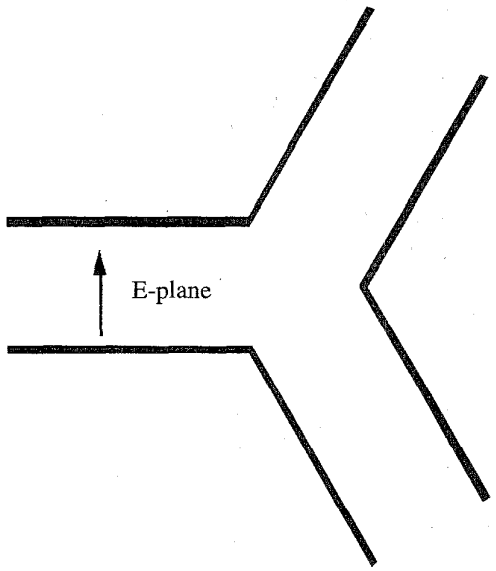

Fig. 9. E-plane section of the Y-junction.

conditions (23). Moreover, by application of (5a)–(5b), we recover exactly the same filter locations as were determined through numerical optimization by the authors of [2].

With reference to the same example, Fig. 8 compares reflection magnitudes appearing at port 3 when port 1 is loaded by $F1$ and port 2 matched (continuous) and when port 1 is matched and port 2 loaded by $F2$ (dashed). In the first case (continuous line) it is apparent a low-reflection window, centred in the midband frequency of the filter $F2$. Conversely, in the second case (dashed line), there is an analogous one about the passband of the filter $F1$. If the bandwidths of each filter exceed the widths of the windows (say at $-25 \div 30$ dB, depending on the diplexer specifications), a deterioration will occur. In that case, it is necessary either to redesign the junction or to optimize the filters.

The second example consists of a simulation; we designed different Ka-band diplexers employing the same E-plane waveguide Y-junction (Fig. 9) modeled by the equivalent circuit of [11] and using given filters. The examples refer to wideband filters, this case being considerably more complicated than the narrow-band one [6].

We checked the method by considering first contiguous filters, then by increasing the separation between the bands of the two filters.

We start by evaluating the maximum bandwidth for which the two-port junction of Fig. 2 has a return loss larger than 26 dB, by considering the phase differentials of the filters to be negligible out of band. By substituting the magnitude of the reflection coefficient of the Y-junction, about 0.35, in (21) we obtain

$$2\Delta\upsilon \leq \frac{1-(0.35)^2}{(0.35)^2}\frac{0.05a}{2l}.$$

Supposing that $l \approx 4$ mm ($\approx \lambda_g/2$), we obtain $2\Delta\beta \leq 44.75$, corresponding to a bandwidth BW ≤ 1.79 GHz.

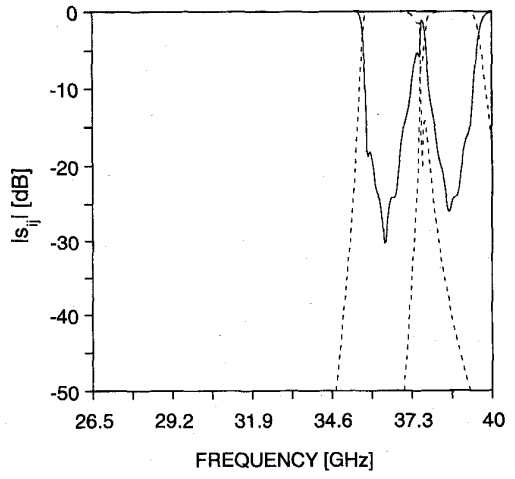

(a)

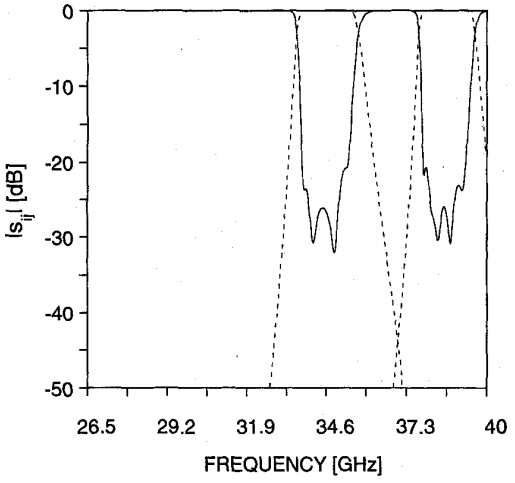

(b)

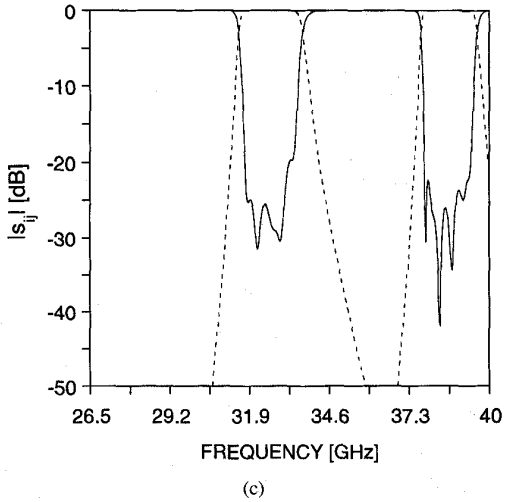

(c)

Fig. 10. Magnitude of the scattering parameters of the three simulated diplexers employing a Y-junction. Continuous lines: $|s_{33}|$, dashed lines: $|s_{13}|$ and $|s_{23}|$. (a) Filters $F1$ and $F2$, (b) filters $F1$ and $F3$, and (c) filters $F1$ and $F4$.

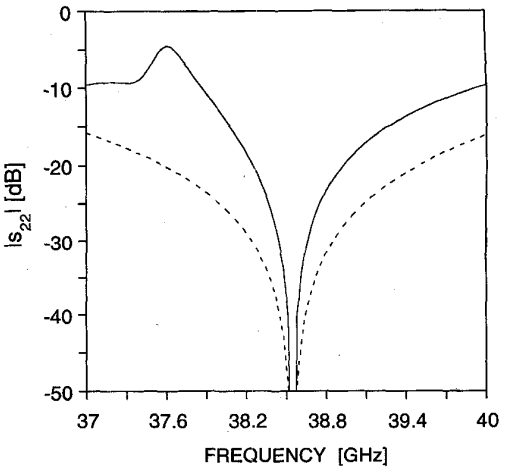

Fig. 11. Magnitude of the reflection coefficient at port 2 of the$Y$-junction when port 1 is closed on $F2$ (continuous) and $F4$ (dashed) respectively.

Having separately designed four E-plane septate 6 poles Tchebysheff filters $F1, \ldots, F4$ of 26 dB mrl and bandwidth 1.55 GHz, centered respectively at $f_1 = 38.5$ GHz, $f_2 = 36.5$ GHz, $f_3 = 34.5$ GHz, $f_4 = 32.5$ GHz, we combined filters and junction so as to obtain the three diplexers whose responses are shown in Fig. 10.

Note that we fixed the upper band filter and changed the lower one. In the first case (filters $F1$ and $F2$), the two filters are very close: There is an evident deterioration of the diplexer response compared with those of the filters that is due mainly to the excessive variation of the phase of one filter in the passband of the other. By measuring the slope of the phase of filter $F1$ at the frequencies f_2 and f_4, it is possible to give a more accurate estimate of the maximum bandwidth of the diplexer. In particular, in a neighborhood of f_2 and of f_4 we have, respectively, $\phi'(v(f_2)) \approx 3$ and $\phi'(v(f_4)) \approx 0.38$. corresponding to 480 MHz and 1.3 GHz bandwidths.

In the next example, we space further out the filter bandwidths. Figs. 10(b) and (c) refer to the diplexer obtained by connecting filters $F1$ and $F3$, $F1$ and $F4$, respectively, to the Y-junction: in both cases the solution is quite good and no further optimization is required.

Finally, we show the magnitudes of the reflection at port 2, when port 1 is loaded by $F2$ and $F4$, respectively, in a neighborhood of the midband frequency of $F1$ (Fig. 11): it is clear from the figure that the matching bandwidth depends on the phase behavior of the filter. We can also see that the bandwidth of the junction corresponding to a return loss of 26 dB is about 1.1 GHz when port 1 is loaded by $F4$ and just 330 MHz when port 1 is closed on $F2$, close enough to the value calculated above.

IV. Conclusion

We present simple analytical criteria for the design of optimum junctions for the realization of diplexers with given filters: these are of general validity, deriving solely from the properties of the scattering matrix of reciprocal, lossless symmetric three-port junctions.

The above criteria also provide explicitly two additional important parameters of the diplexer geometry, namely, the locations of the filters, resulting in a considerable simplification of the overall synthesis.

Results obtained by the application of the foregoing method to the synthesis are good except for the case in which the phase slope of one filter in the passband of the other is too large. Even in this unfavorable case the result can nonetheless be considered as a excellent starting point for an optimization routine.

ACKNOWLEDGMENT

The authors would like to thank Brambilla, Cereda, and Bianconi of Alcatel-Telettra, Vimercate Italy, for helpful discussions.

REFERENCES

[1] J. Dittloff and F. Arndt, "Rigourous design of septate multiplexers with printed circuit elements," in *IEEE MTT-S Dig.*, 1988, pp. 431–434.
[2] ——, "Rigourous field theory design of millimeter-wave *E*-plane integrated circuit multiplexers," *IEEE Trans. Microwave Theory Tech.*, vol. 37, no. 2, pp. 340–350, Feb. 1989.
[3] R. Valdhieck and B. Varailhon de la Filiolie, "Computer-aided design of parallel-connected millimeter-wave diplexers: Multiplexers," in *IEEE MTT-S Dig.*, 1988, pp. 435–438.
[4] H. Yao, A. Abdelmonem, J. Liang, X. Liang, K. Zaki, and A. Martin, "Wide-band waveguide and ridge waveguide *T*-junction for diplexer applications," *IEEE Trans. Microwave Theory Tech.*, vol. 41, no. 12, pp. 2166–2173, Dec. 1993.
[5] J. D. Rhodes, "Direct design of symmetrical interacting bandpass channel diplexer," *Inst. Elec. Eng. J. Microwaves, Optics and Acoustics*, vol. 1, no. 1, pp. 34–40, Sept. 1976.
[6] J. D. Rhodes and R. Levy, "A generalized multiplexer theory," *IEEE Trans. Microwave Theory Tech.*, vol. MTT-27, no. 2, pp. 99–111, Feb. 1979.
[7] ——, "Design of general manifold multiplexer," *IEEE Trans. Microwave Theory Tech.*, vol. MTT-27, no. 2, pp. 111–123, Feb. 1979.
[8] J. Uher, J. Bornemann, and U. Rosemberg, *Waveguide Components for Antenna Feed Systems: Theory and CAD.* Norwood, MA: Artech, 1993.
[9] A. Morini and T. Rozzi, "Design of 'optimum' three-port symmetrical junctions for diplexer application," *IEEE MTT-S Dig.*, 1994, pp. 739–742.
[10] ——, "Analysis of compact *E*-plane diplexers in rectangular waveguide," *IEEE Trans. Microwave Theory Tech.*, vol. 43, pp. 1834–1839, Aug. 1995.
[11] N. Marcuvitz, *Waveguide Handbook.* New York: McGraw-Hill, 1951.

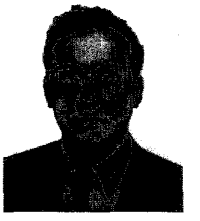

Antonio Morini (M'94) was born in Italy, in 1962. He received the degree in electronic engineering (summa cum laude) from the University of Ancona, Italy, in 1987 and the Ph.D. degree in electromagnetism in 1992.

Since 1992 he has been with the Department of Electronics and Automatics at the University of Ancona as an Assistant Professor. His research is in the modeling and to the synthesis of passive millimetric components, such as filters, multiplexers, and antennas.

Tullio Rozzi (M'66–SM'74–F'90) received the degree of Dottore in physics from the University of Pisa, Italy, in 1965, and the Ph.D. degree in electronic engineering from Leeds University, UK, in 1968. In June 1987 he received the D.Sc. degree from the University of Bath, Bath, U.K.

From 1968 to 1978 he was a Research Scientist at the Philips Research Laboratories, Eindhoven, The Netherlands, having spent one year, 1975, at the Antenna Laboratory, University of Illinois, Urbana. In 1978 he was appointed to the Chair of Electrical Engineering at the University of Liverpool and was subsequently appointed to the Chair of Electronics and Head of the Electronics Group at the University of Bath, in 1981, where he also held the responsibility of Head of the School of Electrical Engineering on an alternate three year basis. Since 1988 he has been Professor of Antennas in the Department of Electronics and Control, University of Ancona, Italy, while remaining a Visiting Professor at Bath University.

In 1975 Dr. Rozzi was awarded the Microwave Prize by the IEEE Microwave Theory and Technique Society. He is also a Fellow of the IEE (U.K.) as well as IEE Council Representative for Italy.

Analysis of Compact E-Plane Diplexers in Rectangular Waveguide

Antonio Morini, *Member, IEEE*, and Tullio Rozzi, *Fellow, IEEE*

***Abstract*—Photolithographic techniques permit the realization of complex circuits totally confined to the E-plane of millimetric rectangular guides with high precision and low cost. This work contains a detailed analysis of an E-plane diplexer configuration recently introduced. Its main feature is the matching section of the three port junction, a simple abrupt E-plane one tuned by means of an inductive post realized on the same mask as the branching filters. On the basis of this analysis, we also demonstrate the application of a recently developed diplexer synthesis technique. Many prototypes, in K_a-band were designed and tested, showing good performances and good agreement between theory and experiment.**

I. Introduction

IN REALIZING millimetric diplexers, it is increasingly expedient both technically and economically to employ reciprocal circuits instead of the traditional microwave circulators [1]–[5]. This is why we recently proposed an E-plane diplexer configuration [6] that is based on the abrupt three-port junction, in lieu of a tapered junction [2]–[4] requiring more expensive mechanical construction. The junction is tuned by means of a single inductive post built on the same mask as the E-plane filters, and placed between the junction and the bifurcation, as shown in Fig. 1. The resulting diplexer consists of just three parts: a single mask containing filters and tuning post and the two halves of the housing wherefrom junction and guides are made. The diplexer is assembled by sandwiching the mask [Fig. 2(b)] between the two halves of the housing [Fig. 2(a)]. Modeling the junction, inclusive of the post, involves a rigorous treatment of the interaction between adjacent discontinuities by the concept of accessible modes [7].

As contrasted to [7], modes of both TE and TM polarization occur depending on two indices with corresponding additional complexity of the analysis.

We now provide a full analytical model for this kind of configuration, that can be coded for running on a PC without recourse to field analysis.

We also demonstrate the utilization of this analysis to the synthesis of various K_a-band prototypes that were actually built and tested, showing good performances and good agreement with predictions.

For the sake of readability of the main text, details of the calculations are reported in Appendix.

Manuscript received June 20, 1994; revised April 24, 1995.

The authors are with the Dipartimento di Elettronica ed Automatica Università di Ancona, 60100 Ancona, Italy.

IEEE Log Number 9412689.

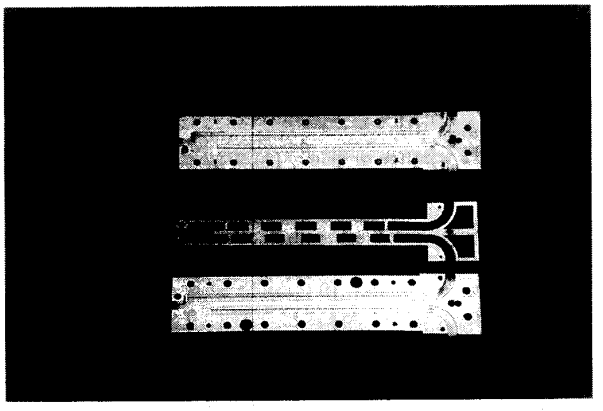

Fig. 1. Compact E-plane diplexer.

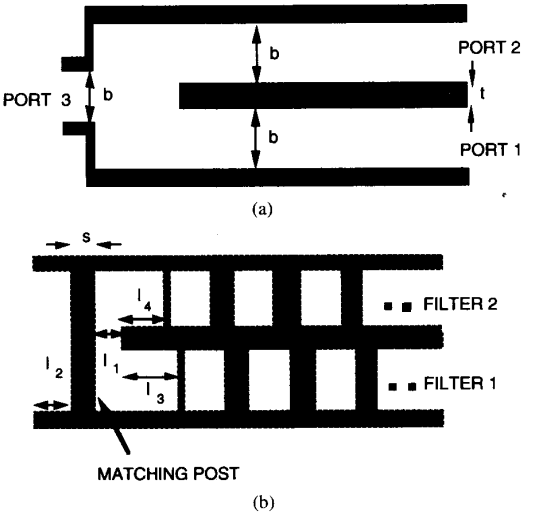

Fig. 2. (a) E-plane section of the three-port junction. (b) Mask containing filters and matching posts.

II. Diplexer Analysis

We shall now focus on the analysis of the junction, whereas reference is made to [7] for that of the filters. Symmetry of the three-port junction about its longitudinal mid-plane [Fig. 2(a)] implies $s_{11} = s_{22}$ e $s_{13} = s_{23}$, so that its scattering matrix becomes

$$\begin{bmatrix} b_1 \\ b_2 \\ b_3 \end{bmatrix} = \begin{bmatrix} s_{11} & s_{12} & s_{13} \\ s_{12} & s_{11} & s_{13} \\ s_{13} & s_{13} & s_{33} \end{bmatrix} \begin{bmatrix} a_1 \\ a_2 \\ a_3 \end{bmatrix}. \quad (1)$$

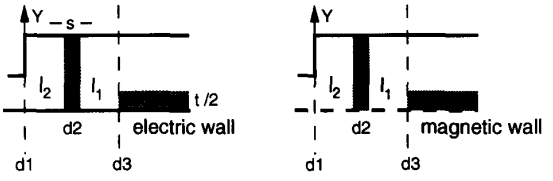

Fig. 3. Even/odd excitation at ports 1 and 2: Resulting structures.

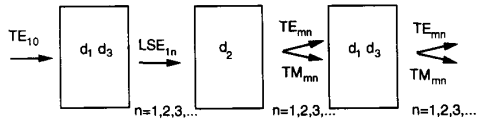

Fig. 4. Scheme of the modal interactions occurring between discontinuities.

By setting separately $a_1 = a_2 = 1$ $a_3 = 0$ and $a_1 = -a_2 = 1$ $a_3 = 0$, corresponding to the even and odd excitation, respectively, at ports 1 and 2, it is possible to characterize the junction. By substituting those values in (1), we obtain, in the even case

$$b_1^e = s_{11} + s_{12} \tag{2a}$$

$$b_3^e = 2s_{13} \tag{2b}$$

and, in the odd case

$$b_1^o = s_{11} - s_{12}. \tag{2c}$$

The parameter s_{33} is recovered by the losslessness condition

$$s_{13}s_{11}^* + s_{13}s_{12}^* + s_{33}s_{13}^* = 0 \tag{2d}$$

which gives

$$s_{33} = -\frac{s_{13}s_{11}^* + s_{13}s_{12}^*}{s_{13}^*}. \tag{2e}$$

Note also that this latter condition implies $|s_{33}| = |b_1^e|$.

By applying even and odd excitations, the three-port junction reduces to the two two-port situations shown in Fig. 3; both comprise the cascade of three discontinuities $d1$, $d2$, and $d3$ separated by short sections of guide and, as such, interacting. These discontinuities are analyzed individually as $2N$-port, N being the number of ' accessible modes ' chosen according to the following considerations.

Owing to their uniformity with respect to x, discontinuities 1 and 3, that is the two E-plane steps, under the excitation of an incident TE_{10}-mode excite in turn just LSE_{1n}-modes with $n = 1, 2, 3 \cdots$.

On the other hand, due to its uniformity with respect to y, discontinuity 2, i.e., the metal septum, when excited by LSE_{1n}-modes excites in turn the TE_{mn} and TM_{mn} families with $m = 1, 3, 5 \cdots$. Finally, the latter impinging on discontinuities 1 and 3 excite TE_{mn} and TM_{mn} modes with $n = 1, 2, 3 \cdots$.

This complex mechanism is summarized in Fig. 4.

For this reason, we preferred to work with the TE and TM families, rather than LSE, LSM for both types of discontinuities. Modes with attenuation larger than 20 dB between successive discontinuities were considered "localized." In order to understand what this assumption implies, consider that for $b \leq \frac{3}{2}a$, the attenuation of the first mode below-cutoff that is being excited, i.e., TE_{13}, is greater than 40 dB/λ_g. In this case, it is sufficient to consider TE_{10}, TE_{11}, TM_{11}, TE_{12}, and TM_{12} as accessible modes obtaining accurate results for discontinuities spaced at least $\lambda_g/2$.

Moreover, it has to be noted that the present approach avoids any numerical instability of the kind discussed in [8]. In fact, the interaction between cascaded discontinuities is accounted for just by those modes that are actually significant and numerical instability due to the weak interactions by higher order modes is thereby avoided.

In practice, once the diplexer is designed on the basis of the five modes model, we have to check its dimensions in order to verify the consistency of the model itself.

If the result is negative, for instance the attenuation of the lowest "localized" mode [9] is less than 20 dB at the upperband edge, we include that mode among the accessible ones.

Each of the six discontinuities occurring is analyzed by deriving a rigorous variational expression of its multiport impedance matrix of the type

$$\begin{bmatrix} \mathbf{V}_{e/o}^l \\ \mathbf{V}_{e/o}^r \end{bmatrix} = \begin{bmatrix} \mathbf{z}_{e/o}^{ll} & \mathbf{z}_{e/o}^{lr} \\ \mathbf{z}_{e/o}^{rl} & \mathbf{z}_{e/o}^{ll} \end{bmatrix}^{(k)} \begin{bmatrix} \mathbf{I}_{e/o}^l \\ \mathbf{I}_{e/o}^r \end{bmatrix} = \mathbf{Z}_k^{e/o} \begin{bmatrix} \mathbf{I}_{e/o}^l \\ \mathbf{I}_{e/o}^r \end{bmatrix} \qquad k = 1, 2, 3 \tag{3}$$

where, $\mathbf{V}$, $\mathbf{I}$ are the amplitude vectors of the transverse components of the E and H-field of the accessible modes, calculated to the left (apex l) and to the right (apex r) of the discontinuity considered. Suffixes e/o stand for even/odd case, respectively.

In the even case, considering TE_{10}, TE_{12}, and TM_{12} as accessible, we get

$$\mathbf{V}_e^s = \begin{bmatrix} V_{e1}^s \\ V_{e2}^s \\ V_{e3}^s \end{bmatrix}, \quad \mathbf{I}_e^s = \begin{bmatrix} I_{e1}^s \\ I_{e2}^s \\ I_{e3}^s \end{bmatrix}, \quad \mathbf{z}_e^{sp} = \begin{bmatrix} z_{e11}^{sp} & z_{e12}^{sp} & z_{e13}^{sp} \\ z_{e21}^{sp} & z_{e22}^{sp} & z_{e23}^{sp} \\ z_{e31}^{sp} & z_{e32}^{sp} & z_{e33}^{sp} \end{bmatrix} \tag{3a}$$

where the indices s, p assume the values l, r.

In the odd case, we take TE_{11}, TM_{11} as accessible, so that each junction reduces to a two-port of the type

$$\mathbf{V}_o^s = \begin{bmatrix} V_{o1}^s \\ V_{o2}^s \end{bmatrix}, \quad \mathbf{I}_o^s = \begin{bmatrix} I_{o1}^s \\ I_{o2}^s \end{bmatrix}, \quad \mathbf{z}_o^{sp} = \begin{bmatrix} z_{o11}^{sp} & z_{o12}^{sp} \\ z_{o21}^{sp} & z_{o22}^{sp} \end{bmatrix}. \tag{3b}$$

Moreover, omitting the suffix e/o, we have in both cases

$$[\mathbf{z}^{sp}]_{ij} = \mathbf{A}_i^{(s)} \cdot \mathbf{Y}^{-1} \cdot \mathbf{A}_j^{(p)} \qquad i, j = 1, 2, 3 \text{ even case } 1, 2 \text{ odd case.} \tag{4}$$

$\mathbf{A}_i^{(l)}$ and $\mathbf{A}_i^{(r)}$ contain the coefficients of the expanding functions used for representing the tangential electric field

of the ith accessible mode at the interface to the left and to the right, respectively, $\mathbf{Y}$ is the discretized Green dyadic admittance.

The latter is obtained by imposing the continuity of the tangential components of the em field at the interface, by following method 3 illustrated in Collin [10], and discretizing the operator so derived by the Ritz–Galerkin method.

The stationarity properties of the impedances $[\mathbf{z}^{sp}]_{ij}$ so obtained are discussed in the same book.

An outline derivation of their expressions and a discussion of the effectiveness of the discretization technique are detailed in the following and in the result section. Here we note just that we use as basis functions for the representation of the tangential electric field at each interface a set of orthonormal polynomials weighted by the correct edge condition. This choice was discussed many times in the past [11]. The main differences with respect to the classical mode expansion can be summarized in the following:

On the one hand, it requires fewer expanding functions to achieve the correct solution and consequently the dimensions of the matrix $\mathbf{Y}$ are smaller; moreover it does not suffer from relative convergence [11]. On the other hand, the computation of the Fourier coefficients and the manipulation of the mode series require more analytical manipulation.

With regard to accuracy obtainable, if the number of expanding functions is adequate in both cases, there are no significant differences between these two choices.

Having computed $\mathbf{Z}_k^e$ and $\mathbf{Z}_k^o$ ($k = 1, 2, 3$) corresponding to the three sub-cases, the behavior of the whole junction is determined by cascading the corresponding transmission matrices $\mathbf{T}_k^e$ and $\mathbf{T}_k^o$.

In fact, denoting by $\mathbf{U}^e(l)$ and $\mathbf{U}^o(l)$ the standard transmission matrices of a waveguide section of length l, for the even/odd excitations, respectively, the global transmission matrix becomes, in the even case

$$\mathbf{T}_E = \mathbf{T}_1^e \cdot \mathbf{U}^e(l_1) \cdot \mathbf{T}_2^e \cdot \mathbf{U}^e(l_2) \cdot \mathbf{T}_3^e \quad : \dim 6 \times 6 \qquad (5a)$$

and, in the odd case

$$\mathbf{T}_O = \mathbf{T}_1^o \cdot \mathbf{U}^o(l_1) \cdot \mathbf{T}_2^o \cdot \mathbf{U}^o(l_2) \cdot \mathbf{T}_3^o \quad : \dim 4 \times 4. \qquad (5b)$$

When the interaction between junction and filters via modes below-cutoff is negligible, the matrices just obtained can be reduced by closing the ports corresponding to those modes on their characteristic impedances, as illustrated in Fig. 5(a) and (b) for the two excitation cases.

From the latter circuits it is easy to derive the scattering parameters (2a)–(c) and then the response of the diplexer by standard network methods.

III. Computation Effort

In order to retain short computation times the following cares need to be taken.

1) For a given geometry, all Fourier coefficients (7), obtained by the overlapping of modes and expanding functions, are computed once only and stored in an array.

2) The admittance matrix of each discontinuity is obtained in a manner conceptually analogous to [7], that is, by considering

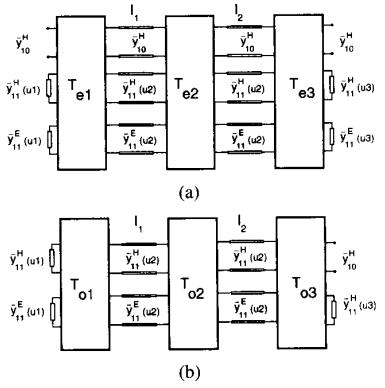

Fig. 5. (a) Equivalent circuit under even excitation at ports 1 and 2: $u1 = b/a$, $u2 = (2b + t)/a$, $u3 = b/a$. (b) Equivalent circuit under odd excitation at ports 1 and 2: $u1 = b/(2a)$, $u2 = (2b + t)/(2a)$, $u3 = b/a$.

an appropriate number of accessible modes. Nonetheless, in the present instance the computation is complicated by the different natures of discontinuities 1, 3, and 2, involving the solution of a vector problem. Their exact expressions involve series of the following form, for example, the yy block of the second discontinuity is given by

$$[y_{yy}]_{ij}^{e/o} = \sum_{m=m_l,\, m_l+2} \left[\bar{y}_{m1}^H(\bar{b}) + \bar{y}_{m1}^E(\bar{b})(\bar{b}m)^2\right] \frac{1}{1+(m\bar{b})^2} \cdot P_{i_y m}(2r) P_{j_y m}(2r) + \sum_{m=m_r,\, m_r+1} \cdot \left[\tilde{y}_{m1}^{He/o}(r)\left(\frac{\bar{b}}{r}\right)^2 + \tilde{y}_{m1}^{Ee/o}(r)\frac{1}{(mr)^2}\right] \cdot \frac{1}{1+[mr/(2\bar{b})]^2} P_{i_y 2m}(1) P_{j_y 2m}(1) \qquad (6)$$

where

$$P_{nm}(u) = \sqrt{2u}c_n \frac{J_{1/6+n}\left(\frac{m\pi}{2}u\right)}{\left(\frac{m\pi}{2}u\right)^{1/6}}. \qquad (7)$$

These functionals depend on the frequency only via the modal admittances. It is expedient, therefore, to use the exact expressions of the modal admittances just for the first few terms of the above series. Subsequent terms, say past the 10th, can be conveniently approximated. For example, for a modal TE admittance we set

$$\bar{y}_{m1}^H(u) = -j\frac{\sqrt{(m/u)^2 - \bar{\omega}^2 - 1 + 1/\bar{b}^2}}{\bar{\omega}} \cong -j\frac{\sqrt{(m/u)^2 - \bar{\omega}_0^2 - 1 + 1/\bar{b}^2}}{\bar{\omega}} \qquad (8)$$

where $\bar{\omega}_0$ is the diplexer effective frequency at midband. The modal series containing the previous approximated terms are then computed just once. The latter approximation, in conjunction with the small size of the admittance matrices arising from a prudent choice of the expanding functions, allows extremely short computation times, while maintaining the original accuracy.

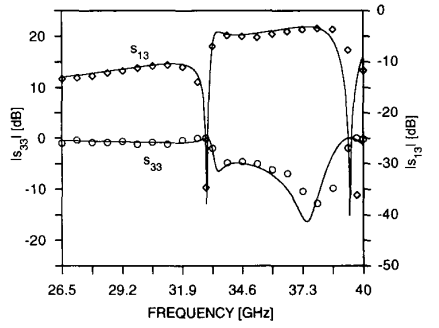

Fig. 6. Comparison between theoretical and experimental scattering parameters of a typical junction. Continuous lines are the theoretical ones, by considering as accessible 5 modes and 7 modes, respectively. Dots are the experimental points.

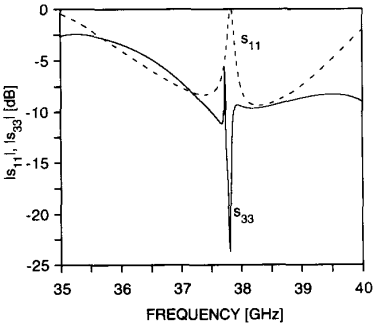

Fig. 7. Reflection magnitudes at ports 1 and 3 of the junction used in the diplexer.

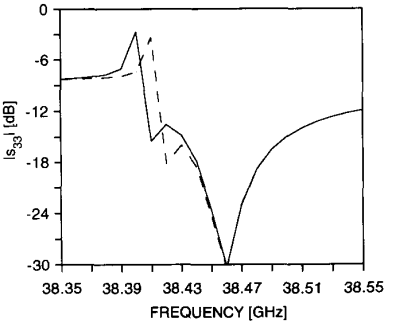

Fig. 8. Comparison between magnitudes of the reflection coefficients at port 1 computed taking account 5 (dashed) and 7 accessible modes (continuous). The junction is the same as that of Fig. 7.

In fact, computing the response of the proposed three-port (5 accessible modes) requires about 6 min on a 486–50 MHz machine, for a full frequency scan (401 points). Computation times increase significantly as more accessible modes are taken into account: for instance, 7 accessible modes require about 11 min.

IV. Results

As a test for the program, Fig. 6 compares experimental and theoretical scattering parameters for a junction of dimensions $a = 7.04$ mm, $b = 3.59$ mm, $t = 1.93$ mm, $d = 0.150$ mm, $s = 0.300$ mm, $l_1 = 1.75$ mm, $l_2 = 4.3$ mm (Fig. 2–3).

It is noted that this is a significant case in as much as the distance between inductive post and bifurcation, l_1, is less than $\lambda_g/4$ at the higher band edge ($\lambda_g = 8.1$ mm at $f = 37$ GHz), implying strong interaction of higher order modes.

The theoretical prediction of the model truncated to 5 accessible modes seems to be in very good agreement with experiment, apart from a slight deviation toward the upper band edge, just where the interaction is strongest. With a view to eliminating this deviation, we increased the number of accessible modes, by including TE_{13} and TM_{13}, but the results were the same as those of the simpler model. Therefore, we concluded that the deviation depends just on mechanical tolerances.

In order to employ the above junction for diplexer applications, its electrical parameters need to be chosen in an appropriate manner. To this end, we adopted the criteria illustrated in [12], briefly stating that over as wide as possible a band, at least over both the bands of the filters, we must have $|s_{11}| = |s_{33}| =$ constant and, preferably, $|s_{11}| \cong 1/3$.

In the case of the following prototypes, it was also required that the characteristics of the two filters were separated by a gap of 1.26 GHz.

The geometry of the junction permitted to approximately satisfy the above requirements just over the two bands of the filters, separated by a region of considerable mismatch, as shown in Fig. 7. This fact did not constitute a limitation in itself, as this region of a mismatch was narrower than the band separating the passbands of the two filters: on the contrary, the isolation between diplexer channels was enhanced. Synthesis, however, was somewhat complicated, by the resonant character of this effect.

Even in this case, we checked the model by increasing the number of accessible modes. As shown in Fig. 8, there is a slight difference just in the resonance region. This constitutes a particularly testing example as small differences between the models of each discontinuity are enhanced by the highly resonant nature of the interposed cavity. In fact, when simulating many nonresonant discontinuities, at even shorter spacings we never encountered deviations comparable with those shown above.

We designed then three diplexers in the band 37–39 GHz by using a single housing with fixed dimensions, tuning only by varying the length of the matching post and its position inside the cavity. This arrangement affords considerable savings in fabrication, as individual diplexers differ only by just an inexpensive mask.

The results obtained, as shown in Fig. 9 for the first diplexer, were satisfactory. Some slight deviations between theoretical and experimental data are due to mechanical tolerances of the filters.

Fig. 10 shows the theoretical response of the lowest of the two 5-poles 26 dB mrl filter employed in the above diplexer. By a comparison with Fig. 9, it can be noted that the diplexer response, designed according the above criteria [12], is seen as transparent by the filters without the need for costly optimization.

Results comparable to those of Fig. 9 are also obtainable from the junction of [2]–[4], but that junction is considerably more expensive than ours. Moreover, it is to be noted that, by suppressing low frequency spurious passbands, selective fre-

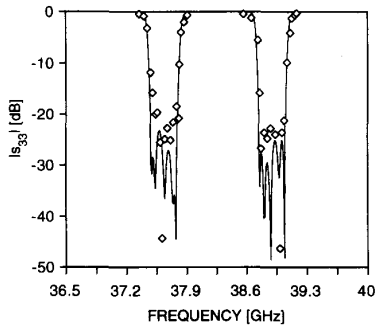

Fig. 9. Comparison between theoretical and experimental (dashed lines) scattering parameters for one of three diplexers realized on the same housing, tuned only by varying position and dimensions of the matching post. Dimensions (in mm) were as follows: Junction: $l_1 = 4.885$, $l_2 = 4.465$, $l_3 = 3.023$, $l_4 = 2.934$, $s = 0.200$, $t = 3.550$. Filters [posts (p), cavities (c)]: filter 1: $p1 = p6 = 1.730$, $c1 = c5 = 7.812$, $p2 = p5 = 5.549$, $c2 = c4 = 7.781$, $p3 = p4 = 6.376$, $c3 = 7.780$; filter 2: $p1 = p6 = 2.026$, $c1 = c5 = 7.301$, $p2 = p5 = 6.422$, $c2 = c4 = 7.259$, $p3 = p4 = 7.360$, $c3 = 7.258$, the thickness of the metallic sheet containing septa is 0.150.

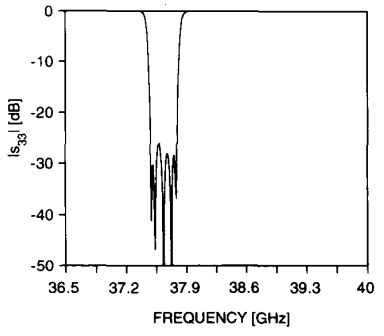

Fig. 10. Theoretical reflection magnitudes of filter 1 employed in the above diplexer.

quency characteristics of the junction allow filters with longer cavities (λ_g, $3/2\lambda_g$) to be employed, which substantially reduce ohmic losses.

Consequently, the arrangement discussed in this work seems to be convenient when the channels are not wide. On the contrary, when specifications require bandwidths wider than 5%, junctions like those of [2]–[4] appear more appropriate.

V. Conclusion

We developed a rigorous analysis for the characterization of a recently proposed "E-plane" diplexer junction of compact and inexpensive fabrication, providing a solution that seems to be expedient when bandwidths are less than 5%.

Different prototypes were built and tested showing good performance, in good agreement with the theoretical predictions.

Appendix
Field Analysis of the Discontinuities

In discretizing the variational expression of the impedances for the three discontinuities under study, we chose polynomials orthonormal over the appropriate intervals as expanding functions. The weight functions take into account the inverse cubic root singularity of the normal electric field in proximity of the 90°-metal corners. By means of integration by parts, the nonsingular component of the electric field was also transformed into a singular function satisfying the same boundary and edge conditions as the normal E-field [11]. In all cases, complete convergence was obtained with just three expanding functions for each field component.

With reference to the coordinate system of Fig. 2, the following expansions were employed.

For discontinuities of the type 1 and 3

$$\frac{b\varepsilon_o}{2\pi}\frac{dE_x}{dy}(x,y) = 2\sqrt{\frac{1}{ab\varepsilon_o}}\cos\frac{\pi}{a}x\sum_{k=1,2}^{3}X_k^{(i)}W \cdot [\eta^{(i)}(y)]f_{\mu(k)}[\eta^{(i)}(y)] \tag{A1a}$$

$$E_y(x,y) = 2\sqrt{\frac{\varepsilon_o}{ab}}\sin\frac{\pi}{a}x\sum_{k=1,2}^{3}Y_k^{(i)}W[\eta^{(i)}(y)] \cdot f_{\nu(k)}[\eta^{(i)}(y)] \tag{A1b}$$

discontinuity 1, even case

$$\mu(k) = 2k,$$
$$\nu(k) = 2(k-1),$$
$$\varepsilon_o = 1,$$
$$\eta^{(1)}(y) = \frac{2y}{b}$$

discontinuity 1, odd case

$$\mu(k) = 2k-1,$$
$$\nu(k) = 2k-1,$$
$$\varepsilon_o = 1$$

discontinuity 3, even case

$$\mu(k) = 2k,$$
$$\nu(k) = 2(k-1),$$
$$\varepsilon_o = 2,$$
$$\eta^{(3)}(y) = \frac{b+t/2-y}{b}$$

discontinuity 3, odd case

$$\mu(k) = 2k,$$
$$\nu(k) = 2(k-1),.$$
$$\varepsilon_o = 2$$

For discontinuities of the type 2

$$E_x(x,y) = \frac{2}{\sqrt{b}}\sqrt{\frac{2}{a-d}}S_x^{e/o}(y)\sum_{k=1,2}^{3}X_k^{(2)} \cdot W\left[\frac{2x}{a-d}\right]f_{\mu(k)}\left[\frac{2x}{a-d}\right] \tag{A2a}$$

$$\frac{dE_y}{dx}(x,y) = \frac{1}{\sqrt{b}}\sqrt{\frac{2}{a-d}}S_{y1}^{e/o}(y)\sum_{k=1,2}^{3}Y_k^{(o)} \cdot W\left[\frac{2x}{a-d}\right]f_{\mu(k)}\left[\frac{2x}{a-d}\right] \tag{3b}$$

$$+\frac{2}{\sqrt{b}}\sqrt{\frac{2}{a-d}}\,S_{y2}^{e/o}(y)\sum_{k=1,2}^{3}Y_k^{(2)}\cdot W\left[\frac{2x}{a-d}\right]f_{\mu(k)}\left[\frac{2x}{a-d}\right] \quad \text{(A2b)}$$

where d is the post thickness, $\mu(k)=2k$; discontinuity 2, even case

$$S_x^e(y)=\sin\frac{\pi}{b+\frac{t}{2}}y,$$
$$S_{y1}^e(y)=1,$$
$$S_{y2}^e(y)=\cos\frac{\pi}{b+\frac{t}{2}}y \quad \text{(A3a)}$$

discontinuity 2, odd case

$$S_x^o(y)=\cos\frac{\pi}{2\left(b+\frac{t}{2}\right)}y,$$
$$S_{y1}^o(y)=0,$$
$$S_{y2}^o(y)=\sin\frac{\pi}{2\left(b+\frac{t}{2}\right)}y \quad \text{(A3b)}$$

$$N_x=N_y=3$$
$$f_k(t)=\frac{1}{N_k}G_k^{1/6}(t) \quad \text{(A4a)}$$
$$W(t)=(1-t^2)^{-1/3}. \quad \text{(A4b)}$$

Where $G_k^{1/6}(t)$ is the kth Gegenbauer polynomial of order 1/6 and the constant N_k was chosen as to satisfy the following orthonormality conditions [13]

$$\int_0^1 dt\,W(t)G_n^{1/6}(t)G_m^{1/6}(t)=N_m^2\delta_{nm} \quad \text{(A4c)}$$

$$N_m=\frac{2^{-1/6}}{\Gamma\left(\frac{1}{6}\right)}\left[\frac{\pi\Gamma\left(\frac{1}{3}+m\right)}{\left(\frac{1}{6}+m\right)m!}\right]^{1/2} \quad \text{(A4d)}$$

ACKNOWLEDGMENT

The authors are indebted to Dr. Gulloch, Dr. Politi, Mr. Brambilla, Mr. Cereda, and Dr. Bianconi of Alcatel-Telettra, Vimercate Italy, for providing experiments and for helpful discussions.

REFERENCES

[1] Y. Shih, L. Q. Bui, and T. Itoh, "Millimeter-wave diplexers with printed circuit elements," *IEEE Trans. Microwave Theory Tech.*, vol. MTT-33, no. 12, pp. 1465–1469, Dec. 1985.

[2] J. Dittloff and F. Arndt, "Rigorous design of septate multiplexers with printed circuit elements," in *IEEE MTT-S Dig.*, 1988, pp. 431–434.

[3] ——, "Rigorous field theory design of millimeter-wave *E*-plane integrated circuit multiplexers," *IEEE Trans. Microwave Theory Tech.*, vol. MTT-37, no. 2, pp. 340–350, Feb. 1989.

[4] R. Vahldieck and B. Varailhon de la Filolie, "Computer aided design of parallel-connected millimeter-wave diplexers/multiplexers," in *IEEE MTT-S Dig.*, 1988, pp. 435–438.

[5] H. Yao, A. Abdelmonem, J. Liang, X. Liang, K. Zaki, and A. Martin, "Wide-band waveguide and ridge waveguide T-junction for diplexer applications," *IEEE Trans. Microwave Theory Tech.*, vol. 41, no. 12, pp. 2166–2173, Dec. 1993.

[6] A. Morini, T. Rozzi, D. De Angelis, and W. Gulloch, "A novel matched diplexer configuration in *E*-plane technology," *IEEE MTT-S Dig.*, 1993, pp. 1077–1080.

[7] T. Rozzi, F. Moglie, A. Morini, W. Gulloch, and M. Politi, "Accurate full-band equivalent circuits of inductive posts in rectangular waveguide," *IEEE Trans. Microwave Theory Tech.*, vol. 40, no. 5, May 1992.

[8] R. R. Mansour and R. Macphie, "An improved transmission matrix formulation of cascaded discontinuities and its application to *E*-plane circuit," *IEEE Trans. Microwave Theory Tech.*, vol. MTT-34, no. 12, Dec. 1986.

[9] T. Rozzi, "Network analysis of strongly coupled transverse apertures in wave-guides," *Int. J. Circuit Theory Applicat.*, vol. 1, pp. 161–178, June 1973.

[10] R. E. Collin, *Field Theory of Guided Waves*, 2nd ed. Piscataway, NJ: IEEE Press, 1990.

[11] F. Alessandri, M. Mongiardo, T. Rozzi, G. Schiavon, and R. Sorrentino, "Alcuni nuovi aspetti sulla convergenza delle tecniche di raccordo modale in strutture guidanti a microonde," in *Proc. VIII RINEM*, 1990, pp. 143–146.

[12] A. Morini and T. Rozzi, "Design of 'optimum' three port symmetrical junctions for diplexer application," in *IEEE MTT-S Dig.*, 1994, pp. 739–742.

[13] S. Gradshtein and I. M. Rhyzik, *Table of Integrals Series and Products*. New York: Academic, 1965.

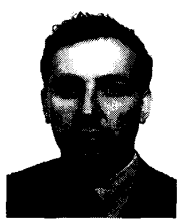

Antonio Morini (M'94) was born in Italy in 1962. He received the degree in electronic engineering (summa cum laude) from the University of Ancona in 1987 and the Ph.D. degree in electromagnetism in 1992.

Since 1992, he has been with the Department of Electronics and Automatics at the University of Ancona as an Assistant Professor. His current research interests are modeling and synthesis of passive millimetric components, such as filters, multiplexers, and antennas.

Tullio Rozzi (M'66–SM–74–F'90) received the dottore degree in physics from the University of Pisa in 1965, and the Ph.D. degree in electronic engineering from Leeds University in 1968. In June 1987, he received the D.Sc. degree from the University of Bath, Bath, UK.

From 1968–1978, he was a Research Scientist at the Philips Research Laboratories, Eindhoven, the Netherlands, having spent one year, 1975, at the Antenna Laboratory, University of Illinois, Urbana. In 1978, he was appointed to the Chair of Electrical Engineering at the University of Liverpool and was subsequently appointed to the Chair of Electronics and Head of the Electronics Group at the University of Bath, in 1981, where he also held the responsibility of Head of the School of Electrical Engineering on an alternate three-year basis. Since 1988, Dr. Rozzi has been Professor of Antennas in the Department of Electronics and Control, University of Ancona, Italy, while remaining a Visiting Professor at Bath University.

Dr. Rozzi was awarded the Microwave Prize by the IEEE Microwave Theory and Technique Society, in 1975. He is also a Fellow of the IEE (UK) as well as IEE Council Representative for Italy.

DESIGN OF 'OPTIMUM' THREE PORT SYMMETRICAL JUNCTIONS FOR DIPLEXER APPLICATION

Antonio Morini, Tullio Rozzi

Dipartimento di Elettronica e Automatica, Università di Ancona
via Brecce Bianche 60100 Ancona, Italy

Abstract

From the properties of the S-matrix of a symmetrical three-port junction, we derive a set of necessary conditions and some sufficient ones to be satisfied in order that the junction be successfully employed in the realisation of a diplexer.

We derive explicit expressions for the positions at which the filters must be placed in the junction arms for optimum diplexer performance. Various examples of application are demonstrated and compared with existing numerical data and with experiments.

Introduction

At millimeter frequencies it is expedient to employ reciprocal circuits for the realization of diplexers and multiplexers and some interesting examples have appeared in the recent literature [1,2]. In view of the considerable difficulty of modelling the physical structures employed, the geometry of the diplexer is normally chosen by making use of routines that optimize global performance, including junction and filters. The optimization is rendered problematic by the fact that the ' error function' is not analytically available and a number of local minima occur. With a view to overcoming such difficulties some researchers have employed sophisticated techniques, achieving some very good results [1,2]. The functionals to be minimized, however, contain some computationally costly redundancies, that is just the purpose of this work to eliminate, with a view to CAD applications.

This contribution provides some necessary and some sufficient conditions for the realization of three-port junctions to be employed in diplexers, involving just the junction as distinct from the filters.

Once the junction is well defined, one obtains by means of a simple analytical formula the distances at which the filters have to be positioned for optimum performance.

It is emphasized that said criteria are based on the analysis of the scattering matrix of the junction and, as much, of general application, independently of the adopted technology.

Analysis

In fig. 1, the diplexer is modelled as lossless reciprocal symmetrical ($s_{11} = s_{22}$) three-port junction (J) with ports 1 and 2 closed by filters F1 and F2, with passbands b_1 and b_2 respectively .

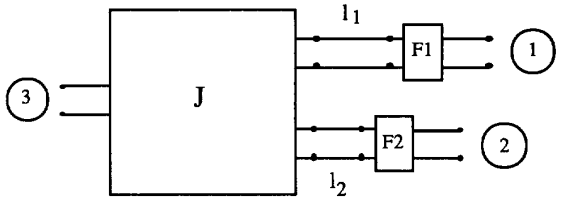

fig.1 Black box equivalent circuit of the diplexer;
J is a three port junction, F1 and F2 the two filters

We require that:

1. Over the band b2 there be perfect transmission between ports 3 and 2 ;

2. Over the band b1, perfect transmission between ports 3 and 1 .

It is easy to find conditions for requirements 1 and 2 to be satisfied at the midband frequencies f_1 and f_2 of the filters [3],

$$|s_{11}| = |s_{22}| \cong |s_{33}| \qquad f = f_1 \ , \ f = f_2 \tag{1}$$

The spacing l_1 and l_2 at which to position the filters in order for the diplexer to be perfectly matched are

$$l_1 = -\frac{1}{2j\beta} \ln\left[\frac{s_{22}}{\Delta s \ s_{33}^{*} \ \rho_{L1}}\right] \qquad f = f_2 \tag{2a}$$

$$l_2 = -\frac{1}{2j\beta} \ln\left[\frac{s_{11}}{\Delta s \ s_{33}^{*} \ \rho_{L2}}\right] \qquad f = f_1 \tag{2b}$$

Where, ρ_{L1}, ρ_{L2} are the reflection coefficients of the filters F1 and F2, closed on matched loads, Δs is the determinant of the scattering matrix of the junction.

It is possible to show that a **necessary** condition in order for (1) to be satisfied is that

$$|s_{33}| \geq 1/3 \qquad (3)$$

We note immediately that an "optimum" junction behaviour for the purpose of realizing a diplexer is rather different from that a power splitter, for which $|s_{33}| = 0$.

Moreover, we derive an upper bound to $|s_{33}|$, by determining the achievable bandwidth of the diplexer; in fact, when closing port 1 of the junction on F1, the reflection coefficient at port 2 of the resulting 2-port network (fig.2) is given by:

$$S_{22}(\beta) = s_{22}(\beta) + \frac{s_{12}^2(\beta)}{\frac{1}{\rho_{L1}(\beta)} - s_{11}(\beta)} \qquad (4)$$

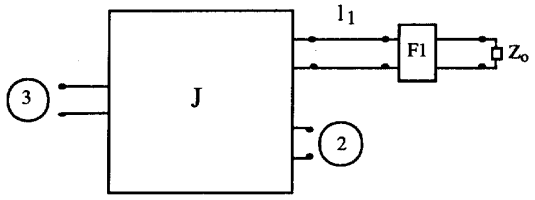

fig.2 two-port obtained by closing port 1 of J by F1

We require that $|S_{22}(\beta)| < \varepsilon$, in the bandpass of the filter $2\Delta\beta$, ε being the maximum return loss of the junction compatible with the specifications on the diplexer.

This condition is satisfied if at f_2 we have

$$\left|\frac{d}{d\beta} S_{22}(\beta)\right| < \frac{\varepsilon}{\Delta\beta} \qquad (5)$$

developing the differential of (4), we see that the best situation occurs when

$$s'_{11} = s'_{12} = s'_{22} \cong 0 \qquad (6a)$$

corresponding to a junction whose parameters do not depend on frequency, as well as

$$\frac{|s_{33}|}{2|s_{12}|} < \sqrt{\xi_o}\ , \qquad \xi_o = \frac{\varepsilon}{8\Delta\beta l} < 1 \qquad (6b)$$

This last inequality gives the maximum normalized bandwidth, centered at f_2, of the two-port junction obtained by closing port 1 by filter F1 (fig.2), vs. the reflection coefficient of the junction, as illustrated in fig.3. The ratio between the maximum return loss ε of the two-port so obtained and the length l, normalized to the guide width a, at which the filter is positioned, is taken as a parameter.

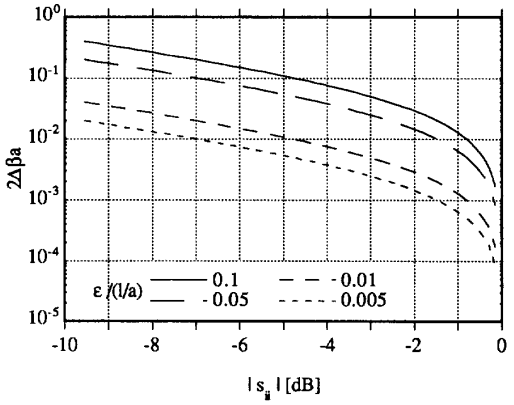

fig.3 Normalized bandwidth $2\Delta\beta a$ vs the return loss of the three-ports junction

We note that in the best case, corresponding to $|s_{33}| = 1/3$ (3), the maximum bandwidth is simply:

$$2\Delta\beta a < \frac{4\varepsilon a}{l} \qquad (7)$$

Having selected a junction whose characteristics are summarized in formulae (1,3,6a-b), the two filters have to be positioned as indicated by (2).

Results

In the following, we report two examples of application of the foregoing method.

The first concerns a diplexer configuration developed in [1,2], employing a symmetrical junction, as shown in fig.4, that was designed by making use of a numerical optimization routine.

fig.4 E-plane section of the three port junction employed in [1,2]

With reference to fig.5, the excellent results obtained there confirm the foregoing criteria. In fact, fig. 6 shows a comparison of the reflection magnitudes at ports 3 and 1; as it can be inferred, in the band of operation of the diplexer, these values are very close to each other, as required by conditions (1), and they also satisfy conditions (3,6a-b).

Moreover, by application of (2a-b), we recover exactly the same filter locations as were determined through numerical optimization by the authors.

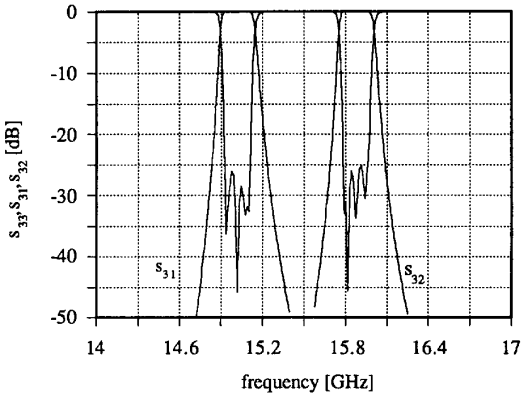

fig.5 Magnitude of scattering parameters for a diplexer realized by the junction used in [2]

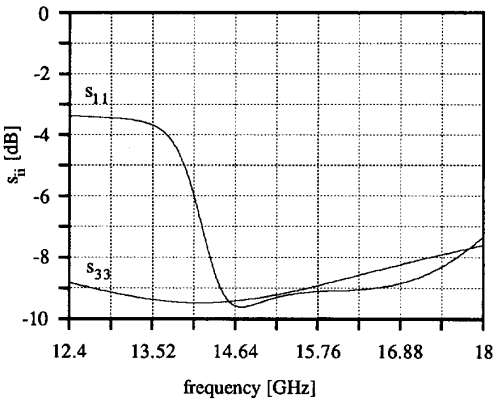

fig.6 reflection coefficients of the junction used in [1,2] at port 1 e 3

A second example concerns a kind of diplexer previously studied by ourselves [4, 5] that employs the junction depicted in fig.7, where an inductive septum, realized by the same E-plane technology as the filters, provides the matching element.

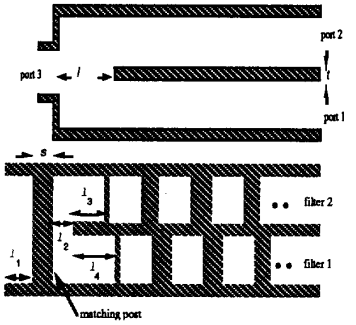

fig.7 E-plane section of the three port junction employed in [7] and mask of the filter

Junction parameters are now computed on the basis of the requirements (1,6a-b), while the filter locations are obtained by means of (2). Fig.8 shows the reflection coefficients at port 3 and 1 of the junction.

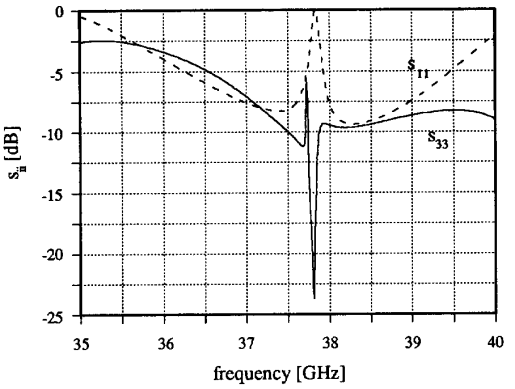

fig.8 reflection coefficients of the junction used in [6] at port 1 e 3

In fig. 9 we plot the reflection magnitude at the common port of the diplexer together with the filter responses. The junction now appears completely transparent to the filters, which property can be understood if one considers the reflection magnitudes at port 3 when port 1 is loaded by F1 and port 2 loaded by F2 (fig.10).

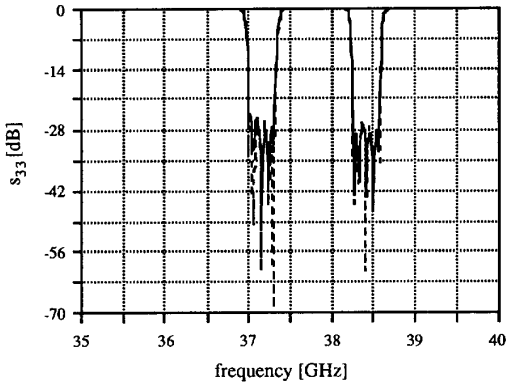

fig.9 Magnitude of scattering parameters for a diplexer realized by ourselves [7], compared with responses of the single filters

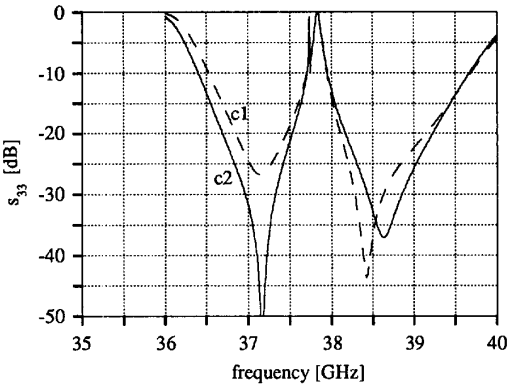

fig.10 Magnitude of the reflection coefficients for the junction [7] at the common port 3 when c1) port 1 is loaded by F1 (fig.2);
c2) port 2 is loaded by F2

Conclusions

We present simple analytical criteria for the design of 'optimum' junctions for diplexer realization.

These are of general validity, deriving solely from the properties of the scattering matrix of a reciprocal, lossless three-port junction.

The above criteria also provide explicitly two additional important parameters of the diplexer geometry, namely, the locations of the filters, resulting in a considerable simplification of the overall synthesis.

References

[1] J. Dittloff, and F. Arndt, "Rigourous design of septate multiplexers with printed circuit elements", IEEE MTT-S Digest 1988, pp.431-434;

[2] J. Dittloff, and F. Arndt, "Rigourous field theory design of millimeter-wave E-plane integrated circuit multiplexers", IEEE Trans. on MTT, vol. MTT-37, No. 2, Feb. 1989, pp 340-350;

[3] C.G. Montgomery, R.H. Dicke, E.M. Purcell: "Principles of microwave circuits", Mc Graw Hill, 1948 ;

[4] T. Rozzi, F. Moglie, A. Morini, W. Gulloch, M. Politi: "Accurate full-band equivalent circuits of inductive posts in rectangular waveguide", IEEE Trans. on MTT, vol. MTT-40, No. 5, May 1992 ;

[5] A. Morini, T. Rozzi, D. De Angelis,W. Gulloch: "A novel matched diplexer configuration in E-plane technology", IEEE MTT-S Digest 1993, pp 1077-1080

A NOVEL MATCHED DIPLEXER CONFIGURATION IN E-PLANE TECHNOLOGY

Antonio Morini, Tullio Rozzi, and Danilo De Angelis

Dipartimento di Elettronica ed Automatica, Università di Ancona, via Brecce Bianche, 60131 Ancona, Italy

William Gulloch
Alcatel Telettra Research, Vimercate (MI), Italy

ABSTRACT

A new arrangement for the realization of waveguide diplexers is proposed.
A single inductive post, located in the cavity between the input waveguide and the bifurcation is used as matching element retaining full planar technology.
This provides a inexpensive and effective solution.

OUTLINE

Modal analyses of the E-plane technology diplexers have been presented in the literature [1,2,3], also including cascaded steps as matching elements.
Although such matching devices do improve the performance of the diplexers, their fabrication is mechanically critical and expensive.
If a single inductive sept , of the kind already used in the realization of branching filters, is employed as a matching device in the cavity between junction and filters, E-plane technology is maintained and considerable mechanical simplification ensues.
The resulting E-plane mask is shown in fig.1a and the abrupt E-plane step provides the housing. (fig.1b)

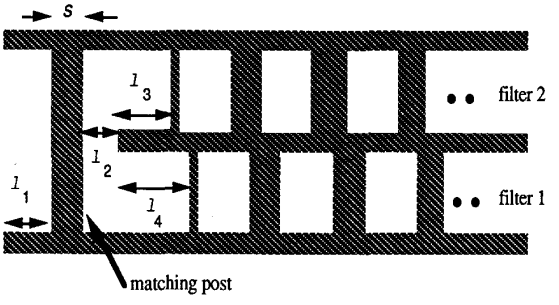

fig.1a mask of filters and matching post

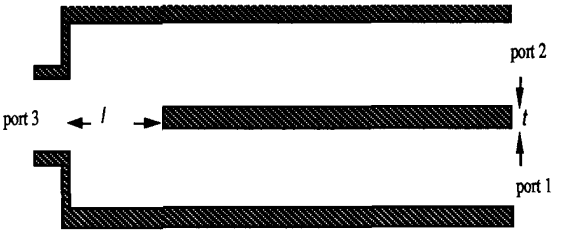

fig.1b longitudinal E-plane section of the housing

ANALYSIS

The structure under study is composed of a three-port junction two arms of which are closed by inductive filters. We focus now on the analysis of the three-port junction, whereas reference is made to [4] for that of the filters.
The problem is reduced by even and odd excitation mode decomposition to the two two-port configuration shown in fig. 2.

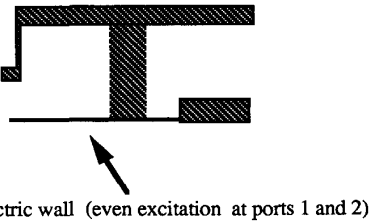

fig. 2a

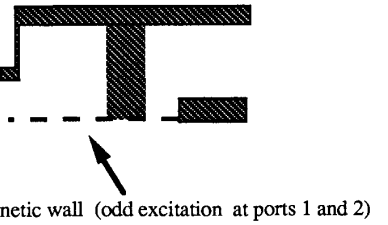

fig. 2b

DD

CH3277-1/93/0000-1077$01.00 © 1993 IEEE

We recognize that each of the latter configurations consists of a cascade of three discontinuities; e.g. in fig. 2a an E-plane step, an inductive post and a second E-plane step. In fig. 2b, the problem is somewhat modified in order to account for the presence of a magnetic wall instead of a electric one over part of the lower boundary.

We employ the concept of 'accessible modes' [5] for each building block discontinuity.

The whole equivalent circuit of the two port, corresponding to the even excitation, is shown in fig. 3a.

Each block T_{ei} represents the transmission matrix of the i-th junction, considering TE_{10}, TE_{11}, TM_{11} and TE_{30} as accessible modes; Y are the corresponding modal characteristic admittances.

In the odd case, the whole equivalent circuit (fig.3b) reduces to a one port because of the absence of modes above cutoff in the regions containing the magnetic wall.

In the odd case the choice of the accessible modes depends on the kind of discontinuity.

For the first two kinds (the E-plane step and the post, both on a magnetic wall), a proper choice is TE_{11} and TM_{11}.

For the third kind (the E-plane step from a guide with a magnetic wall to a standard guide) we take TE_{11} and TM_{11} to the left and TE_{11} and TE_{10} to the right of the juntion.

The parameters of the matrices T_{ei} and T_{oi} are determined by the Galerkin variational method employing singular expanding functions with built in edge conditions [4].

Convergence of the admittance operators is accelerated by accurate asymptotic expansions.

Moreover, by keeping track analytically of the frequency dependence in the waveguide admittance operator, computing time for a simulation over the full band is little different from that of a spot-frequency calculation.

All these analytical manipulations result in a very agile code requiring little memory and capable of being accommodated on a small personal computer.

In term, this renders feasible an effective CAD synthesis of the diplexers with modest computing means.

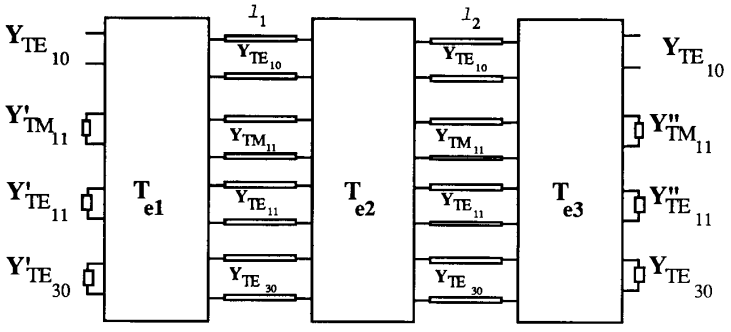

fig. 3a black-box equivalent circuit of the three ports junction under even excitation

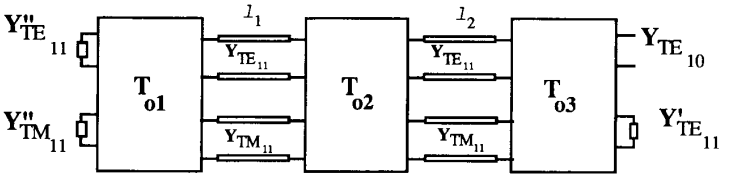

fig. 3b black-box equivalent circuit of the three ports junction under odd excitation

RESULTS

First, we tested the effectiveness of the matching arrangement, by simulating the three-ports junction with the post.

Fig. 4 shows the reflection coefficient at the common port (port3) of this junction for two different values of the lengths of the cavity and with the same post. For this thickness of the wall separating the two output waveguides, the junction would be considerably mismatched, but for the use of the matching post that recovers a good match over a wide band. Moreover, it is apparent how easily the junction can be tuned.

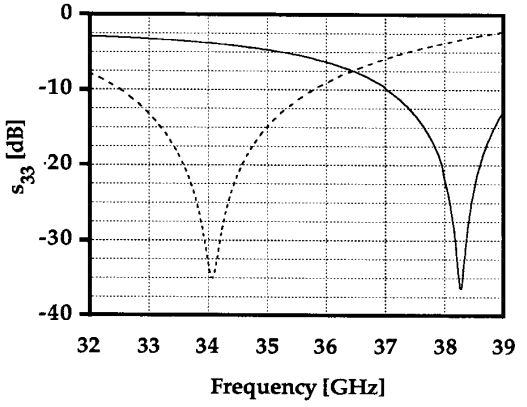

fig.4 Magnitudes of reflection coefficients at the ports of the three ports junction with the matching post: s=0.3mm, t=2mm
--- l_1=5 mm, l_2=5mm; — l_1=4.25 mm, l_2=6mm

Fig.5 shows the predicted performance of a diplexer, containing the filters described in table 1, optimized with the matching post in frequency band 35-39 GHz.

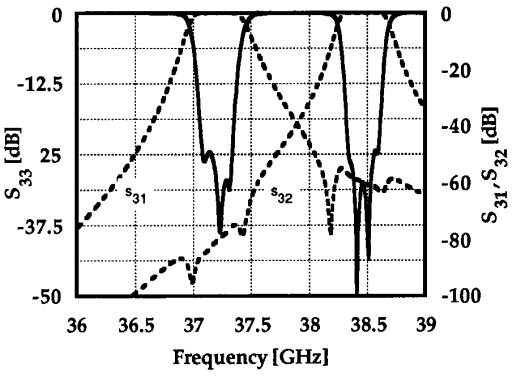

fig.5 Magnitudes of reflection coefficients at the ports of the diplexer with the matching postt l_1=3.952mm, l_2=4.302mm, s=0.3mm, l_3=1.593mm, l_4=2.601mm, t=2mm

length	Filter 1	Filter 2
s_1	2.198	2.540
l_2	3.053	2.798
s_3	6.440	7.367
l_4	3.076	2.774
s_5	7.113	8.120
l_6	3.076	2.774
s_7	6.440	7.367
l_8	3.053	2.798
s_9	2.198	2.540

table 1 lengths of septa (s) and cavities (l) of the simulated filters

In fig.6 we report a comparison between the reflection coefficients at the common port of the diplexer with and without the matching inductive post.In both cases, the dimension of the cavity was optimized to give the minimum insertion loss over the band of the filters.

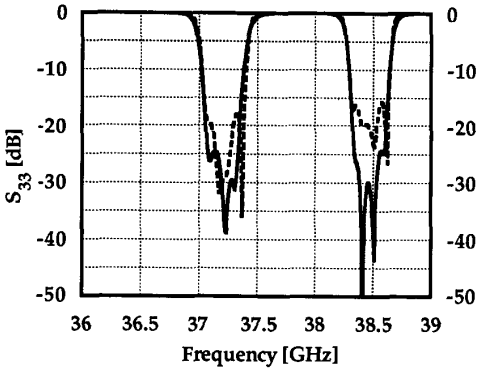

fig.6 Magnitude of reflection coefficient at the common port (port 3) of the diplexer with and without the matching post.

Analogous behaviour was found at different bands

It is also interesting to compare with fig.5, the performances of the individual 4-cavities filters used in both diplexers; this can be seen in fig.7.

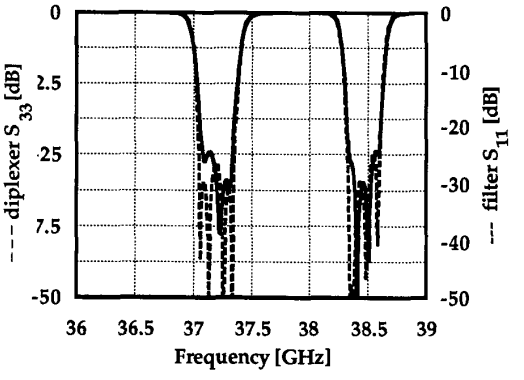

fig.7 Comparison between the magnitude of reflection coefficient at the common port of the diplexer with the matching post and those of the filters.

CONCLUSIONS

We propose a new E-plane solution to the problem of matching diplexer junctions.

The behaviour of the whole matched diplexer is investigated by rigourous field analysis and the numerical predictions of performance are promising.

Experimental prototypes are being constructed

REFERENCES

[1] J. Dittloff, and F. Arndt: "Rigourous design of septate multiplexers with printed circuit elements", IEEE MTT-S Digest 1988, pp.431-434;

[2] R. Vahldieck and B. Varailhon de la Filolie "Computer-aided design of parallel connected millimeter-wave diplexers/multiplexers", IEEE MTT-S Digest 1988, pp.435-438;

[3] J. Dittloff, and F. Arndt: "Rigourous field theory design of millimeter-wave E-plane integrated circuit multiplexers", IEEE Trans. on MTT, vol. MTT-37, No. 2, Feb. 1989, pp 340-350;

[4] T. Rozzi, F. Moglie, A. Morini, W. Gulloch, M. Politi: "Accurate full-band equivalent circuits of inductive posts in rectangular waveguide", IEEE Trans. on MTT, vol. MTT-40, No. 5, May 1992 ;

[5] T. Rozzi: "Network analysis of strongly coupled transverse apertures in waveguide", Int. J. Circuit Theory Appl., vol.1, pp. 161-179,1972 ;

A New Look at the Practical Design of Compact Diplexers

Antonio Morini, *Member, IEEE*, Tullio Rozzi, *Fellow, IEEE*, Marco Farina, *Member, IEEE*, and Giuseppe Venanzoni

***Abstract*—This paper presents a method for the design of compact diplexers, where the common junction is considered part of the filters, thus reducing the diplexer length by roughly one cavity. Starting from two filter prototypes satisfying the desired specifications, the technique provides the design equations in closed form. Effectiveness and accuracy of the proposed method are demonstrated by means of a practical example.**

***Index Terms*—Diplexer, filter, prototype.**

I. Introduction

THE SYNTHESIS of diplexers classically starts from two filters and a three-port junction that are separately designed and combined in such a way as to maximize performance. Unfortunately, simply connecting filters and junction produces an unacceptable deterioration of the response of the two filters in their passbands, which can be restored by modifying the first elements of each filter, as indicated in [1]–[3].

Alternatively, some years ago, we introduced a simple analytical formula, providing the line lengths at which two filters have to be connected to an arbitrary three-port junction, in order to guarantee an optimal design [4], [5].

This approach featured a clear segmentation of the problem and the provision of simple formulas for the combination of filters and junction.

Although the performances of the original filters were not completely preserved in the final diplexer, the response of the channels in the resulting device were very satisfactory, at least in the noncontiguous case and for junctions endowed with some properties. Moreover, in practical cases, the same screws used to tune the cavities could be used to easily compensate for the resulting small deviation.

As a matter of fact, the method ought to be seen as providing a near-optimal starting point from where to apply some efficient optimization.

There is, however, a further aspect that impacts on maximum achievable performance. In fact, in the above approach, two line sections are interposed between the first coupling elements of the two filters and the junction. This makes the diplexer longer than the sum of the filters lengths, possibly challenging the constraints on maximum acceptable size and increasing losses.

Manuscript received February 13, 2006; revised May 19, 2006. This work was supported by the MITEL Srl, Milan, Italy.

The authors are with the Dipartimento di Elettromagnetismo e Bioingegneria, Università Politecnica delle Marche, 60100 Ancona, Italy (e-mail: a.morini@univpm.it).

Color versions of Figs. 2, 3, 7, and 8 are available online at http://ieeexplore.ieee.org.

Digital Object Identifier 10.1109/TMTT.2006.879770

The new method allows to eliminate these additional sections, while preserving the original electrical behaviors of the two filters and the simplicity of design. The latter is guaranteed by means of practical closed formulas, derived in Section II, as no modification of the original prototypes of the two filters is required.

The basic idea is that the junction can be seen as a part of each channel filter. In other words, the junction can be designed so as to mimic the effect of the first coupling elements, i.e., the first K-inverters, of each filter. This task is not very difficult to accomplish, as shown in Section II.

Section III describes a practical example: in the first part, the proposed approach is validated by means of a full-wave analysis performed by Ansoft's High Frequency Structure Simulator (HFSS) [7], while in the second part, we report pictures and measurements of the actual final device.

II. Analysis

It is expedient to split each filter into two cascading blocks, called, respectively, "head," constituted by the first K-inverter, and "tail," involving the remaining part [6].

In this study, the heads are included into the three-port junction, whose scattering matrix $\mathbf{S}$ is given by

$$\begin{bmatrix} b_1 \\ b_2 \\ b_3 \end{bmatrix} = \begin{bmatrix} s_{11} & s_{12} & s_{13} \\ s_{12} & s_{22} & s_{23} \\ s_{13} & s_{23} & s_{33} \end{bmatrix} \begin{bmatrix} a_1 \\ a_2 \\ a_3 \end{bmatrix}. \quad (1)$$

The diplexer is obtained when ports 1 and 2 of this new special junction are connected to the tails of two filters, say, T1 and T2, respectively.

At f_1, the midband frequency of filter F1, the junction must behave as the first inverter $K_1^{(1)}$ of the original filter F1. The superscript j in $K_i^{(j)}$ indicates filter j, and i denotes the ith K inverter of such a filter.

Considering that port 2 of the junction is connected to tail T2, whose reflection is $\Gamma_2(f_1)$, the scattering matrix $\mathbf{S}'$ of the resulting two-port is given by

$$\mathbf{S}' = \begin{bmatrix} s_{11} & s_{13} \\ s_{13} & s_{33} \end{bmatrix} + \frac{\Gamma_2(f_1)}{1-\Gamma_2(f_1)s_{22}} \begin{bmatrix} s_{12}^2 & s_{12}s_{23} \\ s_{12}s_{23} & s_{23}^2 \end{bmatrix}. \quad (2)$$

Note that $|\Gamma_2(f_1)| \approx 1$, as filter F2 is in its out-band at f_1, and, for the same reason, $1 - s_{22}(f_1) \cdot \Gamma_2(f_1) \neq 0$. In fact, the equality would mean that port 2 is matched, i.e., F2 is in-band. In addition, since the junction is assumed to be lossless, we can focus on s'_{11}.

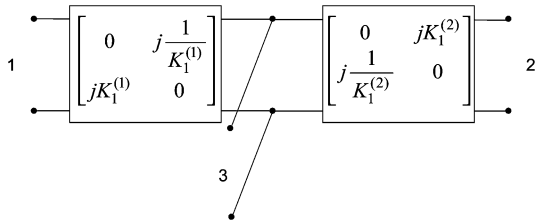

Fig. 1. In its simplest form, the three-port junction to be used is formed by the connection of a Y-junction and the first two K- inverters of each filter (represented in the figure by their $ABCD$-parameters).

According to our strategy, the junction replaces the first k-inverter of filter F1; consequently, its scattering matrix should coincide with the one of $k_1^{(1)}$, whose expression is

$$\mathbf{S}^{K_1^{(1)}} = \begin{bmatrix} \dfrac{\left(K_1^{(1)}\right)^2 - 1}{\left(K_1^{(1)}\right)^2 + 1} & \dfrac{-2jK_1^{(1)}}{\left(K_1^{(1)}\right)^2 + 1} \\ \dfrac{-2jK_1^{(1)}}{\left(K_1^{(1)}\right)^2 + 1} & \dfrac{\left(K_1^{(1)}\right)^2 - 1}{\left(K_1^{(1)}\right)^2 + 1} \end{bmatrix}. \tag{3}$$

Therefore, we require that

$$s_{11} + \frac{s_{12}^2 \Gamma_2(f_1)}{1 - \Gamma_2(f_1) s_{22}} = \frac{\left(K_1^{(1)}\right)^2 - 1}{\left(K_1^{(1)}\right)^2 + 1}. \tag{4}$$

The left-hand side of the above expression has to be carefully analyzed. It is noted that the equality is immediately satisfied if $\left|s_{12}^2\right| \approx 0$ and the reflection coefficient at port 1 of the junction, namely, s_{11}, equates that of the first K-inverter.

This occurs, for instance, when the junction is formed by an ideal Y-junction whose arms 1 and 2 are connected to the first K inverters of the corresponding filters, as shown in Fig. 1. In fact the $ABCD$ matrix of the two-port 1 and 2, obtained by terminating port 3 on its characteristic impedance, is given by

$$\begin{bmatrix} V_1 \\ I_1 \end{bmatrix} = \begin{bmatrix} \dfrac{-1}{K_1^{(1)} K_1^{(2)}} & \dfrac{-K_1^{(2)}}{K_1^{(1)}} \\ 0 & -K_1^{(1)} K_1^{(2)} \end{bmatrix} \begin{bmatrix} V_2 \\ I_2 \end{bmatrix}. \tag{5}$$

Therefore,

$$|s_{12}| = \frac{2}{\dfrac{1}{K_1^{(1)} K_1^{(2)}} + K_1^{(1)} K_1^{(2)} + \dfrac{K_1^{(2)}}{K_1^{(1)}}} \approx 2\left|K_1^{(1)} \cdot K_1^{(2)}\right| \approx 0 \tag{6}$$

as required.

Actually, equality (6) also holds when the "core" junction is more involved than just a simple Y. It turns out that the only needed requirement is that the two inverters be connected to it, as shown in Fig. 1.

Therefore, condition (4) simply becomes

$$s_{11}(f_1) = \frac{\left(K_1^{(1)}\right)^2 - 1}{\left(K_1^{(1)}\right)^2 + 1}. \tag{7}$$

By the same token, at the midband frequency f_2 of filter F2, it is required that

$$s_{22}(f_2) = \frac{\left(K_1^{(2)}\right)^2 - 1}{\left(K_1^{(2)}\right)^2 + 1}. \tag{8}$$

Equations (7) and (8) provide the design formulas for the junction. Note that the right-hand sides of (7) and (8) are real, while the reflection coefficients of a three-port are generally complex. Therefore, phase correction at ports 1 and 2 is required.

This is accomplished by inserting a section of line featuring a negative electrical length

$$\phi_i = \frac{\angle s_{ii}(f_i) - \pi}{2}, \qquad i = 1, 2 \tag{9}$$

in front of ports 1 and 2.

The corresponding physical lengths are given by

$$l_i = -\left|\frac{\angle s_{ii}(f_i) - \pi}{2\beta(f_i)}\right|, \qquad i = 1, 2. \tag{10}$$

In practice, the above negative lengths are absorbed by the first cavities of each filter, thus reducing even more the overall diplexer size.

In conclusion, the junction is designed by considering just the amplitudes of the reflections at ports 1 and 2, at the midband frequencies of the two filters f_1 and f_2, provided that transmission between the two ports is negligible, as discussed above.

In addition, note that when the passbands of the filters are contiguous and bandwidths coincide, their first k-inverters are almost equal, namely, $K_1^{(1)} = K_1^{(2)}$. In this case, it is quite easy to design the junction. For instance, in waveguide technology, this can be done either by placing a metal insert, as shown in Fig. 2, or by using an iris, as will be shown in Section III.

The insert is adjusted in order to obtain the reflection magnitudes required by (7) and (8) at the two filter midband frequencies. This task is easily handled with the help of a full-wave solver, such as Ansoft's HFSS [7].

The phases are finally adjusted by shortening the waveguide sections, which separate the first two k-inverters of each filter, according to (10).

It deserves to be emphasized that the common belief [8] that the junction has to be as neutral as possible is basically wrong.

Of course, the same principle also applies to different technologies, such coaxial and microstrip.

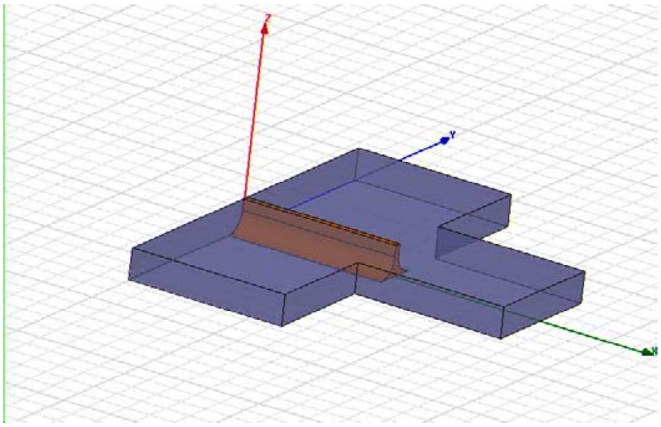

Fig. 2. H-plane metal insert placed into a classical T-junction creates an arbitrary reflection at the main arm, thus satisfying the design conditions expressed by (7) and (8).

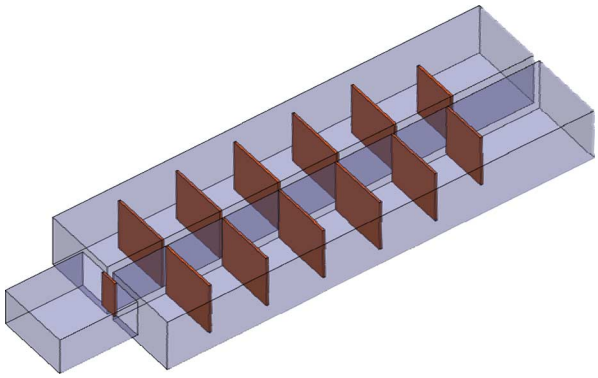

Fig. 3. In the X-band diplexer built, the compact junction was obtained using an H-plane window of the same kind employed for the two six-cavity filters.

III. Results

In order to demonstrate the effectiveness of the proposed method, here we report the details of the design and the results for a WR75-band diplexer, whose sketch is shown in Fig. 3. The diplexer was meant for practical use in a communication system for which a set of specifications was available. These specifications included the possibility to shift the channels by means of tuning screws.

The responses of the Chebyshev ideal filter prototypes, featuring 23-dB minimum return loss and six cavities, are shown in Fig. 4. The bandwidth is 32 MHz for both filters, while the midband frequencies are 12.961 and 13.227 GHz, respectively, corresponding to the higher operating frequencies. Actually, it is well known that the insertion of a screw into a cavity can only shift down its resonant frequency.

The filters were implemented by using inductive asymmetric windows (thickness: 0.5 mm) as coupling elements.

Their dimensions are calculated by using in-house software, which provides the reflections of the windows evaluated at the midband frequencies f_1 and f_2. In particular, the scattering matrices for a discrete set of apertures are stored in a database, and are interpolated during the optimization process. Table I reports the resulting dimensions

The junction is obtained by using an H-plane window of the same thickness as those employed for the filters, as shown in Fig. 5. This choice is quite suitable for the current purpose, as it allows to obtain a (practically) arbitrary reflection.

At this stage, it would be possible to accurately consider the effects of the corner roundness, produced in the fabrication by

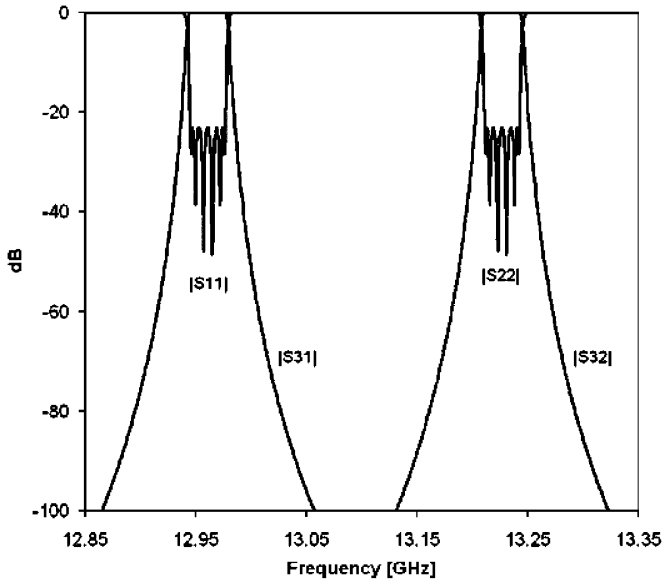

Fig. 4. Prototype response of the two designed six-cavity Chebyshev filters.

TABLE I
Dimensions (in Millimeters) of the Two WR75 H-Window Six-Pole Filters Designed. A_i and C_i are the Width of the ith Aperture and the Length of the ith Cavity, Respectively. All the Window Thicknesses are 0.5 mm

Filter 1	Filter 2	
7.336	7.218	A_1
14.102	13.67	C_1
3.999	3.926	A_2
14.498	14.046	C_2
3.693	3.627	A_3
14.508	14.055	C_3
3.65	3.584	A_4
14.508	14.055	C_4
3.693	3.627	A_5
14.498	14.046	C_5
3.999	3.926	A_6
14.102	13.67	C_6
7.336	7.218	A_7

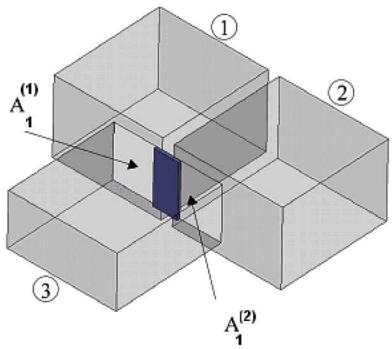

Fig. 5. Sketch of the junction designed. The arrows point to the apertures between the common arm and first cavities of each filter. Note that the waveguide sections connecting the filters to the junction are no longer required, yielding a compact device.

TABLE II
AMPLITUDES AND PHASES OF THE SCATTERING PARAMETERS OF THE JUNCTION OF FIG. 5, CALCULATED AS FUNCTIONS OF THE APERTURE A'S, AT THE MIDBAND FREQUENCY OF THE FIRST FILTER ($f1 = 12.961$ GHz), CONSIDERING 0.1-mm APERTURE STEPS. THE WAVEGUIDES ARE WR75, WHILE THE WINDOW THICKNESS IS 0.5 mm. THE VALUES HAVE BEEN COMPUTED BY ANSOFT'S HFSS [7]

A [mm]	|S11|	ph(S11)	|S31|	ph(S31)	|S21|	ph(S21)
8.025	0.979243	166.68	0.20158	-173.792	0.021179	-24.7776
7.925	0.980544	166.888	0.195165	-172.933	0.019887	-24.4589
7.825	0.981814	167.083	0.188874	-172.06	0.018624	-24.1318
7.725	0.983008	167.253	0.182774	-171.218	0.017416	-23.8326
7.625	0.984121	167.409	0.176803	-170.422	0.016261	-23.5615
7.525	0.985194	167.587	0.170777	-169.647	0.015126	-23.2649
7.425	0.986264	167.811	0.164555	-168.868	0.01399	-22.8975
7.325	0.987324	168.063	0.158185	-168.085	0.01287	-22.5299
7.225	0.988346	168.315	0.151759	-167.307	0.011795	-22.2914
7.125	0.989302	168.553	0.145448	-166.551	0.010794	-22.1672
7.025	0.990173	168.78	0.139496	-165.842	0.009897	-21.92
6.925	0.990955	169.002	0.133982	-165.203	0.009114	-21.3757
6.825	0.991709	169.241	0.128308	-164.591	0.008375	-21.0035
6.725	0.992517	169.522	0.121762	-163.927	0.007591	-21.5786
6.625	0.99336	169.826	0.114648	-163.205	0.00677	-22.7256
6.525	0.994103	170.092	0.108278	-162.541	0.006005	-22.1253
6.425	0.994633	170.282	0.103541	-162.064	0.005388	-17.4718
6.325	0.995038	170.458	0.099514	-161.691	0.004929	-11.558
6.225	0.995466	170.706	0.094875	-161.247	0.004491	-9.78197
6.125	0.995961	171.03	0.089472	-160.671	0.004017	-13.7647

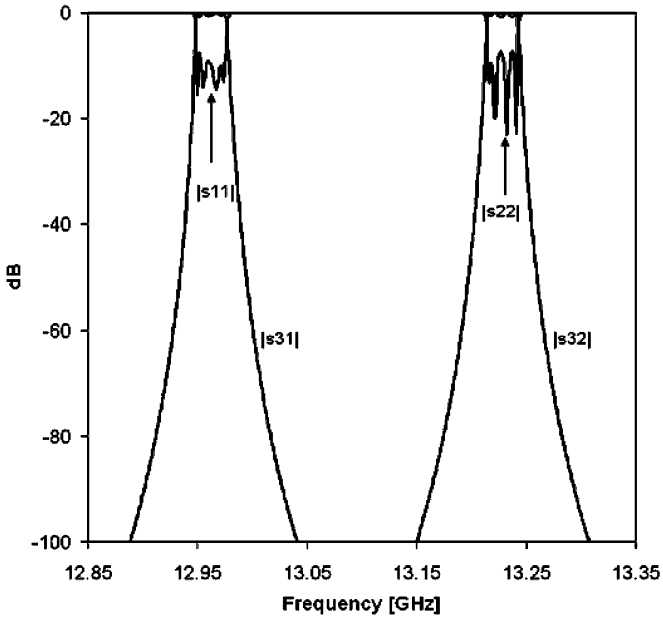

Fig. 6. Ansoft's HFSS simulation of the designed diplexer. This is exactly what results from the design process illustrated, without any adjustment or optimization, which, of course, would significantly improve performance.

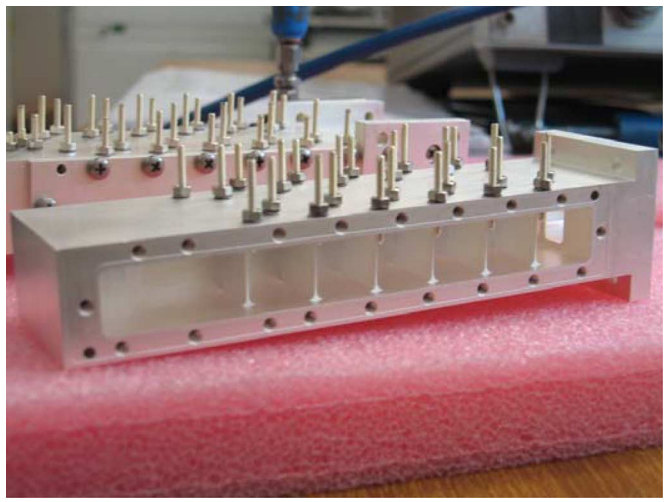

Fig. 7. WR75 diplexer built, as it appears when the lateral walls are removed.

the milling machine. However, we have purposely neglected them. The reason is that, as stated above, the two filters were required to be tunable, by means of tuning screws penetrating cavities and couplings windows. Therefore, we did not spend any effort in optimizing the design, being aware that the implemented structure would deviate somewhat from the designed one. One could argue that this choice weakens the validation of our approach. Actually, the validation is performed by means of Ansoft's full-wave solver HFSS, thus immunizing the proof from the effects of nonideal materials, imperfect realization, and whatever affects real-world devices.

Instead, the realization shows the usefulness of the approach, being a step-by-step example of a real-life diplexer.

The design of the compact junction was obtained by interpolating the data set of junctions computed by Ansoft's HFSS in order to satisfy (7) and (8).

In particular, the values of the K-inverters, corresponding to the first apertures of the two filters are

$$K_1^{(1)} = 0.0834 \quad K_1^{(2)} = 0.0816.$$

Therefore, the compact junction, designed according to (7) and (8), must feature

$$s_{11}(12.961\ \text{GHz}) = -0.986185$$

and

$$s_{22}(13.227\ \text{GHz}) = -0.986771.$$

In addition, negligible transmission is required between the two ports, i.e., $|s_{21}| \approx 0$. Note also that, in the current case, the two reflections are nearly the same.

This simplifies the design. The first step is to select a junction that could meet the requirements, possibly by varying a parameter at a time.

The junction shown in Fig. 5 has the features we are looking for since, for practical values of the apertures, the transmission between ports 1 and 2 is negligible and each aperture only affects the reflection of the corresponding port (and, of course, of the common one). A lookup table (Table II) showing the magnitude of s_{11} for different apertures, calculated by Ansoft's HFSS at the midband frequency of the first filter f_1 (where the two apertures $A_1^{(1)} A_1^{(2)}$ are assumed to be identical), clearly shows this point. The calculation of the aperture corresponding to the first k-inverter of the second filter F2 is conceptually identical. It only requires the recalculation of the above table at the midband frequency of filter 2, i.e., f_2.

In practice, it matters little whether the two apertures $A_1^{(1)}$ and $A_1^{(2)}$ are equal or slightly different. As can be easily checked by direct inspection, the transmission between ports 1 and 3 is

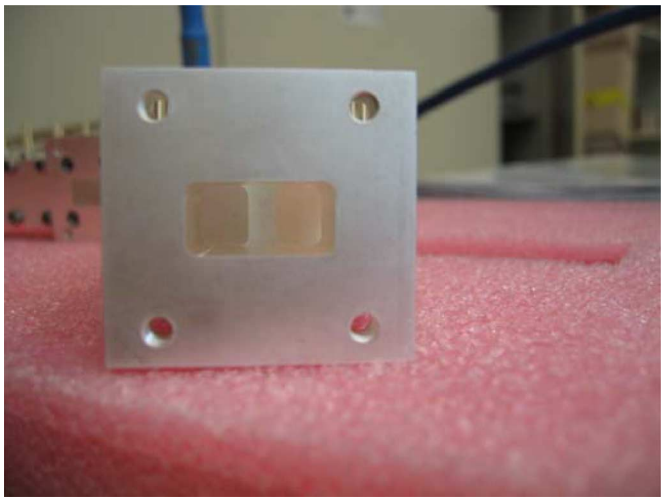

Fig. 8. Diplexer realized as it appears at the common port.

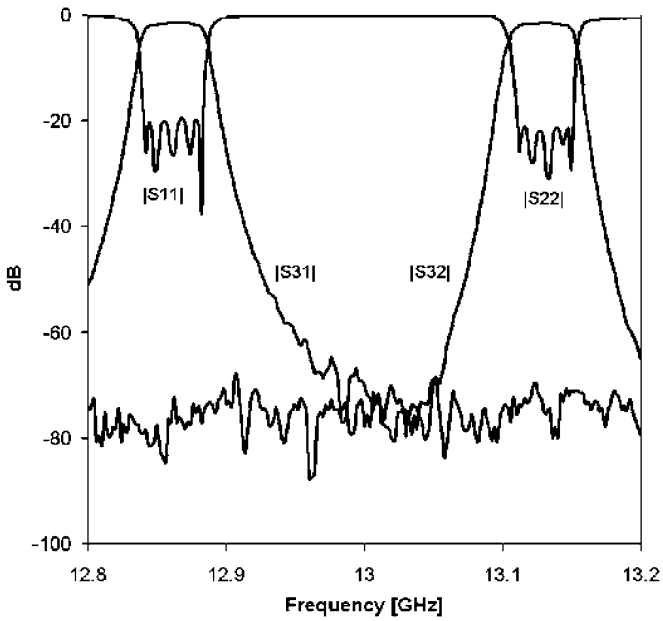

Fig. 9. Measurements of the diplexer designed. The bands of the two filters were slightly widened (40 MHz) by increasing the couplings in order to reduce losses.

essentially independent of the aperture $A_1^{(2)}$ placed across ports 2 and 3.

The resulting window apertures corresponding to the above reflections are as follows.

- Filter 1: $A_1^{(1)} = 7.455$ mm.
- Filter 2:$A_1^{(2)} = 7.275$ mm.

Correspondingly, the lengths of the first cavities are as follows.

- Filter 1: $C_1^{(1)} = 14.037$ mm.
- Filter 2: $C_1^{(2)} = 13.598$ mm.

As can be observed, the latter differ just slightly from the starting values, namely, those of the filters reported in Table I.

The complete diplexer was simulated by Ansoft's HFSS, obtaining the results shown in Fig. 6. They are noteworthy, being obtained *without* any optimization of the overall diplexer.

The diplexer in question was finally built, as shown in Figs. 7 and 8, including the tuning screws and with rounded corners.

Fig. 9 shows the measured scattering parameters. As can be observed, the bandwidths of the two filters were deliberately widened up to 40 MHz in order to reduce losses. This was easily accomplished by increasing the penetration of the screws controlling the couplings.

IV. Conclusion

Diplexer design has been improved by looking at the device as a whole, in contrast to what has been usually done, namely, by considering separately junction and filters. In this way, the junction itself plays the role of the first k-inverter of each filter if suitably designed. As a result, devices are more compact.

We have introduced closed-form design formulas for designing the junction and, consequently, the entire diplexer. The validity of the proposed approach has been assessed by means of full-wave simulations, performed by Ansoft's HFSS. A practical design example, along with its realization and experimental characterization, has also been discussed.

Acknowledgment

The authors are indebted to M. Villa, MITEL Srl, Milan, Italy, not only for helpful discussions and suggestions, but also for the realization and measurement of the prototype shown.

References

[1] G. Matthaei, L. Young, and E. M. T. Jones, *Microwave Filters, Impedance-Matching Networks, and Coupling Structures*. Dedham, MA: Artech House, 1980, pp. 595–595.

[2] J. D. Rhodes and R. Levy, "A generalized multiplexer theory," *IEEE Trans. Microw. Theory Tech.*, vol. MTT-27, no. 2, pp. 99–111, Feb. 1979.

[3] ——, "Design of general manifold multiplexers," *IEEE Trans. Microw. Theory Tech.*, vol. MTT-27, no. 2, pp. 111–122, Feb. 1979.

[4] A. Morini and T. Rozzi, "Constraints to the optimum performances and bandwidth limitations of diplexers employing symmetric three-port junctions," *IEEE Trans. Microw. Theory Tech.*, vol. 44, no. 2, pp. 242–248, Feb. 1996.

[5] A. Morini, T. Rozzi, and M. Morelli, "New formulas for the initial design in the optimization of T-junction manifold multiplexers," in *IEEE MTT-S Microw. Symp. Dig.*, San Diego, CA, Jun. 1997, pp. 1025–1028.

[6] A. Morini and G. Cereda, "Re-configurable reciprocal multiplexers (r-mux) for terrestrial radio links," in *Proc. 31th Eur. Microw. Conf.*, Milan, Italy, Sep. 2002, pp. 105–107.

[7] HFSS. ver. 10, Ansoft, Pittsburgh, PA, 2006.

[8] Uher, J. Bornemann, and U. Rosenberg, *Waveguide Components for Antenna Feed Systems*. Norwood, MA: Artech House, 1993.

Antonio Morini (M'96) received the Laurea degree (*summa cum laude*) in electronics and Ph.D. degree in electromagnetism from the University of Ancona, Ancona, Italy, in 1987 and 1992, respectively.

He is currently an Associate Professor of applied electromagnetism with the Università Politecnica delle Marche, Ancona, Italy. His research activity is mainly devoted to the modeling and design of passive microwave components such as filters and antennas.

Tullio Rozzi (M'66–SM'74–F'90) received the Dottore degree in physics from the University of Pisa, Pisa, Italy, in 1965, the Ph.D. degree in electronic engineering from The University of Leeds, Leeds, U.K., in 1968, and the D.Sc. degree from the University of Bath, Bath, U.K., in 1987.

From 1968 to 1978, he was a Research Scientist with Philips Research Laboratories, Eindhoven, The Netherlands. In 1975, he spent one year with the Antenna Laboratory, University of Illinois at Urbana–Champaign. In 1978, he became the Chair of Electrical Engineering with the University of Liverpool. In 1981, he became the Chair of Electronics and Head of the Electronics Group, University of Bath, where he was also the Head of the School of Electrical Engineering on an alternate three-year basis. Since 1988, he has been a Professor with the Dipartimento di Elettromagnetismo e Bioingegneria, Università Politecnica delle Marche, Ancona, Italy, where he is also Head of the department.

Dr. Rozzi was the recipient of the 1975 Microwave Prize presented by the IEEE Microwave Theory and Technique Society (IEEE MTT-S).

Marco Farina (M'98) received the M. Eng. (*summa cum laude*) degree in electronics and Ph.D. degree from the University of Ancona, Ancona, Italy, in 1990 and 1995, respectively.

From 1991 to 1992, he was a Technical Officer in the Italian Army. Since 1992, he has been with the Department of Electromagnetics and Bioengineering, University of Ancona, where he is an Assistant Professor. In 2002, he became an Associate Professor. He is also a Consulting Engineer in electronics. He coauthored *Advanced Electromagnetic Analysis of Passive and Active Planar Structures* (IEE Press, 1999). He developed the full-wave software package for three-dimensional (3-D) structures EM3DS.

Giuseppe Venanzoni received the Laurea and Ph.D. degrees in electronic engineering from the Università di Ancona, Ancona, Italy, in 2001 and 2004, respectively.

He is currently a Post-Doctoral student with the Università Politecnica delle Marche, Ancona, Italy, where he is involved with electromagnetism and microwaves. His research interests include the design of waveguide passive devices, microwave filters, and antennas.

Elimination of Fine Tuning in High Power, Low-PIM Diplexers for Combined Transmit/Receive Antennas

G.G. Connor

1 Abstract

The use of combined transmit/receive antennas on spacecraft can reduce the mass by a considerable amount. Such a configuration normally requires the diplexion of the receive and transmit bands onto a common feed. Due to the difference in power levels, problems can arise if passive intermodulation (PIM) products from the transmit carriers fall within the receive band at power levels of the same order as the receive carriers.

The design and performance of a low-PIM diplexer is described. It is shown that a transmission line model may be used for the precise design of rectangular waveguide manifold diplexers which maintain the Chebyshev transfer function properties of the low-pass prototype. The use of mode matching in the final stages of realisation allows the unit to be constructed in two halves and the performance maintained without the need for tuning screws. By reducing the number of metal to metal contacts lower PIM levels can be achieved. It is shown that for two 100W carriers input to the transmit port, the 3rd order PIM level is lower than -140dBm, ie -190dBC, over a temperature range of -40deg C to +120 deg C. The variation of PIM level with both power and PIM order is presented.

The advantages of the present method are discussed. In particular, it is shown that precision designs are feasible without the need for intensive optimisation of the diplexer using mode matching, the results of which do not necessarily reproduce the desired transfer functions and can lead to increased tolerance sensitivity. Instead, the presented technique uses transmission line models until the final stage of the design process, in which all equivalent circuit elements are converted, using mode matching, into physical dimensions.

2 Introduction

Satellite communication systems commonly reduce the mass of the antenna subsystems by combining the receive and transmit functions into a single unit. This, however, requires a diplexer to perform the frequency division between the transmit and receive signals. A common solution to this requirement at Ku Band is the waveguide manifold diplexer, where two filters, transmit and receive, are connected onto a common path (figure 1). This arrangement allows the high power transmit carriers to generate intermodulation products in the receive band. These products can be at a similar power level to the received signals and can therefore pose a severe problem in systems design. Passive intermodulation (PIM) products are generated in waveguide diplexers by bad metal to metal contacts, dissimilar metal contacts, microcracks and so forth. The reduction of PIM levels is therefore dependent on the cleanliness of the surfaces and the nature of the metal contacts.

An additional problem can arise if the antenna subsystem uses multiple beams. Here the relative phase and amplitude of the different beams is of crucial importance to the antenna coverage patterns. If diplexers are used in the antenna feeds, it is essential that these diplexers do not introduce large phase and amplitude variations; the diplexers must "track" in phase and amplitude.

This paper deals with the design and performance of diplexers for a combined transmit/receive multiple beam antenna system at Ku Band. Throughout the design, emphasis was placed on the preservation of the initial Chebyshev response in order to control the sensitivity of the final unit. This allowed estimates to be made of the critical phase tracking between the different units. The

The author is with British Aerospace (Space Systems) Ltd., UK

electrical design is described and the various stages to the process outlined. The fabrication techniques, upon which the cost, tolerance and PIM performance largely depend, are described. The performance of the diplexers is given, including the critical PIM and tracking results.

3 Design Techniques

The design begins with the generation of a suitable prototype filter. Here we used doubly terminated Chebyshev function lumped low-pass prototypes. After conversion to waveguide using the usual techniques [eg 1], the response of each filter was optimised, as a transmission line equivalent circuit (Figure 2), until the Chebyshev response was restored (some small deviations from Chebyshev are inevitable in the transformation from lumped low-pass to waveguide bandpass).

These transmission line simulations of the rectangular waveguide filters were then used as starting points for the diplexer optimisation. The optimisation was performed on the equivalent circuit shown in Figure 3, the E-plane T-junction model being based on that given in Marcuvitz [2]. Initially, only the manifold and branch guide lengths of transmission line were optimised. Gradually more components were added to the optimisation until the first three resonances and couplings from each filter were modified to recover the return loss response on the manifold.

The next stage of the design process involved the realisation of transmission line elements as physical waveguide dimensions. This was accomplished using in-house modal analysis software. The analysis, at an appropriate frequency, of a symmetric, thick iris in rectangular waveguide, yields complex scattering matrix elements S11 and S21. This complex pair completely characterizes the iris at this frequency and so may be used to derive an appropriate equivalent circuit. The equivalent circuit so derived is shown in Figure 4. The shunt susceptance of the iris is symmetrically embedded in a length of waveguide. This is a significant effect due to the use of thick irises, the major result of which would be incorrect resonant frequency for each resonator.

The final stage of the design was the check on the physical dimensions by the use of modal analysis for the diplexer filters [3]. The analysis for a typical asymmetric bandpass filter of order 6 takes just under 2 seconds for each frequency point. After analysis of the diplexer components, the predicted response may be assessed and any final optimisation performed. This is usually unnecessary if the correct iris model is used for the earlier optimisation.

The predicted performance of the diplexer is shown in Figures 5 and 6.

4 Fabrication

Since the diplexers were to be tested for phase tracking in addition to the normal performance characteristics, five in total were actually manufactured. Three units were manufactured in the same fashion: machined and spark eroded in two halves from aluminium alloy, the piece parts were then silver plated and bolted together at high torque to ensure 70MPa contact pressure. From experience with other components, this pressure has been found to be sufficient to penetrate any oxide or sulphide layers on the silver plated piece parts and so minimise the PIM level. The split in each unit was along the broad wall of the filters and manifold to ensure very low electrical current across the interface. The remaining two units were electroformed. In the first instance, gold-flashed copper electroformed units were produced, the thickness of gold being sufficient only to preserve the copper from corrosion. The final diplexer was electroformed from copper and silver plated. In all cases, a high pressure, low-PIM connecting flange was provided at the common port of the diplexer.

A spark eroded diplexer is shown in Figure 7.

5 Results

The measured performance of the diplexers is given in figures 8 to 11. In all cases the measured performance closely resembles the predicted performance and proves the design technique to be efficient and accurate. Of particular interest are the measured phase tracking results. These show that even without fine tuning it is still possible to achieve phase tracking of better than 2.5 degrees.

The PIM performance of the diplexers is shown in figures 12 and 13. It is clear that the silver to silver joint on the spark eroded diplexers contributes very low PIM levels whereas the gold/copper combination produces a much higher level. Investigations into the reduction of PIM level with order and carrier power revealed a rapid roll-off characteristic (figures 14 and 15). This allows estimates of PIM levels for future diplexers to be assessed more easily and with greater justification.

6 Conclusions

It has been shown that diplexers may be designed accurately and efficiently by a combined approach using both transmission line models and the more accurate modal analysis method. The resulting precision design allows the production of phase tracking diplexers without the need for tuning screws. The silver plated diplexers have been shown to produce very low levels of 3rd order PIM, even for two 100W carriers. Additional investigations into PIM order and power roll-off have been presented and show a rapid decrease in PIM level for lower powers and higher orders.

7 References

[1] Microwave Filters, Impedance-Matching Networks, and Coupling Structures
George L. Matthaei, Leo Young, E.M.T. Jones
McGraw-Hill 1964

[2] Waveguide Handbook
N. Marcuvitz
McGraw-Hill 1951

[3] Double Plane Steps in Rectangular Waveguide and their Application to Transformers, Irises and Filters
Hartmut Patzelt and Fritz Arndt
IEEE Trans. on Microwave Theory and Techniques
Vol. MTT-30, No.5 May 1982

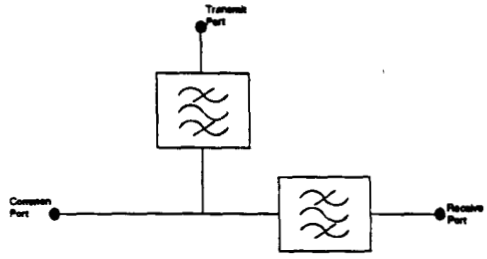

Figure 1. Diplexer Schematic

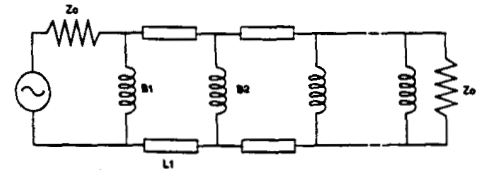

Figure 2. Equivalent Circuit of a Filter

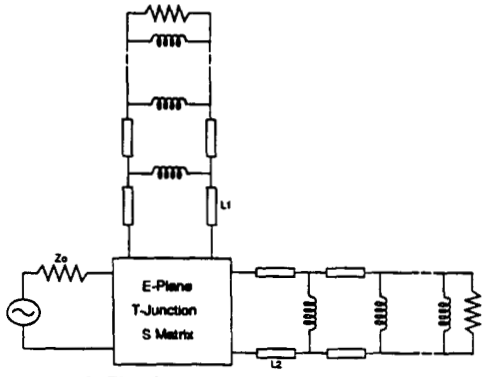

Figure 3. Equivalent Circuit of the Diplexer

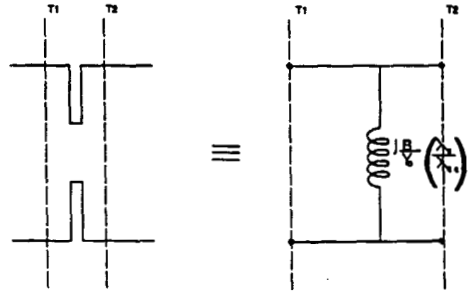

Figure 4 Equivalent Iris

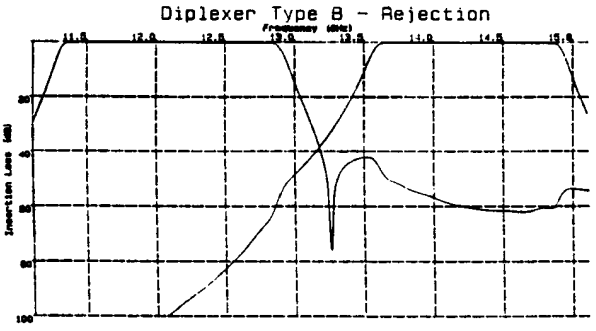

Figure 5 Computed Return Loss

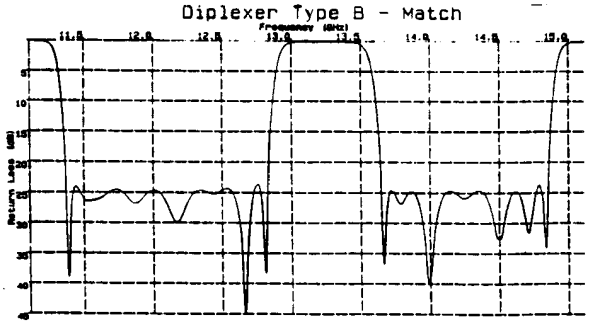

Figure 6 Computed Transmission

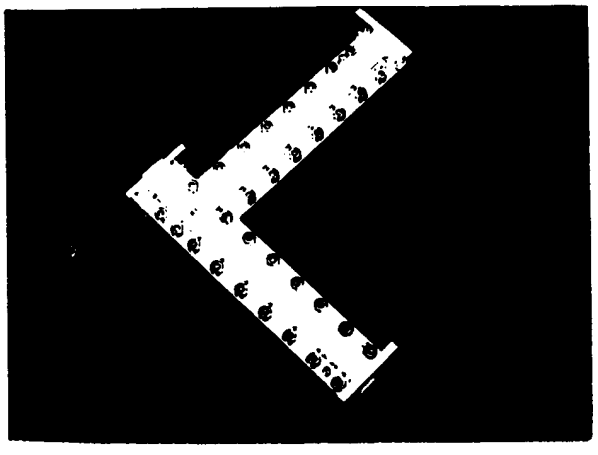

Figure 7 Photograph of a Diplexer

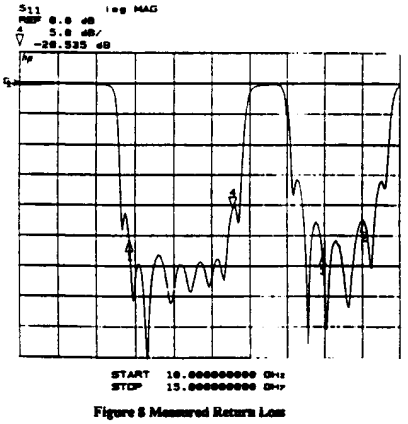

Figure 8 Measured Return Loss

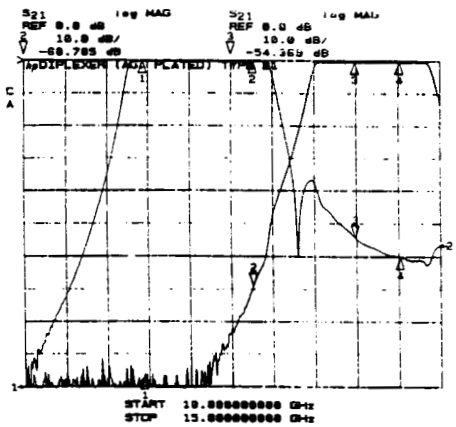

Figure 9 Measured Transmission

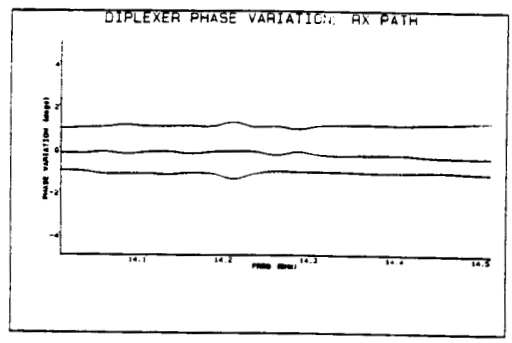

Figure 10 Rx Path Phase Tracking

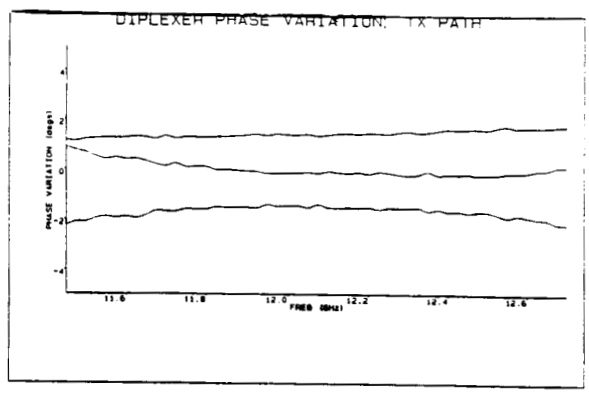

Figure 11 Tx Path Phase Tracking

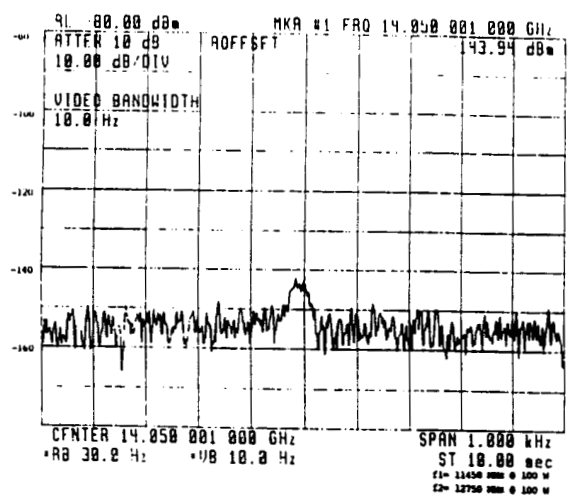

Figure 12 Measured 3rd Order PIM, 2x100W, Spark Eroded Diplexer

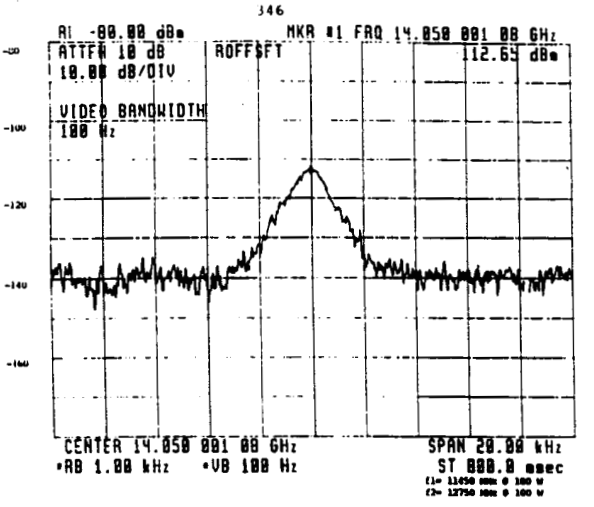

Figure 13 Measured 3rd Order PIM, 2x100W, Electroformed Diplexer

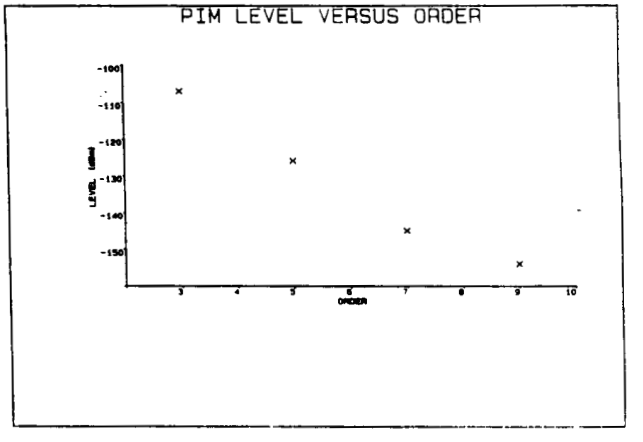

Figure 14 PIM Order Roll-off

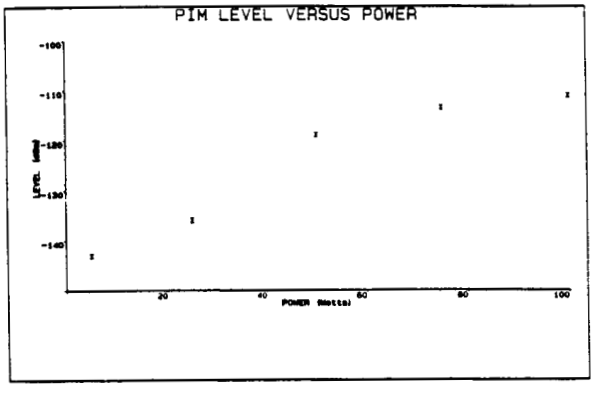

Figure 15 PIM Power Roll-off

SYNTHESIS OF NON-CONTIGUOUS DIPLEXERS USING BROADBAND MATCHING THEORY

R. Levy

Introduction

Closed-form formulas for the design of contiguous diplexers based on singly-terminated prototypes are well known, but no such formulas have been available for the Chebyshev lowpass/highpass non-contiguous diplexer prototype, as derived in this paper.

The non-contiguous diplexer consists of lowpass and highpass filters connected at a common junction, as shown in Fig. 1, which illustrates a series connection. The two filters are assumed to have Chebyshev response characteristics with all transmission zeros at the extreme frequencies , although more general cases are amenable to somewhat different treatment.

Synthesis of non-contiguous multiplexers having several narrow bandwidth channels has been described [1]. This relies on the development of the input admittance of each channel as a Taylor series expansion in a term dependent on the inter-channel spacings. The method is suitable for total bandwidths up to one octave, and is not applicable to the lowpass/highpass case.

This paper describes an approximate but very accurate analytical method based on the theory of broadband matching. Each filter is designed as a broadband matching network over its respective low or high passband, with the immittance of the other filter representing the load network to be matched. It is found that excellent results are obtained when only the first element of the "other" filter is taken into account in the load network. Good results almost to fully contiguous operation are obtained for high-degree Chebyshev lowpass/highpass diplexers.

Theory

Fig. 2 illustrates the diplexer characteristics for low and high pass filters designed using the same prototype, leading to the reciprocal relationship

$$\omega \rightarrow 1/\omega \qquad (1)$$

with equi-ripple pass band edges ω_1 and $1/\omega_1$.

When ω_1 is sufficiently small the problem is solved with acceptable results by designing independent doubly-terminated filters, but this requires $\omega_1 < 0.5$ for reasonable VSWR.
At the other extreme we have the contiguous situation which effectively defines an upper limit to ω_1 lying typically in the range .7 - .9, depending on degree n and ripple level. Here we are interested in the solution for intermediate cases.

As stated above the method is to design each filter as a matching network, with the first element of the other filter in shunt across the common port impedance representing the load network to be matched. There are two sets of conditions to be simultaneously satisfied, one for each filter.

R. Levy is a Consultant at 1897 Caminito Velasco, La Jolla, CA 92037, USA.

Consider the matching problem of Fig 3. having the closed form solution given previously [2]. Since the network has n+1 reactive elements, n for the filter and 1 for the load element due to the other channel, it is logical to modify the notation given in [3] so that the load element is g_0 and the filter elements have indices from 1 to n, leading to the formulas

$$g_0 = \frac{2\sin(\pi/2N)}{x - y} \tag{2}$$

$$g_r g_{r+1} = \frac{4 \sin(2r-1)\pi/2N \sin(2r+1)\pi/2N}{x^2 + y^2 + \sin^2 r\pi/N - 2xy\cos r\pi/N} \tag{3}$$

for

$$r = 0,1,2,.....n, \quad \text{with} \quad N = n+1 \tag{4}$$

and

$$S = (g_n/g_0).(x+y)/(x-y) \tag{5}$$

The matching network possesses an equi-ripple response with the reflection coefficient varying between

$$\rho_{max} = \frac{\cosh N\sinh^{-1}y}{\cosh N\sinh^{-1}x} \quad (6) \quad \text{and} \quad \rho_{min} = \frac{\sinh N\sinh^{-1}y}{\sinh N\sinh^{-1}x} \quad (7)$$

The value of the terminating resistance is equal to the VSWR $S = (1+\rho)/(1-\rho)$ calculated from (6) when N is even and is equal to 1/S calculated from (7) when N is odd.

In matching theory the value of the maximum pass band reflection coefficient (6) is minimized under the constraint imposed by the load network, but here we have a different set of conditions to be satisfied, namely that the reactive part of the load network is equal to that of the first element of the other channel. Referring to Fig 1, this gives the condition

$$\frac{g_0\omega}{\omega_1} = \frac{\omega\omega_1}{g_1}, \text{ i.e. } g_0 g_1 = \omega_1^2 \tag{8}$$

When the similar set of conditions are written down for the matching of the highpass filter it is found that the identical equation (8) results, as expected from the reciprocity.

Hence the desired set of g values for a given VSWR is obtained by solving for the known maximum reflection coefficient (6) under the constraint imposed by (8), i.e. there are two equations to solve for the two unknowns x and y. Actually it is necessary to modify the theory to allow for the value of the terminating resistances ($1/S_{max}$ for N even or S_{min} for N odd), noting that when we replace these by unity, the actual VSWR will increase to S_{max} for N even and to $S_{max}S_{min}$ for N odd. Thus in the case of N even we must design for a VSWR of $\sqrt{S_{max}}$, and since in practice there is little difference between S_{max} and S_{min} we use the same modified VSWR for N odd.

In the more general case when the low and high pass filters have different degrees, we will have 4 equations with 4 unknowns, readily solvable by iteration.

Results

To illustrate the utility of the method, results for 10 section non-contiguous diplexers are shown in Fig. 4 for a return

loss of 26 dB with normalized band edge parameters ω_1 of .4, .7 and .81, the latter being 98% of the contiguous case.

The return loss is practically identical to the design level almost everywhere, the only notable deterioration being to 20 dB for the almost-contiguous case. As ω_1 decreases the actual bandwidth increases, which may be corrected by compensation, and one or two of the return loss poles become suppressed.

Element values for a number of cases, including those plotted in Fig. 4, are given in Table 1, together with the doubly- and singly-terminated values for purposes of comparison. The non-contiguous design is fairly asymptotic to the singly terminated values at the high ω_1 end, but not to the doubly terminated values at the low end. The return loss of the latter is only 15 dB.

References

[1]. J. D. Rhodes and R. Levy, "A generalized multiplexer theory", IEEE Trans. on Microwave Theory and Techniques, vol. MTT-27, pp. 99-111, Feb. 1979.

[2]. R. Levy, "Explicit formulas for Chebyshev impedance-matching networks, filters and interstages", Proc. IEE Vol. 111, No.6, pp. 1099-1106, June 1964.

Table 1 Element values for diplexers

g	1	2	3	4	5	6	7	8	9	10
Doubly-term.	0.8299	1.4406	1.8280	1.7306	1.9435	1.7580	1.9132	1.6535	1.5926	0.7507
0.4	0.6379	1.0558	1.1752	1.4615	1.4130	1.6192	1.4755	1.5484	1.2596	0.7299
0.5	0.7842	1.2447	1.3369	1.6193	1.5370	1.7387	1.5707	1.6765	1.3285	0.7685
0.6	0.9228	1.3990	1.4595	1.7271	1.6209	1.8129	1.6317	1.7300	1.3695	0.7870
0.7	1.0520	1.5235	1.5525	1.8017	1.6796	1.8603	1.6726	1.7618	1.3949	0.7950
0.81	1.1841	1.6287	1.6325	1.8542	1.7278	1.8887	1.7047	1.7753	1.4092	0.7880
Contig. (0.8277)	1.2326	1.6551	1.5358	1.7060	1.5387	1.6846	1.4917	1.5706	1.2355	0.7112

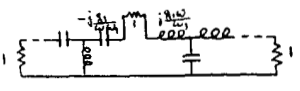

Fig. 1 Diplexer circuit

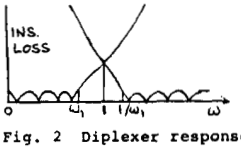

Fig. 2 Diplexer response

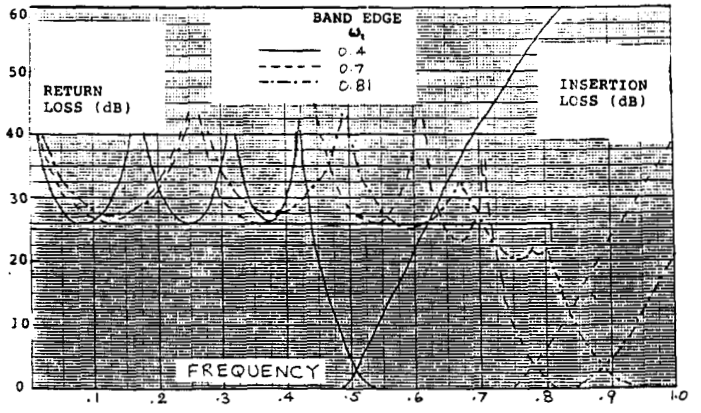

Fig. 4 Example diplexer characteristics

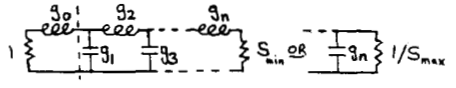

Fig. 3 Lowpass matching nework

DESIGN AND PERFORMANCE OF A W-BAND BROADBAND FINLINE DIPLEXER WITH OVER 20 GHz BANDWIDTH

Cam Nguyen and Kai Chang
TRW
One Space Park
Redondo Beach, CA 90278

ABSTRACT

This paper describes the design and performance of a contiguous 90- to 112-GHz diplexer using the integrated finline technique. State-of-the-art results of 1.5 dB insertion losses have been achieved. There is good agreement between the experimental results and those predicted theoretically; these results demonstrate a significant technological advance of millimeter-wave multiplexers using printed circuit techniques. Results of an extremely wideband H-plane tee with a VSWR of less than 1.4 over the full W-band (75 to 110 GHz) are also presented.

INTRODUCTION

Rapidly increasing activities in millimeter-wave receiver technology have created strong interest in the development of wideband, low cost, low loss diplexers. Recently, a W-band narrowband non-contiguous diplexer with a guard band of 4 GHz was reported(1). Wideband contiguous diplexers are required for most practical channelized downconverters. This paper presents the design and performance of a contiguous broadband diplexer (90 to 112 GHz) using the integrated finline technique. Excellent results have been obtained with insertion losses of 1.5 dB in the 90- to 101-GHz channel, and 1.7 dB in the 101- to 112-GHz channel. The use of printed circuits offers the advantages of light weight, small size, and good reproducibility.

An H-plane tee plays an important role in the diplexer design; the broadband matching of this component has been difficult to achieve, especially at millimeter-wave frequencies. In this paper, an extremely broadband H-plane tee is reported over the 75- to 110-GHz range with more than 15 dB return loss.

DIPLEXER ANALYSIS

In this section, the scattering matrix for the diplexer will be determined in terms of the S-matrices of individual components based on the multiport connection method(2). The diplexer shown in Figure 1 consists of two finline bandpass filters located in the two sidearms of an H-plane tee. A block diagram of the diplexer is illustrated in Figure 2.

Two-port networks A and B, representing channels A and B, respectively, consist of finline bandpass filters in cascade with waveguides as shown in Figure 3. $A_1(B_1)$ and $A_2(B_2)$ are dielectric-slab-loaded waveguides of lengths $\theta_{A1}(\theta_{B1})$ and $\theta_{A2}(\theta_{B2})$, respectively. $A_3(B_3)$ and $A_4(B_4)$ are empty or dielectric-slab-loaded waveguides of lengths $\theta_{A3}(\theta_{B3})$ and $\theta_{A4}(\theta_{B4})$, respectively, and $F_A(F_B)$ is a finline bandpass filter, characterized by a scattering matrix $S^{FA}(S^{FB})$. The analyses of these filters are well established(3,4). Three-port component C, characterized by a scattering matrix S^C, stands for an H-plane tee-junction, and two-port component D, characterized by S^D, represents the main waveguide of length θ_D. The scattering matrix of the two-port component K (K stands for A or B) is given by

$$S^K = \begin{bmatrix} S_{11}^{FK} e^{-2j(\theta_{K1}+\theta_{K3})} & S_{12}^{FK} e^{-j(\theta_{K1}+\theta_{K2}+\theta_{K3}+\theta_{K4})} \\ S_{12}^{FK} e^{-j(\theta_{K1}+\theta_{K2}+\theta_{K3}+\theta_{K4})} & S_{11}^{FK} e^{-2j(\theta_{K2}+\theta_{K4})} \end{bmatrix}$$

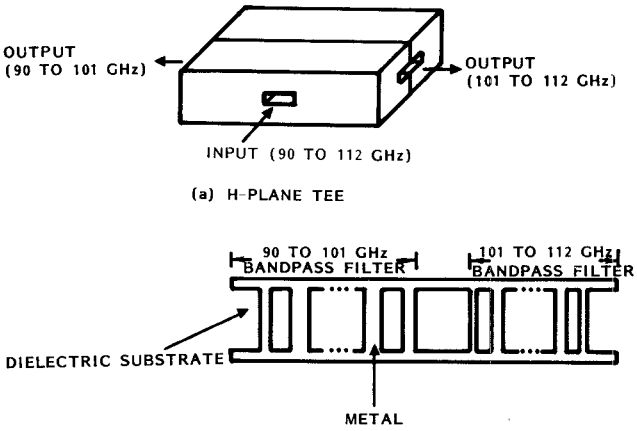

Figure 1. Finline diplexer.

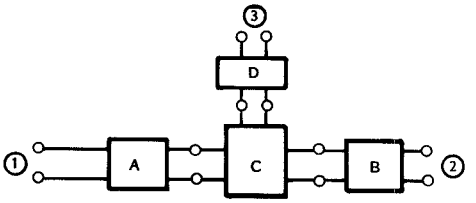

Figure 2. Block diagram of diplexer.

0149-645X/85/0000-0349

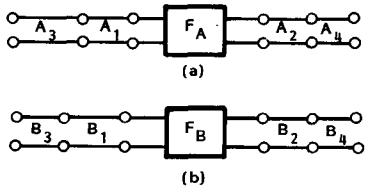

Figure 3. Schematic of (a) network A (b) network B.

The scattering matrix, S, of the diplexer can now be obtained by applying the multiport connection method(2) to the diplexer network considered in Figure 2, and is given by

$$S = S_{pp} + S_{pc}(\Gamma - S_{cc})^{-1} S_{cp}$$

where

$$S_{pp} = \begin{bmatrix} S_{11}^{A} & 0 & 0 \\ 0 & S_{22}^{B} & 0 \\ 0 & 0 & S_{22}^{D} \end{bmatrix}$$

$$S_{pc} = \begin{bmatrix} S_{12}^{A} & 0 & 0 & 0 & 0 & 0 \\ 0 & 0 & 0 & 0 & S_{21}^{B} & 0 \\ 0 & 0 & 0 & 0 & 0 & S_{21}^{D} \end{bmatrix}$$

$$S_{cp} = \begin{bmatrix} S_{21}^{A} & 0 & 0 \\ 0 & 0 & 0 \\ 0 & 0 & 0 \\ 0 & 0 & 0 \\ 0 & S_{12}^{B} & 0 \\ 0 & 0 & S_{12}^{D} \end{bmatrix}$$

$$S_{cc} = \begin{bmatrix} S_{22}^{A} & 0 & 0 & 0 & 0 & 0 \\ 0 & S_{11}^{C} & S_{12}^{C} & S_{13}^{C} & 0 & 0 \\ 0 & S_{21}^{C} & S_{22}^{C} & S_{23}^{C} & 0 & 0 \\ 0 & S_{31}^{C} & S_{32}^{C} & S_{33}^{C} & 0 & 0 \\ 0 & 0 & 0 & 0 & S_{11}^{B} & 0 \\ 0 & 0 & 0 & 0 & 0 & S_{11}^{D} \end{bmatrix}$$

and

$$\Gamma = \begin{bmatrix} 0 & 1 & 0 & 0 & 0 & 0 \\ 1 & 0 & 0 & 0 & 0 & 0 \\ 0 & 0 & 0 & 0 & 1 & 0 \\ 0 & 0 & 0 & 0 & 0 & 1 \\ 0 & 0 & 1 & 0 & 0 & 0 \\ 0 & 0 & 0 & 1 & 0 & 0 \end{bmatrix}$$

DIPLEXER DESIGN AND PERFORMANCE

The finline bandpass filters used in the diplexer were seven-pole, 0.1-dB ripple Chebyshev filters, and were realized on a 0.127-mm (0.005-in.) thick Duroid substrate. These filters can be analyzed individually using the technique described in (3). For the H-plane tee, tremendous reflections occur when power is sent toward the junction from any of the three arms because of the severe geometrical discontinuities characterizing each junction. These reflections may be reduced or substantially eliminated by the incorporation within the junction of suitable reactance, such as metal rods or plates. If these tuning elements are disposed in a sufficiently symmetrical manner, the original shunt character of the junction can be preserved. The H-plane tee used in the diplexer has been matched by using a cylindrical post located in a symmetrical plane inside the junction. The measured return losses at the common port and insertion losses from this port to sidearm ports are shown in Figures 4 and 5. In Figure 4, the curves show the return loss at the common port before and after the matching device was added. An insertion loss of 0.5 dB and VSWR of less than 1.4 over the 75- to 110-GHz frequency range have been achieved. It can be seen that an extremely good balance has been obtained for the junction. A cross-section of the matched H-plane tee is illustrated in Figure 6. The same technique can also be used to design very wideband H-plane tees in other frequency bands. The diplexer was constructed using two finline bandpass filters and the H-plane tee. The performance of the diplexer is shown in Figure 7. Insertion losses of 1.5 and 1.7 dB were achieved in the 90- to 101-GHz and 101- to 112-GHz channels, respectively. The measured band-edge frequencies of any channel are within 1 percent of the crossover frequency. Stopband attenuation of more than 25 dB apart from 0.8 and 1.3 percent of the crossover frequency for the higher and lower channels, respectively, has been achieved. Good agreement between the measured and calculated results has also been observed. A photograph of the diplexer is shown in Figure 8.

CONCLUSIONS

The design and performance of a W-band broadband (90 to 112 GHz) finline diplexer have been presented with state-of-the-art results. An extremely wideband (75 to 110 GHz) H-plane tee has also been

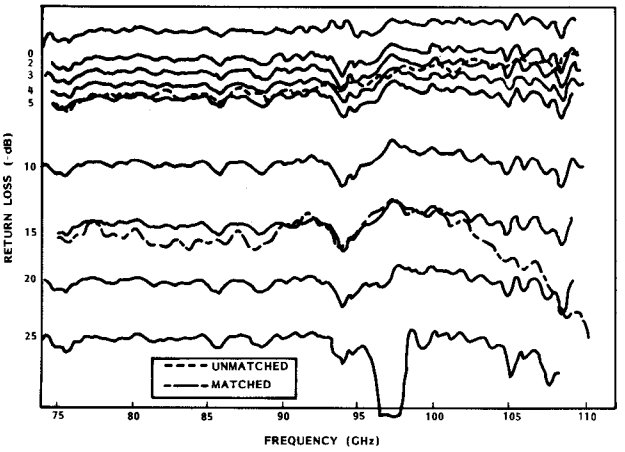

Figure 4. Measured return loss at common port of an H-plane tee.

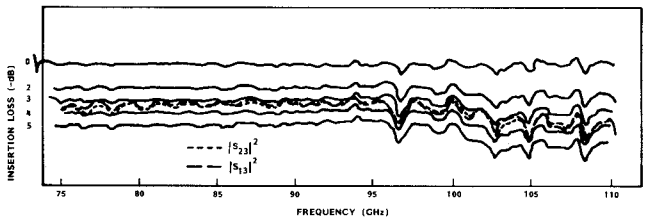

Figure 5. Measured insertion losses from common port to sidearm ports.

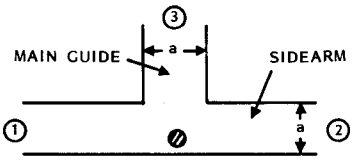

Figure 6. Cross-section of matched H-plane tee.

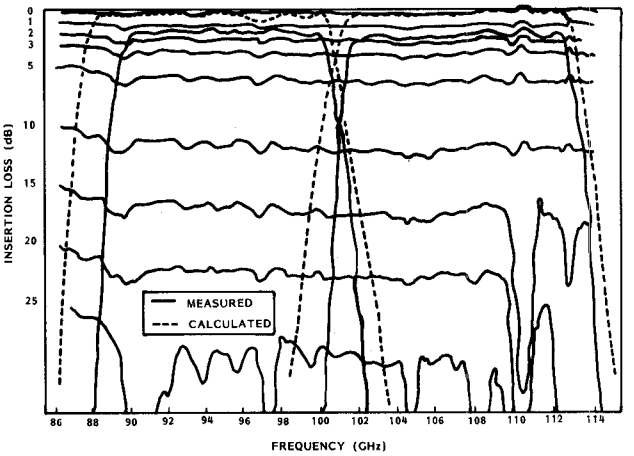

Figure 7. Transmission loss response of diplexer.

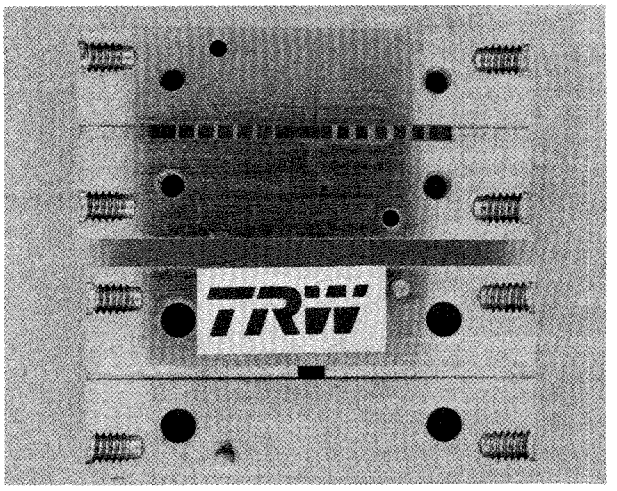

Figure 8. Photograph of diplexer.

developed. The results represent a significant advance in the development of low cost, low loss diplexers. The diplexer together with other high performance broadband components(5) demonstrate the practicality of wideband, high performance, low cost millimeter-wave channelized receivers.

REFERENCES

1. L. D. Cohen, N. Worontzoff, J. Levy, and A. Harvey, "Millimeter Wave Multiplexer with Printed Circuit Elements for the 88- to 100-GHz Frequency Range," IEEE 1984 MTT-S Int. Microwave Symposium Digest, pp. 233-235.

2. V. A. Monaco and P. Tiberio, "Computer-Aided Analysis of Microwave Circuits," IEEE Trans. Microwave Theory Tech., Vol. MTT-22, No. 3, pp. 249-263, Mar. 1974.

3. Y. C. Shih, T. Itoh, and L. Q. Bui, "Computer-Aided Design of Millimeter-Wave E-Plane Filters," IEEE Trans. Microwave Theory Tech., Vol. MTT-31, No. 2, pp. 135-141, Feb. 1983.

4. F. Arndt et al., "Low-Insertion-Loss Finline Filters for Millimeter Wave Applications," 11th European Microwave Conference, Amsterdam, The Netherlands, Sept. 7-10, 1981, pp. 309-314.

5. R. S. Tahim, G. M. Hayashibara, and K. Chang, "Design and Performance of W-band Broadband Integrated Circuit Mixers," IEEE Trans. Microwave Theory Tech., Vol. MTT-31, pp. 177-183, Mar. 1983.

WAVEGUIDE AND RIDGE WAVEGUIDE T-JUNCTIONS FOR WIDE BAND APPLICATIONS

Hui-Wen Yao, Amr Abdelmonem, Ji-Fuh Liang
Xiao-Peng Liang and Kawthar A. Zaki

Electrical Engineering Department
University of Maryland
College Park, MD. 20742

Alain Martin

Mitec Electronics Ltd.
104 Gun Avenue, Pointe Claire, QC, Canada H9R 3X3

R

ABSTRACT

Scattering parameters of waveguide and ridge waveguide stepped T-junctions are obtained using an extension of the three plane mode matching method [1]. An optimization process is applied to find the T-junctions and steps dimensions that yield low reflection coefficient in one of the T-junction arms over a wide frequency band. The optimized wide band T-junctions are useful in the design of wide band high power dividers, diplexers and multiplexers. An example of the design of a wide band T-junction diplexer is presented. Experimental results on the optimized T-junction and the T-junction diplexer are presented. The experimental results of both the T-junction and the diplexer showed excellent agreement with their computed optimum results, respectively.

I. INTRODUCTION

Waveguide T-junctions are important components in many microwave applications. Since these junctions are lossless reciprocal three ports, all three ports cannot be matched simultaneously. However, in some applications [2], it is desirable to have the T-junction with one of its ports well matched over a reasonable wide frequency band. This paper extends the three plane mode matching method [1] to the analysis and optimization of stepped waveguides and ridge waveguides T-junctions, to achieve wide bandwidth match of one of the ports. The optimized T-junctions are used in the design of a wide bandwidth, low loss, high power diplexer. The diplexer filters are waveguide inductive iris type filters. The theoretical performance of the optimized T-junctions computed using mode matching is verified experimentally. Using the optimized T-junction, a network model of the diplexer with two inductive iris filters is developed. The filter iris are analyzed rigorously by mode matching and their S-parameters are used in the network model to optimize the wide band diplexer performance. Results of the computed optimized diplexer response and the measured diplexer response are presented. The two responses agreed remarkably without further adjustment.

II. STEPPED WAVEGUIDE AND RIDGE WAVEGUIDE T-JUNCTIONS

Fig. 1-a and Fig. 1-b show stepped E-plane T-junctions for waveguide and ridge waveguide, respectively.

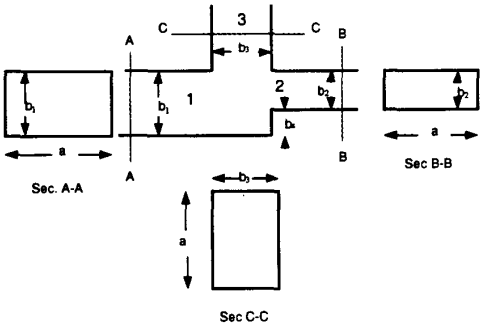

Fig. 1-a Stepped E-plane waveguide T-junction

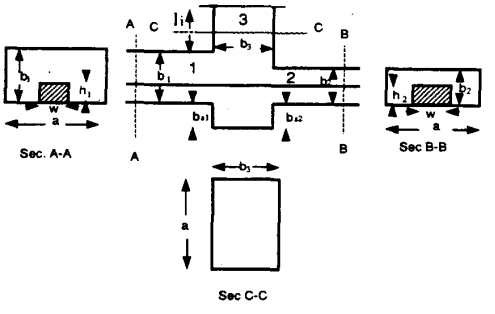

Fig. 1-b Stepped E-plane ridge waveguide T-junction

CH3277-1/93/0000-0601$01.00 © 1993 IEEE

Each of these two junctions can be analyzed using the three plane mode matching method [1]. In this method the three port scattering matrix of the T-junction is determined from three 2-port scattering matrices computed (or measured) by placing three different lengths of short circuit lines in port 3 of the T-junctions. The resulting two port structures are treated as three lengths of different cross sections of uniform waveguides (or ridge waveguides), and their scattering matrices are easily determined using mode matching. For the case of the ridge waveguide the appropriate ridge waveguide modes must first be found for each of the three regions 1, 2 and 3, and used in the analysis. Note that the center region in Fig. 1-b with the short circuit in port 3 will also be a ridge waveguide with cross section $a \times (b_1 + b_{s1} + \ell_i)$, where ℓ_i are the distances of the short circuits from port 3 reference plane, length b_3, and ridge cross section $w \times h$.

The optimum T-junctions will have minimum reflections in port 1 over the widest possible frequency band, while the powers to ports 2 and 3 are divided equally. To optimize the T-junction dimensions, the S-parameters are computed as a function of frequency with b_2 and b_3 as parameters. Fig. 2 shows the computed S-parameters of

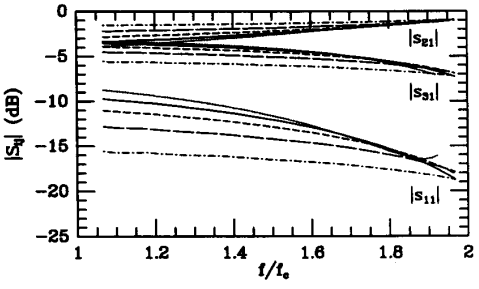

Fig. 2. S-parameters of E-plane T-junction for different b_3 with b_1/a = b_2/a = 0.5 and b_s/a = 0

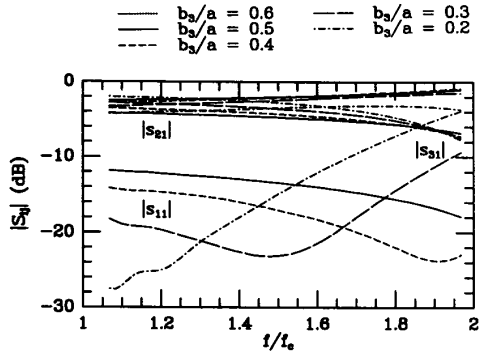

Fig. 3. S-parameters of E-plane T-junction for different b_2 with b_1/a = 0.5, b_3/a = 0.35, $(b_2+b_s)/a$ = 0.5

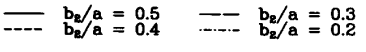

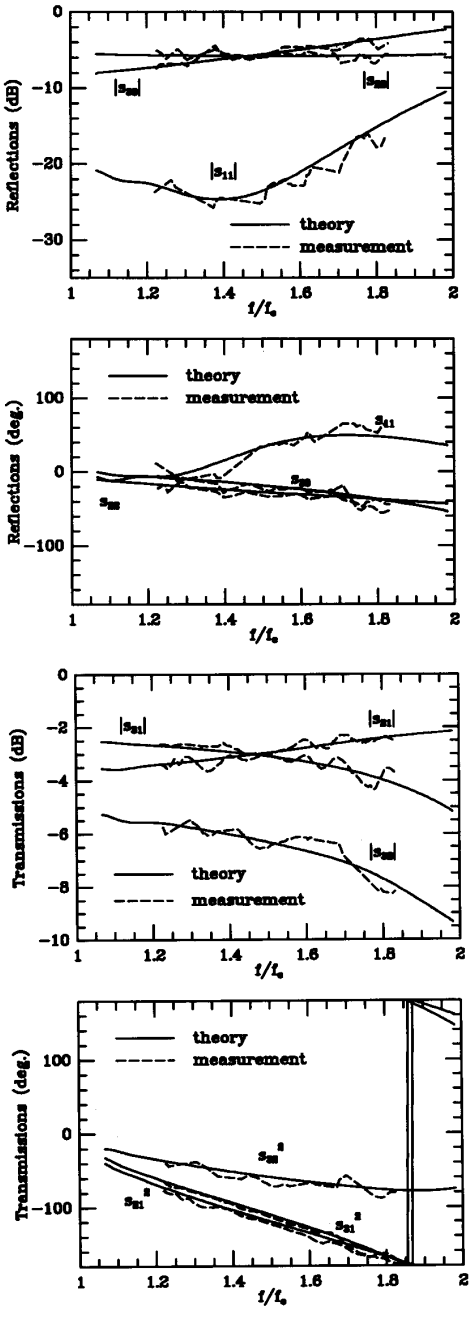

Fig. 4. Measured results of an E-plane T-junction with optimized dimensions compared with theory. T-junction dimensions: a=0.9", b_1=0.4", b_2=0.21", b_3=0.275", b_s=0.19"

an E-plane T-junction without step in the straight arm. As the width b_3 of port 3 is reduced, the reflection coefficient in port 1 decreases, while the transmission to ports 2 and 3 from port 1 become less frequency sensitive, but unequal. Fig. 3 shows the computed S-parameters with the step height (or b_2) as a parameter, for a fixed b_3. As seen in Fig. 3, with the increase of the step height, more power is forced into port 3, and the reflection in port 1 decreases over the band, then starts to increase again, particularly at higher frequencies. This implies that their is an optimum dimension for the junction over the frequency band of interest. This optimum was obtained using simple search process of the variables b_2 and b_3. The computed and measured results for the optimum junction are shown in Fig. 4. The measured results were obtained by using three short circuits of different lengths on both ports 2 and 3, and measuring the reflection coefficient in port 1 as a function of frequency 9 times. The complete scattering matrix elements of the T-junction were extracted from these measurements.

A similar process was used for the ridge waveguide T-junction and the results are shown in Fig. 5 and Fig. 6. Note that the bandwidth for the optimum ridge waveguide stepped T-junction is wider than the regular waveguide case.

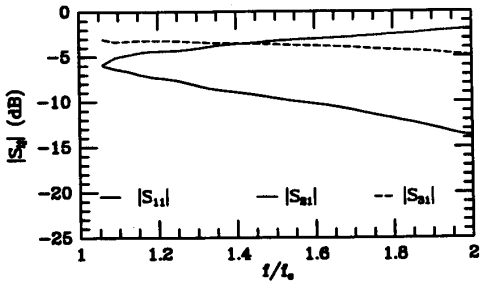

Fig. 5 Ridged waveguide T-junction charectaristics before optimization with a1=1.872, $b_1=b_2=b_3=0.872$ $b_{s1}=b_{s2}=0.0$, $h_1=h_2=0.4$

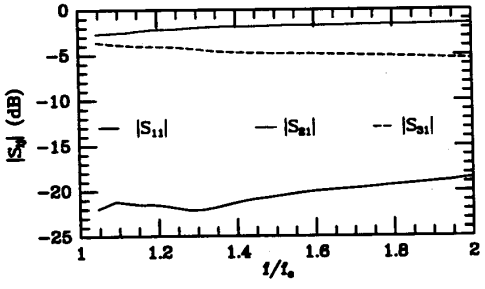

Fig. 6 Optimized ridged waveguide T-junction charectaristics with a1=1.872, $b_1=0.672, b_2=0.672$, $b_3=0.2$, $b_{s1}=0.2$, $b_{s2}=0.0$, $h_1=0.2$, $h_2=0.4$

III. DIPLEXER MODELING AND OPTIMIZATION

Typical requirements of a broad band diplexer is given in Table 1. Broad band diplexers using snaked stripline and printed circuit elements were reported in [3]-[5]. These types of diplexers provide less than 15 dB pass band return loss, have relatively high insertion loss and cannot handle high power. To achieve the high quality requirements, waveguide type diplexers are the most suitable configuration. Previous waveguide diplexers reported in [6]-[7] are narrow band.

Table 1. Broad-band Diplexer Requirements

Parameter	Requirements
Channel 1 pass band	3.52-4.2 GHz
Channel 2 pass band	4.35-5.0 GHz
Min. pass band return loss	>22 dB
Max. pass band insertion loss	0.25 dB
Min. pass band insertion loss (Ch. 1)	> 20 dB from 4.35-5.0 GHz
Min. pass band insertion loss (Ch. 2)	> 20 dB from 3.52-4.2 GHz
Power handling capability (C.W.)	Min. 1 K.W. for each Channel

The diplexer considered here consists of two band pass filters connected to ports 2 and 3 of the optimized T-junction whose response is shown in Fig. 7. Initial filters designs were chosen as inductive iris, doubly terminated, .01 dB ripple Tchebycheff filters of orders 13 and 9. The channel filters are modeled by their S-parameters. These S-parameters are computed by cascading the S-parameter matrices of each individual inductive window and the lengths of waveguides forming the resonators. The S-parameters of inductive windows are computed by mode matching. The reflection and transmissions of the diplexer are computed by cascading the S-parameters of the filters and the T-junction

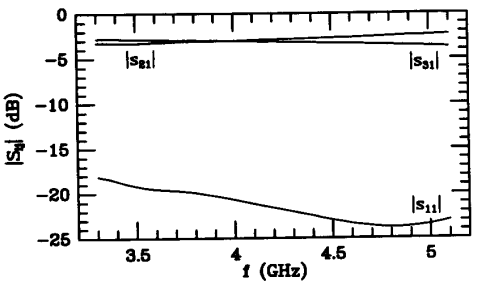

Fig. 7. S-parameters of E-plane T-junction used for the C-band diplexer. a = 1.872 inch, b_1 = 0.872 inch, b_2 = 0.522 inch, b_3 = 0.6 inch

All inductive window widths and cavity lengths of both filters are optimized. The objective function used in the optimization is a weighted least square sums of the deviation of the return loss and isolation from their specified values. Fig. 8 shows the optimized diplexer response, while Fig. 9 gives the measured diplexer response.

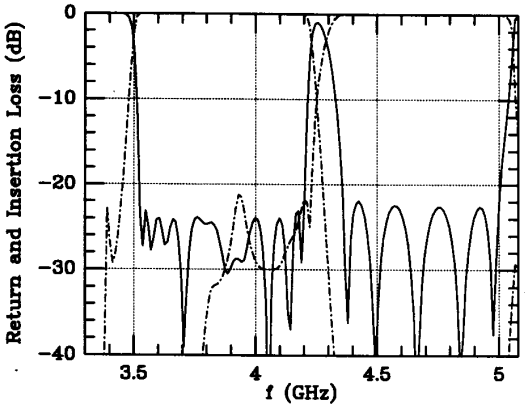

Fig. 8. Designed results of the C-band diplexer

—— Return loss -·-·- Insertion Loss

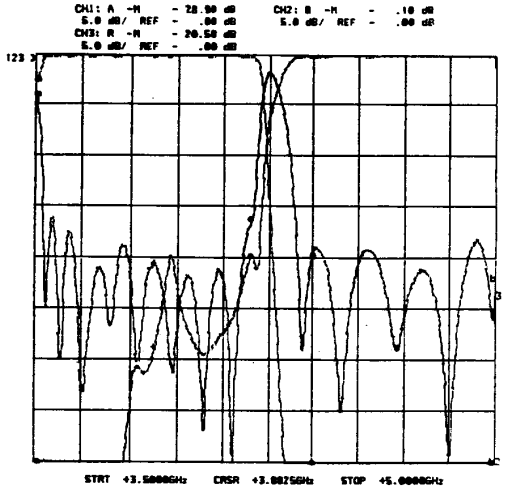

Markers

No.	Frequency (Hz)	Chan. 1 (dB)	Chan. 2 (dB)	Chan. 3 (dB)
1	3.5E+09	- 42.708	- 2.568	- 3.975
2	4.197SE+09	- 19.834	- .239	- 16.159
3	4.399999E+09	- .096	- 46.584	- 19.614
act	4.999999E+09	- .062	- 48.491	- 21.965

Couplers

1	3.8825E+09	- 28.898	- .096	- 28.581

Fig. 9. Measured response of the C-band diplexer

IV. CONCLUSION

A procedure for the design of E-plane wide band T-junction diplexers is described. The properties of E-plane waveguide and ridge waveguide step T-junctions are analyzed. A wide band 3 dB T-junction which is an important component in the design of the wide band diplexer is optimized and verified by measurement. An optimization model for the wide band diplexer is implemented. Using this model, a C-band T-junction waveguide diplexer with total 31% band width and return loss better than 22 dB in pass bands is designed.

Acknowledgment

The authors would like to thank Dr. A.M.K. Saad of Scientific Microwave Corp., Ontario, Canada, for his valuable suggestions and participation in this project.

REFERENCES

[1] X. -P. Liang, K. A. Zaki, and A. E. Atia, "A rigorous three plane mode-matching technique for characterizing waveguide T-junctions, and its application in multiplexer design," *IEEE Trans. Microwave Theory Tech.*, vol. MTT-39, pp. 2138-2147, December 1991.

[2] F. Arndt, I.Ahrens, U. Papziner, U. Wiechmann, and R. Wilkeit, "Optimized E-plane T-junction series power dividers," *IEEE Trans. Microwave Theory Tech.*, vol. MTT-35, pp. 1052-1059, Nov. 1987.

[3] M. Miyazaki, H. Asao, and O. Ishida, "A broad dielectric diplexer using a snaked strip-line," *1991 IEEE MTT-s Dig.*, pp.551-554.

[4] C. Nguyen and K. Chang, "W-band wideband low loss planar integrated circuit diplexer," *Microwave J.*, vol. 28., pp. 157-161, July 1985.

[5] Y.-C. Shih, L. Q. Bui, and T. Itoh, "Millimeter-wave diplexers with printed circuit elements," *IEEE Trans. Microwave Theory Tech.*, vol. MTT-33, pp. 1465-1469, December 1985.

[6] J. Dittloff and F. Arndt, "Computer-aided design of slit-coupled H-plane T-junction diplexers with E-plane metal-insert filters," *IEEE Trans. Microwave Theory Tech.*, vol. MTT-36, pp. 1833-1840, December 1988.

[7] J. L. Haine and J. D. Rhodes, "Direct design formulas for asymmetric bandpass channel diplexers," *IEEE Trans. Microwave Theory Tech.*, vol. MTT-25, pp. 807-814, Oct. 1977.

Direct Synthesis of General Chebyshev Bandpass Filters with A Frequency Variant Complex Load

Meng Meng and Ke-Li Wu

Department of Electrical Engineering, the Chinese University of Hong Kong, Hong Kong, PRC

***Abstract* — This paper presents a direct approach to the synthesis of a general Chebyshev coupled resonator filter with a frequency variant complex load. The new approach is based on the power wave renormalization of admittance parameters of a matched filter with a complex load to unitary load. When the port reference is changed from a complex load to a real load, a set of new expressions of admittance parameters can be obtained for the same filter. By introducing a piece of dispersive transmission line to the original matched filter, the poles of the original admittance parameters are retained, which greatly facilitates the extraction of the new admittance parameters, and consequently the synthesis of the coupling matrix. The approach is applicable to the synthesis of an optimal channel filter of a diplexer and a multiplexer, where the load presented at a port of the filter is a frequency variant complex load in a wide frequency range.**

***Index Terms* — Microwave filters, filter synthesis, diplexer, Chebyshev filter, impedance matching**

I. INTRODUCTION

Frequency division multiplexing (FDM) is the most popular architecture in communication systems for channel division. To implement an FDM system, filters are always integrated with a manifold or a T-junction to form a multiplexer and diplexer. The most practical technique of designing such FDM system starts from the synthesis of the filter circuit models whose electric performances in the content of a multiplexer or diplexer meet the design requirement. Such filter synthesis still largely depends on non-linear optimization and manually tuning based on human experience. Although directly synthesizing of a general Chebyshev filter is a straightforward process, the direct synthesis of a multiplexer or a diplexer remains challenging.

Most of design techniques for multiplexers are based on the theory of singly terminated filters [1]. The theory provides a general solution to the design of contiguous multiplexer. Using this theory, filters are first designed as singly terminated ones and then tuned to meet the requirements concerning the matching condition and the crossover between channels.

Once the manifold and the stub length connecting each filter to the manifold is designed by trading off the return loss and the isolation, as well as suppressing the spurious modes, the reminding task in designing a multiplexer is the design of a circuit model for each channel filter [2]. Designing a channel filters involves optimization of the circuit model to meet the requirements of matching and separation [3]. The most employed approach used in the industry today still relies on non-linear optimization, by which the manifold dimension and channel filter models are adjusted in the same time [4]. The research efforts for more effective design approach never stops. For instance, a new design approach by optimizing the rational polynomial expressions of a diplexer was presented in [5]. Nevertheless, an ultimate approach of designing channel filters in a multiplexer and diplexer would be a direct approach so that the design process would be deterministic and the solution would be optimal in certain sense.

The objective of this work is to find a direct approach to the design of a channel filter while the manifold is presented as a complex load. Considering the complex loading effects gains a new perspective of designing a channel filter [6]. In fact, the rational polynomials for a matched filter, which define the reflection and transfer functions, are virtually referenced to two matched impedances of any values. Using the theory of power wave renormalization [7], the fundamental polynomial functions with a presumed matched complex load can be renormalized to a new set of polynomials with real unitary load at both filter ports, so that the existing direct synthesis techniques can still be employed. However, the new concept proposed in [6] was only explored for the case in which only a constant complex load at the centre frequency was considered. Although the implementation is straight forward, its applications are restricted to a very narrowband case.

In this paper, the concept of complex load is reinvestigated from different angle for more practical case, in which the complex reference impedance (load) will be a function of frequency over a wide band of frequency. Instead of only matching to constant complex impedance, the variation of the complex impedance vs. frequency is also taken into consideration in the proposed approach. It will be seen that by equivalently adding a piece of dispersive transmission line to the original filter prototype, designing a matched filter with a frequency variant complex load becomes a simple matter of determining a polynomial of n-th order by curve-fitting a designated behavior over the frequency band of interest.

II. ADMITTANCE PARAMETERS SYNTHESIS

In designing a channel filter for a multiplexer, the reference impedance at the port connecting to the manifold junction can

be regarded as a frequency variant complex load, whereas the load at the other port is unitary impedance associated to the matched transmission line connected to the filter as shown in Fig. 1. The work presented in [6] shows that when a channel filter is detached from the junction, the reference impedance at the detached port should be amended to the same characteristic impedance as that of the other port. When the frequency band of interest is narrow, the complex impedance at center frequency can be used to represent the condition of entire pass band.

Fig. 1. A filter network connecting to complex load Z_L

Assuming that the scattering matrix [S] of a 2-port filter network is given, the scattering matrix is referenced with the unitary impedance at port 1 and ZL at port 2, respectively. If the referenced impedances at port 2 is changed from ZL to the unitary load, the new scattering matrix [S'] can be expressed in terms of the original [S] and the reflection coefficient.

It is shown in [6] that a constant complex load can lead to a new set of rational polynomials for [S'] of the same order. For frequency variant load, obtaining the explicit polynomials of the same orders for [S'] is impossible for all the frequencies. Since the rational polynomial expressions of the same orders can be obtained by least square fitting of the numerical values of [S'] over a certain frequency band, a direct coupling matrix synthesis can be done in a limited frequency band with an approximated rational polynomials of [S'].

The renormalization of S-parameters with respect to another reference impedance is analogous to observing a system with a different angle, as the filter network itself is unchanged. The admittance matrix of a filter network is independent to the impedance reference. Suppose the S-parameters of a matched filter, whose reference impedances of ports 1 and 2 are unitary and Z_L respectively, is known, the intrinsic admittance parameters can be found by

$$y'_{11} = \frac{(1-s_{11})(Z_L^* + Z_L s_{22}) + Z_L s_{21}^2}{(1+s_{11})(Z_L^* + Z_L s_{22}) - Z_L s_{21}^2} \quad (1a)$$

$$y'_{22} = \frac{(1+s_{11})(1-s_{22}) + s_{21}^2}{(1+s_{11})(Z_L^* + Z_L s_{22}) - Z_L s_{21}^2} \quad (1b)$$

$$y'_{21} = \frac{-2\sqrt{\mathrm{Re}(Z_L)}s_{21}}{(1+s_{11})(Z_L^* + Z_L s_{22}) - Z_L s_{21}^2} \quad (1c)$$

As the S parameters of a general Chebyshev filter can be expressed by the fundamental polynomials as,

$$s_{11} = \frac{F_{11}(s)}{\varepsilon_R E(s)}, \quad s_{21} = \frac{P(s)}{\varepsilon E(s)}, \quad \text{and } s_{22} = \frac{F_{22}(s)}{\varepsilon_R E(s)} \quad (2)$$

using the equality of $F_{11}(s)\cdot F_{22}(s) + P(s)\cdot P^*(s) = E(s)\cdot E^*(s)$ of the fundamental polynomials for lossless filters, the admittance parameters can be found by:

$$y'_d = (E(s) + F_{11}(s))Z_L^* + \left((E(s) + F_{11}(s))Z_L^*\right)^* \quad (3a)$$

$$y'_{11n} = (E(s) - F_{11}(s))Z_L^* - \left((E(s) - F_{11}(s))Z_L^*\right)^* \quad (3b)$$

$$y'_{22n} = (E(s) - F_{22}(s))Z_L^* - \left((E(s) - F_{22}(s))Z_L^*\right)^* \quad (3c)$$

$$y'_{21n} = -2\sqrt{\mathrm{Re}(Z_L)}P(s) \quad (3d)$$

When the load impedance is frequency variant, the degrees of the new polynomials in (3) must be higher than those of the original ones. It means that it is impossible to find a coupling matrix of the same order that matches to the frequency variant complex load at all the frequencies. However, in a practical design, people are only interested in a good matching is a finite frequency band of interest. That is to say, if a set of polynomials of the same orders for the admittance parameters can be found in a certain frequency band through (3), by imposing legitimate constrains over the parameters, the coupling matrix of a channel filter with a complex load can be directly synthesized using existing techniques.

III. MODIFIED ADMITTANCE PARAMETERS

It is know that the filter response is very sensitive to its eigen-values and the eigen-values are determined by the system poles. If the polynomial fitting of (3) is done in a finite frequency band, the obtained poles may have multiple solutions. Some of the solutions come with unreasonable eigen-values, such as the number of poles does not match or the value of a pole is an extreme value, which lead to an unrealizable filter coupling matrix. In order to preserve the original eigen-values of the filter that is presumably matched to a frequency variant complex load and are determined by required filter specifications, a modification of admittance parameters needs to be made. For a Chebyshev filter matched to a complex load, its fundamental polynomials $E(s)$, $F_{11}(s)$, $F_{22}(s)$ and $P(s)$ can be modified by

$$E_m(s) = E(s)/Z_L^*(s) \quad (4a) \qquad F_{m11}(s) = F_{11}(s)/Z_L^*(s) \quad (4b)$$

$$F_{m22}(s) = F_{22}(s)/Z_L(s) \quad (4c) \qquad P_m(s) = P(s)/\left|Z_L(s)\right| \quad (4d)$$

Note that the modification above is equivalent to adding a piece of dispersive transmission line at port 2, therefore, for the modified polynomials, the equality of

$$F_{m11}(s)\cdot F_{m22}(s) + P_m(s)\cdot P_m^*(s) = E_m(s)\cdot E_m^*(s) \quad (5)$$

is still satisfied. Using the modified polynomials, the modified admittance parameters, which corresponds to the original matched filter with an extra piece of dispersive transmission line at port 2, are obtained as follows:

$$y'_{md} = \left(E(s) + F_{11}(s)\right) + \left(E(s) + F_{11}(s)\right)^* \quad (6a)$$

$$y'_{m11n} = \left(E(s) - F_{11}(s)\right) - \left(E(s) - F_{11}(s)\right)^* \quad (6b)$$

$$y'_{m22n} = \left(E(s)/Z_L^* - F_{22}(s)/Z_L\right) - \left(E(s)/Z_L^* - F_{22}(s)/Z_L\right)^* \quad (6c)$$

$$y'_{m21n} = -2\sqrt{\mathrm{Re}(Z_L)}P(s)/|Z_L| \quad (6d)$$

The benefits of the above modified admittance parameters are obvious. If (3) was used, one would need to curve-fit all the polynomials by n-th degree polynomials in general when frequency variant complex load is presented. There is no warranty that all the poles of the admittance parameters obtained with (3) exhibit good sense. On the other hand, it can be seen that the modified admittance parameters have the same poles as those of the matched filter. As a result, only the polynomial for the numerator of y_{22} needs to be determined in the direct synthesis approach.

Having had the characteristics of the filter network that can match to a given frequency variant load, the corresponding coupled resonator circuit model can be simply synthesized once the residues of y_{11} and y_{22} are determined as the poles of the admittance parameters are known and are the same as those of the matched filter. The residues of y'_{m11} can be found through the following relation:

$$y'_{m11}\prod_{i=1}^{n}(\Omega - \lambda(i)) = \sum_{i=1}^{n}\left[r'_{m11}(i)\prod_{\substack{j=1 \\ j\neq i}}^{n}(\Omega - \lambda(j))\right] \quad (7)$$

where *(i)* is the *i*-th pole of the admittance parameters, $r'_{m11}(i)$ is the *i-th* residue of y'_{11} and is the transformed lowpass frequency variable. The residues of y'_{m21} can be found by the same token.

With the values of poles and residues of the admittance parameters founded, the coupling matrix of a channel filter matched to a complex load can be found by a well known matrix orthogonal transformation method given in [8]. The modifications to the fundamental polynomials by (4), and consequently the admittance polynomials in (6) provide a different solution of a matched filter as compared to the solution using (3). Both solutions lead to a matched filter but the phase of S_{21} and S_{22} are different.

IV. A DESIGN EXAMPLE

One design example is given in this short paper to demonstrate the validation and its effectiveness of the proposed direct synthesis approach. The example concerns the design of a waveguide diplexer with two 5th degree all-pole filters and an H-plane T-junction as illustrated in Fig.2. The center frequencies of the two filters are 12.9 GHz and 13.9 GHz, and the bandwidth for the two filters is 0.6GHz. WR75 waveguide is used as the interfacing waveguide and for the T-junction.

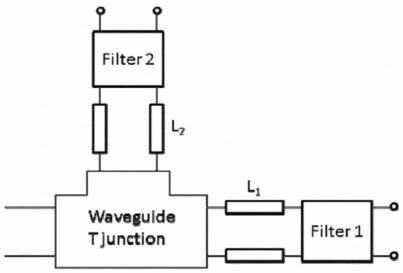

Fig. 2. A diplexer with two waveguide filters connecting to a waveguide T junction.

The first step in the diplexer design is the determination of the stub lengths of L_1 and L_2. In this example, a simple numerical search is used to find the stub lengths with which the derivative of the real part of the complex load w.r.t. frequency reaches to a small value when the other port of the junction is connected to the filter model designed with unitary reference loads. Having determined the stub lengths, the direct synthesis starts with the design of a matched Chebyshev filter with return loss of -22 dB and the filter order of 5. The matched filter is presumed to be connected to a unitary load at one port and a frequency variant complex load at the other port. Then the admittance parameters of the filter are renormalized from the complex reference load Z_L to the unitary reference load. The renormalization process leads to unmatched filter responses whose reflection coefficient is shown in Fig.3. The iterative design technique proposed in [6] for diplexer design and the proposed direct synthesis method are jointly used. Only two iterations are enough to get a convergent result. The return loss of the synthesized filter model is also superimposed in Fig.3, showing very good match to the desired response of the filter when it is connected to a unitary load at the two ports. Theoretically, if the admittance parameters can be curve-fitted well over a sufficiently wide frequency band, when the directly synthesized filter is connected to the actual frequency variant complex load, the filter response should be the same as the matched responses.

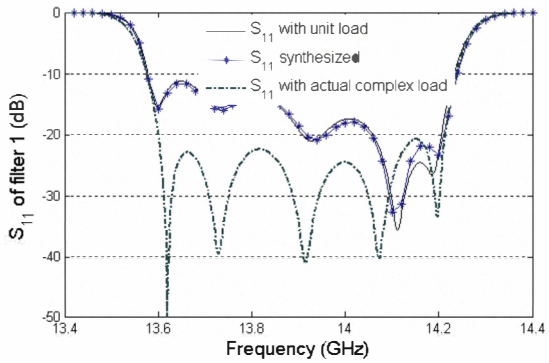

Fig.3 The reflection coefficients of filter 1: (1) matched filter with actual complex load; (2) ideal filter with real unitary reference load; and (3) the synthesized filter model with unitary reference load.

The synthesized coupling matrices of both channels are compared to the originally designed filter with unitary load in Table.I.

TABLE I
COUPLING MATRIES IN THE DIPEXER DESIGN

Coupling matrix	Original	Filter 1	Filter 2
M_{11}	0.0000	0.0037	-0.0085
M_{22}	0.0000	0.0004	-0.0085
M_{33}	0.0000	0.0167	-0.0280
M_{44}	0.0000	0.0237	0.0288
M_{55}	0.0000	0.2066	0.8461
M_{s1}	1.0570	1.0590	1.0575
M_{12}	0.9068	0.9076	0.9024
M_{23}	0.6533	0.6531	0.6473
M_{34}	0.6533	0.6553	0.6529
M_{45}	0.9068	0.7994	0.9196
M_{5l}	1.0570	0.8404	1.1402

Fig.4 shows the designed diplexer responses that are obtained by cascading the filter responses of the synthesized filter circuit model with the S-parameters of the T-junction. It can be seen that the return loss at the common port of the directly designed diplexer is nearly equal-rippled and is below -20dB. The initial physical dimensions of the channel filters are designed based on the synthesized circuit models. The dimensions can be fine tuned if time permits. The overall responses simulated by the in-house mode-matching software are also superposed in Fig. 4, demonstrating that the synthesized filter model is realizable.

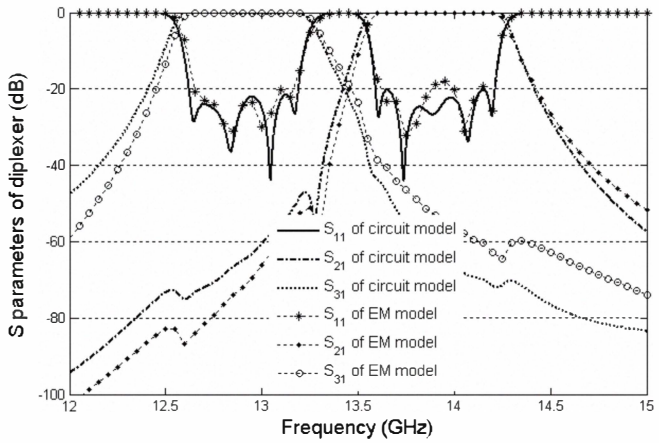

Fig.4 S-parameters of the diplexer of directly synthesized and the EM designed.

The physical realization of the diplexer is designed with an H-plane T-junction and two H-plane waveguide filters using an in-house mode-matching based EM simulation software. The structure is illustrated in Fig.5

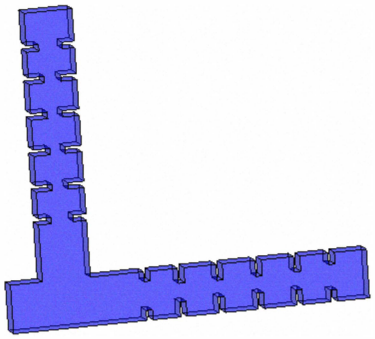

Fig.5 Designed EM model of this diplexer.

V. CONCLUSION

A novel approach to a direct synthesis of admittance polynomials and the corresponding coupling matrix for a general Chevbshev filter that matches to a frequency variant complex load is presented in this paper. Having modified the fundamental polynomials *E(s)*, *F(s)* and *P(s)* by equivalently adding a piece of dispersive transmission line at the port with complex load, synthesizing a matched filter with a complex load becomes a simple matter of finding an *n*-th order polynomial in the frequency band of interest. An example of analytically designing a waveguide diplexer is given to show the effectiveness of the new approach. The approach can be widely used in a direct synthesis of a microwave diplexer or a multiplexer. More applications of the approach will be presented in the symposium.

REFERENCE

[1] R.J. Wenzel, W.G. Erlinger, "Narrowband Contiguous Multiplexing Filters with Arbitrary Amplitude and Delay Response," *Microwave Symposium Digest, MTT-S International* , vol.76, no.1, pp. 116-118, Jun 1976

[2] J.D. Rhodes, R. Levy, "Design of General Manifold Multiplexers," *IEEE Trans. Microwave Theory & Tech* , vol.27, no.2, pp. 111-123, Feb 1979

[3] J.D. Rhodes, R. Levy, "A Generalized Multiplexer Theory," *IEEE Trans. Microwave Theory & Tech* , vol.27, no.2, pp. 99-111, Feb 1979

[4] R.J. Cameron, Ming Yu, "Design of manifold-coupled multiplexers," *Microwave Magazine, IEEE* , vol.8, no.5, pp.46-59, Oct. 2007

[5] G. Macchiarella, S. Tamiazzo, "Novel Approach to the Synthesis of Microwave Diplexers," *IEEE Trans. Microwave Theory & Tech*, vol.54, no.12, pp.4281-4290, Dec. 2006

[6] K.-L. Wu, W. Meng, "A Direct Synthesis Approach for Microwave Filters With a Complex Load and Its Application to Direct Diplexer Design," *IEEE Trans. Microwave Theory & Tech*, vol.55, no.5, pp.1010-1017, May 2007

[7] K. Kurokawa, "Power Waves and the Scattering Matrix", *IEEE Trans. Microwave Theory & Tech.,* Mar. 1965, pp194-202

[8] R.J. Cameron, "Advanced coupling matrix synthesis techniques for microwave filters," *IEEE Trans. Microwave Theory & Tech* , vol.51, no.1, pp. 1-10, Jan 2003

COMPUTER-AIDED DESIGN OF PARALLEL-CONNECTED MILLIMETER-WAVE DIPLEXERS/MULTIPLEXERS

by

R. Vahldieck and B. Varailhon de la Filolie
University of Victoria
Department of Electrical and Computer Engineering
Victoria, B.C. V8W 2Y2 Canada

ABSTRACT

This paper describes the analysis and design of a novel integrated millimeter wave diplexer. The structure is simple and can easily be extended to a multiplexer configuration. The diplexer is composed of ladder-shaped E-plane metal insert filters which are fabricated on a single metallic sheet and embedded in a split block housing.The theoretical design procedure is based on the generalized scattering matrix method which includes mutual parasitic loading effects between the filters as well as higher order mode interaction. Thus, no physical fine tuning of the component is necessary.

Introduction

Conventional design methods for diplexers/multiplexers follow in principle a two step procedure: First, the design of the band-select filters and second, physical fine tuning of the individual filter positions in the channels relative to their common input port. This procedure is time consuming and particulary difficult at millimeter wave frequencies. Furthermore, T-junctions are commonly used to connect the individual channels with the main input waveguide (i.e. [1], [7]). T-junctions, however, are typically narrow bandwidth devices and it is difficult to compensate for the rapid change of the junction reactance over frequency. Thus, this scheme is not suitable if wide-band channels are required. To alleviate this problem a low-cost W-band diplexer design has been published in [3] which utilizes a wide-band printed probe transition from waveguide to suspended-stripline. E-plane filters were printed on the same substrate to select the frequency bands and computer-aided design methods were used to account for the loading effect of the filters to ensure a good overall response.

However, the application range of this structure is limited to low-power signals and it is difficult to extend this structure with the same simplicity to a multiplexer network.

Therefore, the present paper describes a new low-cost design for millimeter wave diplexers which can easily be extended to multiplexer applications. The principle structure was suggested in [5]. However, the design was based on equivalent network theory and did not include the transition between the standard waveguide and the power divider section to feed the individual channels.

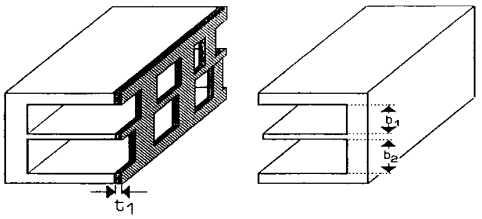

Fig.1a Perspective view of the diplexer arrangement with E-plane filters.

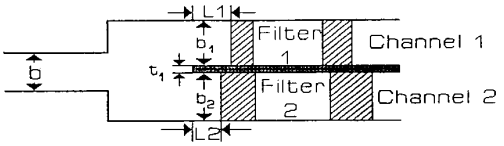

Fig.1b Side view of the diplexer connected to the input port by an abrupt E-plane step transition

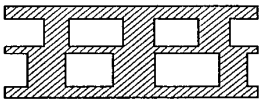

Fig.1c Dual ladder-shaped E-plane metal insert

0149-645X/88/0000-0435$01.00 © 1988 IEEE

Diplexer Design

Fig.1 shows the principle configuration of the diplexer. The structure consists of an E-plane bifurcation and two E-plane metal insert filters. The advantage of this design approach is obvious. Firstly, in comparison to the E-or H-plane T-junction the E-plane bifurcation (or n-furcation for multiplexers) is a rather broadband transition for the TE10-mode. Secondly, since the output waveguides have common broadwalls, the ladder-shaped E-plane metal insert filters can be fabricated on a single metallic sheet. Thus, their positions in the channels with respect to the common port are automatically adjusted in a single manufacturing step. Finally, the present solution is not only suitable for high power signals but also provides extremely low insertion loss when needed due to the absence of a lossy substrate material in the filter structure [2].

To compensate for the mutual loading effect between the filters the lengths L1, L2 (Fig.1b) must be optimized as well as L to ensure a good match between the input waveguide and the output channels. Instead of using an abrupt step transition as shown in Fig.1, a tapered transition improves the return loss of the power divider up to an average of 30dB over 20 GHz in W-band. The optimum dimensions for the taper as well as for L1, L2 and L have been obtained by computer optimization which is an indispensible part of the design procedure. On the other hand the best optimization routine is useless if the analysis method is not accurate.

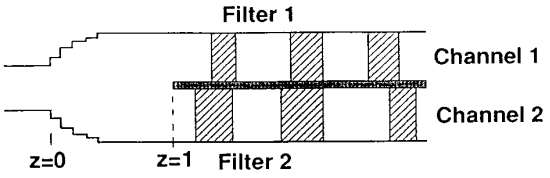

Fig.2a Diplexer connected to the input port by a tapered E-plane waveguide transition

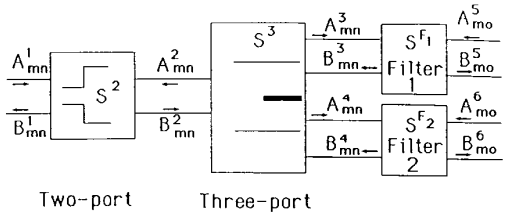

Fig.2b S-matrix representation of the various discontinuities involved in the structure of Fig.2a.

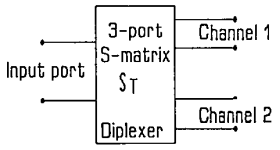

Fig.2c Overall 3-port S-matrix of the diplexer.

Therefore, we used a rigorous mode matching approach to calculate the generalized scattering matrix of the entire component and then we optimized the dimensional parameters for best circuit performance. The individual steps are outlined in Fig.2: First, we find the optimum dimensions for the E-plane band-select filters and the corresponding s-matrices. This can be done using the method described in [2]. Second we optimize the transformer section and combine its s-matrix with that of the E-plane bifurcation. Finally, the resulting three-port s-matrix is combined with the individual filter s-matrices, and the parameters L1, L2 and L are optimized to yield the best overall diplexer response. The same procedure applies to the design of multiplexers.

Analysis

For the mode matching method the structure is decomposed into two classes of discontinuities:

1) The E-plane bifurcation which includes the abrupt step in waveguide heigth (Fig.1).

2) The H-plane bifurcation in the filter sections.

The H-plane bifurcation was treated in detail in [2] in conjunction with E-plane metal insert filters. E-and H-plane n-furcations have in common that the field components at the discontinuities can be derived from the x component of the magnetic Hertz potential. However, instead of only three field components (Ey, Hx,Hz) at the H-plane discontinuity, an incident TE10-mode will excite five field components (Ey,Ez,Hy,Hx,Hz) at the E-plane discontinuity. The generalized scattering matrix in this case is then derived from the matching condition for Ey and Hy or Ey and Hx field components.

$$Ey^{\nu} = j\omega\mu \sum_{n=0}^{N} \sum_{m=1}^{M} C_{nm}^{\nu} \sin(kx_m^{\nu} x) \cos(ky_n^{\nu} y) \cdot$$

$$\cdot (A_{nm}^{\nu} + B_{nm}^{\nu}) e^{\mp jkz_{nm}^{\nu} z} \quad (1)$$

$$Hx^{\nu} = \sum_{n=0}^{N}\sum_{m-1}^{M}(ko^2-(kz_{nm}^{\nu})^2)C_{nm}^{\nu}\sin(kx_m^{\nu}x)\cdot$$

$$\cdot\cos(ky_n^{\nu}y)(A_{nm}^{\nu}+B_{nm}^{\nu})e^{\mp jk_{nm}^{\nu}z} \qquad (2)$$

The abbreviations Amn and Bmn in (1) and (2) denote the incident and reflected wave amplitudes and Cmn is a factor to normalize the wave amplitudes to 1 W.

From the matching conditions at the two principle interface planes, z=0 and z=1 (Fig.2a), one obtains the two-port scattering matrix for the abrupt step transition

$$\begin{bmatrix} B_{mn}^1 \\ B_{mn}^2 \end{bmatrix} = S^2 \begin{bmatrix} A_{mn}^1 \\ A_{mn}^2 \end{bmatrix} \qquad (3)$$

and the three-port s-matrix for the E-plane bifurcation

$$\begin{bmatrix} A_{mn}^2 \\ A_{mn}^3 \\ A_{mn}^4 \end{bmatrix} = S^3 \begin{bmatrix} B_{mn}^2 \\ B_{mn}^3 \\ B_{mn}^4 \end{bmatrix} \qquad (4)$$

The algorithm to cascade two-port s-matrices necessary in the taper section has been given in [7]. Cascading the three-port s-matrix with the filter two-ports in each channel yields the following algorithm: At first we combine the three-port with the two-port of the filter in channel 1

$$\begin{aligned}
S_{11}^0 &= S_{11}^3 + S_{12}^3 * S_{11}^{F_1} * W * S_{21}^3 \\
S_{21}^0 &= S_{21}^{F_1} * W * S_{21}^3 \\
S_{31}^0 &= S_{31}^3 + S_{32}^3 * S_{11}^{F_1} * W * S_{21}^3 \\
S_{12}^0 &= \left[S_{12}^3 * S_{11}^{F_1} * W * S_{22}^3 + S_{12}^3\right] * S_{21}^{F_1} \\
S_{13}^0 &= S_{13}^3 + S_{12}^3 * S_{11}^{F_1} * W * S_{23}^3 \\
S_{22}^0 &= S_{22}^{F_1} + S_{21}^{F_1} * W * S_{22}^3 * S_{12}^{F_1} \\
S_{23}^0 &= S_{21}^{F_1} * W * S_{23}^3 \\
S_{32}^0 &= \left[S_{32}^3 * S_{11}^{F_1} * W * S_{22}^3 + S_{32}^3\right] * S_{12}^{F_1} \\
S_{33}^0 &= S_{33}^3 + S_{32}^3 * S_{11}^{F_1} * W * S_{23}^3 \\
W^0 &= \left[E - S_{22}^3 * S_{11}^{F_1}\right]^{-1}
\end{aligned}$$

In a second step the overall s-matrix of the diplexer is obtained by combining S^0 with the filter in the second channel using the same algorithm again but replacing S^3_{nm} by S^0_{nm} and S^{F1}_{nm} by S^{F2}_{nm}. For multiplexers the procedure must be repeated according to the number of channels involved.

There are only TE^x_{1m} -modes in the vicinity of an E-plane discontinuity. Nevertheless, we consider in equ.'s (1) and (2) the more general case of TE^x_{nm} -modes. This is so because the s-matrix of the E-plane bifurcation must be cascaded with the s-matrix of the channel filters which contain only TE^x_{no} -modes. To cascade both types of matrices we must consider only those scattering elements in S (Fig.2b) which correspond to B1o, B3o, B5o (etc.) wave amplitudes. This results in diagonal matrices for S11, S12 etc. Since TE^x_{no} -modes of higher order than 2 to 3 (odd modes) are negligible a short distance from the first filter discontinuity, the size of the matrices to be cascaded is considerably reduced accelerating the computer program significantly. The E-plane discontinuities are sufficiently described by taking into account 8 to 12 even higher order TE^x_{1m} -modes. This is shown for the E-plane power divider and the five step tapered transition in Fig.3.

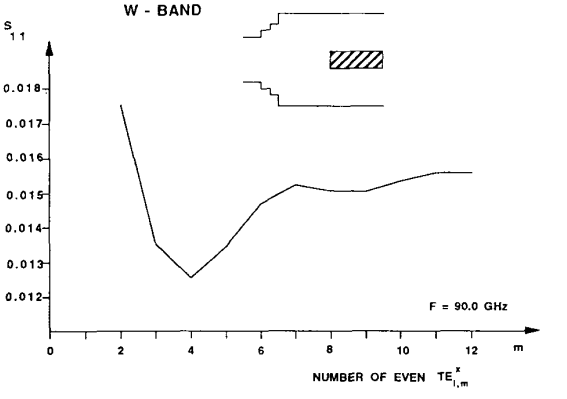

Fig.3 Convergence analysis of a five step E-plane taper with bifucation in W-band(a=2.54,b/a=0.5) d1=0.0195, d2=0.109, d3=0.288,d4=0.538,d5=0.68,s1=1.24,s2=1.174, s3=1.083,s4=1.135 L=1.82 (dimensions in mm)

Results

Fig.4 shows the frequency response of the same taper over a 20 GHz bandwidth in W-band. The tapered transition was necessary since the abrupt step transition between the input standard waveguide and the bifurcated power divider section was rather large (2b). The corresponding return loss was below 10dB. With the optimized taper the return loss remains above 30dB in the average.

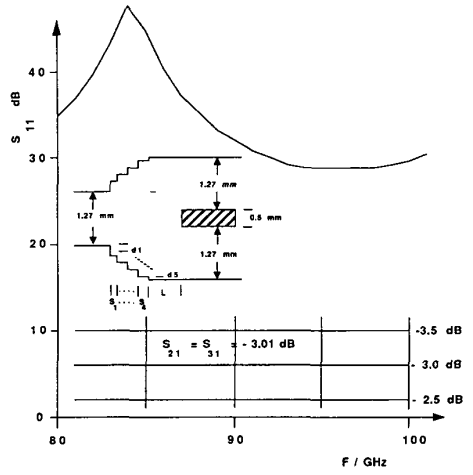

Fig.4 Frequency response of the tapered power divider given in Fig.3

Fig.5 shows the response of noncontiguous diplexers in Ka- and W-band with a guard band between 29 and 32 GHz and 94.5 and 95.5 GHz, respectively. Both diplexers are fed by tapered transitions. The predesigned bandpass filters show excellent performance as stand-alone components. In

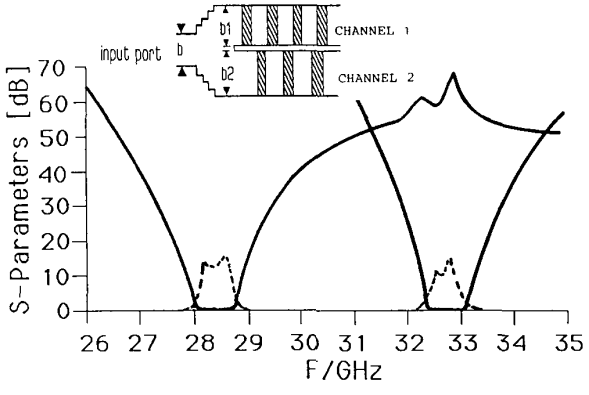

Fig.5 Frequency response of a noncontiguous Ka-band diplexer. Filter 1 resonators, 1.: 6.311mm; 2.: 6.397mm; coupling sections, 1.: 0.525mm; 2.: 2.539mm; Filter 2 resonators, 1.:4.372mm; 2.:4.4mm; coupling sections, 1.:0.647mm; 2.:3.446mm; 3.:4.056mm. Both filters are symmetrical about resonator 2 and coupling section 3, respectively. Metallization thickness t=127.um

Fig.6 Frequency response of a noncontiguous W-band diplexer. Filter 1 resonators, 1.:1.471mm; 2.:1.473mm; coupling sections 1.:0.586mm; 2.:1.829mm; 3.:1.98mm. Filter 2 resonators, 1.:1.555mm 2.:1.557mm; coupling sections, 1.:0.591mm; 2.:1.829; 3.:1.98mm. Both filters are symmetrical about 3.coupling section. t=127.um

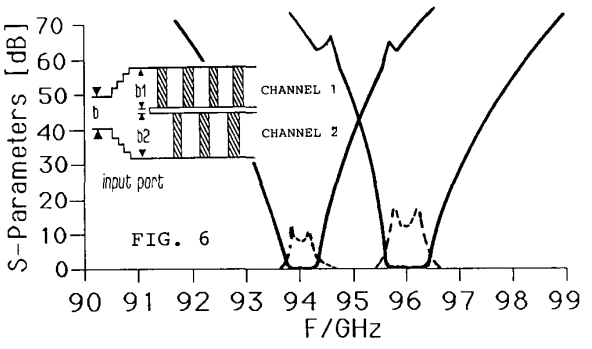

FIG. 6

the diplexer arrangement, however, their passband insertion loss increases somewhat (0.3 dB) and the return loss deteriorates down to 15 dB. The typical CPU time required to optimize a diplexer is approximately 30 min. on a PC (AT) with DSI20 coprocessor.

Conclusion

A parallel-connected diplexer configuration has been introduced which can easily be extended to a multiplexer component. Fabrication costs are reduced to a minimum due to the applicability of low-cost photolithographic techniques and the use of accurate CAD software, which makes fine tuning unnecessary. Furthermore, due to a computer time efficient but accurate numerical procedure the design software is operational on Personal Computers.

References

[1] Matthaei,G., L.Young and E.M.T. Jones,"Microwave Filters, Impedance-Matching Networks, and Coupling Structures", Artech House, Inc. 1980.

[2] Vahldieck, R., J. Bornemann, F. Arndt and D. Grauerholz," Optimized Waveguide E-Plane Metal Insert Filters for Millimeter Wave Applications", IEEE Trans., MTT-31, pp.65-69, January 1983.

[3] Shih, Y.-C., L.Q. Bui and T. Itoh, "Millimeter-Wave Diplexers with Printed Circuit Elements", IEEE Trans. MTT-33, pp.1465-1469, December 1985.

[4] Dittloff,J.,J.Bornemann and F.Arndt, "Computer Aided Design of Optimum E- or H-plane N-Furcated Waveguide Power Divider", Conference Proceedings 17th European Microwave Conference,1987, pp. 181-186.

[5] Reiter, G. and T. Kolumban," Diplexer Arrangement utilizing E-plane Filters", 15Proc. 15th Europ. Microwave Conference, pp.859-864, 1985.

[6] Marshall, T., J. Christopher and S. Kluger,"The Definicon 68020 Coprocessor", Part 1 and 2 published in Byte Magazin July and August 1986, pp.120-144 and pp.108-114.

[7] Vahldieck, R. and W.J.R. Hoefer,"Finline and Metal Insert Filters with improved Passband Separation and Increased Stopband Attenuation", IEEE Trans. Microwave Theory Tech., vol. MTT-33, No.12, Decemb. 1985

[8] Arndt, F., J. BOrnemann,D. Grauerholz," Waveguide E-plane Integrated-Circuit Diplexer", Electronics Letters, 4th July, 1985, Vol.21, No.14, pp.615-617

Progress In Electromagnetics Research C, Vol. 17, 203–218, 2010

COMPUTER-AIDED DESIGN OF Y-JUNCTION WAVEGUIDE DIPLEXERS

F. M. Vanin † **and F. Frezza**

Department of Information Engineering, Electronics, and Telecommunications
La Sapienza University of Rome
Via Eudossiana 18, Roma 00184, Italy

D. Schmitt

European Space Agency — European Space Research and Technology Centre (ESA-ESTEC)
Keplerlaan 1, 2201AZ Noordwijk, The Netherlands

Abstract—Waveguide diplexer designs are widely used for telecommunications, space, and terrestrial applications. Although mathematical models and design procedures for waveguide filters are known, diplexer designs still remain complex and time consuming. This paper describes how to obtain an equivalent circuit network model and a complete design of non-contiguous diplexers using a computer-aided approach with a classic Y-junction. Results are satisfactory in terms of reduced design time and performance. Examples including physical dimensions are provided.

1. INTRODUCTION

Diplexers are used in a large variety of applications in communication systems. They typically follow the antenna in the RF chain allowing simultaneously transmit and receive functions. A diplexer is a device that splits a signal into two groups according to predefined frequency ranges, or combines two signals, each occupying a separate frequency range, into a single collection of signals. Diplexers subdivide a wide frequency band in two narrower bands or, reciprocally, combine

Received 20 September 2010, Accepted 2 November 2010, Scheduled 12 November 2010
Corresponding author: Felice Maria Vanin (felice.vanin@esa.int).
† Also with European Space Agency — European Space Research and Technology Centre (ESA-ESTEC), Keplerlaan 1, 2201AZ Noordwijk, The Netherlands.

frequency bands into a common port. There are mainly two types of diplexer, contiguous and non-contiguous ones. In a non-contiguous diplexer, the bands of the filters are separated in frequency with a frequency separation called 'guardband' whereas, in the contiguous case, the bands are adjacent.

This paper focuses on diplexers realized in rectangular waveguides connecting two inductive iris bandpass filters. The design typically starts with the establishment of the main RF specifications, e.g., Transmit/Receive frequency ranges, insertion loss variation, return loss, and rejection at Transmit/Receive bands. Each filter is then modelled and physical dimensions calculated i.e., waveguide lengths and iris dimensions. Subsequently, the filters are combined at the common port. This connection can be done, for example, with N-furcation, T-junctions, or Y-junction. In this article, the Y-junction is chosen as connection between the two filters. The connection of the two filters at the common port requires typically optimization loops of the entire structure. To ease the dimensional design process in terms of time and complexity, excessive use of optimisation should be prevented, especially in diplexer structures where there are numerous dimensions to be optimised.

Accurate transfer functions for calculating network models of bandpass filters and diplexers are known and published for example in [1–3]. In addition information on how to derive physical dimensions of bandpass filters and diplexers is also provided in [4] and [5] but without indicating how diplexer circuit models can be calculated.

The aim of this work is to provide practical formulas to derive a Y-junction diplexer network model (see Figure 1) giving examples of diplexer network synthesis, including physical dimensions and fullwave analyses. A FORTRAN software code has been written to assist engineers in the design of diplexers limiting the optimization variables following an automatic and systematic approach as indicated in [5]. This prevents the use of common techniques requiring time-consuming global fullwave optimization. The FORTRAN programming language was chosen due to its accurate numerical computation, speed, and portability with respect to operative system.

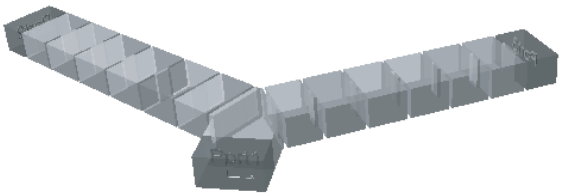

Figure 1. 3D cad drawing of a diplexer.

2. MATHEMATICAL MODEL

2.1. Diplexer Admittance Matrix

The object of this section is to provide formulas to be used in the definition of a diplexers network model.

Since a diplexer is a three port device, it can be modeled using a 3×3 either admittance or impedance matrix. Figure 2 indicates the block diagram of a diplexer network model, where the junction is represented by the admittance matrix Y, and the two filters by the admittance matrices Y^{F1} and Y^{F2}.

The matrix Y can be written as:

$$Y = \begin{pmatrix} Y_{11} & Y_{12} & Y_{13} \\ Y_{21} & Y_{22} & Y_{23} \\ Y_{31} & Y_{32} & Y_{33} \end{pmatrix} \tag{1}$$

while the two admittance filter matrices Y^{F1} and Y^{F2}:

$$\begin{cases} Y^{F1} = \begin{pmatrix} Y_{11}^{F1} & Y_{21}^{F1} \\ Y_{21}^{F1} & Y_{22}^{F1} \end{pmatrix} \\ Y^{F2} = \begin{pmatrix} Y_{11}^{F2} & Y_{21}^{F2} \\ Y_{21}^{F2} & Y_{22}^{F2} \end{pmatrix} \end{cases} \tag{2}$$

Considering the voltages V_1, V_2, V_3 and currents I_1, I_2, I_3 respectively at port 1, 2, 3, the following can be written:

$$\begin{pmatrix} I_1 \\ I_2 \\ I_3 \end{pmatrix} = Y^{Dip} \cdot \begin{pmatrix} V_1 \\ V_2 \\ V_3 \end{pmatrix} \tag{3}$$

Using the network in Figure 2, the Kirchhoff equations can be written and solved in Y^{Dip} in terms of Y^{F1} and Y^{F2}:

$$Y^{Dip} = \begin{pmatrix} Y_{11}^{Dip} & Y_{12}^{Dip} & Y_{13}^{Dip} \\ Y_{21}^{Dip} & Y_{22}^{Dip} & Y_{23}^{Dip} \\ Y_{31}^{Dip} & Y_{32}^{Dip} & Y_{33}^{Dip} \end{pmatrix} \tag{4}$$

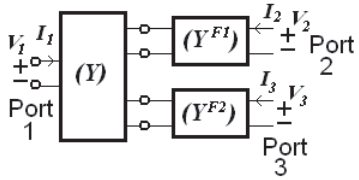

Figure 2. Diplexer network model.

Note that the network can be solved also in terms of the impedance matrix rather than the admittance matrix (clearly both models are electrically equivalent).

The complete analytical expression for matrix (4) is given in the Appendix (the case of Z matrix representation is also provided). The explicit expression of Y^{Dip} can be used to create a mathematical model of the Diplexer. Such equations are independent of the practical realization of the junction and therefore are still valid for junctions different from the Y-junction.

2.2. Y-Junction and Filter Admittance Matrices

In order to complete the analytical model of the diplexer, explicit expressions for the matrices Y^{F1}, Y^{F2}, and Y are necessary. The objective is to show how to calculate those matrices and to derive consequently a diplexer response. It is first indicated how to calculate the junction admittance matrix and then the filter admittance matrices.

Since lumped element models for the junction typically do not include the frequency dependence of waveguide structures (unless advanced models are used), it is preferred to use standard fullwave simulators to derive accurate results. With the use of a fullwave simulator (in our case [9]), it is possible to calculate the S matrix response of a Y-junction in the frequency range of interest. The S matrix can be then converted in Y matrix just using analytical matrix transformations.

This way of proceeding ensures a very accurate model of the Y-junction which includes the frequency dependency of the junction structure. The Y admittance matrix of the junction is then calculated.

In order to calculate the filter admittance matrices Y^{F1} and Y^{F2}, it is necessary to choose the filter network model. Typically, waveguide bandpass filters exhibiting Chebychev characteristics are represented either with coupling matrices [6] or with a model based on impedance inverters cascaded with transmission lines as indicated in [1, 5]. In this article the model is chosen based on impedance inverters which give a direct link between network characteristics and physical model as indicated in Figure 3.

A possible realization in rectangular waveguide of a Chebychev bandpass filter is composed of a cascade of resonators separated by inductive irises. Figure 3(a) contains a schematic of a 4-pole filter and the equivalent network model based on a cascade of impedance inverters and transmission lines with characteristic impedance Z_0. The widths of irises, represented by a frequency independent impedance

inverter K_{ij}, are denoted as W_1, W_2, W_3, and the letters R_1, R_2 indicate the resonator lengths, represented by transmission lines. Thus, the geometrical structure is mapped into a network model. To be noted that this circuit model clearly simplifies the actual behavior of waveguides: for example, it does not include higher order modes and the frequency dependence of the coupling elements. In any case, the model given in Figure 3(b) is a good approximation of a waveguide filter when these effects can be ignored, namely for narrow bandwidth (BW) applications.

The filter network model is completed when the values of the impedance inverters, the resonator lengths, and the characteristic impedance of the line have been determined.

We assume that all resonators are tuned to the same centre frequency $f_0 = BW/2$ and therefore, in the network model, the lengths of the resonators (i.e., of the transmission lines) are identical and given by:

$$l = m\frac{\lambda_{g0}}{2} \quad m = 1, 2, \ldots \tag{5}$$

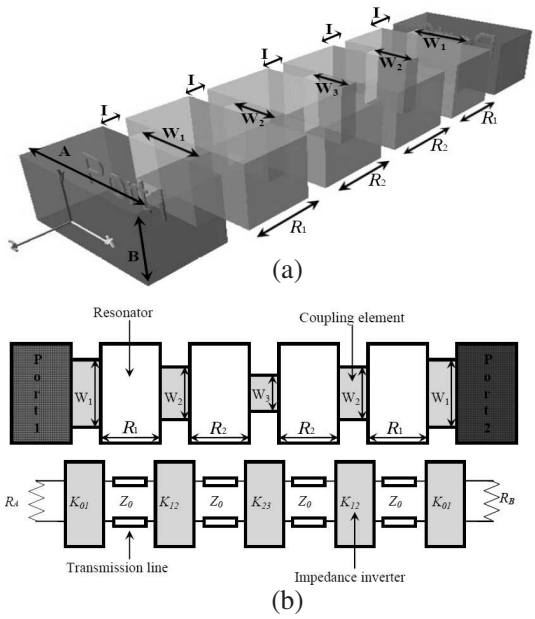

Figure 3. (a) 3D drawing of a 4-pole bandpass filter in rectangular waveguide. (b) Top-view of a bandpass filter in rectangular waveguide and its network model.

where λ_{g0} is the guide-wavelength at the centre frequency, and m the number of half wavelengths. For the example, the TE_{101} mode has been selected and therefore the value for m is 1.

The remaining network model parameters are Z_0 and K_{ij}. The characteristic impedance Z_0 can be set to any real value. For simplicity we choose the value of $Z_0 = 1\,\Omega$.

For a given filter degree n of fractional bandwidth $w = BW/f_0$, the impedance inverters are defined as given in [6]:

$$\begin{cases} K_{01} = k_{01}\sqrt{R_A \cdot x \cdot w} \\ K_{j,j+1}\big|_{j=1,n-1} = w \cdot x \cdot k_{j,j+1} \\ K_{n,n+1} = k_{n,n+1}\sqrt{R_B \cdot x \cdot w} \end{cases} \tag{6}$$

where the normalised coupling elements $k_{j,j+1}$ are calculated from the lowpass prototype elements defined in [6] for Chebychev filters by the following:

$$k_{i,i+1}\big|_{i=0,\ldots,n} = \frac{1}{\sqrt{g_i g_{i+1}}} \tag{7}$$

In Equation (6), R_A and R_B are the resistances which close the line on the left- and right-hand side of the network in Figure 3(b). These resistances are the normalising elements for calculating the S-parameters and usually taken to the value of Z_0 (i.e., in this case, both equal to 1). x is the reactance slope parameter of the series resonator given by:

$$x = \frac{\pi}{2} Z_0 \left(\frac{\lambda_{g0}}{\lambda_0}\right)^2 \tag{8}$$

where λ_0 is the wavelength at the centre frequency f_0.

Having dimensioned all network elements, the filter model is completed. In general, for an n-pole filter, the transfer matrix T_{ij} is obtained by multiplying the transfer matrix elements of the circuit as follows:

$$\begin{aligned} \begin{pmatrix} T_{11} & T_{12} \\ T_{21} & T_{22} \end{pmatrix} = & \begin{pmatrix} \cos(\beta L) & jZ_0 \sin(\beta L) \\ \frac{j}{Z_0}\sin(\beta L) & \cos(\beta L) \end{pmatrix} \cdot \begin{pmatrix} 0 & iK_{01} \\ \frac{i}{K_{01}} & 0 \end{pmatrix} \\ & \cdot \begin{pmatrix} \cos\left(\pi\frac{\lambda_{g0}}{\lambda_g}\right) & iZ_0 \sin\left(\pi\frac{\lambda_{g0}}{\lambda_g}\right) \\ \frac{i\sin\left(\pi\frac{\lambda_{g0}}{\lambda_g}\right)}{Z_0} & \cos\left(\pi\frac{\lambda_{g0}}{\lambda_g}\right) \end{pmatrix} \cdot \begin{pmatrix} 0 & iK_{12} \\ \frac{i}{K_{12}} & 0 \end{pmatrix} \\ & \cdots \begin{pmatrix} \cos\left(\pi\frac{\lambda_{g0}}{\lambda_g}\right) & iZ_0 \sin\left(\pi\frac{\lambda_{g0}}{\lambda_g}\right) \\ \frac{i\sin\left(\pi\frac{\lambda_{g0}}{\lambda_g}\right)}{Z_0} & \cos\left(\pi\frac{\lambda_{g0}}{\lambda_g}\right) \end{pmatrix} \cdot \begin{pmatrix} 0 & iK_{n+1} \\ \frac{i}{K_{n+1}} & 0 \end{pmatrix} \end{aligned} \tag{9}$$

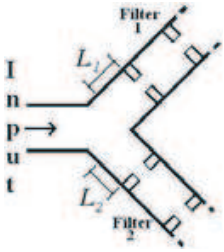

Figure 4. Connection of the filters to the Y-junction, detail of L_1 and L_2.

Note that in Equation (9), a transmission line of length L is positioned at the left side of the first coupling representing the waveguide connecting the filter to the common junction. In order to ensure adequate electrical matching between the filters and the junction, the lengths L_1 and L_2 respectively connecting filter 1 and 2 to the common port have to be appropriately chosen, as indicated in Figure 4.

An analytical solution to calculate L_1 and L_2 is possible as indicated in [8] using the phase information for the two filters and the scattering parameters characterizing the junction. For convenience, the formulas, (A3) and (A4), are provided in the appendix.

After calculating L_1 and L_2, Equation (9) can be finally transformed into the admittance matrices Y^{F1} and Y^{F2} with the simple use of network formulas.

Using now the three matrices Y, Y^{F1}, and Y^{F2}, Y^{Dip} can be calculated using the formula (A1) given in the appendix. The S matrix can be then derived using:

$$S = \left(I + Y^{Dip}\right)^{-1} \left(I - Y^{Dip}\right) \tag{10}$$

3. SUMMARY OF THE NETWORK DESIGN PROCEDURE AND EXAMPLES

A FORTRAN code has been written including all the equations previously described. In this section, a digest of the diplexer design procedure is given including 2 examples.

The network diplexer synthesis proceeds as follows:

1) The waveguide type for the Y-junction and the filters shall be selected according to the working frequency range, and a suitable iris thickness chosen.
2) The Y-junction shall be analysed with a fullwave simulator to calculate S-parameters and then convert them into the Y matrix.

3) In accordance with Figure 3(b) and with the RF specifications, the network models of the filters shall be calculated: the impedance inverters using (6), and the resonator lengths using (5).
4) The transfer matrix T_{ij} of the filters shall be calculated using (9) (including L_1 and L_2 by using (A3)) and converted into Y^{F1} and Y^{F2} using matrix transformations.
5) The diplexer admittance matrix shall be calculated using (4) and (A1) of the appendix, and the S-parameters with (10).

Two examples of diplexer network design are now discussed. The specifications are for typical Rx/Tx for Telecommunication satellites in Ku band and given in Table 1 and Table 3.

Table 1. RF specification example 1.

	Filter 1 (Tx)	**Filter 2 (Rx)**
Order	5	4
Frequency Bands	12.5–12.75 [GHz]	14–14.25 [GHz]
Return Loss	> -20 [dB]	> -20 [dB]

After running the program, the network results are summarized as follows in Table 2 (a return loss of 25 dB is assumed):

Table 2. Network analysis results.

	Filter 1 (Tx)	**Filter 2 (Rx)**
$\boldsymbol{f_0}$	12.625 [GHz]	14.125 [GHz]
$\boldsymbol{L_{1,2}}$	3.46 [mm]	2.12 [mm]
Inverters	0.252768 ($K_{0,1} = K_{5,6}$)	0.231325 ($K_{0,1} = K_{4,5}$)
	0.049528 ($K_{1,2} = K_{4,5}$)	0.041959 ($K_{1,2} = K_{3,4}$)
	0.034711 ($K_{2,3} = K_{4,5}$)	0.031100 ($K_{2,3}$)

The S-parameters calculated are shown in Figure 5. The matching on both channels and the excellent diplexer response can be observed. This model did not require any optimization at network level, resulting in a computation time of just few seconds.

The second example of diplexer design considers a bandwidth of 750 MHz for the first filter and 500 MHz for the second one as indicated in Table 3.

Table 3. RF specification example 2.

	Filter 1 (Tx)	**Filter 2 (Rx)**
Order	12	10
Frequency Bands	10.95–11.7 [GHz]	14–14.5 [GHz]
Return Loss	> -20 [dB]	> -20 [dB]

Table 4. Network analysis results.

	Filter 1 (Tx)	**Filter 2 (Rx)**
f_0	11.325 [GHz]	14.25 [GHz]
$L_{1,2}$	3.22 [mm]	1.79 [mm]
Inverters	0.482308 ($K_{0,1} = K_{12,13}$)	0.304014 ($K_{0,1} = K_{10,11}$)
	0.178933 ($K_{1,2} = K_{11,12}$)	0.071112 ($K_{1,2} = K_{3,4}$)
	0.121689 ($K_{2,3} = K_{10,11}$)	0.048402 ($K_{2,3}$)
	0.111251 ($K_{3,4} = K_{9,10}$)	0.044324 ($K_{3,4} = K_{10,11}$)
	0.107722 ($K_{4,5} = K_{8,9}$)	0.043047 ($K_{3,4} = K_{10,11}$)
	0.106329 ($K_{5,6} = K_{7,8}$)	0.042726 ($K_{5,6}$)
	0.105946 ($K_{6,7}$)	–

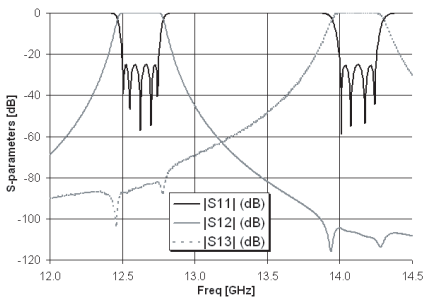

Figure 5. Network S-parameters response of the Diplexer (5 and 4 pole filters).

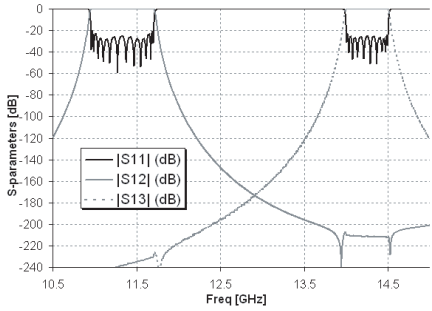

Figure 6. Network S-parameters response of the Diplexer (12 and 10 pole filters).

After running the program, the network results are summarized as follows in Table 4.

The S-parameters calculated are shown in Figure 6. It can be observed the matching on both channels and the excellent diplexer response. The return loss is better than 20 dB on both channels.

In conclusion, the S-parameter results show good performance of the presented network model. The FORTRAN program calculates the S-parameters in few seconds for both cases. This permits to easily predict the performance of diplexers.

4. EXAMPLE OF DIPLEXERS IN RECTANGULAR WAVEGUIDE

A simple and reliable automatic diplexer design procedure has been described for non-contiguous diplexers, substantially reducing the overall computational time from the RF specifications to the final dimensions [5]. This procedure resulted in a FORTRAN code able to assist engineers in diplexer modeling. The procedure ensures fast optimization by the appropriate choice of only six dimensions to be adjusted. Electromagnetic simulations are run with a limited number of variables independent of the filter order.

The software code was run for the two examples previously described. The dimensions found for the first diplexer are reproduced in Table 5. The second structure is given in Table 6. For both cases, WR75 was used and the iris thickness I is 1 mm (see Figure 3(a)). The mathematical computation took less than five minutes.

Table 5. Dimensions of the Diplexer [mm].

	Filter 1 (Tx)	**Filter 2 (Rx)**
WG type	WR75	WR75
Iris length	1	1
$L_{1,2}$	1.855	0.908
Resonator lengths	Resonator 1 13.300	Resonator 1 11.237
	Resonator 2 and 4 14.460	Resonator 2 and 3 12.206
	Resonator 3 14.554	Resonator 4 11.251
	Resonator 5 13.260	–
Iris widths	Iris 1 8.027	Iris 1 7.350
	Iris 2 and 5 4.583	Iris 2 and 4 4.058
	Iris 3 and 4 4.076	Iris 3 3.685
	Iris 6 7.989	Iris 5 7.197

Table 6. Dimensions of the Diplexer [mm].

	Filter 1 (Tx)	**Filter 2 (Rx)**
WG type	WR75	WR75
Iris length	1	1
$L_{1,2}$	0.282	0.237
Resonator lengths	Resonator 1 14.110	Resonator 1 10.766
	Resonator 2 and 11 16.174	Resonator 2 and 9 11.811
	Resonator 3 and 10 16.612	Resonator 3 and 8 11.951
	Resonator 4 and 9 16.705	Resonator 4 and 7 11.979
	Resonator 5 and 8 16.738	Resonator 5 and 6 11.988
	Resonator 6 and 7 16.750	Resonator 10 10.660
	Resonator 12 14.090	–
Iris widths	Iris 1 10.744	Iris 1 7.924
	Iris 2 and 12 7.652	Iris 2 and 10 4.801
	Iris 3 and 11 6.714	Iris 3 and 9 4.232
	Iris 4 and 10 6.506	Iris 4 and 8 4.112
	Iris 5 and 9 6.430	Iris 5 and 7 4.073
	Iris 6 and 8 6.407	Iris 6 4.063
	Iris 7 6.399	Iris 11 7.906
	Iris 13 11.003	–

The S-parameters of the diplexer analyzed with a fullwave simulator [9] are given in Figure 7. The response shows a return loss better than 20 dB, however this is not equal ripple. This limitation is linked to the dimensional synthesis of the filters themselves and not to the design methodology of the diplexer (i.e., to the choice of the dimensions to adjust via optimization). The limitation of the filter synthesis is linked to the network model which uses frequency independent couplings. An optimization of the individual filter can be useful to achieve equal-ripple performance before finalizing the

diplexer design process. In these specific cases, it was preferred to leave the dimensions as they came directly from the synthesis without any optimization at diplexer (nor filter) level to demonstrate the capability of the design procedure and possible limits.

The S-parameters of the structure analyzed with a fullwave simulator [9] are given in Figure 8. The return loss is better than 18 dB on the first channel and better than 20 dB on the second one. Also in this case the limitation on the achieved return loss is due to the initial fullwave response of the TX filter.

Figure 9 shows the field analysis of the diplexer of Figure 8 at the center frequency of the TX channel ($f = 11.325$ GHz). It can be noted that the electric field is maximum in the TX channel and minimum in the RX channel as expected.

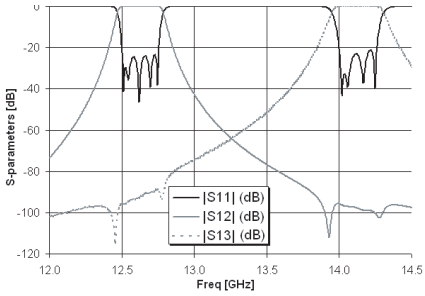

Figure 7. Fullwave response of the Diplexer (5 and 4 pole filters).

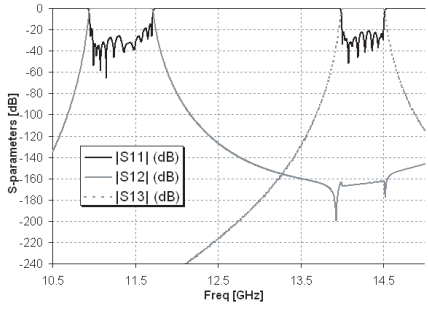

Figure 8. Fullwave response of the Diplexer (12 and 10 pole filters).

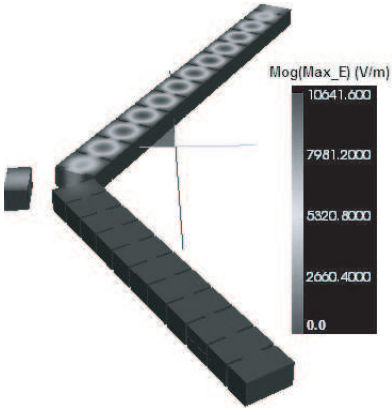

Figure 9. Field analysis at the center frequency of the TX channel ($f = 11.325$ GHz).

5. APPLICABILITY OF THE METHOD

The presented computer-aided design of Y-junction waveguide diplexers is limited to the case of non contiguous diplexers, meaning that the rejection provided by the TX channel to the RX channel and opposite is sufficiently high ($< 50\,\mathrm{dB}$). Depending on the filter, this is often achieved if the guard-band is in the order of the bandwidth of the wider channel. Note that this has to include any additional spurious that can possibly fall in the second channel.

This is because the impedance inverters as calculated in this paper are based on doubly terminated networks. It is also possible to design a contiguous diplexer using the same procedure but with appropriate couplings based on singly-terminated filters. However, the quality of the synthesis depends on guard-band and the filter types chosen. Therefore optimization of the diplexer is typically necessary to achieve the specified RF performance.

Note that diplexer design and utilization depends upon the applicability range of the waveguide. In any case the entire diplexer band (both channels) has to fall within the applicability range of the waveguide; in the described examples WR75.

6. CONCLUSIONS

A software tool has been developed to support engineers in the design of non-contiguous diplexers using waveguide Y-junctions. The software calculates a mathematical model of the diplexer and can be used for example in establishing the filter order of each frequency band. Examples of designs have been given showing adequate return loss matching of each filter. This model and the equation provided are generic and can be used also for any other junction type by just using another admittance junction matrix.

The software code written in FORTRAN calculates the diplexer dimensions using a procedure already presented by some of the authors and validated with measurements [5]. The use of the mathematical model, supported with automatic dimensional synthesis procedures, allows fast analysis and assessments. This can lead to quick corrections simply by reiterating automatic designs. The applicability and limits of the method are also discussed.

The FORTRAN software code can be further improved allowing diplexer designs using other junction and filter types, but using the same basic approach and formulas as given in the paper.

APPENDIX A.

The Diplexer admittance matrix Y^{Dip} (4) is given analytically using the following expressions:

$$\begin{cases} Y_{11}^{Dip} = Y_{11} - \dfrac{\begin{array}{c}+Y_{11}^{F2}Y_{12}Y_{21} + Y_{13}\left(Y_{11}^{F1}+Y_{22}\right)Y_{31} \\ -Y_{12}Y_{23}Y_{31} - Y_{13}Y_{21}Y_{32} + Y_{12}Y_{21}Y_{33}\end{array}}{-Y_{23}Y_{32}+\left(Y_{11}^{F1}+Y_{22}\right)\left(Y_{11}^{F2}+Y_{33}\right)} \\ Y_{12}^{Dip} = -\dfrac{Y_{12}^{F1}\left(Y_{11}^{F2}Y_{12}-Y_{13}Y_{32}+Y_{12}Y_{33}\right)}{Y_{11}^{F2}Y_{22}-Y_{23}Y_{32}+Y_{22}Y_{33}+Y_{11}^{F1}\left(Y_{11}^{F2}+Y_{33}\right)} \\ Y_{13}^{Dip} = -\dfrac{Y_{12}^{F2}\left(Y_{11}^{F1}Y_{13}+Y_{13}Y_{22}-Y_{12}Y_{23}\right)}{Y_{11}^{F2}Y_{22}-Y_{23}Y_{32}+Y_{22}Y_{33}+Y_{11}^{F1}\left(Y_{11}^{F2}+Y_{33}\right)} \\ Y_{21}^{Dip} = -\dfrac{Y_{12}^{F1}\left(-Y_{11}^{F2}Y_{21}+Y_{23}Y_{31}-Y_{21}Y_{33}\right)}{Y_{11}^{F2}Y_{22}-Y_{23}Y_{32}+Y_{22}Y_{33}+Y_{11}^{F1}\left(Y_{11}^{F2}+Y_{33}\right)} \\ Y_{22}^{Dip} = Y_{22}^{F1} - \dfrac{\left(Y_{12}^{F1}\right)^2\left(Y_{11}^{F2}+Y_{33}\right)}{Y_{11}^{F2}Y_{22}-Y_{23}Y_{32}+Y_{22}Y_{33}+Y_{11}^{F1}\left(Y_{11}^{F2}+Y_{33}\right)} \\ Y_{23}^{Dip} = \dfrac{Y_{12}^{F1}Y_{12}^{F2}Y_{23}}{Y_{11}^{F2}Y_{22}-Y_{23}Y_{32}+Y_{22}Y_{33}+Y_{11}^{F1}\left(Y_{11}^{F2}+Y_{33}\right)} \\ Y_{31}^{Dip} = \dfrac{Y_{12}^{F2}\left(-Y_{11}^{F1}Y_{31}-Y_{22}Y_{31}+Y_{21}Y_{32}\right)}{Y_{11}^{F2}Y_{22}-Y_{23}Y_{32}+Y_{22}Y_{33}+Y_{11}^{F1}\left(Y_{11}^{F2}+Y_{33}\right)} \\ Y_{32}^{Dip} = \dfrac{Y_{12}^{F1}Y_{12}^{F2}Y_{32}}{Y_{11}^{F2}Y_{22}-Y_{23}Y_{32}+Y_{22}Y_{33}+Y_{11}^{F1}\left(Y_{11}^{F2}+Y_{33}\right)} \\ Y_{33}^{Dip} = Y_{22}^{F2} - \dfrac{\left(Y_{12}^{F2}\right)^2\left(Y_{11}^{F1}+Y_{22}\right)}{Y_{11}^{F2}Y_{22}-Y_{23}Y_{32}+Y_{22}Y_{33}+Y_{11}^{F1}\left(Y_{11}^{F2}+Y_{33}\right)} \end{cases} \tag{A1}$$

In case impedance matrices Z are used, the following expression is valid:

$$\begin{cases} Z_{11}^{Dip} = Z_{11} - \dfrac{\begin{array}{c}+Z_{11}^{F2}Z_{12}Z_{21} + Z_{13}\left(Z_{11}^{F1}+Z_{22}\right)Z_{31} \\ -Z_{12}Z_{23}Z_{31} - Z_{13}Z_{21}Z_{32} + Z_{12}Z_{21}Z_{33}\end{array}}{-Z_{23}Z_{32}+\left(Z_{11}^{F1}+Z_{22}\right)\left(Z_{11}^{F2}+Z_{33}\right)} \\ Z_{12}^{Dip} = \dfrac{Z_{12}^{F1}\left(Z_{11}^{F2}Z_{12}-Z_{13}Z_{32}+Z_{12}Z_{33}\right)}{Z_{11}^{F2}Z_{22}-Z_{23}Z_{32}+Z_{22}Z_{33}+Z_{11}^{F1}\left(Z_{11}^{F2}+Z_{33}\right)} \\ Z_{13}^{Dip} = \dfrac{Z_{12}^{F2}\left(Z_{11}^{F1}Z_{13}+Z_{13}Z_{22}-Z_{12}Z_{23}\right)}{Z_{11}^{F2}Z_{22}-Z_{23}Z_{32}+Z_{22}Z_{33}+Z_{11}^{F1}\left(Z_{11}^{F2}+Z_{33}\right)} \\ Z_{21}^{Dip} = \dfrac{Z_{21}^{F1}\left(Z_{11}^{F2}Z_{21}-Z_{23}Z_{31}+Z_{21}Z_{33}\right)}{Z_{11}^{F2}Z_{22}-Z_{23}Z_{32}+Z_{22}Z_{33}+Z_{11}^{F1}\left(Z_{11}^{F2}+Z_{33}\right)} \\ Z_{22}^{Dip} = Z_{22}^{F1} - \dfrac{Z_{12}^{F1}Z_{21}^{F1}\left(Z_{11}^{F2}+Z_{33}\right)}{Z_{11}^{F2}Z_{22}-Z_{23}Z_{32}+Z_{22}Z_{33}+Z_{11}^{F1}\left(Z_{11}^{F2}+Z_{33}\right)} \\ Z_{23}^{Dip} = \dfrac{Z_{12}^{F2}Z_{21}^{F1}Z_{23}}{Z_{11}^{F2}Z_{22}-Z_{23}Z_{32}+Z_{22}Z_{33}+Z_{11}^{F1}\left(Z_{11}^{F2}+Z_{33}\right)} \\ Z_{31}^{Dip} = -\dfrac{Z_{21}^{F2}\left(Z_{11}^{F1}Z_{31}+Z_{22}Z_{31}-Z_{21}Z_{32}\right)}{Z_{23}Z_{32}-\left(Z_{11}^{F1}+Z_{22}\right)\left(Z_{11}^{F2}+Z_{33}\right)} \\ Z_{32}^{Dip} = -\dfrac{Z_{12}^{F1}Z_{21}^{F2}Z_{32}}{Z_{23}Z_{32}-\left(Z_{11}^{F1}+Z_{22}\right)\left(Z_{11}^{F2}+Z_{33}\right)} \\ Z_{33}^{Dip} = Z_{22}^{F2} + \dfrac{Z_{12}^{F2}Z_{21}^{F2}\left(Z_{11}^{F1}+Z_{22}\right)}{Z_{23}Z_{32}-\left(Z_{11}^{F1}+Z_{22}\right)\left(Z_{11}^{F2}+Z_{33}\right)} \end{cases} \tag{A2}$$

L_1 and L_2 have to be calculated alternatively using the formula (A3). As indicated in [8], and repeated for simplicity, it is always possible to minimize the reflectivity of the two-port junction realized by closing an arm of a reciprocal and lossless three-port junction, say port 2, on a reactive load jX, provided that the load is position at a distance L:

$$L(f) = \frac{\psi - \phi}{2\beta} \tag{A3}$$

where $e^{j\psi}$ is the reflection of the reactive load, β the propagation constant of the feed waveguides and ϕ is a quantity that depends on the scattering parameters of the junction.

Using the property of the Y-junction $S_{11} = S_{22} = S_{33}$, the formulas given in [8], reduces to the form:

$$\phi = 2\tan^{-1}\left(\frac{-b + \sqrt{a^2 + b^2 - c}}{c - a}\right) \tag{A4}$$

where

$$\begin{aligned} a &= \left(1 + a_{11}^2\right)\sin\left(\phi_s - 2\phi_{11}\right) - 2a_{11}\sin\left(\phi_{11}\right) \\ b &= \left(1 + a_{11}^2\right)\cos\left(\phi_s - 2\phi_{11}\right) - 2a_{11}\cos\left(\phi_{11}\right) \\ c &= 2a_{11}\sin\left(3\phi_{11} - \phi_s\right) \end{aligned}$$

with,

$$\phi_s = \measuredangle\left(S_{11}^3 - 3S_{11}S_{12}^2 + 2S_{12}^3\right)$$

In (A4), $S_{11} = a_{11}e^{j\phi_{11}}$ and $S_{12} = a_{12}e^{j\phi_{12}}$ are the scattering parameter at the input port and ϕ_s is the phase of the determinant of the scattering matrix of the three-port junction computed at the frequency f (i.e., alternatively the center frequency of channel one and two). If L is negative then it is necessary to add $\lambda_g/2$.

REFERENCES

1. Cohn, S. B., "Direct-coupled-resonator filters," *Proc. IRE*, Vol. 45, 187–196, Feb. 1957.
2. Levy, R., "Theory of direct coupled cavity filters," *IEEE Trans. on Microwave Theory and Techniques*, Vol. 11, 340–348, Jun. 1967.
3. Rhodes, J. D. and R. Levy, "A generalized multiplexer theory," *IEEE Trans. on Microwave Theory and Techniques*, Vol. 27, 99–111, Feb. 1979.
4. Vanin, F. M., D. Schmitt, and R. Levy, "Dimensional synthesis of wideband waveguide filters," *2004 IEEE MTT-S Symposium Digest*, Vol. 2, 463–466, Jun. 2004.

5. Vanin, F. M., D. Schmitt, and R. Levy, "Dimensional synthesis of wideband waveguide filters and diplexers," *IEEE Trans. on Microwave Theory and Techniques*, Vol. 52, No. 11, 2488–2495, Nov. 2004.
6. Cameron, R. J., R. R. Mansour, and C. M. Kudsia, *Microwave Filters for Communication Systems: Fundamentals, Design and Applications*, Hardcover, Jul. 27, 2007.
7. Matthaei, G. L., L. Young, and E. M. T. Jones, *Microwave Filters, Impedance-matching Networks and Coupling Structures*, McGraw-Hill, New York, 1964.
8. Morini, A., T. Rozzi, and M. Morelli, "New formulae for the initial deisgn in the optimization of T-junction manifold multiplexers," *1997 IEEE MTT-S International Microwave Symposium Digest*, Vol. 2, 1025–1028, Jun. 1997.
9. FEST3D, "Fullwave electromagnetic simulation tool," www.fest3d.com.

A Direct Synthesis Approach for Microwave Filters With a Complex Load and Its Application to Direct Diplexer Design

Ke-Li Wu, *Senior Member, IEEE*, and Wei Meng

***Abstract*—This paper presents a direct synthesis approach for general Chebyshev filters terminated with a complex load. The new approach is based on the fact that the polynomial functions for synthesizing the filters are composed for any matched loads. By normalizing the polynomial functions with assumed complex matched load impedance by a real reference load impedance using power waves normalization, a set of new polynomial functions for the same filter, but with real load impedance, can be formulated, from which the coupling matrix for the physical filter design can be obtained using a standard direct filter synthesis approach.**

This new direct synthesis approach can find many applications. A practical application is the direct diplexer design with a realistic junction model being taken into account. With the diplexer design is concerned, a fast-converged iterative scheme is proposed. The effectiveness and the validation of the proposed scheme are demonstrated by two design examples.

***Index Terms*—Chebyshev filter, diplexer, filter synthesis, impedance matching.**

I. Introduction

THE SYNTHESIS of microwave filters has attracted a great deal of attention over the last few decades. The most significant work for the exact synthesis of microwave filters includes the multicoupled resonator filter network by Atia and Williams [1] and Atia *et al.* [2] and the direct synthesis approach for general Chebyshev filters by Cameron [3], [4].

All of these *direct* synthesis techniques assume that the two-port filter network is terminated by real valued reference impedances at the two ends. In fact, this reference impedance is a symbolic substitute for the characteristic impedance of the transmission line connected to the microwave filter. Generally, the two reference impedances at the two ports of a filter network, i.e., Z_1 and Z_2 in Fig. 1, can be arbitrary impedance values. However, the filters synthesized by the existing direct approaches can only be used for the applications where the two ports of a filter are interfaced to the same reference impedance.

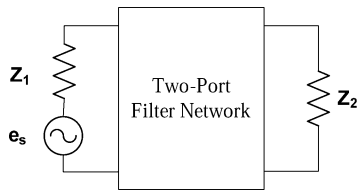

Fig. 1. Filter network terminated with reference impedances Z_1 and Z_2.

In many applications, a filter network is used in the circumstance in which the reference impedance at one end is a complex valued impedance, whereas the other end of the filter is terminated by a real valued reference impedance. Such complex valued impedance could be the input impedance of an antenna prefixed to the filter or the output impedance of a power amplifier suffixed to the filter in a front-end system. In the scenario of a diplexer design, the complex impedance would be the input impedance looking into the junction of the diplexer where the channel filters are attached to. However, the issue of how to directly synthesize a general Chebyshev filter with a complex reference impedance has never been systematically addressed.

Synthesis of a diplexer is a classic subject in the community and has led to a large amount of literature. An early work on direct synthesis techniques can be found in the paper by Haine and Rhodes [5] published in the 1970s. The effort has been continued by many researchers, such as in [6]–[8] and a very recent work [9]. An investigation on how to optimize the performance of a diplexer using a symmetric junction was also performed [10]. The major limitations in [5]–[9] include: 1) the junction is modeled by a simple series resistance or a shunt reactance, which has a large variation from the actual junction and 2) the parameters for the two channel filters are initially derived at the same working frequency. Very recently, people has attempted to incorporate the actual effect of the junction into the channel filter design by modifying the first irises and cavities next to the junction of the two channel filters to compensate for the complex impedance effect of the junction [11].

On the other hand, the diplexer design could start from an actual junction model and two channel filters that are separately designed. Nonlinear optimization is then used to find a satisfactory overall performance of a diplexer [12]–[14]. Although the optimization approaches are considered to be practical and can give reasonable results for most of cases if the junction meets the required conditions and the initial starting point is lucky enough,

Manuscript received October 24, 2006; revised January 15, 2007. This work was supported by the Research Grants Council of the Hong Kong Special Administrative Region under Grant 2150499.

K.-L. Wu is with the Department of Electronic Engineering, The Chinese University of Hong Kong, Shatin, Hong Kong (e-mail: klwu@ee.cuhk.edu.hk).

W. Meng was with the Department of Electronic Engineering, The Chinese University of Hong Kong, Shatin, Hong Kong. He is now with the Department of Electrical and Computer Engineering, University of Maryland at College Park, College Park, MD 20742 USA.

Color versions of one or more of the figures in this paper are available online at http://ieeexplore.ieee.org.

Digital Object Identifier 10.1109/TMTT.2007.895175

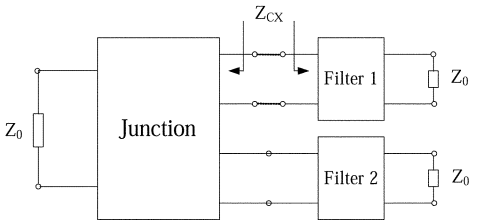

Fig. 2. Schematic diagram of a diplexer; all ports are terminated by the matched reference impedances.

people have never stopped seeking an efficient, systematic, and mathematically elegant direct technique for synthesizing microwave diplexers. A more systematic design technique that can take into account the actual junction effect is desirable.

This paper will firstly propose a new concept for direct synthesis of a general Chebyshev microwave filter with a complex load as the reference impedance. The concept is based on the fact that the rational polynomial functions that define the reflection and transfer functions of a filter are virtually referenced to two matched impedances of any value. Using the theory of power waves normalization [15], the rational functions with an assumed matched complex load can be normalized by real valued loads at the both filter ends so that the existing direct synthesis techniques for general Chebyshev filters, such as [3], can still be employed. In other words, all the existing direct approaches can be extended to the cases in which the filter is terminated by a complex load at one end and a real valued load on the other.

As depicted in Fig. 2, when the common port of the junction is connected to the matched reference impedance Z_0 and the right-bottom port of the junction is loaded with channel filter 2, the input impedance $Z_{\rm CX}$ looking into the above-right port of junction can be viewed as the complex load impedance at the port of channel filter 1. Via the new concept proposed in this paper, channel filter 1 can be synthesized straightforwardly. Obviously the same procedures can be applied to channel filter 2. Therefore, a diplexer with a specific junction model can be designed in an iterative manner.

Before the iterative design approach is detailed, the new concept for direct synthesis of a general Chebyshev microwave filter with a complex load will be formulized. The new concept is justified by two diplexer design examples: a coaxial diplexer with a simple wire Y-junction and a waveguide diplexer using an E-plane T-junction with a coupled slit, respectively.

II. Synthesis of a Filter With a Complex Load

The starting point for the direct synthesis of generalized Chebyshev filter is to construct three polynomials, i.e., $E(s), F(s)$, and $P(s)$, using a well developed procedure with pre-described transmission zeros (TZs), a reflection level, and the order of the filter [3]. The transfer function S_{21} and the reflection functions S_{11} are then defined from these polynomials. It is worth mentioning that the terminating conditions to evaluate the transfer and reflection functions do not stipulate any specific impedance value. Therefore, a filter with equiripple responses can be interpreted to be with a complex reference impedance at one end and a real reference impedance at the other end.

The main idea of this new concept is to normalize the assumed complex matched impedance at one end of the filter to the same real valued matched impedance as that at the other end of the filter. Being aware of that, the evaluation of transfer and reflection functions depends on the terminal conditions [15], three new polynomials $E'(s), F'(s)$, and $P'(s)$ for real valued terminations can be formulated from those with a complex termination and the complex load. It is obvious that the responses of a filter with two real valued load impedances correspond to the measurement of a standalone filter.

A. Renormalization of Reference Impedances

Suppose that the scattering matrix $[S]$ of a two-port network is given and is referenced by the matched impedance Z_1 at port 1 and Z_2 at port 2, as shown in Fig. 1.

If the terminal impedances of the two-port network are changed from Z_i to Z_i' ($i = 1$ and 2), the new scattering matrix $[S']$ can be expressed in terms of the original $[S]$ and the reflection coefficient r_i of Z_i' with respect to Z_i^* [15] as

$$[S'] = [A]^{-1}([S] - [\Gamma]^+)([I] - [\Gamma][S])^{-1}[A]^+ \tag{1}$$

where $[I]$ is the identity matrix, $[\Gamma]$ and $[A]$ are the diagonal matrices with their ith diagonal elements being

$$\Gamma_i = r_i = \frac{Z_i' - Z_i}{Z_i' + Z_i^*} \tag{2}$$

$$A_i = \frac{1 - r_i^*}{|1 - r_i|}\sqrt{|1 - r_i r_i^*|} \tag{3}$$

and the superscript "-1" and $^+$ represent the matrix inverse and matrix complex conjugate transpose, respectively.

Considering that

$$([S] - [\Gamma]^+) = \begin{bmatrix} S_{11} & S_{12} \\ S_{21} & S_{22} \end{bmatrix} - \begin{bmatrix} r_1^* & 0 \\ 0 & r_2^* \end{bmatrix} = \begin{bmatrix} S_{11} - r_1^* & S_{12} \\ S_{21} & S_{22} - r_2^* \end{bmatrix} \tag{4}$$

$$([I] - [\Gamma][S])^{-1} = \left(\begin{bmatrix} 1 - r_1 S_{11} & -r_1 S_{12} \\ -r_2 S_{21} & 1 - r_2 S_{22} \end{bmatrix} \right)^{-1} = \begin{bmatrix} \dfrac{1 - r_2 S_{22}}{\Delta_S} & \dfrac{r_1 S_{12}}{\Delta_S} \\ \dfrac{r_2 S_{21}}{\Delta_S} & \dfrac{1 - r_1 S_{11}}{\Delta_S} \end{bmatrix} \tag{5a}$$

where

$$\Delta_S = (1 - r_1 S_{11})(1 - r_2 S_{22}) - r_1 r_2 S_{12} S_{21} \tag{5b}$$

the new scattering matrix after the change of the terminal impedances from Z_i to Z_i' ($i = 1$ and 2) becomes (6), shown at the bottom of the following page.

In designing a channel filter for a diplexer, the reference impedances at two ports of a channel filter, when detached from the junction, are the same reference impedance associated to the transmission line connected to the filter. When the filter is loaded on the junction, the reference impedance at the connecting port will be amended to a complex number to reflect the

presence of the junction. However, in this scenario, only the reference impedance at one port is changed.

Without losing generality, assuming port 2 of a filter is originally connected to a complex load and is to be changed to the same real valued impedance as that of port 1, i.e., $Z_2' = Z_1' = Z_1 = Z_0$, where Z_0 is a positive real number standing for the characteristic impedance of the transmission line connected to the ports of the filter, and $Z_2 = Z_{\rm CX}$, which is a complex value related to the complex load, the above equations can be greatly simplified as

$$\begin{aligned} r_1 &= 0 \\ r_1^* &= 0 \\ \Delta_S &= (1 - r_1 S_{11})(1 - r_2 S_{22}) - r_1 r_2 S_{12} S_{21} \\ &= 1 - r_2 S_{22} \\ S_{11}' &= S_{11} + \frac{S_{12} r_2 S_{21}}{(1 - r_2 S_{22})} \\ &= \frac{S_{11} - r_2 S_{11} S_{22} + r_2 S_{12} S_{21}}{(1 - r_2 S_{22})} \end{aligned} \tag{7}$$

$$S_{11}' = S_{11} + \frac{S_{12} r_2 S_{21}}{(1 - r_2 S_{22})} = \frac{S_{11} - r_2 S_{11} S_{22} + r_2 S_{12} S_{21}}{(1 - r_2 S_{22})} \tag{8a}$$

$$S_{12}' = \frac{\sqrt{|\mathrm{Re}\, Z_2'|}}{\sqrt{|\mathrm{Re}\, Z_2|}} (1 - r_2) \frac{S_{12}}{1 - r_2 S_{22}} \tag{8b}$$

$$S_{21}' = \frac{\sqrt{|\mathrm{Re}\, Z_2'|}}{\sqrt{|\mathrm{Re}\, Z_2|}} (1 - r_2) \frac{S_{21}}{1 - r_2 S_{22}} \tag{8c}$$

$$S_{22}' = \frac{(1 - r_2)}{(1 - r_2^*)} \frac{S_{22} - r_2^*}{1 - r_2 S_{22}}. \tag{8d}$$

Since the real part of input impedance of a passive network is always positive, the following relation has been used in deriving S_{21}' in (8c):

$$\frac{\sqrt{|\mathrm{Re}\, Z_2|}}{\sqrt{|\mathrm{Re}\, Z_2'|}} \frac{(1 - r_2 r_2^*)}{(1 - r_2^*)} = \frac{\sqrt{|\mathrm{Re}\, Z_2'|}}{\sqrt{|\mathrm{Re}\, Z_2|}} (1 - r_2). \tag{9}$$

B. Transformation of Transfer and Reflection Functions

It is our hypothesis that a general Chebyshev filter that is with equiripple return loss in its passband and is with a complex load is to be designed. The transfer and reflection polynomials for a matched general Chebyshev filter can be composed by an existing standard procedure [3] in the format of

$$\begin{aligned} S_{11} &= \frac{F_{11}(s)}{E(s)} \\ S_{22} &= \frac{F_{22}(s)}{E(s)} \end{aligned} \tag{10a}$$

$$S_{12} = S_{21} = \frac{P(s)/\varepsilon}{E(s)} \tag{10b}$$

where ε is a normalization constant related to the prescribed return loss level. According to the procedure, for a matched Chebyshev characteristics, there is

$$F_{11}(s) = F_{22}(s) = F(s). \tag{10c}$$

It is assumed that the polynomials $E(s)$, $F(s)$, and $P(s)$ have been normalized to their respective highest degree coefficients. Both $E(s)$ and $F(s)$ are Nth-degree polynomials, N is the degree of the filtering function, whereas $P(s)$, which contains the finite-position prescribed TZs, is of degree $n_{\rm fz}$, where $n_{\rm fz}$ is the number of finite-position TZs. It is also noticed that the polynomials $E(s), F(s)$, and $P(s)$ are related by

$$F(s) \cdot F(s) - P(s)/\varepsilon \cdot P(s)/\varepsilon = E(s) \cdot E^*(s) \tag{11}$$

where the roots of polynomial $E^*(s)$ form mirror imaginary pairs about the imaginary axis with corresponding roots of polynomial $E(s)$, and $E(s)$ is a Hurwitz polynomial and all of its roots are located in the left half-plane of the complex s-plane.

Substituting (10) into (8) yields

$$\begin{aligned} S_{11}' &= \frac{\dfrac{F(s)}{E(s)} - r_2 \dfrac{F(s)}{E(s)} \dfrac{F(s)}{E(s)} + r_2 \dfrac{P(s)/\varepsilon}{E(s)} \dfrac{P(s)/\varepsilon}{E(s)}}{1 - r_2 \dfrac{F(s)}{E(s)}} \\ &= \frac{E(s)F(s) - r_2 E(s) E^*(s)}{E(s)(E(s) - r_2 F(s))} \\ &= \frac{F(s) - r_2 E^*(s)}{E(s) - r_2 F(s)} \end{aligned} \tag{12a}$$

$$\begin{aligned} S_{12}' &= S_{21}' \\ &= \frac{\sqrt{|\mathrm{Re}\, Z_2'|}}{\sqrt{|\mathrm{Re}\, Z_2|}} (1 - r_2) \frac{P(s)/\varepsilon}{E(s) - r_2 F(s)} \end{aligned} \tag{12b}$$

$$S_{22}' = \frac{(1 - r_2)}{(1 - r_2^*)} \frac{F(s) - r_2^* E(s)}{E(s) - r_2 F(s)}. \tag{12c}$$

Therefore, the new transfer and reflection polynomials, after changing the terminal impedance at port 2 from Z_2 to Z_0, can be transformed as

$$E'(s) = E(s) - r_2 F(s) \tag{13a}$$

$$F_{11}'(s) = F(s) - r_2 E^*(s) \tag{13b}$$

$$F_{22}'(s) = F(s) - r_2^* E(s) \tag{13c}$$

$$[S'] = [A]^{-1}([S] - [\Gamma]^+)([I] - [\Gamma][S])^{-1}[A]^+ = \begin{bmatrix} \left(\frac{S_{11} - r_1^*}{(1 - r_1^*)} \frac{1 - r_2 S_{22}}{\Delta_S} + \frac{S_{12}}{(1 - r_1^*)} \frac{r_2 S_{21}}{\Delta_S} \right)(1 - r_1) & \frac{\sqrt{|\mathrm{Re}\, Z_1|}}{\sqrt{|\mathrm{Re}\, Z_1'|}} \frac{\sqrt{|\mathrm{Re}\, Z_2'|}}{\sqrt{|\mathrm{Re}\, Z_2|}} (1 - r_2) \left(\frac{S_{11} - r_1^*}{(1 - r_1^*)} \frac{r_1 S_{12}}{\Delta_S} + \frac{S_{12}}{(1 - r_1^*)} \frac{1 - r_1 S_{11}}{\Delta_S} \right) \\ \frac{\sqrt{|\mathrm{Re}\, Z_1'|}}{\sqrt{|\mathrm{Re}\, Z_1|}} \frac{\sqrt{|\mathrm{Re}\, Z_2|}}{\sqrt{|\mathrm{Re}\, Z_2'|}} (1 - r_1) \left(\frac{S_{21}}{(1 - r_2^*)} \frac{1 - r_2 S_{22}}{\Delta_S} + \frac{S_{22} - r_2^*}{(1 - r_2^*)} \frac{r_2 S_{21}}{\Delta_S} \right) & \left(\frac{S_{21}}{(1 - r_2^*)} \frac{r_1 S_{12}}{\Delta_S} + \frac{S_{22} - r_2^*}{(1 - r_2^*)} \frac{1 - r_1 S_{11}}{\Delta_S} \right)(1 - r_2) \end{bmatrix} \tag{6}$$

TABLE I
5–1 FILTERING FUNCTION: ROOTS OF $E(s)$, $F(s)$, AND $P(s)$ POLYNOMIALS

	Roots of *P(s)*	Roots of *F(s)*	Roots of *E(s)*
1	+j 1.42	-j0.9375	-0.2802 - j1.1977
2	--	-j0.4901	-0.6840 - j0.6070
3	--	+j0.1636	-0.7180 + j0.2381
4	--	+j0.7064	-0.4269 + j0.8773
5	--	+j0.9695	-0.1126 + j1.1010
	$\varepsilon = 1.5479$		

	S	1	2	3	4	5	L
S	0	1.0540	0	0	0	0	0
1	1.0540	0.0366	0.7544	0.4941	0	0	0
2	0	0.7544	-0.6410	0.5101	0	0	0
3	0	0.4941	0.5101	0.1053	0.6526	0	0
4	0	0	0	0.6526	0.0506	0.9018	0
5	0	0	0	0	0.9018	0.0366	1.0540
L	0	0	0	0	0	1.0540	0

(a)

	S	1	2	3	4	5	L
S	0	1.0540	0	0	0	0	0
1	1.0540	0.0366	0.7544	0.4941	0	0	0
2	0	0.7544	-0.6410	0.5101	0	0	0
3	0	0.4941	0.5101	0.1053	0.6526	0	0
4	0	0	0	0.6526	0.0506	0.9018	0
5	0	0	0	0	0.9018	-1.6296	1.6665
L	0	0	0	0	0	1.6665	0

(b)

Fig. 3. (a) Coupling matrix $[M]$ synthesized from polynomials $E(s), F(s)$, and $P(s)$. (b) Coupling matrix $[M']$ from polynomials $E'(s), F'(s)$, and $P'(s)$.

and

$$P'(s) = P(s). \tag{13d}$$

It can be shown that $E'(s)$ is still a Hurwitz polynomial and the roots of $F'_{11}(s)$ and $F'_{22}(s)$ form mirror imaginary pairs as expected for an unmatched filter. In fact, (13) gives all the required polynomials for the same general Chebyshev filter that was originally terminated by one complex load and this complex load has been replaced by the same real load as that connected to the other end of the filter. Note that the complex load is evaluated at the center frequency of the filter.

C. Illustration Example

To illustrate the new concept, an example is given here for a fifth-degree 22-dB equiripple return-loss filter with a TZ positioned at $+j1.42$ in the normalized s-plane to give a rejection sidelobe of 30 dB on the upper side of the passband.

Following the standard procedure [3], the polynomials $E(s), F(s)$, and $P(s)$ according to the filter requirement can be easily constructed. The roots of the polynomials are given in Table I.

For unit reference impedance Z_0 at two ports, the $N+2$ coupling matrix $[M]$ according to the polynomials $E(s), F(s)$, and $P(s)$ can be synthesized and is given in Fig. 3(a). Theoretically, the S-parameters directly derived from this coupling matrix should give an equiripple response in the passband and a TZ at normalized frequency 1.42.

TABLE II
5–1 FILTERING FUNCTION: ROOTS OF $E'(s)$, $F'(s)$, AND $P'(s)$ POLYNOMIALS

	Roots of *P'(s)*	Roots of $F'_{11}(s)$	Roots of $F'_{22}(s)$	Roots of *E'(s)*
1	+j 1.42	0.1764 - j1.0092	-0.1764 - j1.0092	-0.2477 - j1.0782
2	--	0.3594 - j0.2709	-0.3594 - j0.2709	-0.5484 - j0.2970
3	--	0.2801 + j0.5760	-0.2801 + j0.5760	-0.4199 + j0.6344
4	--	0.0818 + j1.0133	-0.0818 + j1.0133	-0.1082 + j1.0502
5	--	-2.5638 + j1.7689	2.5638 + j1.7689	-2.5639 + j1.7688
	$\varepsilon = 1.5479$			

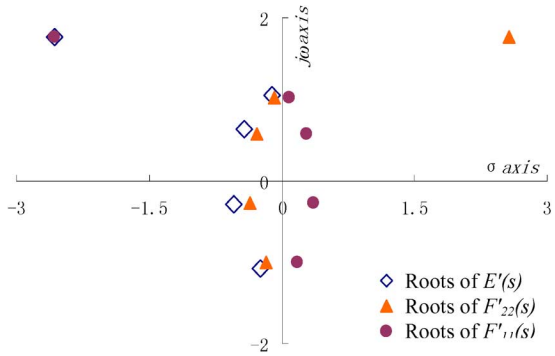

Fig. 4. Locations of roots of $E'(s), F'_{11}(s)$, and $F'_{22}(s)$ on the complex s-plane.

In order to synthesize the coupling matrix $[M']$ having the same responses, but with a complex reference impedance at one port, say, at port 2, a new set of polynomials $E'(s), F'(s)$, and $P'(s)$ must be sought. Without losing generality, the complex reference impedance $Z_2 = 0.4 + j0.6$ is considered in this example. By setting Z'_2 to unit impedance Z_0, the reflection coefficient r_2 will be $r_2 = (Z'_2 - Z_2)/(Z'_2 + Z_2^*) = 0.5172 - \text{j}0.2069$.

Using (13), the new polynomials $E'(s), F'_{11}(s), F'_{22}(s)$, and $P'(s)$ can be found, the roots of which are given in Table II. It is shown in Fig. 4 that the roots of $F'_{11}(s)$ and $F'_{22}(s)$ form mirror image pairs about the imaginary axis, and the roots of $E'(s)$ still satisfy the Hurwitz condition, all of which lie in the left plane of the complex s-plane.

An existing coupling matrix synthesis procedure can be applied to the new polynomials to obtain a new coupling matrix $[M']$, as given in Fig. 3(b). Moreover, the lossless condition of a two-port network has to be guaranteed, which means that an additional coefficient must be used to adjust the S-parameters. In this case, a coefficient $\varepsilon_n = 1.5811$ can be found to be multiplied to polynomial $P'(s)$ in addition to the coefficient ε. Comparing the two coupling matrices in Figs. 3(a) and (b), the only changes happen on coupling values of the load coupling from the last resonator to the load Z_2 and the resonant frequency of the last resonator next to the load.

Three sets of S-parameters curves are superimposed in Fig. 5. The "matched" and "unmatched" cases correspond to the responses of coupling matrix $[M]$ with any matched loads and $[M']$ with real impedance Z_0 at the two ends of the filter, respectively. For "verification" purposes, the circuit model simulation results of coupling matrix $[M']$ with port 1 terminated by Z_0 and port 2 terminated by $Z_2 = 0.4 + j0.6$ are also provided in

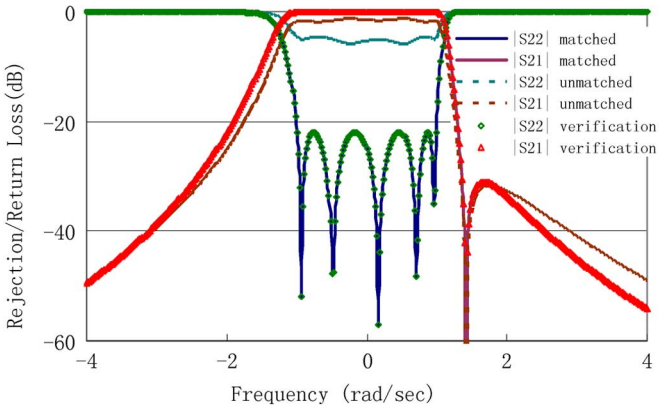

Fig. 5. Comparison of S-parameters for the matched, unmatched, and verification filters.

this figure. As expected, the "verification" curves are identical to those of the "matched" case.

III. Direct Diplexer Design

The most common approach to realize a diplexer is to use two bandpass filters that are combined through a three-port junction. Different types of junction configurations have been seen for various of applications. For RF coaxial diplexers for mobile phone base-station applications, a star-shaped wire Y-junction is commonly used, whereas for the microwave diplexers consisting of waveguide channel filters, a waveguide junction should be employed, commonly including E- or H-plane waveguide T- or Y-junctions. For designing broadband diplexers, one needs to optimize the performances of the junctions to satisfy certain necessary conditions, e.g., using a symmetric Y-junction [10] or a waveguide T-junction with a tuning conductor post [16].

Since the two channel filters are electrically connected to each other through a junction, the parameters of the two filters must be considered together in conjunction with the properties of the chosen junction in order to take into account the interaction among the filters and the junction. As depicted in Fig. 2, assuming that channel filter 2 of a diplexer with center frequency f_2 has been appropriately designed and the common port of the junction is matched, looking into the junction at the port where channel filter 1 is connected, one can find a load impedance $Z_{\rm CX}$ at f_1, which is the center frequency of channel filter 1. If the reference impedance Z_0 (which corresponds to Z_2') is given and the load impedance $Z_{\rm CX}$ (which corresponds to Z_2) is known, the polynomials for channel filter 1 can be determined by (13). Consequently, the related coupling matrix $[M_1]$ for a designated filter topology can be easily obtained from the polynomials by using an existing direct filter synthesizing approach.

It will be an *iterative* process to design the coupling matrices for the two channel filters. Having understood how channel filter 1 is directly synthesized under the assumption that the design of channel filter 2 is converged, one can alternatively apply the same scheme to channel 2 and channel 1 until the solution for the two channel filters converged.

It needs to be pointed out that since the load impedance at the center frequency of a channel is used, the approach is, in principle, a narrowband approach. However, if the slope of the complex load with respect to frequency is small, the approach can be extended to a diplexer design with moderate bandwidth.

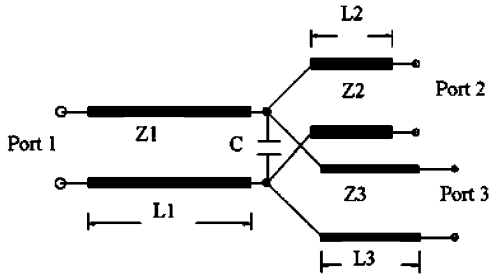

Fig. 6. Transmission line model of a wire Y-junction with a shunt capacitor.

In the proposed design procedure, appropriate lengths for the transmission lines between the junction and the channel filters have been incorporated in the junction model. In fact, the lengths need to be carefully optimized although there are some empirical rules-of-thumb to follow. From a theoretical point-of-view, the lengths should be chosen in the way that the slopes of the complex loads at the ports facing to the two filters become minimum. How to analytically design the lengths using the proposed theory is still a future research topic.

IV. Practical Design Examples

A. Diplexer With Wire Y-Junction

The first design example is with a wire Y-junction as the common junction connecting to two channel filters. Fig. 6 shows a generic transmission line model for a wire Y-junction with a shunt capacitor. It is assumed that port 1 of the junction is connected to the common port, and ports 2 and 3 are connected to the low and high channel filters, respectively.

The channel filters in this example are synthesized by the approach discussed in Section III. The input impedance looking into port 2 at f_1 (center frequency of the low channel filter), when a high channel filter is connected at port 3, is, in general, a complex number. The impedance will be used as the complex load impedance in synthesizing the low channel filter. Similarly, the input impedance looking into port 3 at f_2 (center frequency of the high channel filter), when a low channel filter is connected at port 2, is the complex load impedance in synthesizing the high channel filter. By default, port 1 is always terminated by the unit reference impedance.

To simplify the design, the characteristic impedances Z_1, Z_2, and Z_3 of the three sections of the transmission line in Fig. 6 are assumed to be the same, and the lengths L_1, L_2, and L_3 are adjustable. The two channel filters are initially designed as fifth-degree 22-dB return-loss Chebyshev filters with a TZ at $+j1.52$ for the low channel filter and a TZ at $-j1.52$ for the high channel filter, respectively. The center frequencies of two filters are at $f_1 = 1.74$ GHz and $f_2 = 1.85$ GHz, respectively, and the bandwidth of both filters is approximately 0.08 GHz.

To begin with, the coupling matrices for the two channels with matched loads are obtained and are listed in Table III in the columns of the zeroth iteration. Connecting two channel filters

TABLE III
COUPLING MATRICES OF LOW AND HIGH CHANNEL FILTER IN EACH ITERATION

	Low Channel			*High Channel*		
	0th	1st	2nd	0th	1st	2nd
M_{01}	1.0545	***0.9518***	***0.9063***	1.0545	***1.1816***	***0.9838***
M_{11}	0.0333	***1.0683***	***0.8219***	-0.0333	***-1.7225***	***-1.0079***
M_{12}	0.9026	0.9026	0.9026	0.9026	0.9026	0.9026
M_{22}	0.0464	0.0464	0.0464	-0.0464	-0.0464	-0.0464
M_{23}	0.6525	0.6525	0.6525	0.6525	0.6525	0.6525
M_{33}	0.0982	0.0982	0.0982	-0.0982	-0.0982	-0.0982
M_{34}	0.5361	0.5361	0.5361	0.5361	0.5361	0.5361
M_{35}	0.4495	0.4495	0.4495	-0.4495	-0.4495	-0.4495
M_{44}	-0.5865	-0.5865	-0.5865	0.5865	0.5865	0.5865
M_{45}	0.7827	0.7827	0.7827	0.7827	0.7827	0.7827
M_{55}	0.0333	0.0333	0.0333	-0.0333	-0.0333	-0.0333
M_{56}	1.0545	1.0545	1.0545	1.0545	1.0545	1.0545

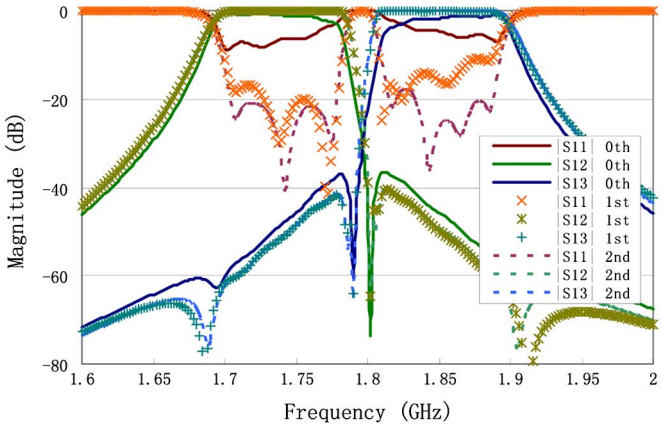

Fig. 7. Responses of the diplexer design using a wire Y-junction.

TABLE IV
INPUT IMPEDANCES AT THE PORTS OF Y-JUNCTION

	Port 2 at f_1	*Port 3 at f_2*
1st	0.4365 + j0.4063	0.3796 - j0.5767
2nd	0.4915 + j0.3486	0.4923 - j0.4315

directly onto the Y-junction, the circuit response of the diplexer in this iteration is marked by "0th" and is shown in Fig. 7.

Table IV lists the input impedances looking into ports 2 and 3, while the channel filter at the other channel that is designed in the previous iteration is connected. The coupling matrices directly synthesized for each iteration are given in Table III. The circuit responses of the diplexer for each iteration are superimposed in Fig. 7. It should be mentioned that the diplexer design reaches its satisfactory converged response only by three iterations. Notice that the responses in Fig. 7 are simulated based on the circuit model of the Y-junction and the circuit model of channel filters. A possible realization of this diplexer in a coaxial combline structure is proposed in Fig. 8.

B. Diplexer Design Using an E-Plane T-Junction

The performance of a waveguide T-junction is of great importance in designing a waveguide diplexer. The standard T-junction is widely used for narrowband diplexers. In practice, additional adjusting elements, such as coupled slit [14], inductive post [16], and reflection stub [12], [13] are required to minimize the slope of the reflection with respect to frequency over the frequencies of the channel filters. This example will demonstrate a waveguide diplexer designed using a slit-coupled E-plane T-junction with a bandwidth of 600 MHz.

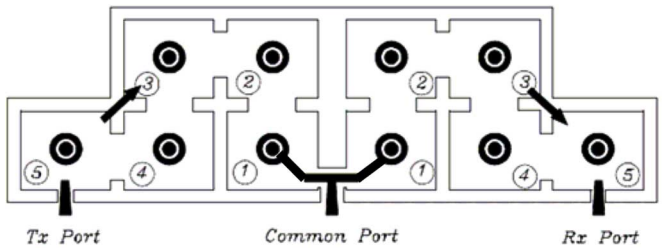

Fig. 8. Coaxial combline diplexer with two five-pole channel filters.

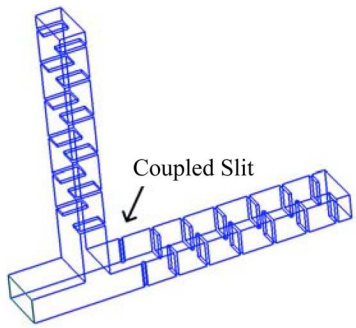

Fig. 9. Waveguide diplexer using an E-plane T-junction with a coupled slit.

TABLE V
INPUT IMPEDANCES AT THE PORTS OF E-PLANE T-JUNCTION

	Port 2 at f_1	*Port 3 at f_2*
1st	0.2909 + 0.1072i	0.7474 - 0.1072i
2nd	0.5916 + 0.0667i	0.7823 + 0.1771i
3rd	0.5888 + 0.0523i	0.7585 + 0.1838i

TABLE VI
CHANGED COUPLING ELEMENTS OF CHANNEL FILTERS IN EACH ITERATION

	0th	1st	2nd	3rd
	Low Channel			
M_{01}	1.0570	***0.6076***	***0.8182***	***0.8143***
M_{11}	0.000	***0.4117***	***0.1260***	***0.0992***
	High Channel			
M_{01}	1.0570	***0.9232***	***0.9586***	***0.9472***
M_{11}	0.000	***-0.1603***	***0.2529***	***0.2707***

Fig. 9 shows the waveguide diplexer using an E-plane T-junction with a coupled slit. The two channel filters are required to be fifth-degree 22-dB return-loss pure Chebyshev filters with two channel center frequencies at $f_1 = 12.6$ GHz and $f_2 = 14.2$ GHz, respectively. The bandwidth of both filters is approximately 600 MHz. The diplexer specifications were used for a communication satellite. A WR 75 waveguide is used as the interface.

A similar design process as that for the first design example is carried out. Again, only three iterations are required. The complex load impedances in each iteration for each channel filter are summarized in Table V. Only the changed coupling elements for the filters are given in Table VI. The circuit model responses of the diplexer in each iteration are shown in Fig. 10.

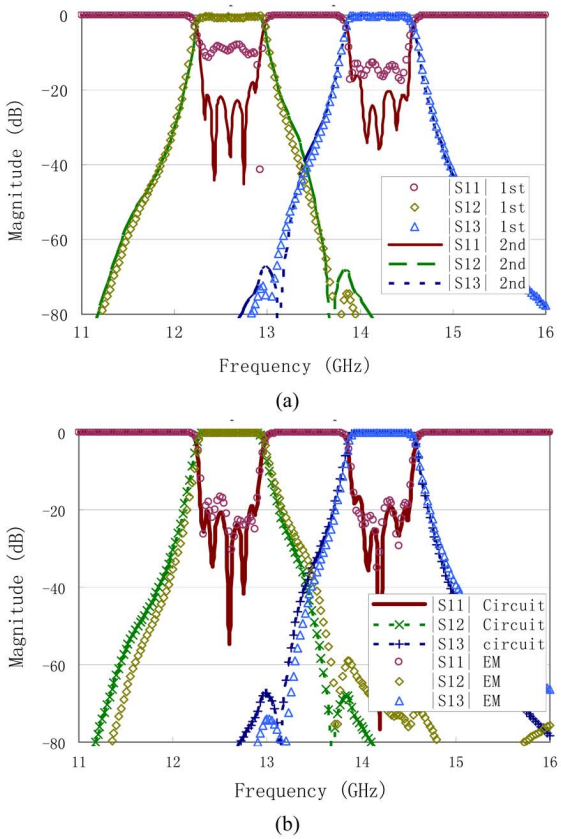

Fig. 10. Responses of the diplexer using E-plane T-junction. (a) First iteration and second iteration. (b) Circuit simulation (third iteration) and EM simulation.

It is noted that the simulation of the diplexer is based on the electromagnetic (EM) mode-matching (MM) T-junction model and the circuit channel filter model. The circuit model of the channel filters is converted into the physical model with physical dimensions by an MM program that has been fully verified for communication satellite payload applications. The complete physical model of the designed diplexer has also been simulated by the EM-based MM program. It is anticipated that the EM model will reflect the dispersion effects of the waveguide filters outside of the passband. An excellent agreement between the responses of the designed circuit model and the EM model can be observed.

V. Conclusion

A direct synthesis approach for microwave filters with a complex load impedance at one end and a real load impedance at the other end has been presented. A new set of filter design polynomials for the synthesizing required coupling matrix can be obtained by the power waves impedance normalization. The standard direct filter synthesis theory can be applied to the modified polynomials to derive the filter coupling matrix. The capability to incorporate a complex load impedance in the design of general Chebyshev filters makes this approach very useful to many applications. The approach can particularly be used for designing a diplexer with a realistic junction model. A novel iterative scheme for direct synthesizing the channel filters has also been proposed. The validation of the proposed scheme is firmly made through two design examples.

References

[1] A. E. Atia and A. E. Williams, "Narrow-bandpass waveguide filters," *IEEE Trans. Microw. Theory Tech.*, vol. MTT-20, no. 4, pp. 258–265, Apr. 1972.

[2] A. E. Atia, A. E. Williams, and R. W. Newcomb, "Narrow-band multiple-coupled cavity synthesis," *IEEE Trans. Circuits Syst.*, vol. CAS-21, no. 9, pp. 649–655, Sep. 1974.

[3] R. J. Cameron, "General coupling matrix synthesis methods for Chebyshev filtering functions," *IEEE Trans. Microw. Theory Tech.*, vol. 47, no. 4, pp. 433–442, Apr. 1999.

[4] ——, "Advanced coupling matrix synthesis techniques for microwave filters," *IEEE Trans. Microw. Theory Tech.*, vol. 51, no. 1, pp. 1–10, Jan. 2003.

[5] J. L. Haine and J. D. Rhodes, "Direct design formulas for asymmetric bandpass channel diplexer," *IEEE Trans. Microw. Theory Tech.*, vol. MTT-25, no. 10, pp. 807–814, Oct. 1977.

[6] J. D. Rhodes and R. Levy, "A generalized multiplexer theory," *IEEE Trans. Microw. Theory Tech.*, vol. MTT-27, no. 2, pp. 99–111, Feb. 1979.

[7] ——, "Design of general manifold multiplexer," *IEEE Trans. Microw. Theory Tech.*, vol. MTT-27, no. 2, pp. 111–123, Feb. 1979.

[8] R. Levy, "Synthesis of non-contiguous diplexers using broadband matching theory," in *IEEE MTT-S Int. Microw. Symp. Dig.*, Boston, MA, Jun. 10–14, 1991, pp. 543–546.

[9] G. Macchiarella and S. Tamiazzo, "Synthesis of diplexers based on the evaluation of suitable characteristic polynomials," in *IEEE MTT-S Int. Microw. Symp. Dig.*, San Francisco, CA, Jun. 2006, pp. 111–114.

[10] A. Morini and T. Rozzi, "Constrains to the optimum performance and bandwidth limitations of diplexers employing symmetric three-port junctions," *IEEE Trans. Microw. Theory Tech.*, vol. 44, no. 2, pp. 242–248, Feb. 1996.

[11] A. Morini, T. Rozzi, M. Farina, and G. Venanzoni, "A new look at the practical design of compact diplexers," *IEEE Trans. Microw. Theory Tech.*, vol. 54, no. 9, pp. 3515–3520, Sep. 2006.

[12] H.-W. Yao, A. E. Abdelmonem, J.-F. Liang, X.-P. Liang, and K. A. Zaki, "Wide-band waveguide and ridge waveguide T-junctions for diplexer applications," *IEEE Trans. Microw. Theory Tech.*, vol. 41, no. 12, pp. 2166–2173, Dec. 1993.

[13] Y. Rong, H.-W. Yao, K. A. Zaki, and T. Dolan, "Millimeter-wave Ka-band H-plane diplexers and multiplexers," *IEEE Trans. Microw. Theory Tech.*, vol. 47, no. 12, pp. 2325–2330, Dec. 1999.

[14] J. Dittloff and F. Arndt, "Computer-aided design of slit-coupled H-plane T-junction diplexers with E-plane metal-insert filters," *IEEE Trans. Microw. Theory Tech.*, vol. 36, no. 12, pp. 1833–1840, Dec. 1988.

[15] K. Kurokawa, "Power waves and the scattering matrix," *IEEE Trans. Microw. Theory Tech.*, vol. MTT-13, no. 3, pp. 194–202, Mar. 1965.

[16] K.-L. Wu and H. Wang, "A rigorous modal analysis of H-plane waveguide T-junction loaded with a partial-height post for wideband applications," *IEEE Trans. Microw. Theory Tech.*, vol. 49, no. 5, pp. 893–901, May 2001.

Ke-Li Wu (M'90–SM'96) received the B.S. and M.Eng. degrees from Nanjing University of Science and Technology, Nanjing, China, in 1982 and 1985, respectively, and the Ph.D. degree from Laval University, Quebec, QC, Canada, in 1989.

From 1989 to 1993, he was with the Communications Research Laboratory, McMaster University, Hamilton, ON, Canada, as a Research Engineer and a Research Group Manager. In March 1993, he joined the Corporate Research and Development Division, Com Dev International, where he was a Principal Member of Technical Staff in charge of developing advanced electromagnetic (EM) design software for passive microwave subsystems for communication satellites. Since October 1999, he has been with the Department of Electronic Engineering, The Chinese University of Hong Kong, Shatin, Hong Kong, where he is currently a Professor. He has authored or coauthored

numerous publications in the areas of EM modeling, microwave, and antenna engineering. His current research interests include numerical and analytical methods in electromagnetics, passive microwave circuits, filters, antennas for communication systems, low-temperature co-fired ceramic (LTCC)-based multichip modules (MCMs) for wireless communications, and RF identification (RFID) technologies.

Wei Meng received the B.Eng. degree (with first-class honors) and M.Phil. degree in electronic engineering from The Chinese University of Hong Kong, Shatin, Hong Kong, in 2003 and 2006, respectively, and is currently working toward the Ph.D. degree in electrical and computer engineering at the University of Maryland at College Park.

His research is focused on the modeling and design of passive microwave components, especially on the synthesis and design techniques of microwave filters.

DIPLEXER DESIGN USING PRE-SYNTHESIZED WAVEGUIDE FILTERS WITH STRONGLY DISPERSIVE INVERTERS

Smain Amari[*], Jens Bornemann[*], Wolfgang Menzel[#] and Ferdinando Alessandri[+]

[*]University of Victoria, Canada, [#]University of Ulm, Germany, [+]University of Perugia, Italy

Abstract: An approximate synthesis technique for strongly dispersive inverters is introduced. The technique allows the prescription of transmission zeros at finite frequencies on either side of the filter passband - symmetrically or asymmetrically - as required for diplexer applications. Several direct-coupled resonator filters with additional attenuation poles and a related diplexer design at 18.5 GHz are presented. The computerized design procedure is based on CIET (coupled-integral-equations technique) and MMT (mode-matching technique) modules. Excellent agreement between measurements and theoretical predictions is achieved.

I. INTRODUCTION

Direct-coupled resonator filters are commonly used in front-end diplexer applications,. Accurate synthesis and design techniques for this type of filters have been known for many decades, e.g., [1] - [4].

While design techniques to generate elliptic or pseudo-elliptic responses are also widely known, e.g. [5], [6], such filter are used only in L- or S- band diplexers with stringent frequency specifications. In Ku- to Ka-band diplexers, due to increased manufacturing accuracies, cost and more relaxed channel separation, the use of direct-coupled resonator filters has prevailed.

However, recent diplexer specifications with closer frequency spacing between Rx and Tx channels and asymmetric responses inspired the generation of additional attenuation poles at finite frequencies in direct-coupled resonator filters. But only a few attempts have been made to create such poles in direct-coupled waveguide filters. The most common mechanism used consist in overmoding the resonators, thereby generating poles only in the upper stopband. In waveguide filters, this approach results in all coupling sections being irises, e.g. [7]-[9].

A different technique comprises the use of inverter sections which simultaneously provide a transmission zero and the correct inverter value for the filter design. The basic principle of operation has been verified in [10] and [11].

This paper presents a design procedure for pre-synthesized, strongly dispersive inverters with application in waveguide filters and diplexers. Excellent agreement between measured and computed filter responses in the 15 and 38 Gigahertz range is demonstrated. A branching-type diplexer design operates at 18.5 GHz.

II. FILTER DESIGN

The filter design follows standard synthesis procedures to calculate impedance inverters which can be realized as low dispersive irises (Fig. 1a) or strongly dispersive stubs or T-junctions (Fig. 1b, c). If transmission zeros are not needed, then the model of the (possibly asymmetric) inverter is a shunt reactance X_p with two series reactances X_{s1}, X_{s2} and associated phases ϕ_1 and ϕ_2. Using coupled-integral-equations techniques (CIET) or mode-matching techniques (MMT), the scattering parameters of the inverter are related to the model by the following expressions:

$$jX_{s1} = \frac{[1+S_{11}][1-S_{22}]+S_{21}^2-2S_{21}}{[1-S_{11}][1-S_{22}]-S_{21}^2} \quad (1)$$

$$jX_{s2} = \frac{[1-S_{11}][1+S_{22}]+S_{21}^2-2S_{21}}{[1-S_{11}][1-S_{22}]-S_{21}^2} \quad (2)$$

$$jX_p = \frac{2S_{21}}{[1-S_{11}][1-S_{22}]-S_{21}^2} \quad (3)$$

$$\begin{bmatrix}\phi_1\\ \phi_2\end{bmatrix} = -\arctan\left\{\frac{X_{s1}+X_{s2}+2X_p}{1-X_{s1}X_{s2}-X_p(X_{s1}+X_{s2})}\right\} \mp \arctan\left\{\frac{X_{s1}-X_{s2}}{1+X_{s1}X_{s2}+X_p(X_{s1}+X_{s2})}\right\} \quad (4)$$

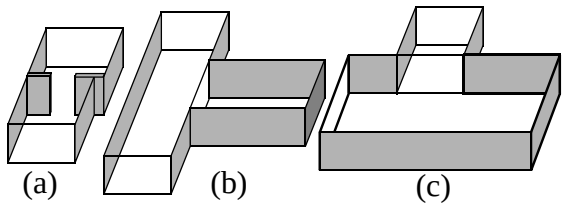

Fig. 1 *Examples of waveguide circuits used as impedance inverters: asymmetric iris (a), stub (b) and shorted T-junction (c).*

A search algorithm varies the dimensions of the circuit until the prototype inverter values K are obtained.

$$K = \sqrt{\left|\frac{1+\Gamma\exp(-j\phi_1)}{1-\Gamma\exp(-j\phi_1)}\right|} \qquad (5)$$

$$\Gamma = \frac{(jX_{s1}+jX_p-1)(jX_{s1}+jX_p+1)+X_p^2}{(jX_{s1}+jX_p+1)(jX_{s1}+jX_p+1)+X_p^2} \qquad (6)$$

In order to prescribe one or two transmission zeros at frequencies ω_{z1} and ω_{z2} to an inverter, we are solving the following equations

$$K_{Prototype} = K_{dispersive}(\omega_0, \text{dimensions}) \; . \qquad (7)$$

$$S_{21}(\omega=\omega_{z1}) = 0 \quad , \quad S_{21}(\omega=\omega_{z2}) = 0 \qquad (8)$$

simultaneously by minimizing the cost function

$$F_{cost} = [K_{Prototype} - K_{dispersive}(\omega_0, \text{dimensions})]^2 + \left|S_{21}(\omega=\omega_{z1})\right|^2 + \left|S_{21}(\omega=\omega_{z2})\right|^2 \qquad (9)$$

In a special case, where a highly dispersive element is added to a filter without acting as inverter simultaneously, the cost function is modified as

$$F_{cost} = \sum_i [1 - \left|S_{21}(\omega_i)\right|]^2 + \left|S_{21}(\omega=\omega_{z1})\right|^2 + \left|S_{21}(\omega=\omega_{z2})\right|^2 \qquad (10)$$

where ω_i are the passband frequency samples. The typical inband return loss achieved by such an approximate synthesis is in the order of 10 dB (c.f. Fig. 6) - as compared to several trial-and-error approaches which usually fall only in the 2 - 4 dB return-loss range. A final optimization, e.g. [12], of the entire filter structure is required to fine tune the return loss while maintaining the transmission zeros.

Two prototype structures involving strongly dispersive inverters have been manufactured. Fig. 2 shows the photograph of a four-pole Ku-band filter with four finite transmission zeros. Computed and measured performances are depicted in Fig. In this design, only the shorted T-junction at the lower right of the circuit (Fig. 2) is used as an inverter which generates the transmission zero (attenuation pole) at 14.175 GHz. The remaining three zeros are generated by the additional H-plane stub which does not act as an inverter. The measured insertion loss is between 0.2 and 0.3 dB within a 20dB return loss bandwidth.

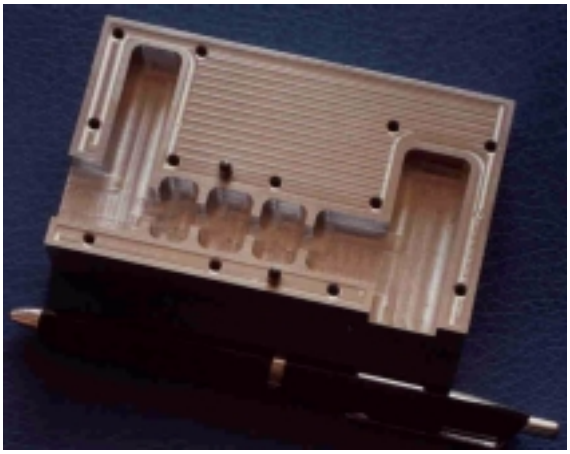

Fig. 2 *Ku-band prototype of waveguide filter with dispersive inverters.*

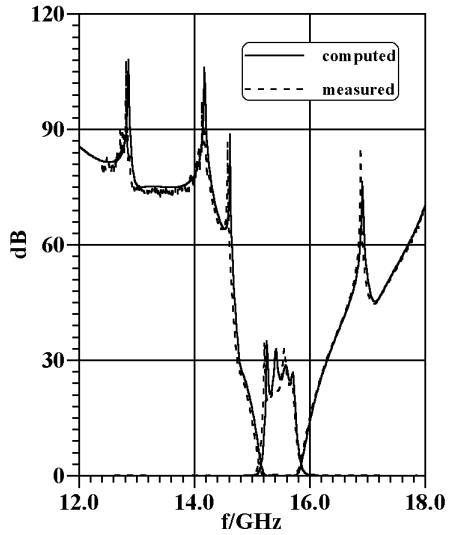

Fig. 3 *Measured and computed performance of Ku-band prototype filter (c.f. Fig. 2).*

The second example is a three-pole Q-band (WR22) filter with nearly maximally flat performance. Emphasis was placed on symmetric

skirts with sharp cutoffs. Fig. 4 shows the principle layout and Fig. 5 the computed and measured results. In this design, both shorted T-junctions act as inverters. Since the shorted sections are longer than a wavelength, they produce a number of transmission zeros but only one each in the frequency range shown. The measured insertion is between 1.1 and 1.5 dB over the 20 dB return-loss bandwidth of 230 MHz.
Note that for both prototypes, excellent agreement between measurements and the CIET/ MMT analysis techniques is demonstrated.

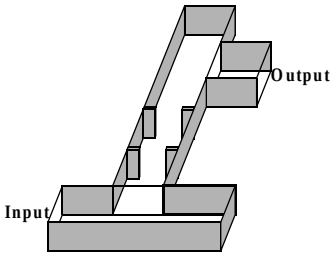

Fig. 4 *Principle layout of 38.5 GHz filter.*

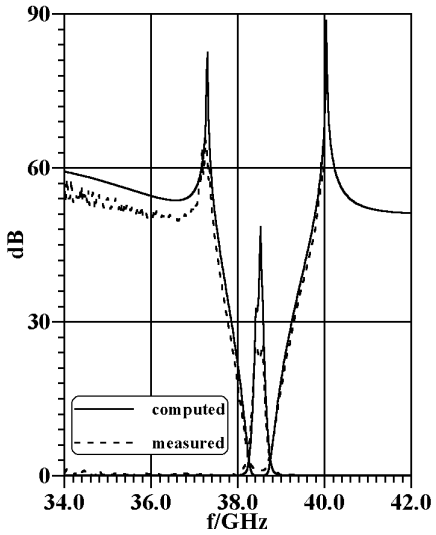

Fig. 5 *Measured and computed response of Q-band prototype filter (c.f. Fig. 4)*

III. DIPLEXER DESIGN

Using the procedure outlined in the previous section, a diplexer was designed according to the following specifications: 17.9GHz - 18.3GHz and 18.7-19.1GHz passbands with 24dB return loss, 60dB isolation. The minimum manufacturable thickness was set to 0.75mm (appr. 0.03”). As an additional requirement, Rx and Tx port locations were to be right beside each other.
Fig. 6 shows the computed performances of the pre-synthesized and fine-optimized five-pole channel filters with one attenuation pole each. Note that the pre-synthesized design is ideally suited as initial data for fine optimization. In this specific case, the optimization even varied the entire waveguide width for the benefit of a better return loss. However, the attenuation poles were kept at the same frequencies.

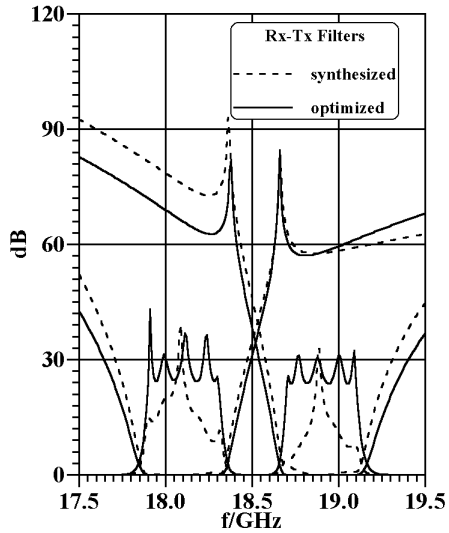

Fig. 6 *Responses of synthesized (dashed lines) and optimized (solid lines) diplexer channel filters.*

The principle layout of the branching-type diplexer is shown in Fig. 7. In order to facilitate a small spacing between the two filters, irises and stubs are pointing toward opposite sides. A combined CIET-MMT code, which is has been verified in [13], is used as analysis tool in the final diplexer fine-optimization. The resulting response is depicted in Fig. 8. In addition to the attenuation poles provided by the two stubs, the diplexer exibits the typical peaks at the cross-over frequencies of the respective other channel ([4], [13]). However, the attenuation poles are responsible for achieving the specified isolation of 60 dB. A similar diplexer design based on five-pole iris filters without strongly dispersive inverters (not shown here) achieves only 54 and 36 dB isolation at the respective inband frequencies and would require six- and seven-order filters to match the isolation performance of the design in Fig. 8.

IV. CONCLUSIONS

Pre-synthesized waveguide filters with strongly dispersive inverters offer an attractive solution

in diplexers whose specifications would otherwise require higher-order filters. Several design examples presented here demonstrate that this is a viable option in Ku- to Ka-band diplexer applications.

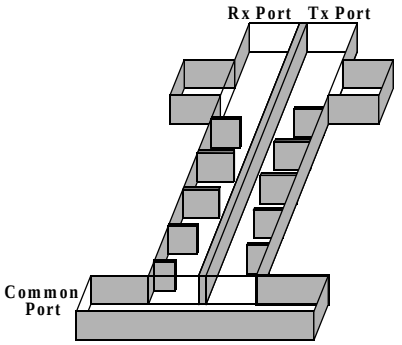

Fig. 7 *Principle layout of 18.5 GHz diplexer.*

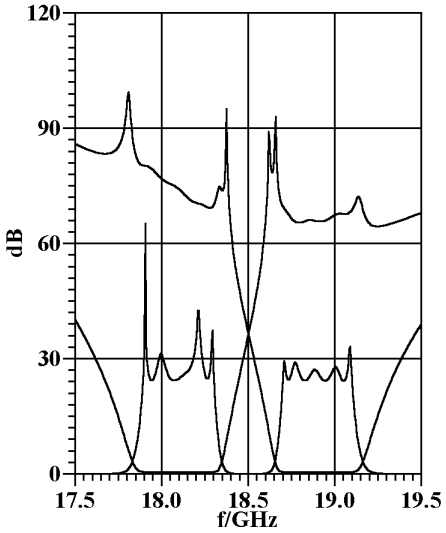

Fig. 8 *Performance of 18.5 GHz diplexer*

REFERENCES

[1] S. B. Cohn, "Direct-coupled-resonator filters", Proc. IRE, vol. 45, pp. 187-196, Feb. 1957.

[2] R. Levy, "Theory of direct-coupled-cavity filters", IEEE Trans. Microwave Theory Techn., vol. MTT-15, pp. 340-348, June 1967.

[3] G. L. Matthaei, L. Young and E. M. T. Jones, Microwave Filters, Impedance Matching Networks and Coupling Structures, McGraw-Hill, New York 1964.

[4] J. Uher, J. Bornemann and U. Rosenberg, Waveguide Components for Antenna Feed Systems. Theory and CAD. Artech House Inc., Norwood 1993.

[5] A. Atia and Williams, "New type of waveguide bandpass filters for satellite transponders", COMSAT Tech. Rev., vol. 1, No. 1, pp. 21-43, 1971.

[6] U. Rosenberg, "New 'planar' waveguide cavity elliptic function filters", Proc. 25th European Microwave Conf., Bologna, pp. 524-527, Sep. 1995.

[7] F. Arndt, T. Duschak, U. Papziner and P. Rollape, "Asymmetric iris coupled cavity filters with stopband poles", IEEE MTT-S Int. Microwave Symp. Dig., pp. 215-218, Dallas, May 1990.

[8] K. Iguchi, M. Tsuji and H. Shigesawa, "Mode-selective negative coupling for implementing multiple attenuation poles in evanescent-modewaveguide filters", IEEE MTT-S Int. Microwave Symp. Dig.,pp. 513-516, Orlando, May 1995.

[9] M. Guglielmi, "Accurate CAD of integrated band-pass and second harmonic band-reject microwave filters", IEEE MTT-S Int. Microwave Symp. Dig., pp. 813-816, Baltimore, June 1998.

[10] W. Menzel, F. Alessandri, A. Plattner and J. Bornemann, "Planar integrated waveguide diplexer for low-loss millimeter-wave applications", Proc. 27th European Microwave Conf., pp. 676-680, Jerusalem, Sep. 1997.

[11] S. Amari and J. Bornemann, "Using frequency-dependent coupling to generate finite attenuation poles in direct-coupled resonator bandpass filters", IEEE Microwave Guided Wave Lett., Vol. 9, pp. 404-406, Oct. 1999.

[12] K. Madsen, H. Schaer-Jacobsen and J. Voldby, "Automated minimax design of networks," IEEE Trans. Circuits Systems, Vol. CAS-22, pp. 791-796, Oct. 1975.

[13] J. Bornemann, S. Amari and R. Vahldieck, "A combined mode-matching and coupled-integral-equations technique for the design of narrow-band H-plane waveguide diplexers", IEEE AP-S Int. Symp. Dig., pp. 950-953, Orlando, USA, July 1999.

EFFICIENT FULL-WAVE CAD OF WAVEGUIDE DIPLEXERS

J. Bornemann[(*)], **J. Uher**[(**)] and **K. N. Patel**[(**)]

[(*)]Dept. of ECE, University of Victoria, BC V8W 3P6
[(**)]Spar Aerospace Ltd., Ste-Anne-de Bellevue, PQ H9X 3R2

ABSTRACT

The paper presents an efficient CAD algorithm for the design of waveguide front-end diplexers. Three different types of junctions can be employed: E-plane T-junction, H-plane T-junction and E-plane bifurcation. Channel filter configurations currently include - but are not limited to - waveguide stub filters and inductive-iris filters.The diplexer design is performed in three basic steps: synthesis, analysis and optimization. In order to improve the computing efficiency of the design algorithm, highly accurate transmission line models are used in the initial component design and optimization stages. The final optimization and the analysis of the entire diplexer makes use of a full-wave mode-matching model, which can include waveguide transformers at all ports.
The CAD routine is verified against measurments, and excellent agreement between predicted and measured results is obtained.

I. INTRODUCTION

Waveguide front-end diplexers are typically used in fixed satellite service (FSS) antenna systems with common transmit and receive feeds. The diplexers are employed behind each feed in order to separate Tx and Rx channels.
While it is well known that waveguide diplexers can be optimized on the basis of full-wave models, e.g. mode matching, and additional matching elements [1] - [3], such a component design is often tedious and time-consuming due to the extremely high CPU-time required. Equivalent-circuit models [4], [5], on the other hand, produce results much faster, but their applications are limited to certain dimensional constraints, due to proximity effects, where the degree of validity of such models is practically uncertain. For waveguide cross-section ratios around b/a=0.1 to 0.15, excellent diplexer designs are usually obtained by equivalent-circuit modelling of E-plane T-junctions [4] and waveguide stub filters [1]. Although such designs have been used for many years, power levels and multipactor specifications of modern satellite communication systems no longer permit reduced-height rectangular waveguide components. However, already at a ratio of 0.2 - 0.25, equivalent-circuit designs no longer produce reliable designs, hence demanding full-wave methods to be employed.

Therefore, this paper focuses on an efficient diplexer design which combines the advantages of the equivalent circuit approach with full-wave mode-matching algorithms. The software package currently contains subroutines for the following configurations (Fig. 1):

Waveguide Junctions:
- E-plane T-junctions
- E-plane bifurcations
- H-plane T-junctions

Rx and/or Tx Filters:
- Inductive-iris filters
- Single-sided stub filter
- Double-sided stub filters

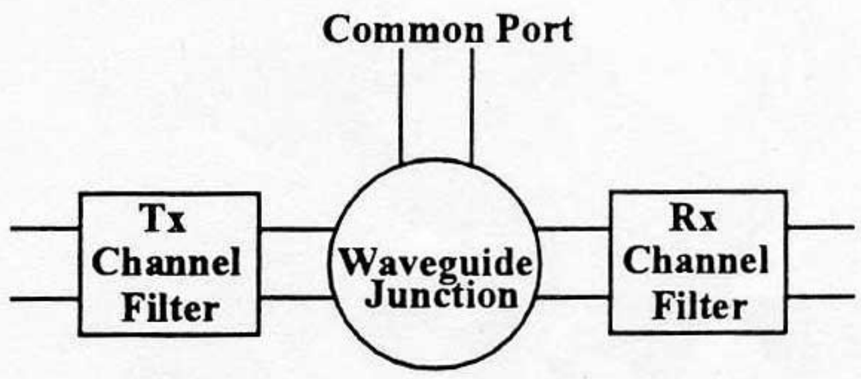

Fig. 1: *Block diagram of waveguide diplexer.*

II. ANALYSIS

The engine of the software package is a mode-matching based analysis for various discontinuities that are required in the diplexer assembly. Compared to standard mode matching algorithms, the CPU-time efficiency is significantly increased due to two measures. Firstly, the TE_{xmn} - mode approach is utilized, which has a proven record of successful designs with single- or double-plane step discontinuities and junction blocks involved [1], [6]. Secondly, the number of modes used in individual combinations of discontinuities automatically adapts to the problem at hand. For discontinuity calculations, the number of modes is selected according to the cross-section ratios of the connected waveguides. Although one of these numbers is usually high, the connection of this discontinuity with others over a finite distance of waveguide requires only a few modes.
In each different cross-section of rectangular waveguide, the x-component of a magnetic vector potential component is written as

$$A_{hx} = \sum_{q=1}^{Q} \sqrt{\frac{\omega \mu_o / k_{zq}}{A\left[k_o^2 - k_{xm}^2\right]}} \; T_{mn}(x,y) \cdot \left[F_q exp\,(-jk_{zq}z) - B_q exp\,(jk_{zq}z)\right] \quad (1)$$

where F_q and B_q are the wave amplitudes travelling in the positive and negative z direction, respectively, and A is the cross-section of the individual region. T_{mn} (=T_q), where index q is related to combinations (m,n) with respect to increasing cutoff frequencies, are the cross-section functions satisfying the boundary conditions.

$$T_{mn}(x,y) = \sin\left[\frac{m\pi}{a}(x-e)\right] \frac{\cos\left[\frac{n\pi}{b}(y-d)\right]}{\sqrt{1+\delta_{0n}}} \quad (2)$$

δ_{0n} is the Kronecker delta, a and b the waveguide cross-section dimensions, and e and d distances to the origin.
In case of a T-junction, e.g. in the E-plane with cross-section dimensions $a \times c$ (I) and $a \times b$ (II,III), the vector potential is obtained from a superposition of functions

$$T_{mn}^{I} = C_{mn}^{I} \sin\left(\frac{m\pi}{a}x\right) \frac{\cos\left(\frac{n\pi}{c}z\right)}{\sqrt{1+\delta_{0n}}} \cos\left(k_{ymn}^{I}y\right) \quad (3)$$

$$T_{ik}^{II} = C_{ik}^{II} \sin\left(\frac{i\pi}{a}x\right) \frac{\cos\left(\frac{k\pi}{b}y\right)}{\sqrt{1+\delta_{0k}}} \cos\left(k_{zik}^{II}z\right) \quad (4)$$

$$T_{jl}^{III} = C_{jl}^{III} \sin\left(\frac{j\pi}{a}x\right) \frac{\cos\left(\frac{l\pi}{b}y\right)}{\sqrt{1+\delta_{0l}}} \cos\left[k_{zjl}^{III}(z-c)\right] \quad (5)$$

where superscript I identifies the common port, II and III follow clockwise, and k_z^i are the phase constants in waveguide i with the remaining two ports shorted. For further details, especially the derivations of single-junction and cascaded scattering matrices, the reader is referred to [1].
If the entire diplexer component comprises exclusively E-plane (H-plane) discontinuities, the mode spectra are reduced to those of TE^x_{1n} (TE^x_{m0}) modes. In case of both discontinuities being present in the component, a combination of modes is used as outlined in [6]. Good agreement between theory and measurements is already obtained for three to five modes in the matrix-connecting algorithms. Individual discontinuities are analyzed with up to 45 modes.
A loss prediction is carried out on the basis of the fundamental-mode attenuation constant and the resonator unloaded Q-efficiency in the design frequency range.

III. DESIGN

The design is carried out in three steps. First, the channel filters are synthesized for given diplexer specifications. Standard filter synthesis and a combined equivalent-circuit / mode-matching approach is used to ensure filter performance. Secondly, if the b/a ratio permits the T-junction to be represented by an equivalent circuit, the diplexer is pre-optimized with the equivalent-circuit approach. Thirdly, a subsequent analysis based entirely on mode matching either confirms the equivalent-circuit results or identifies a need for further optimization using mode-matching routines exclusively. At this point, waveguide transformers, if required, at all three ports can be incorporated, and all dimensions can be individually selected as optimization parameters. The optimazation strategy itself is based on a minimax algorithm [7]. Note that, contrary to comparable diplexer configurations in [1] - [3], additional matching elements such as inductive irises are not required. Therefore, this design concept leads to more compact diplexer configurations.
The entire software package is operational on personal computers. Depending on diplexer specifications of various degrees of difficulty and restrictions, with which the software has been tested, complete designs of diplexer components take between five minutes and four hours on a Pentium 90 computer.

IV. RESULTS

The excellent agreement between mode-matching analysis and measurements is demonstrated in Figs. 2 for two different diplexer configurations. Fig. 2a shows an E-plane T-junction diplexer with waveguide stub filters. For interface purposes with standard waveguide equipment, impedance transformers have been added at all three ports.
Fig. 2b shows a similar comparison for an E-plane T-junction diplexer with inductive-iris filters. Again, excellent agreement is obtained within the 70dB-dynamic range of the measurement equipment.
A comparison between the equivalent-circuit approach and mode matching is demonstrated in Fig. 3 for an E-plane T-junction single-sided stub-filter diplexer (similar configuration as in Fig. 2a, but without transformers) with a waveguide height-to-width ratio of b/a=0.13. Excellent agreement is observed, and a mode-matching analysis is used simply to confirm the results. In certain high-power applications, it is necessary to design the diplexer with maximum height. In this situation, the diplexer stub dimensions become very small and are not manufacturable.
A solution to this problem is depicted at the top of Fig.4. The stub-filter synthesis based on the equivalent-circuit approach is still used, but it is applied to only half the actual structure and, therefore, uses only half the waveguide height. By mirroring such a stub-filter design, the original waveguide height is restored, and double-sided stub filters are obtained. The mode-matching software currently developed includes the double-sided stub-filter diplexer design. The options for the stub location are: 1) pointing towards the common port, 2) pointing away from the common port as shown in Fig. 2a, and 3) the double-stub approach in Fig. 4.

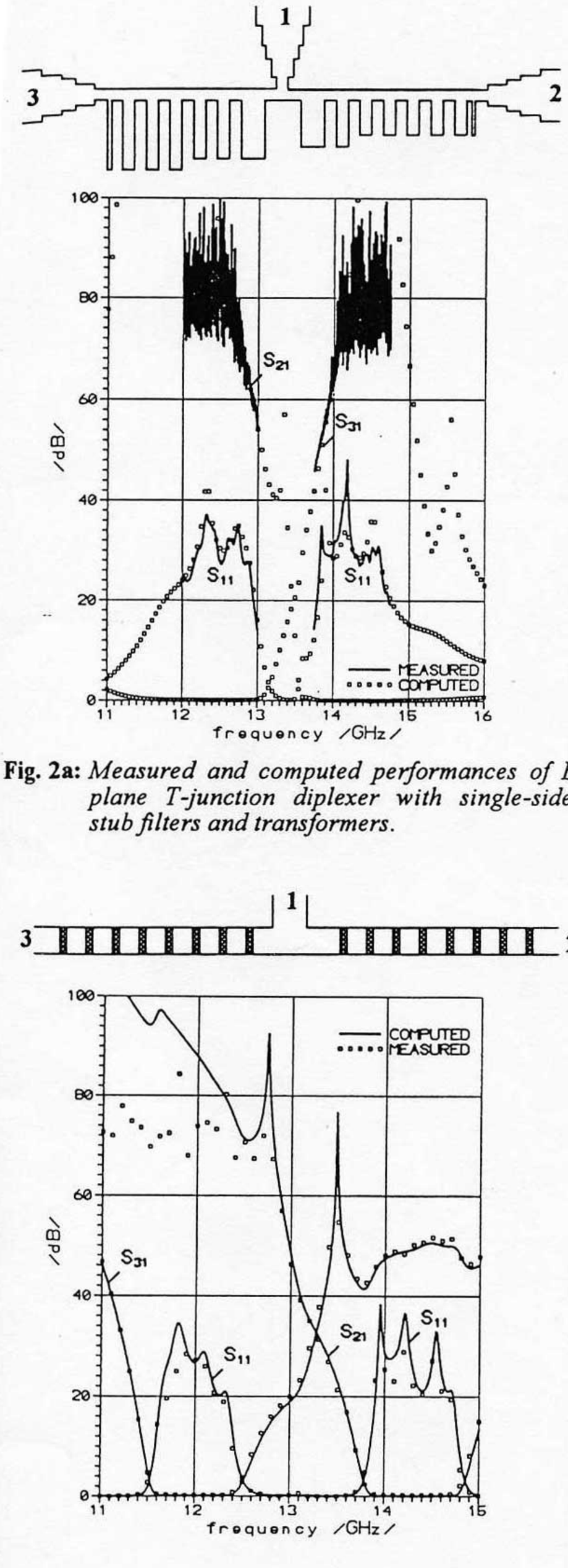

Fig. 2a: *Measured and computed performances of E-plane T-junction diplexer with single-sided stub filters and transformers.*

Fig. 2b: *Measured and computed performances of E-plane T-junction diplexer with inductive-iris filters.*

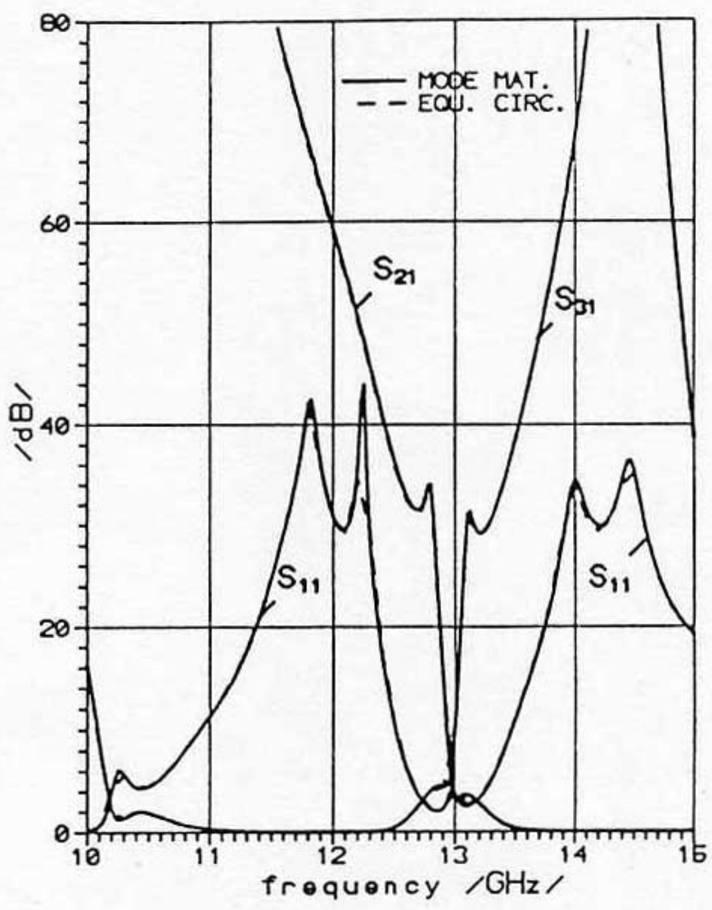

Fig. 3: *Comparison between equivalent-circuit approach and mode matching for E-plane T-junction single-sided stub-filter diplexer at b/a=0.13.*

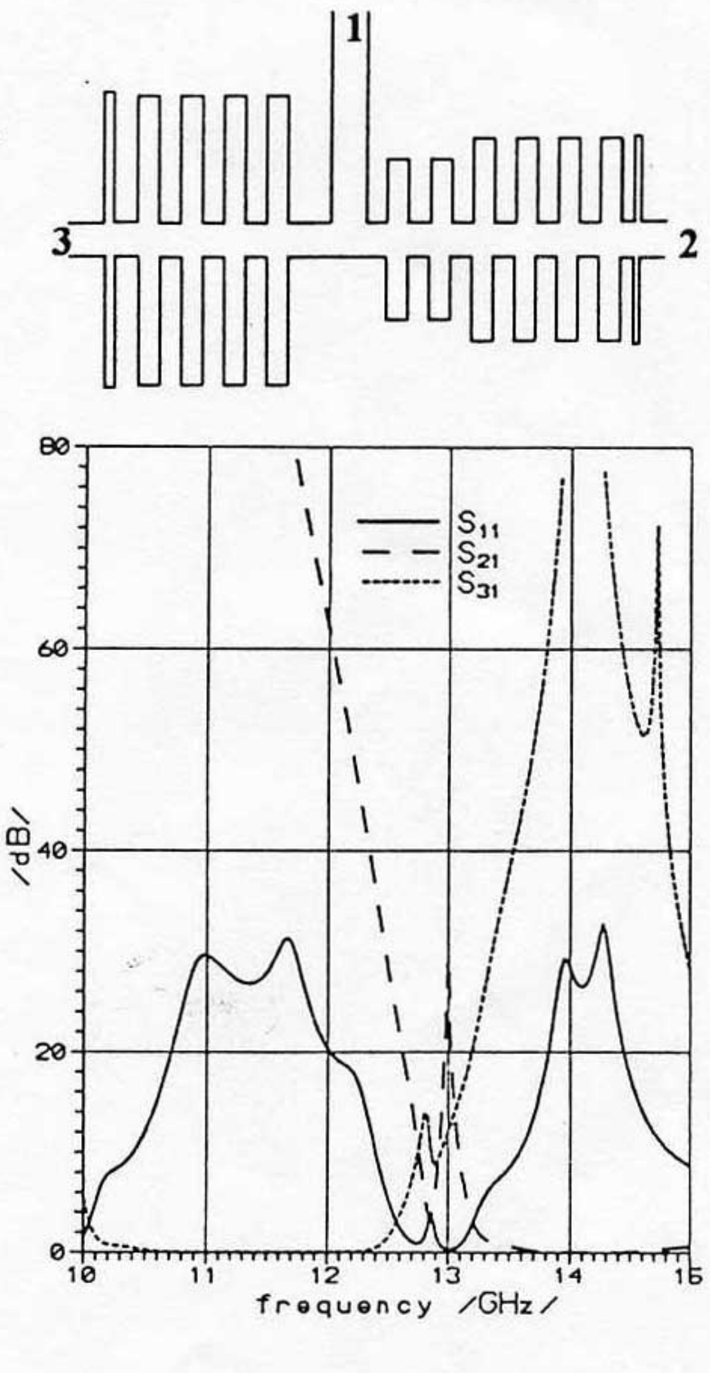

Fig. 4: *Computed performance of E-plane T-junction double-sided stub-filter diplexer (b/a=0.27).*

Once the stub filters are synthesized, the optimization of the entire diplexer is carried out with mode-matching analysis routines only. The performance of the optimized design is shown in Fig.4. Note that specifications required unequal Rx and Tx bandwidths. The design goal for optimization was set to 26dB return loss and 60 dB isolation.

For even higher ratios of *b/a*, stub filters are no longer recommended, and inductive-iris filters are used in the current software setup. The E-plane bifurcation diplexer with inductive-iris as shown in Fig. 5 provides good performance up to the full regular waveguide height (*b/a*=0.5). The input power divider and channel filters are synthesized according to [1], and the optimization software varies the transformer profile and filter dimensions for optimum performance. Alternatively, an H-plane configuration as shown in Fig. 6 can be used. This design is independent of the waveguide height.

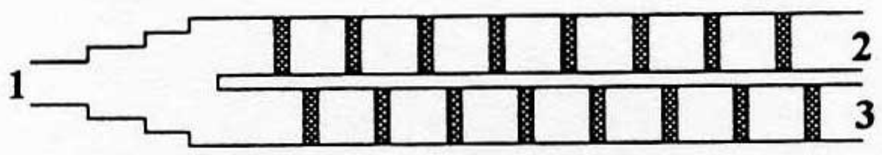

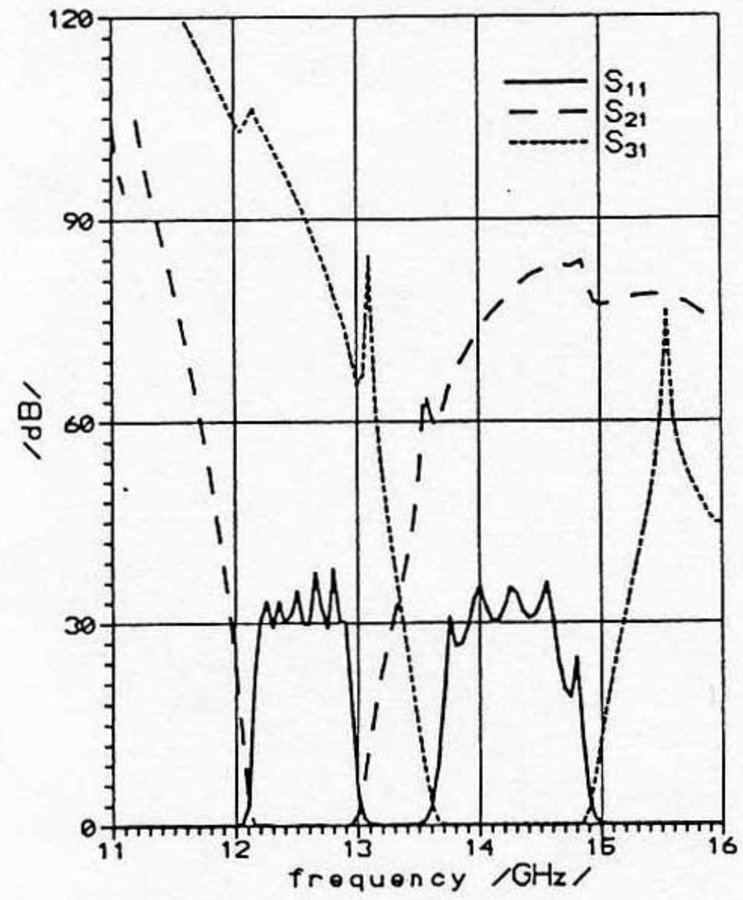

Fig. 5: *Computed performance of E-plane bifurcation diplexer with inductive-iris filters (b/a=0.5).*

V. CONCLUSIONS

An efficient CAD strategy for waveguide front-end diplexers in fixed satellite service antenna systems is presented. Channel filter and junction components are presynthesized by equivalent-circuit or mode-matching routines. In order to provide the design engineer with a fast and reliable design, a minimax optimization scheme and mode-matching analysis is used in the final step of the design process. Waveguide height restrictions can be efficiently overcome, and an option for trans formers at all three ports is included. The final design is compact as additional tuning elements are not required. The software is operational on standard Pentium personal computers.

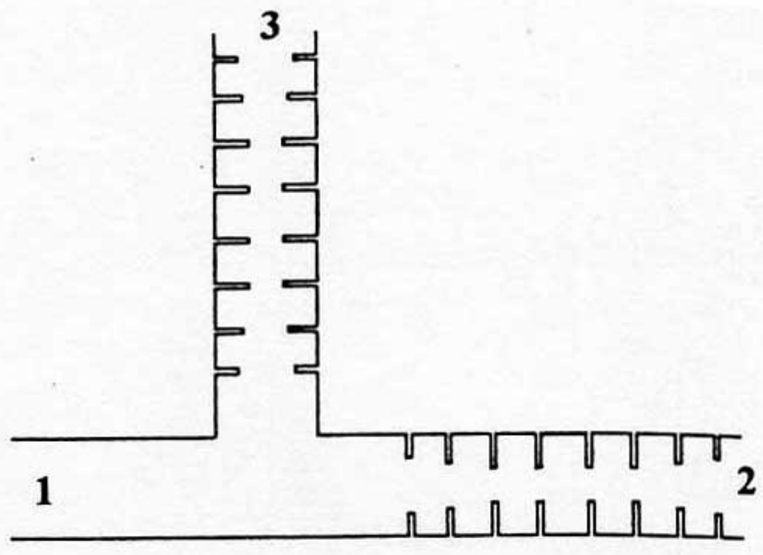

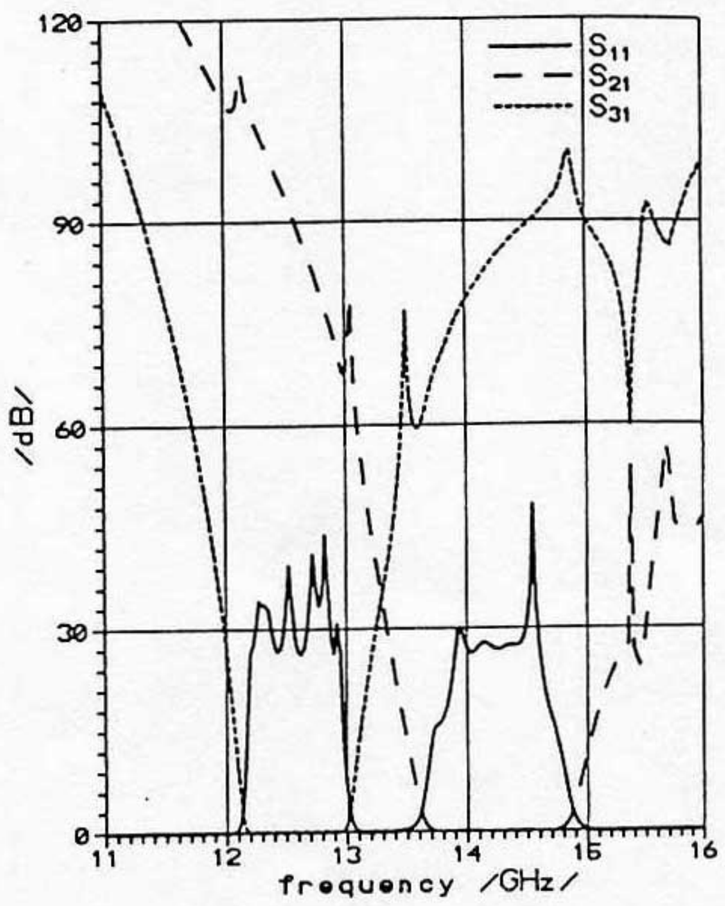

Fig. 6: *Computed performance of H-plane T-junction diplexer with inductive-iris filters (b/a=0.5).*

REFERENCES

[1] J. Uher, J. Bornemann and U. Rosenberg, *Waveguide Components for Antenna Feed Systems. Theory and CAD*, Norwood: Artech House, 1993.

[2] J. Dittloff and F. Arndt, "Computer-aided design of slit-coupled H-plane T-junction diplexers with E-plane metal-insert filters," *IEEE Trans. Microwave Theory Tech.*, Vol.36, pp. 1833-1840, Dec. 1988.

[3] J. Dittloff and F. Arndt, "Rigorous field theory design of millimeter-wave E-plane integrated circuit multiplexers," *IEEE Trans. Microwave Theory Tech.*, Vol.37, pp. 340-350, Feb. 1989.

[4] N. Marcuvitz, *Waveguide Handbook*, New York: Dover, 1965.

[5] G. Matthaei, L. Young and E.M.T. Jones, *Microwave Filters, Impedance-Matching Networks, and Coupling Structures*, Dedham: Artech House, 1980.

[6] J. Bornemann, "Selectivity-improved E-plane filter for millimetre-wave applications," *Electronics Letters*, vol. 27, pp. 1891-1893, Oct. 1991.

[7] K. Madsen, H. Schaer-Jacobsen and J. Voldby, "Automated minimax design of networks," *IEEE Trans. Circuits Systems*, Vol. CAS-22, pp. 791-796, Oct. 1975.

MULTI-CARRIER MULTIPACTOR ANALYSIS OF HIGH POWER ANTENNA TX-TX DIPLEXER FOR SATCOM APPLICATION

PRESENTED AT:

4TH INTERNATIONAL WORKSHOP ON MULTIPACTOR, CORONA AND PASSIVE INTERMODULATION IN RF SPACE HARDWARE

8/9/10/11 SEPTEMBER 2003

ESTEC, NOORDWIJK, THE NETHERLANDS

ORGANIZED BY THE EUROPEAN SPACE AGENCY

PRESENTED BY: K.S.PARIKH

SPACE APPLICATIONS CENTRE

INDIAN SPACE RESEARCH ORGANISATION, INDIA.

DIPLEXER FUNCTIONAL REQUIREMENT:

- TO COMBINE THE OUTPUTS OF A 12-CHANNEL & A 6-CHANNEL OUTPUT MULTIPLEXERS BEFORE FEEDING TX ANTENNA
- AT C-BAND, LENGTH OF 18-CHANNEL OMUX WITH “COMBLINE” CONFIGURATION USING CONVENTIONAL CIRCULAR WAVEGUIDE DUAL MODE FILTERS IS TOO LARGE TO BE ACCOMODATED ON THE SATELLITE PANEL
- OMT (ORTHO MODE TRANSDUCER) BASED DIPLEXER COMPLICATES THE DESIGN OF DUAL MODE FEED
- FILTER BASED DIPLEXER (THIS DESIGN) IS ACCOMODATED IN THE PART OF THE WAVEGUIDE RUN LEADING UP TO THE FEED AND DOES NOT IMPOSE ADDITIONAL MASS AND SPACE PENALTY

BLOCK SCHEMATIC OF DIPLEXER

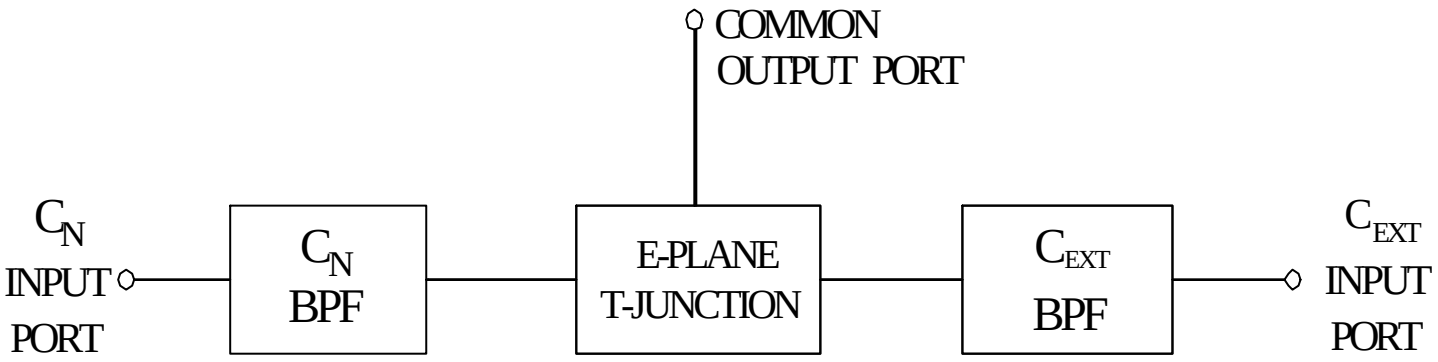

DIPLEXER ELECTRICAL DESIGN:

- INDUCTIVE IRIS COUPLED BPFS MOUNTED ON E-PLANE T-JUCNTION
- C_N FILTER WITH 7-SECTION & C_{EXT} FILTER WITH 5-SECTION CHEBYSHEV CHARACTERISTICS
- FILTERS WITH TE_{101} WR229 RECTANGULAR WAVEGUIDE RESONATORS
- DIPLEXER DOES NOT HAVE ANY TUNING SCREWS TO AVOID GENERATION OF PIM
- DIPLEXER CONSTRUCTED USING ALUMINUM ALLOY 6061T & SILVER PLATED INTERNALLY TO ACHIEVE LOWEST POSSIBLE INSERTION LOSS

DIPLEXER DESIGN PRINCIPLE:

- DESIGN APPROACH BASED ON THE PRINCIPLE OF EQUAL REFLECTION COEFFICIENTS AT ALL PORTS OF THE COMMON JUNCTION
- AN H-PLANE INDUCTIVE IRIS INTRODUCED IN THE COMMON JUNCTION TO MEET THE ABOVE REQUIREMENT
- DIPELXER DESIGNED & OPTIMIZED USING FE/MM PROGRAM (μ-WAVE WIZARD - MICIAN)

ELECTRICAL SPECIFICATIONS:

- C_N CHANNEL : 3705 – 4185 MHz
- C_{EXT} CHANNEL : 4510 – 4770 MHz
- RETURN LOSS : > 23 dB
- ISOLATION : > 35 dB
- POWER HANDLING : C_N CHANNEL: 12 CARRIERS, 15 W EACH
  C_{EXT} CHANNEL: 6 CARRIERS, 15 W EACH

SIMULATED FREQUENCY RESPONSE OF DIPLEXER USING FE/MM PROGRAM (μ-Wave Wizard)

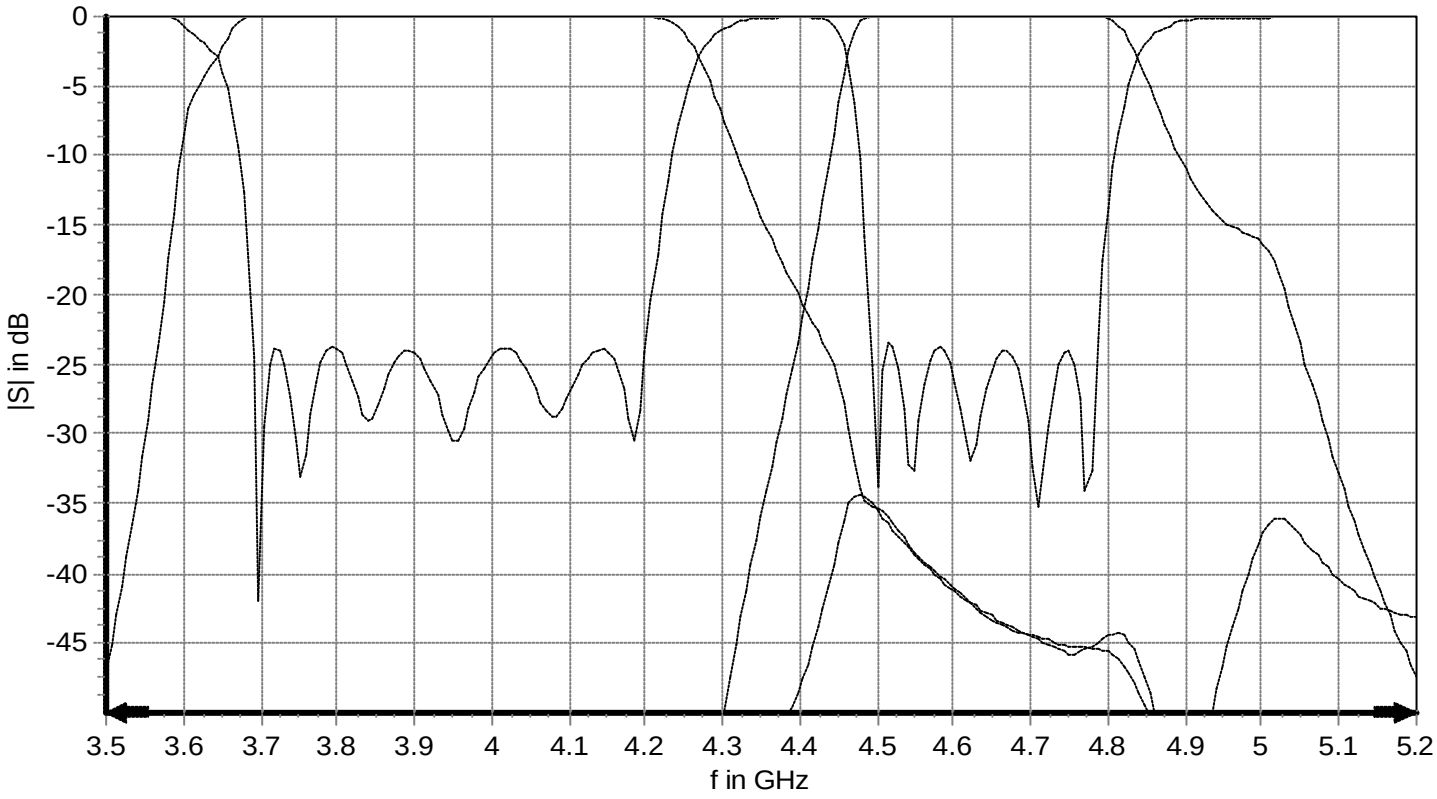

MEASURED FREQUENCY RESPONSE OF DIPLEXER

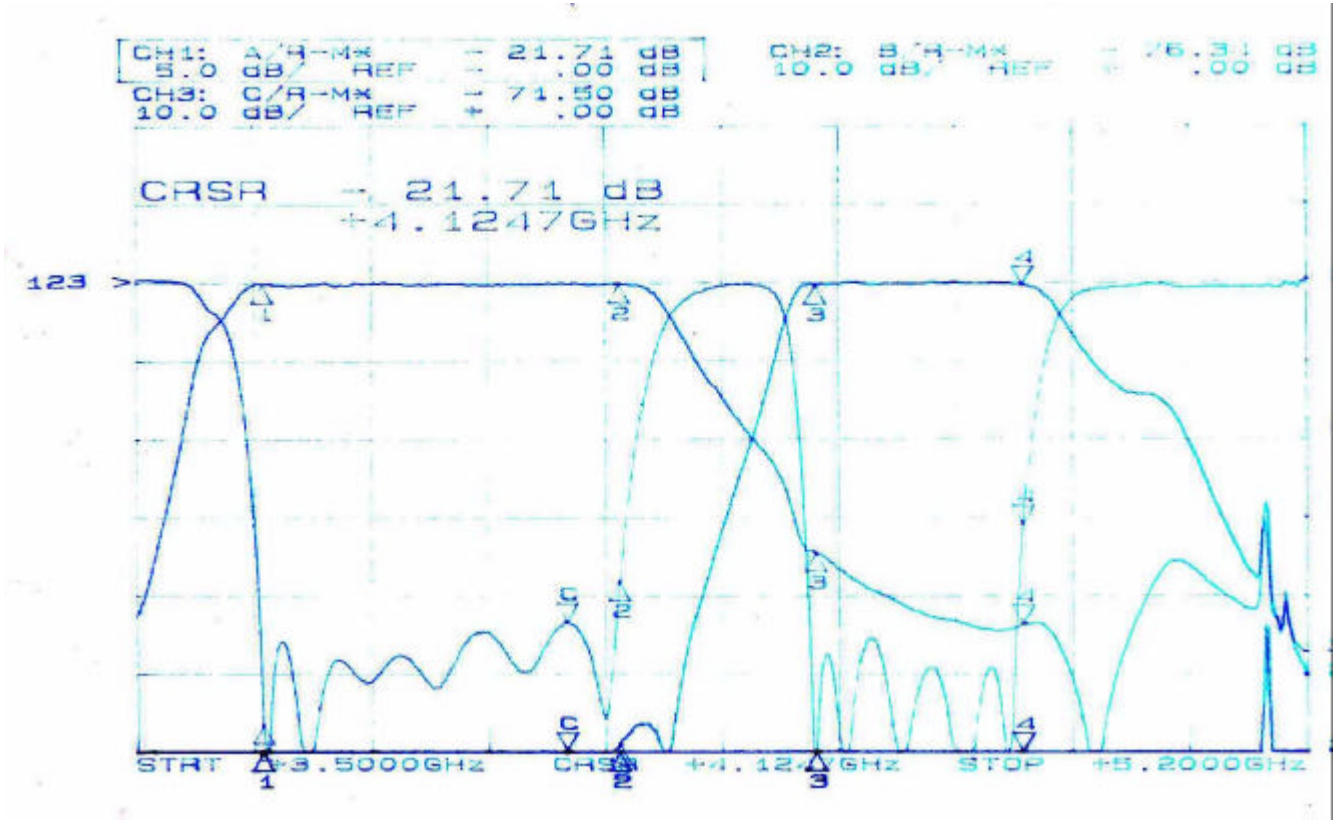

MULTIPACTOR ANALYSIS:

SINGLE CARRIER MULTIPACTION THRESHOLD:

- MAXIMUM E FIELD OCCURS AT THE CENTRE OF BROAD-WALL OF WG (TE_{10} MODE)
- MAXIMUM E FIELD OCCURS AT CENTRE OF RESONATORS (ALONG THE LENGTH) OF FILTER (TE_{101} RESONATOR)
- PEAK VOLTAGE IN CENTRE OF RESONATOR HIGHER THAN THE INCIDENT PEAK VOLTAGE
- VMF (VOLTAGE MAGNIFICATION FACTOR)

  = PEAK VOLTAGE IN RESONATOR / PEAK INCIDENT VOLTAGE

• EVALUATION OF VMF (VOLTAGE MAGNIFICATION FACTOR):

- USE OF SCATTERING MATRICES CALCUALTED USING FE/MM PROGRAM
- DOMINANT MODE (TE_{10} MODE) PROPAGATION ASSUMED FOR THE ANALYSIS
- NETWORK ASSUMED TO BE LOSELESS

DIPLEXER 3-PORT NETWORK (MULTIPACTION ANALYSIS PLANE)

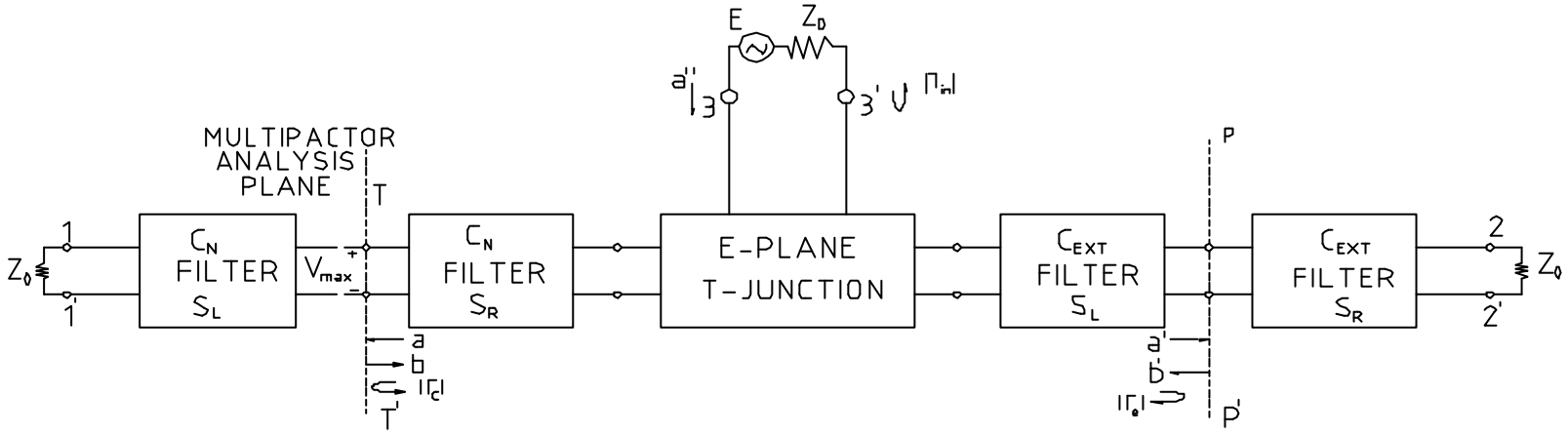

DESCRIPTION OF METHOD (VMF CALCULATION):

$$\text{I}\,NPUT\,POWERTO\ \text{DIPLEXER} = \text{P}_{\text{in}} = \frac{\text{V}_{\text{in}}^{+2}}{\sqrt{\text{Z}_0}}\left(1-\left|\text{G}_{\text{in}}\right|^2\right)$$

$$NET\ POWER\,FLOW\ AT\ PLANE\ T-T' = \text{P}_c = a^2\left(1-\left|\Gamma_c\right|^2\right)$$

$$NET\ POWER\ FLOW\ AT\ PLANE\,P-P' = \text{P}_e = a'^2\left(1-\left|\Gamma_e\right|^2\right)$$

$$FOR\,LOSSLESS\,NETWORK,\ P_{in} = \text{P}_c + P_e$$

$$PEAK\,VOLTAGE\,AT\ \ VOLTAGE\ ANALYSIS\ PLANE,\ T-T' = V_{\max} = a\sqrt{Z_0}\left(1+\left|\Gamma_c\right|\right)$$

$$VMF = \frac{V_{max}}{V_{in}^{+}} = \frac{\left(1+\left|\Gamma_c\right|\right)\sqrt{1-\left|\Gamma_{in}\right|^2}}{\sqrt{\left(1-\left|\Gamma_c\right|^2\right)+\frac{a'^2}{a^2}\left(1-\left|\Gamma_e\right|^2\right)}}$$

$$BY\,CHOOSING\,PLANE\,P-P'\,IN\,C_{ext}\ FILTER\ AT\ THE\,LOAD\,END,\ \left|\Gamma_e\right| = 0$$

$$\therefore\ VMF = \frac{V_{max}}{V_{in}^{+}} = \frac{\left(1+\left|\Gamma_c\right|\right)\sqrt{1-\left|\Gamma_{in}\right|^2}}{\sqrt{\left(1-\left|\Gamma_c\right|^2\right)+\left|S_{23}\right|^2\Big/\left|S'_{13}\right|^2}}$$

VMF (C_N FILTER & C_{EXT} FILTER):

- E FIELD APPEARS IN C_N FILTER RESONATORS (R_{C1}, R_{C2},…..,R_{C7}) & C_{EXT} FILTER RESONATORS (R_{E1}, R_{E2},…..,R_{E5}) DUE TO EXCITATION IN C_N BAND
- E FIELD ALSO APPEARS IN C_{EXT} FILTER RESONATORS (R_{E1}, R_{E2},…..,R_{E5}) & C_N FILTER RESONATORS (R_{C1}, R_{C2},…..,R_{C7}) DUE TO EXCITATION IN C_{EXT} BAND
- E FIELD APPEARS IN CONNECTING WAVEGUIDES (R_{C0}, R_{E0}) DUE TO EXCITATION IN C_N BAND & C_{EXT} BAND

- VMF HIGHER FOR CENTRAL RESONATORS THAN TOWARDS INPUT AND OUTPUT
- VMF HIGHER AT BAND EDGES THAN AT CENTRE FREQUENCY OF PASS BAND
- VMF ALSO CALCULATED USING 3D FEM PROGRAM (ANSOFT HFSS) FOR COMPARISON WITH FE/MM METHOD

HFSS FIELD SIMULATION OF DIPLEXER (C_N PORT EXCITATION)

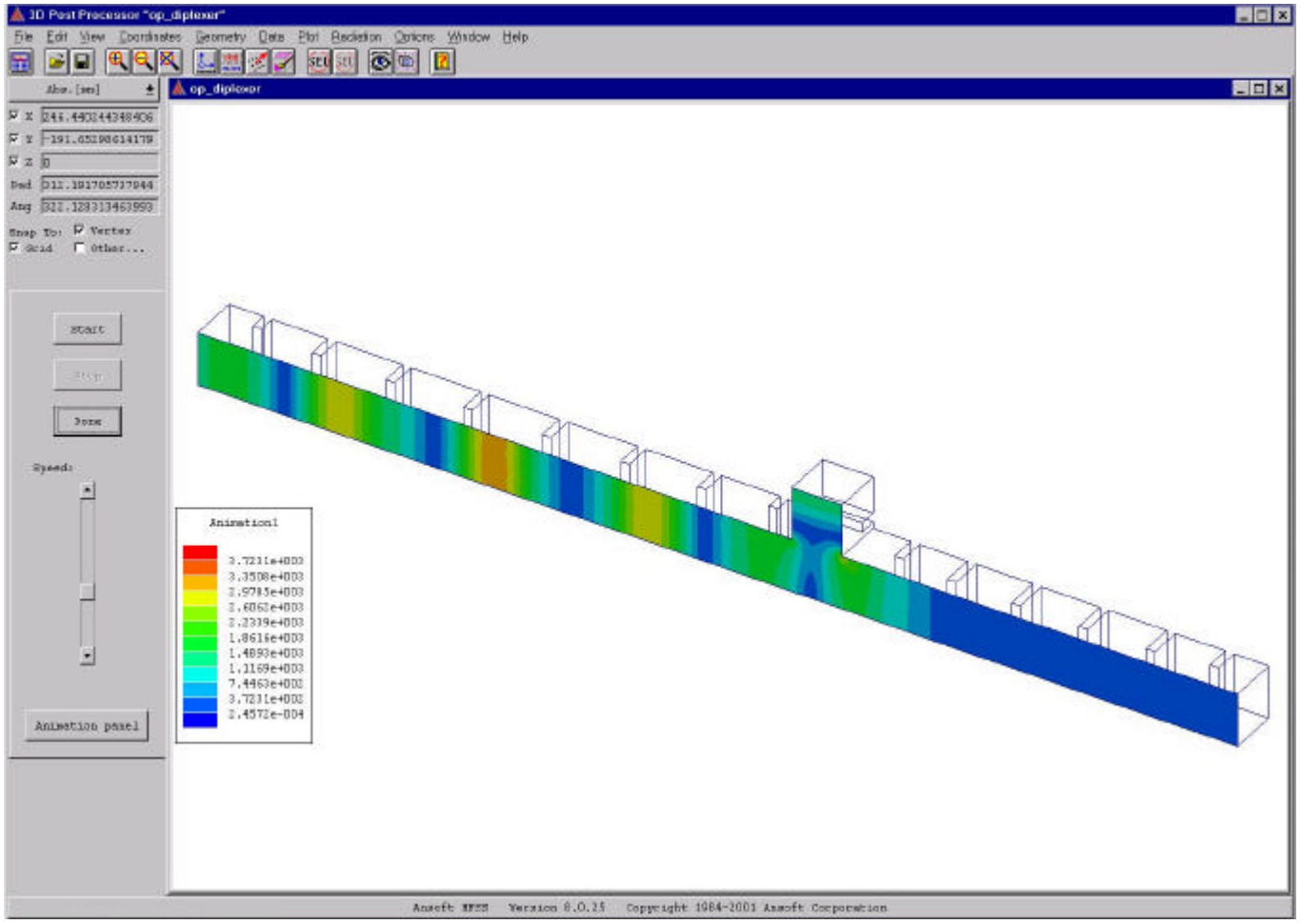

VOLTAGE MAGNIFICATION FACTOR FOR C_N FILTER

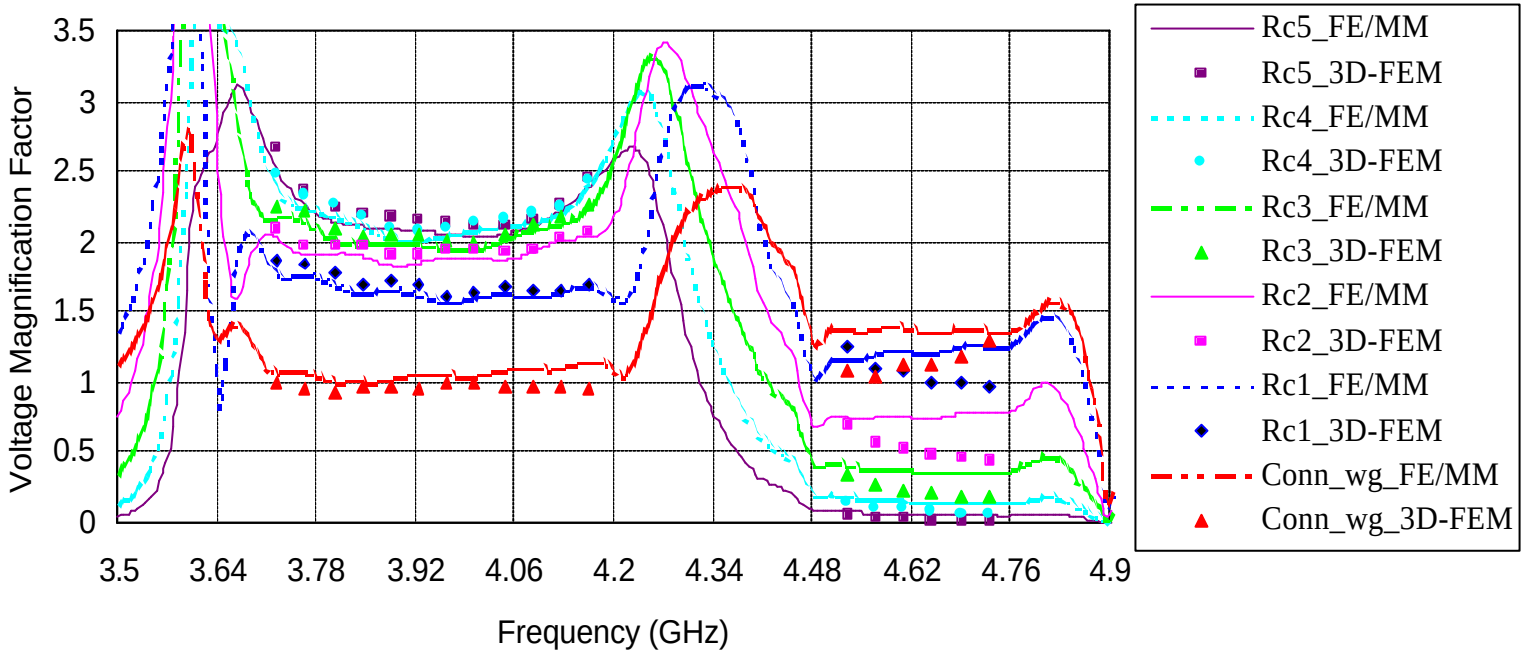

VOLTAGE MAGNIFICATION FACTOR FOR C_{EXT} FILTER

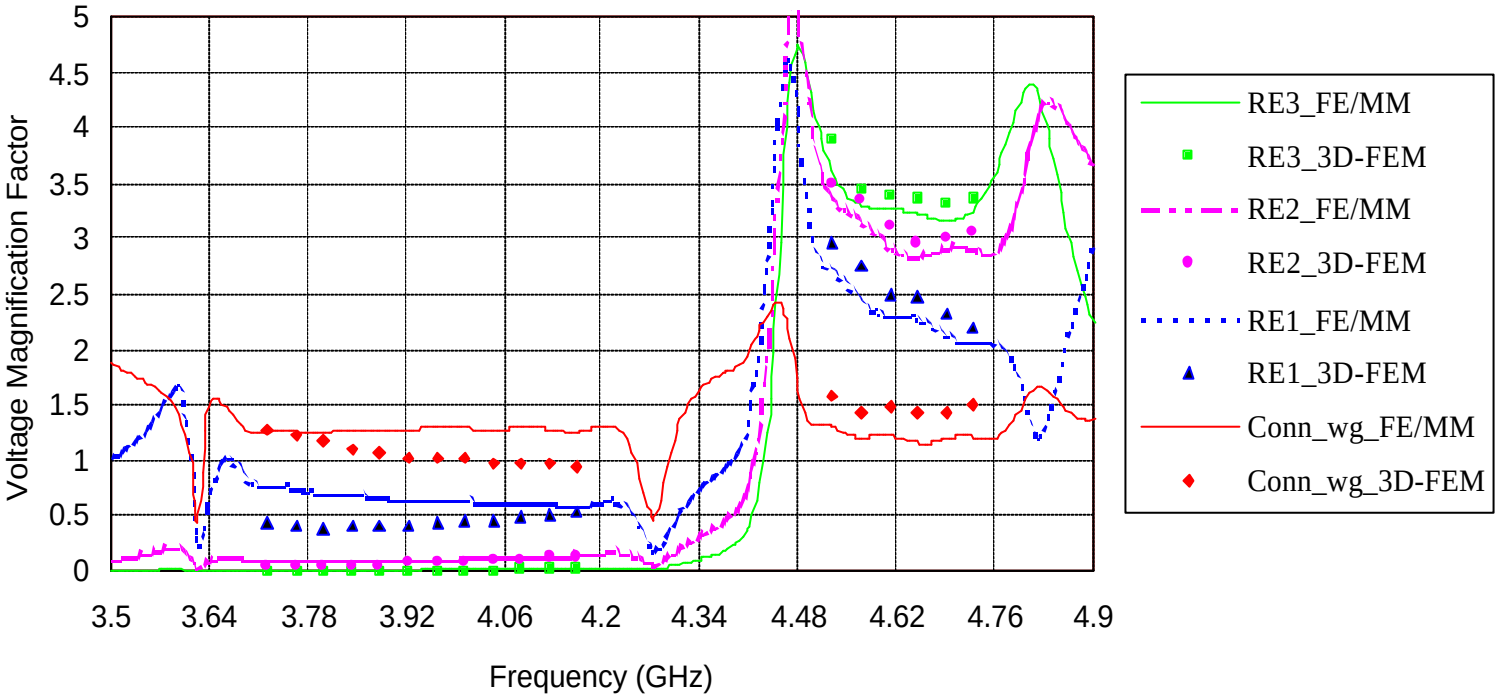

SINGLE CARRIER MULTIPACTION THRESHOLD:

$$SINGLE\ CARRIER\ MULTIPACTION\ THRESHOLD = P_{sc} = \frac{V_{th}^2}{2\,Z_0\,VMF^2}$$

$Z_0 = WAVEGUIDE\ IMPEDANCE$

$VMF = VOLTAGE\ MAGNIFICATION\ FACTOR$

$V_{th} = PEAK\ GAP\ VOLTAGE\ FROM\ ESA\ CURVES\ FOR\ SILVER\ PLATED\ ALUMINUM$

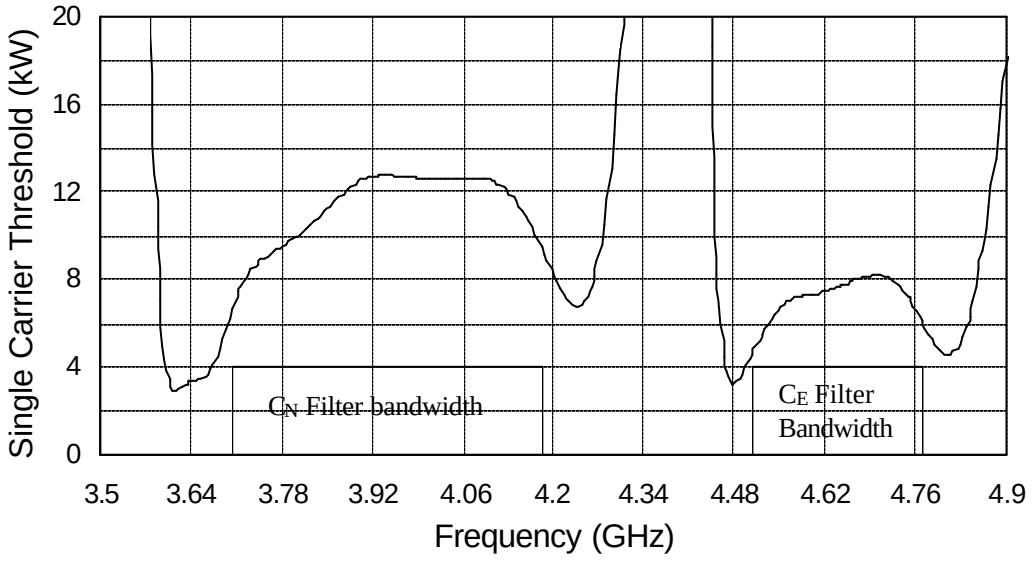

REALISTIC MULTIPACTOR MARGINS:

- PEAK POWER FOR DIPLEXER = N^2 x P_i = (18)2 x 15 = 4.86 kW
- SINGLE CARRIER THRESHOLD (P_{SC}) FOR C_N FILTER = 5.86 kW
- SINGLE CARRIER THRESHOLD (P_{SC}) FOR C_{EXT} FILTER = 4.60 kW

$$V_{peak,total} = \sum_{i=1}^{N} V_{peak}\left(f_i\right)$$

$$MULTIPACTOR\ MARGIN = 10\log\left(\frac{V_{th}\left(f_1\right)}{V_{peak,total}}\right)^2$$

- WHEN C_N PORT IS EXCITED WITH 12 CARRIERS & C_{EXT} PORT IS EXCITED WITH 6 CARRIERS WITH 15 W/CARRIER
  (ASSUMING WORST-CASE CONDITION OF IN-PHASE CARRIERS)
  WHERE, $f_1, f_2, \ldots f_n$ = CHANNEL CENTRE FREQUENCIES OF TRANSPONDERS
  N = NUMBERS OF CARRIERS

REALISTIC MULTIPACTOR MARGINS:

	RESONATOR /WAVEGUIDE	Vpeak,total (Volts)	Multipactor Margin (dB)
C_N FILTER	R_{C5}	3348	6.18
	R_{C4}	3342	6.20
	R_{C3}	3274	6.38
	R_{C2}	3281	6.36
	R_{C1}	3256	6.43
	CONNECTING WG	2229	9.72
C_{EXT} FILTER	R_{E3}	2446	8.91
	R_{E2}	2340	9.30
	R_{E1}	2436	8.95
	CONNECTING WG	2589	8.42

MULTIPACTION THRESHOLD FOR MULTI-CARRIER OPERATION:

- FOR MULTI-CARRIER COMPONENTS WITH LARGE N & P_i , PEAK POWER LEVEL IS VERY HIGH
- IT IS NOT POSSIBLE TO MEET THE CUSTOMARY "$N^2 P_i + 3$ dB" or "$N^2 P_i + 6$ dB" MULTIPACTOR MARGINS
- MAXIMUM POWER PERMISSIBLE PER CARRIER IS CALCULATED USING "20-GAP-CROSSING-RULE" RECOMMENDED BY ESA
- IT ALLOWS THE COMPONENT TO BE OPERATED AT LARGER POWER PER CARRIER ESPECIALLY FOR COMPONENTS WITH LARGE N & WITH LARGE GAPS AFTER CRITICAL ANALYSIS
  f x d PRODUCT > 100 GHz-mm (FOR DIPLEXER)
- ANALYSIS DEPENDS ON NUMBER OF CARRIERS N, FREQ PLAN, MULTIPACTION MODE ORDER n; MODE ORDER > 51 (FOR DIPLEXER)

MULTIPACTION THRESHOLD FOR MULTI-CARRIER OPERATION:

PARAMETER	C_N FILTER		C_{EXT} FILTER	
	RESONATOR R_{C5}	CONNECTING GUIDE	RESONATOR R_{E3}	CONNECTING GUIDE
NUMBER OF CARRIERS, N	12	18	6	18
SINGLE CARRIER THRESHOLD, P_{SC}	5.86 kW	5.86 kW	4.6 kW	4.6 kW
MAXIMUM ALLOWABLE POWER PER CARRIER, P_{MC}	488 W	326 W	767 W	255 W

- MINIMUM OF P_{MC} WILL DECIDE POWER HANDLING OF DIPLEXER, WHICH WILL BE 326 W FOR C_N FILTER & 255 W FOR C_{EXT} FILTER

EXPERIMENTAL RESULTS:

- MAXIMUM VOLTAGE OCCURS IN CENTRAL RESONATORS (R_{C4}-R_{C5}) OF C_N FILTER
- PEAK POWER = $N^2 \times P_i = (12)^2 \times 15 = 2.16$ kW
- TEST POWER FOR C_N FILTER = 3.05 kW (AT LOWEST FREQUENCY 3705 MHz)
- SINGLE CARRIER MULTIPACTION MARGIN = 1.5 dB (BY TEST)

- MAXIMUM VOLTAGE OCCURS IN CENTRAL RESONATOR (R_{E3}) OF C_{EXT} FILTER
- PEAK POWER = $N^2 \times P_i = (6)^2 \times 15 = 540$ W
- TEST POWER FOR C_{EXT} FILTER = 760 W (AT LOWEST FREQUENCY 4510 MHz)
- SINGLE CARRIER MULTIPACTION MARGIN = 1.5 dB (BY TEST)

MULTIPACTION TEST (DIPLEXER):

- C-BAND TRAVELING WAVE RING RESONATOR:
  - TWTA OUTPUT POWER = 350 W
  - TEST FREQUENCY = 3705 MHz
  - PULSE DUTY CYCLE = 6 %
  - PRF = 1kHz
  - RING GAIN = 10 dB
  - RING FORWARD POWER = 3500 W
  - RING RETURN LOSS (DURING TEST) > 26 dB

- DETECTION SYSTEMS USED:
  - FORWARD / REVERSE POWER NULL DETECTION
  - SECOND HARMONIC DETECTION
  - RING REVERSE POWER DETECTION
  - NEAR BAND NOISE DETECTION

C-BAND RING RESONATOR TEST SET UP (DIPLEXER IN TVAC CHAMBER)

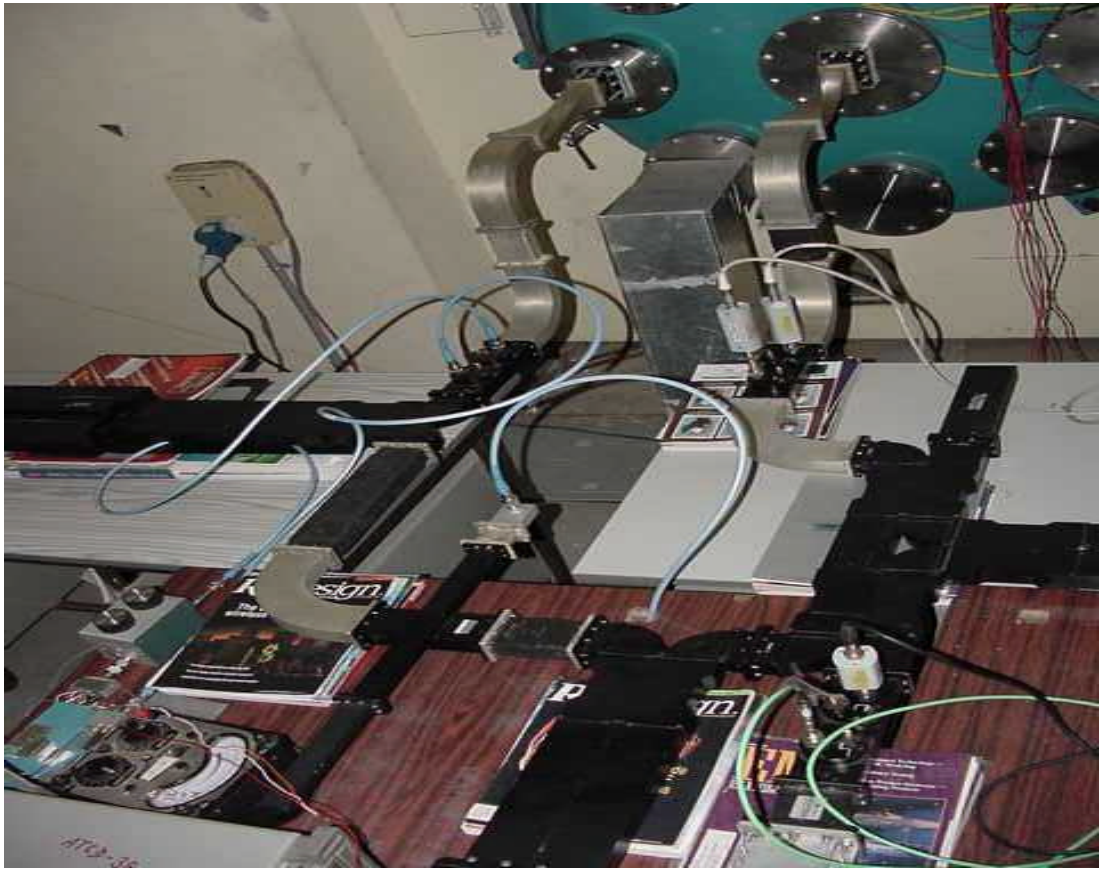

FLIGHT MODEL UNIT OF DIPLEXER

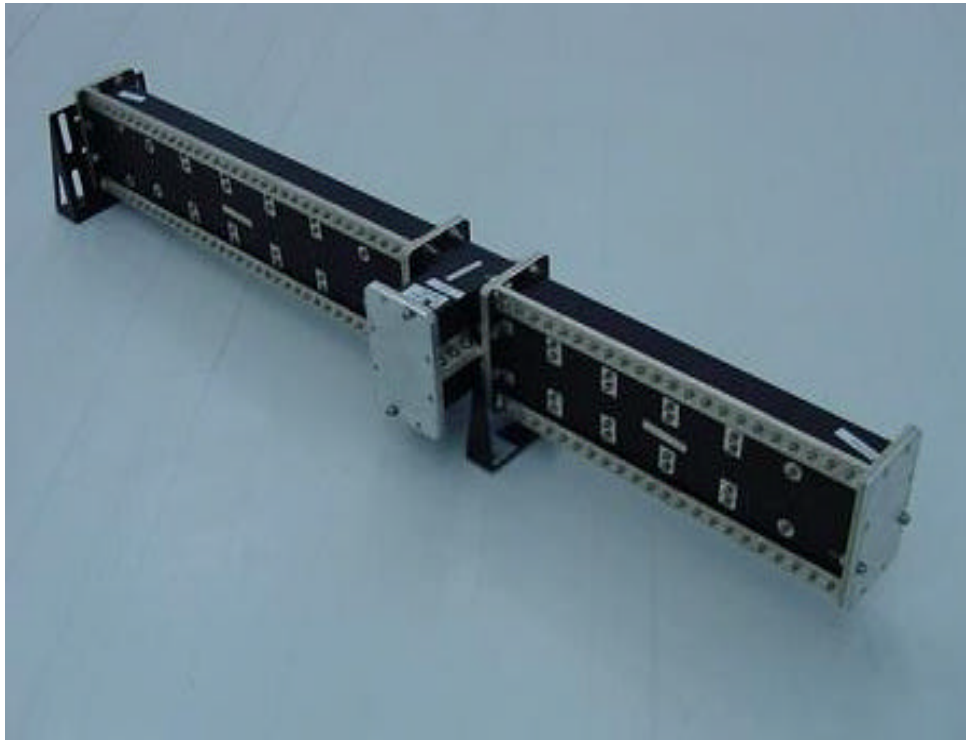

HIGH POWER TEST FACILTIY (SAC-ISRO):

C-BAND HIGH POWER TEST SET UPS:

- MULTIPACTION TEST SET UP:
  - TRAVELING WAVE RING RESONATOR (RING GAIN = 10 dB)
  - MUILTI-CARRIER TEST
- PIMP TEST SET UP

- HIGH POWER SOURCES:
  - HIGH POWER PULSE TWTA
    - POWER OUTPUT: 5 kW
    - FREQUENCY RANGE: 2.5 - 5.0 GHz
    - PULSE DUTY CYCLE: 0 - 4 %
    - PRF: VARIABLE (0.1-100 kHz)

  - HIGH POWER (CW/PULSE) TWTA (12 Nos.)
    - POWER OUTPUT: 300 W TO 400 W
    - FREQUENCY RANGE: 2.5 - 5.0 GHz
    - PULSE DUTY CYCLE: 0 - 100 %
    - PEAK POWER: 30 kW

HIGH POWER TEST FACILTIY (SAC-ISRO):

Ku-BAND HIGH POWER TEST SET UPS:

- MULTIPACTION TEST SET UP:
  - TRAVELING WAVE RING RESONATOR (RING GAIN=7 dB)
  - MUILTI-CARRIER TEST
- PIMP TEST SET UP

- HIGH POWER SOURCES:
  - HIGH POWER PULSE TWTA
    - POWER OUTPUT: 5 kW
    - FREQUENCY RANGE: 10.0 – 13.0 GHz
    - PULSE DUTY CYCLE: 0 - 4 %
    - PRF: VARIABLE (0.1-100 kHz)
    - RING FORWARD POWER = 20 kW

  - HIGH POWER (CW/PULSE) TWTA (12 Nos.)
    - POWER OUTPUT: 350 W
    - FREQUENCY RANGE: 10.0 – 13.0 GHz
    - PULSE DUTY CYCLE: 0 - 100 %
    - PEAK POWER: 30 kW

HIGH POWER TEST FACILTIY (SAC-ISRO):

THERMO-VACUUM CHAMBERS:

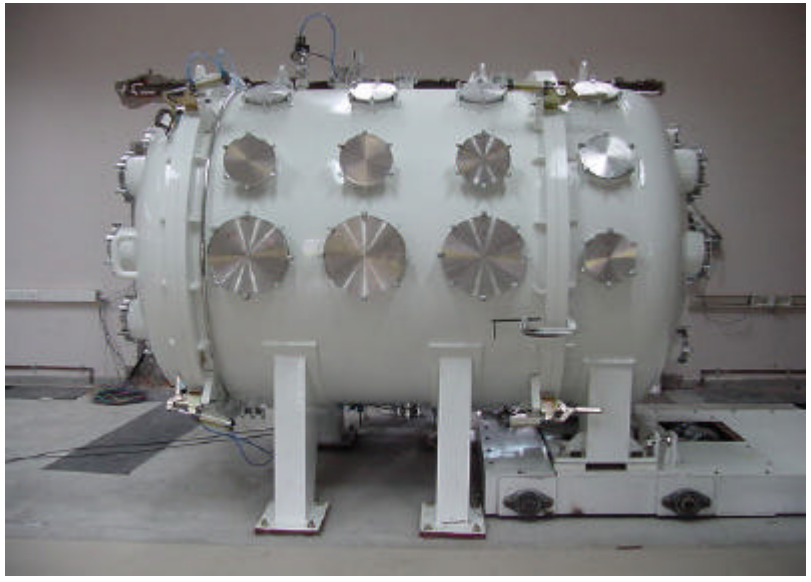

THANK YOU

Direct Design Formulas for Asymmetric Bandpass Channel Diplexers

JOHN L. HAINE AND J. DAVID RHODES, MEMBER, IEEE

Abstract—**This paper gives direct design formulas for asymmetric bandpass channel diplexers, which allow rapid design of diplexers using narrow-band direct-coupled resonator filters. Computed results for a prototype diplexer are given, and results are presented for a 5.8-GHz asymmetric waveguide diplexer, which demonstrate the high performance possible using this design technique.**

I. Introduction

THIS PAPER gives direct design formulas for asymmetric bandpass channel prototype diplexers, which can be transformed into narrow-band diplexers using direct-coupled resonator filters. These formulas are a generalization of ones given for the symmetrical case in an earlier paper by Rhodes [1].

The asymmetric bandpass diplexer consists of two dissimilar bandpass filters connected in series. To compensate for the interaction between the filters, each is internally modified, and a series annulling reactance is introduced. The design procedure forces the reflection coefficient at the common port to be approximately zero at a finite set of frequencies in each channel. The reflection coefficient at each of the other ports is automatically forced to be zero to the same degree of approximation at the set of frequencies in the corresponding channel.

Compared to the filters operating in isolation, each channel of the diplexer shows a significant increase in skirt selectivity over the passband of the other, which may allow a reduction of degree to meet a given specification. The return loss at each port is only slightly degraded, and this may be allowed for by improving the specification of the original bandpass filters.

Section II quotes the formulas without proof: the proof is given in Section III. Section IV gives computed responses for a typical prototype diplexer, and proceeds to consider the design of a waveguide diplexer at 5.8 GHz. The measured response of this diplexer agrees closely with theory.

II. The Design Formulas

The essentials of the type of diplexer considered here are shown in Fig. 1. It consists of a pair of bandpass filters, whose input impedance in the stopband tends to a short circuit, connected in series. The input impedance at the common port of the diplexer approximates to a constant resistance in the passband of each filter. Since the stopband input impedance of each filter is actually finite and complex, the filters interact unless their passbands are very widely separated. To compensate for this interaction, each filter is modified internally, and the frequency-invariant annulling reactance X_0 is connected in series with the filters.

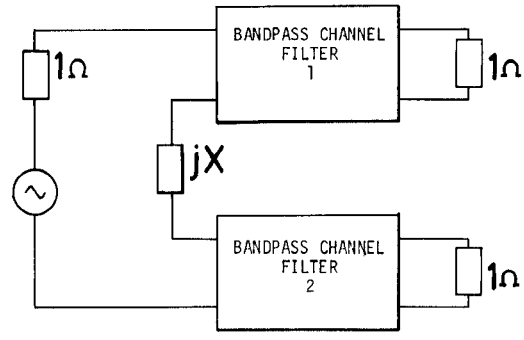

Fig. 1. An elementary series connected diplexer.

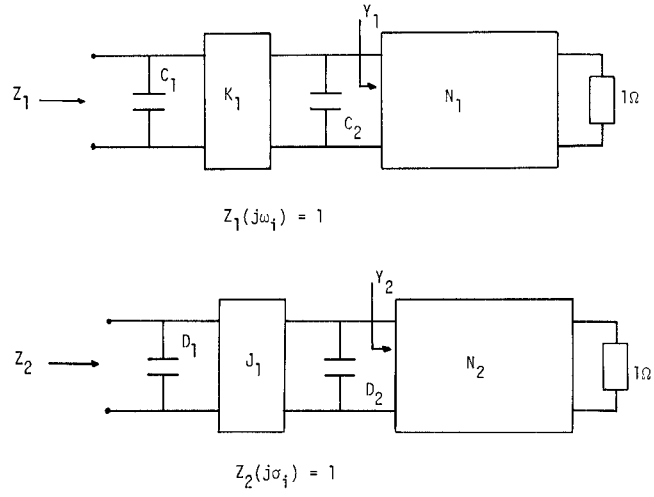

Fig. 2. Low-pass prototype networks used in the design procedure.

Let the bandpass filters be based on the normalized, doubly terminated low-pass prototype networks shown in Fig. 2. Each prototype begins with a pair of capacitors coupled through an admittance inverter, the rest of the network being arbitrary. The derivation of the design formulas requires that the input impedance of each prototype be unity at some set of frequencies in the passband, and each filter must have at least a second-ordered transmission zero at infinity. Since the networks are assumed lossless, the first condition implies that they have zero insertion loss at the same sets of frequencies. Prototype element values for Chebyshev, Butterworth, or even linear-phase filters are available from explicit formulas or fairly simple synthesis procedures [2].

Manuscript received December 1, 1976; revised April 11, 1977. J. L. Haine receives a U.K. Science Research Council studentship.

J. L. Haine was with the Department of Electrical and Electronic Engineering, The University of Leeds, Leeds LS2 9JT, England. He is now with Marconi Communication Systems, Marrable House, Great Baddow, Chelmsford, Essex, England.

J. D. Rhodes is with the Department of Electrical and Electronic Engineering, The University of Leeds, Leeds LS2 9JT, England.

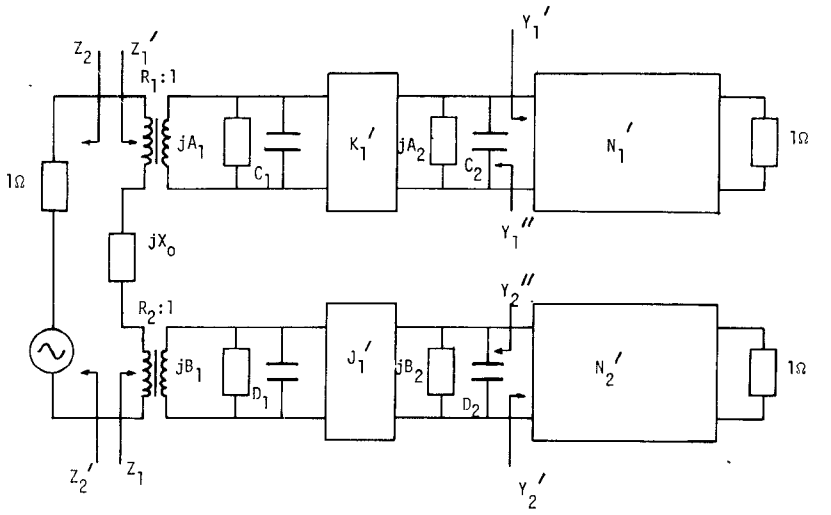

Fig. 3. The prototype diplexer circuit.

Fig. 3 shows the diplexer prototype circuit. The channels have been transformed to bandpass filters at center frequencies $\pm\alpha$. The section of each prototype following the first two shunt capacitors is transformed by the direct frequency transformation:

$$\omega \rightarrow \omega \mp \alpha. \tag{1}$$

The elements in the first two "resonators" of each filter are obtained from the formulas (2)–(10) below, which are equivalent to (1) as $\alpha \rightarrow \infty$. If the prototypes are identical, these formulas reduce to those given in [1].

The approximate improvements in the insertion loss of each channel in the center of the passband of the other are given in (11) and (12). ΔL_u is the increase in insertion loss of the upper filter in the center of the passband of the lower filter, compared to the filter in isolation, and correspondingly for ΔL_L.

Referring to Fig. 3, the design formulas are as follows:

$$X_0 = \frac{1}{2\alpha}\left(\frac{1}{D_1} - \frac{1}{C_1}\right) \tag{2}$$

$$A_1 = -C_1\left(\alpha + \frac{1}{2C_1^2\alpha} + \frac{1}{8D_1^2C_1\alpha^3}\left[\frac{J_1^2}{D_2} - \frac{1}{C_1}\right]\right) \tag{3}$$

$$A_2 = -C_2\left(\alpha + \frac{K_1^2}{8C_1^2C_2D_1\alpha^3}\right) \tag{4}$$

$$B_1 = D_1\left(\alpha + \frac{1}{2D_1^2\alpha} + \frac{1}{8C_1^2D_1\alpha^3}\left[\frac{K_1^2}{C_2} - \frac{1}{D_1}\right]\right) \tag{5}$$

$$B_2 = D_2\left(\alpha + \frac{J_1^2}{8D_1^2D_2C_1\alpha^3}\right) \tag{6}$$

$$R_1^2 = 1 + \frac{1}{4C_1\alpha^2}\left(\frac{1}{C_1} - \frac{1}{D_1}\right) \tag{7}$$

$$R_2^2 = 1 + \frac{1}{4D_1\alpha^2}\left(\frac{1}{D_1} - \frac{1}{C_1}\right) \tag{8}$$

$$K_1'^2 = K_1^2\left(1 - \frac{1}{4C_1D_1\alpha^2}\right) \tag{9}$$

$$J_1'^2 = J_1^2\left(1 - \frac{1}{4C_1D_1\alpha^2}\right) \tag{10}$$

$$\Delta L_u = 6 + 10\log_{10}\left(1 + \frac{1}{4C_1^2\alpha^2}\right)\text{dB} \tag{11}$$

$$\Delta L_L = 6 + 10\log_{10}\left(1 + \frac{1}{4D_1^2\alpha^2}\right)\text{dB}. \tag{12}$$

III. Proof of the Design Formulas

The element values in (2)–(10) are given in terms of the band separation factor α. The transformation $\alpha \rightarrow -\alpha$ should clearly interchange the channels, and the further transformation $\omega \rightarrow -\omega$ will interchange them again. Thus application of both transformations must result in a network which is indistinguishable at its ports from the original. Considering the affects which these transformations have on the frequency invariant susceptances of the original network, these susceptances must be odd functions of α. Similarly, the transformers and admittance inverters must be even functions of α.

As the separation between the channels becomes very large, the interactions between them become vanishingly small; thus, writing the element values as power series in α^{-1}, they must be of the following form:

$$X_0 = \frac{x_1}{\alpha} + \frac{x_3}{\alpha^3} + \varepsilon(\alpha^{-5}) \tag{13}$$

$$A_1 = -C_1\left(\alpha + \frac{a_{11}}{\alpha} + \frac{a_{13}}{\alpha^3} + \varepsilon(\alpha^{-5})\right) \tag{14}$$

$$A_2 = -C_2\left(\alpha + \frac{a_{21}}{\alpha} + \frac{a_{23}}{\alpha^3} + \varepsilon(\alpha^{-5})\right) \tag{15}$$

$$B_1 = D_1\left(\alpha + \frac{b_{11}}{\alpha} + \frac{b_{13}}{\alpha^3} + \varepsilon(\alpha^{-5})\right) \tag{16}$$

$$B_2 = D_2\left(\alpha + \frac{b_{21}}{\alpha} + \frac{b_{23}}{\alpha^3} + \varepsilon(\alpha^{-5})\right) \tag{17}$$

$$R_1^2 = 1 + \frac{r_1}{\alpha^2} + \varepsilon(\alpha^{-4}) \tag{18}$$

$$R_2^2 = 1 + \frac{r_2}{\alpha^2} + \varepsilon(\alpha^{-4}) \tag{19}$$

$$K_1'^2 = K_1^2\left(1 + \frac{k_1}{\alpha^2} + \varepsilon(\alpha^{-4})\right) \tag{20}$$

$$K_2'^2 = K_2^2\left(1 + \frac{k_2}{\alpha^2} + \varepsilon(\alpha^{-4})\right). \tag{21}$$

In these equations, $\varepsilon(-)$ means "an error of the order of $(-)$."

All the other elements in the network are obtained from the direct transformation (1), and thus only the first two resonators in each filter are modified from the values they have when the filter is working in isolation.

Let the prototype filters of Fig. 2 have an input impedance of unity, and, hence, zero insertion loss, at the sets of frequencies $\{\omega_i\}, \{\sigma_i\}$. Since there is maximum power transfer through the filter at these frequencies, it follows that, at these frequencies, the input admittances $Y_1(j\omega_i)$ and $Y_2(j\sigma_i)$ are a conjugate match to the admittances looking towards the first two elements of each filter. After applying the frequency transformation $\omega \to \omega \mp \alpha$ to the subnetworks N_1 and N_2 to get N_1' and N_2', respectively (Fig. 3), it follows that

$$Y_1'(j(\omega_i + \alpha)) = -j\omega_i C_2 + \frac{K_1^2}{-j\omega_i C_1 + 1} \tag{22}$$

$$Y_2'(j(\sigma_i - \alpha)) = -j\sigma_i D_2 + \frac{J_1^2}{-j\sigma_i D_i + 1}. \tag{23}$$

We may now derive a power series expansion of the impedance $Z_1(j(\omega_i + \alpha))$, which is the input impedance of the lower filter in the passband of the upper filter:

$$Z_1(j(\omega_i + \alpha)) = \frac{1 + r_2/\alpha^2}{j(\omega_i + \alpha)D_1 + jD_1\left(\alpha + \frac{b_{11}}{\alpha} + \frac{b_{13}}{\alpha^3}\right) + \frac{J_1^2(1 + k_2/\alpha^2)}{j(\omega_i + \alpha)D_2 + jD_2(\alpha + \cdots)}}$$

$$= \frac{1 + r_2/\alpha^2}{2j\alpha D_1 + j\omega_i D_1 + \frac{j}{\alpha}\left(D_1 b_{11} - \frac{J_1^2}{2D_2}\right) + \varepsilon(\alpha^{-2})} \tag{24a}$$

$$= \frac{z_1}{\alpha} + \frac{z_2}{\alpha^2} + \frac{z_3}{\alpha^3} + \varepsilon(\alpha^{-4}). \tag{24b}$$

Multiplying (24a) and (24b) by the denominator of (24a), and equating terms of equal degree in α, we get

$$2jD_1 z_1 = 1, \qquad z_1 = \frac{-j}{2D_1}$$

$$\frac{\omega_i}{2} + 2jD_1 z_2 = 0, \qquad z_2 = \frac{j\omega_i}{4D_1}$$

$$\frac{1}{2D_1}\left(D_1 b_{11} - \frac{J_1^2}{2D_2}\right) - \frac{\omega_i^2}{4} + 2jD_1 z_3 = r_2,$$

$$z_3 = \frac{j}{2D_1}\left(\frac{b_{11}}{2} - \frac{J_1^2}{4D_1 D_2} - \frac{\omega_i^2}{4} - r_2\right).$$

Thus

$$Z_2(j(\omega_i + \alpha)) = 1 + \frac{j}{\alpha}\left(x_1 - \frac{1}{2D_1}\right) + j\frac{\omega_i}{4D_1\alpha^2} + \frac{j}{\alpha^3}\left[x_3 + \frac{1}{2D_1}\left(\frac{b_{11}}{2} - \frac{J_1^2}{4D_1 D_2} - \frac{\omega_i^2}{4} - r_2\right)\right] + \varepsilon(\alpha^{-4}). \tag{25}$$

Knowing Z_2, we can calculate $Y_1''(j(\omega_i + \alpha))$:

$$Y_1''(j(\omega_i + \alpha)) = j(\omega_i + \alpha)C_2 - jC_2(\alpha + a_{21}/\alpha + a_{23}/\alpha^3) + \frac{K_1^2(1 + k_1/\alpha^2)}{j(\omega_i + \alpha)C_1 - jC_1(\alpha + a_{11}/\alpha + a_{13}/\alpha^3) + \frac{(1 + r_1/\alpha^2)}{1 + z_1/\alpha + z_2/\alpha^2 + z_3/\alpha^3}}. \tag{26}$$

Now (26) can be expanded as a power series in α^{-1}. Letting $\alpha \to \infty$ in (26), we obtain the leading term of the power series, which is

$$Y_1'' = j\omega_i C_2 + \frac{K_1^2}{j\omega_i C_i + 1}$$

a conjugate match for Y_1', (22). We must therefore choose the unknowns in (13)–(21) so that the higher order terms in the expansion of Y_1'' are zero: this is possible up to the third degree in α. Before going on to consider the equations in the unknowns that this gives, note that similar equations can be obtained for the upper filter in the passband of the lower filter, at the set of frequencies $\{\sigma_i - \alpha\}$, to force similar conditions on Y_2''.

Expanding Y_1'' and Y_2'' and equating the coefficients of the first-, second-, and third-degree terms in α^{-1} to zero we get

the following equations: from the α^{-1} terms:

$$-a_{21}+\frac{1}{2D_1}-x_1-C_1a_{11}=0 \tag{27a}$$

$$b_{21}+D_1b_{11}-x_1-\frac{1}{2C_1}=0 \tag{27b}$$

from the α^{-2} terms:

$$k_1(1+j\omega_iC_1)-\left[r_1-\left(x_1-\frac{1}{2D_1}\right)^2-\frac{j\omega_i}{4D_1}\right]=0 \tag{28a}$$

$$k_2(1+j\sigma_iD_1)-\left[r_2-\left(x_1+\frac{1}{2C_1}\right)^2-\frac{j\sigma_i}{4C_1}\right]=0. \tag{28b}$$

From the ω_i dependent terms in (28a) and (28b) we get the following independent equations:

$$k_1C_1+\frac{1}{4D_1}=0 \qquad k_2D_1+\frac{1}{4C_1}=0$$

$$k_1=k_2=-\frac{1}{4C_1D_1}. \tag{29}$$

The α^{-3} terms are more complicated:

$$\begin{aligned}&-jC_2a_{23}(1+j\omega_iC_1)^2\\&\quad-K_1^2\left\{\frac{\omega_i}{4D_1}\left(\frac{1}{2D_1}-x_1\right)-j\left(x_1-\frac{1}{2D_1}\right)\right.\\&\qquad\cdot\left(r_1-\left[x_1-\frac{1}{2D_1}\right]^2-j\frac{\omega_i}{4D_1}\right)\\&\qquad-j\left(x_3+\frac{1}{2D_1}\left[\frac{b_{11}}{2}-\frac{J_1^2}{4D_1D_2}-\frac{\omega_i^2}{4}-r_2\right]\right)\\&\qquad\left.-jC_1a_{13}\right\}=0\end{aligned} \tag{30a}$$

$$\begin{aligned}&jD_2b_{23}(1+j\sigma_iD_1)^2\\&\quad+J_1^2\left\{\frac{\sigma_i}{4C_1}\left(x_1+\frac{1}{2C_1}\right)+j\left(x_1+\frac{1}{2C_1}\right)\right.\\&\qquad\cdot\left(r_2-\left[x_1+\frac{1}{2C_1}\right]^2-j\frac{\sigma_i}{4C_1}\right)\\&\qquad+j\left(x_3-\frac{1}{2C_1}\left[\frac{a_{11}}{2}-\frac{K_1^2}{4C_1C_2}-\frac{\sigma_i^2}{4}-r_1\right]\right)\Bigg\}\\&\qquad-jD_1b_{13}=0.\end{aligned} \tag{30b}$$

The ω_i^2 term from (30a) gives

$$jC_1^2C_2a_{23}-j\frac{K_1^2}{8D_1}=0, \qquad a_{23}=\frac{K_1^2}{8C_1^2C_2D_1} \tag{31}$$

and the σ_i^2 term from (30b) gives

$$-jD_1^2D_2b_{23}+j\frac{J_1^2}{8C_1}=0, \qquad b_{23}=\frac{J_1^2}{8D_1^2D_2C_1}. \tag{32}$$

Substituting into (30a) and (30b) and solving for the ω_i terms gives, from (30a),

$$\frac{1}{2C_1}-\frac{1}{2D_1}+x_1=0, \qquad x_1=\frac{1}{2}\left(\frac{1}{D_1}-\frac{1}{C_1}\right) \tag{33}$$

and this result is also given by (30b).

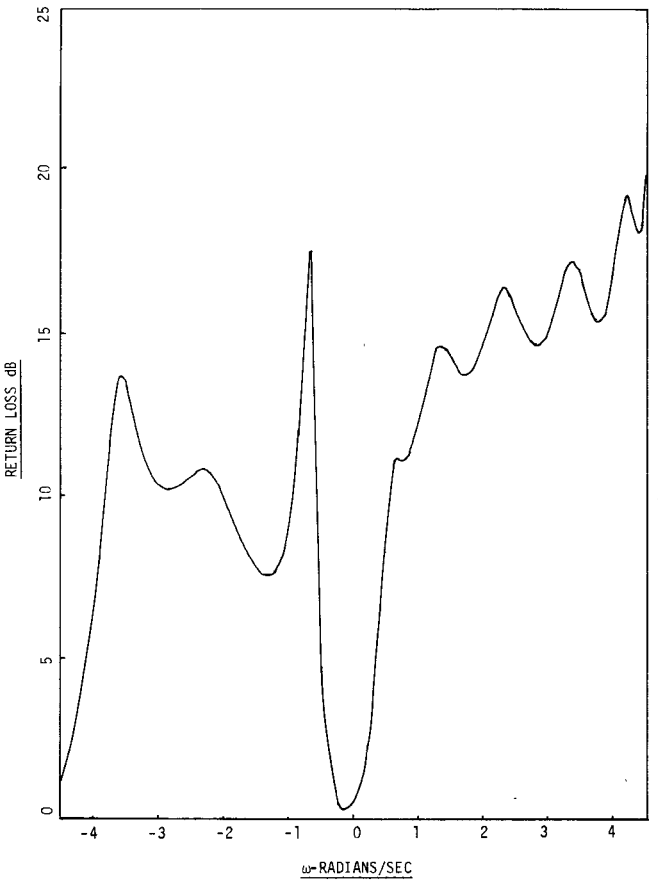

Fig. 4. Common-port return loss of unmodified filters connected in series.

Substituting for x_1 in (27a) and (27b), both a_{21} and b_{21} can be zero with no loss of generality, and we obtain

$$a_{11}=\frac{1}{2C_1^2} \tag{34}$$

$$b_{11}=\frac{1}{2D_1^2}. \tag{35}$$

Eliminating x_1, k_1, and k_2 in (28a) and (28b), we get

$$r_1=\frac{1}{4C_1}\left(\frac{1}{C_1}-\frac{1}{D_1}\right) \tag{36}$$

$$r_2=\frac{1}{4D_1}\left(\frac{1}{D_1}-\frac{1}{C_1}\right). \tag{37}$$

Finally, substituting into (30a) and (30b) and solving for the constant term, we find that x_3 can be zero without loss of generality, and

$$a_{13}=\frac{1}{8D_1^2C_1}\left(\frac{J_1^2}{D_2}-\frac{1}{C_1}\right) \tag{38}$$

$$b_{13}=\frac{1}{8C_1^2D_1}\left(\frac{K_1^2}{C_2}-\frac{1}{D_1}\right). \tag{39}$$

Equations (29) and (31)–(39) are the coefficients in (2)–(10).

Consider the upper filter in Fig. 3. The design procedure forces

$$Y_1''(j(\omega_1+\alpha))=Y_1'^*(j(\omega_i+\alpha))+\varepsilon(\alpha^{-4})$$

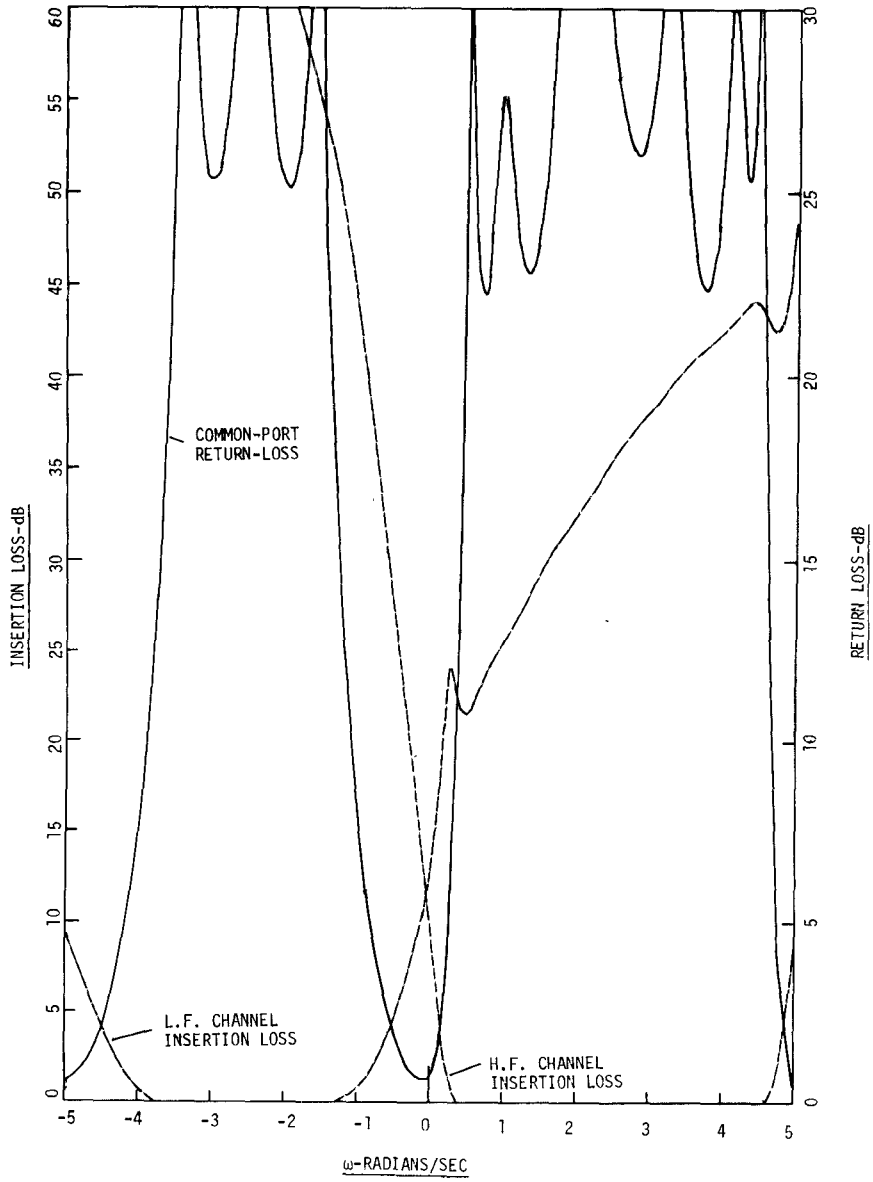

Fig. 5. Response of the prototype diplexer example.

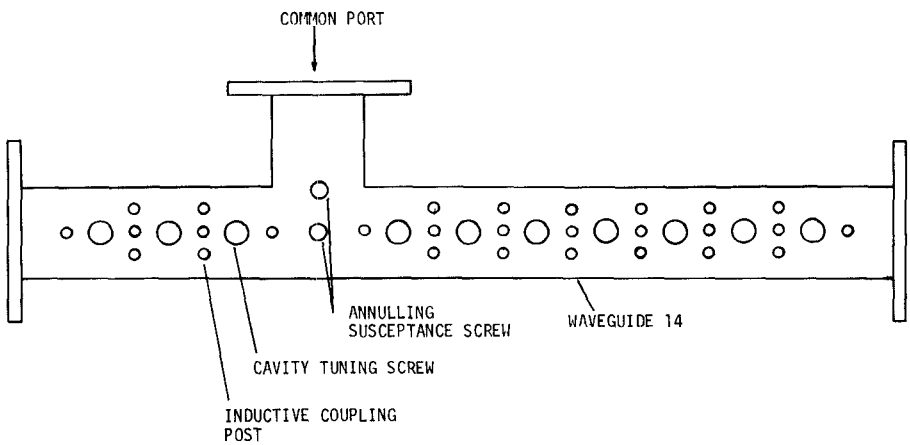

Fig. 6. Diplexer in waveguide 14.

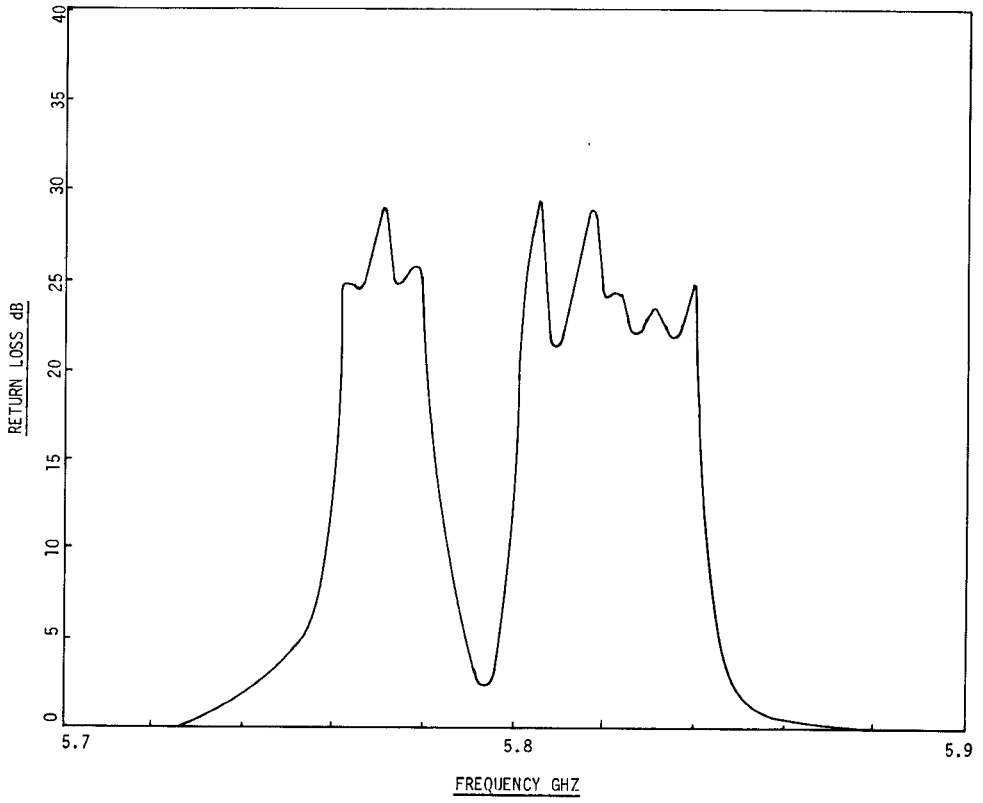

(a)

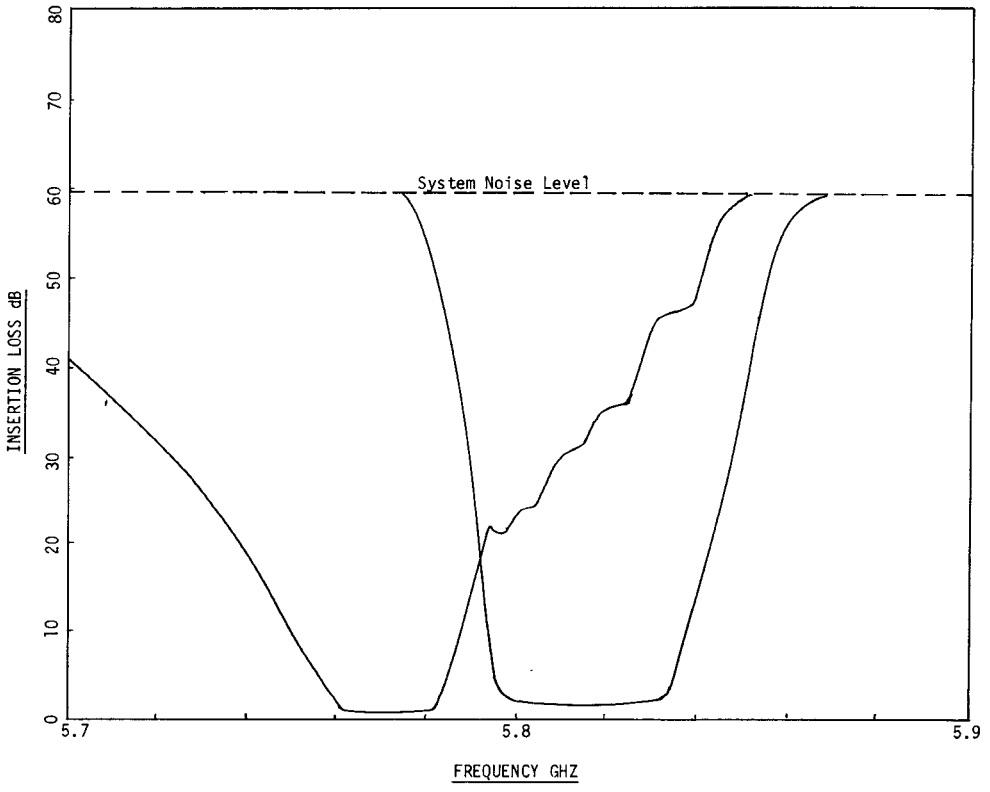

(b)

Fig. 7. Response of the waveguide diplexer. (a) Return loss. (b) Insertion loss.

and, except for an error of the order of α^{-4}, there must therefore be maximum power transfer into N'_1. Since the lower filter, in its stopband, has an input impedance which is purely reactive up to the order of α^{-4}, it follows that, to this order of approximation, there is maximum power transfer from the source to the whole network. Also, since N'_1 is lossless, there is maximum power transfer from N'_1 to its load. Thus it follows that

$$S_{11}(j(\omega_i + \alpha)) = 0 + \varepsilon(\alpha^{-4})$$

$$S_{22}(j(\omega_i + \alpha)) = 0 + \varepsilon(\alpha^{-4})$$

and similar conditions hold for the common port and the output port of the other channel at the set of frequencies $\{\sigma_i - \alpha\}$.

Now consider the upper filter of Fig. 3 at the center of the passband of the lower filter. The increase in the insertion loss of the filter is due to the potential-divider action which results from the passband input impedance of the lower filter and the annulling reactance being connected in the series with the source resistance. Considering the modifications to the filters, it is easy to show that the increase in insertion loss is given by

$$\Delta L_u \approx 6 + 10 \log_{10}\left(1 + \frac{1}{4C_1^2\alpha^2}\right) \tag{40}$$

and similarly

$$\Delta L_H \approx 6 + 10 \log_{10}\left(1 + \frac{1}{4D_1^2\alpha^2}\right). \tag{41}$$

This process can be continued, and corrections of the fourth and higher degrees in $1/\alpha$ obtained. However, the magnitude of the corrections becomes small compared with manufacturing tolerances, and the principle corrections are to the resonant frequencies of the elements and are inevitably made during tuning of the diplexer.

In [1], Rhodes showed that the symmetrical diplexer performed well even when the channels were contiguous. This is not true of the asymmetric diplexer, unless the selectivities of the individual filters are comparable at their band edges, and this criterion must be used to determine the filter specification for a given application.

IV. Performance of a Typical Diplexer

Consider the following diplexer example.

	Center Frequency (rad/s)	Bandwidth (rad/s)	Return Loss ripple (dB)	Degree
Low-Frequency Channel	−2.5	2.0	26	3
High-Frequency Channel	+2.5	4.0	27.31	7

Each filter has a conventional Chebyshev response and the explicit element values given in [2]. The degree and ripple level have been chosen such that the insertion losses of each channel are equal at zero frequency.

The common-port return-loss response of the two filters connected directly in series is shown in Fig. 4; clearly, the interactions between the filters cause an unacceptable degradation of performance.

In contrast, Fig. 5 shows the performance obtained by modifying the filters according to the design procedure given in Section II: the improvement over Fig. 4 is very marked. The in-channel return loss is better than 22 dB, and the lower frequency channel shows very little degradation. The insertion-loss curves also show the predicted improvement.

A waveguide diplexer has been designed from this prototype. This was made in waveguide 14, at a center frequency of 5.8 GHz and channel bandwidths of 20 and 40 MHz; the channel separation is hence 50 MHz. The design of the diplexer was straightforward, and is sketched in Fig. 6. The filters were designed using direct-coupled half-wave cavities, coupled via shunt inductive post irises. The individual filters were designed using the procedure in [3], and the common port was realized by a T-junction with tuning screws at the center of the junction to provide a capacitive annulling susceptance. The frequency-invariant susceptances in parallel with the capacitors in the prototype produce relative differences in the cavity resonant frequencies and were absorbed by adjustments to the tuning screws.

The response of the waveguide diplexer agreed closely with theory, as is shown in Fig. 7.

V. Conclusions

The direct design formulas given for asymmetric bandpass channel diplexers can be used to design high-performance diplexer prototypes. These prototypes can be directly transformed into narrow-band diplexers using direct-coupled resonator filters.

A 5.8-GHz waveguide diplexer has been designed and built using the new formulas, and its response agreed closely with theory.

References

[1] J. D. Rhodes, "Direct design of symmetrical interacting bandpass channel diplexers," *Inst. Elec. Eng. J. Microwaves, Optics, and Acoustics*, vol. 1, no. 1, pp. 34–40, Sept. 1976.
[2] ——, *Theory of Electrical Filters*. New York: Wiley, 1976.
[3] S. B. Cohn, "Direct-coupled-resonator filters," *Proc. IRE*, vol. 45, pp. 187–196, Feb. 1957.